

**IRON AND MANGANESE SPECIATION AND METHOD  
DEVELOPMENT FOR THE ANALYSIS OF WATER  
FROM PROCESSING PLANTS**

**RUGAYA MUHAMED SANIN**

**A thesis submitted in partial fulfilment of the requirements of  
Liverpool John Moores University for the degree of Doctor of  
Philosophy**

**June 2019**

## **Acknowledgement**

In the name of Allah Most Gracious Most Merciful.

My sincerest thanks go to my supervisors Dr. Alistair Fielding, Linda Seton and Ian Bradshaw for continuous support during my Ph.D study and the opportunity to work on this project, and also for their patience, immense knowledge, encouragement and motivation. I am very grateful to them for their guidance that helped me during the research and the writing of this thesis. It was their continued confidence in me that enabled this work to be completed.

I would like also to express gratitude to United Utilities for providing us the water samples involved in this project. A special thank you goes to research technicians; Phil Salmon and Nicola Dempster, for their help. Additionally, I would also like to acknowledge all my lab colleagues, in particular Samar Thiab, for their support and care, and all my friends especially, Adel Mohamed, Afaf AL Groshi, Ruba Bayan and Nashwa Osman, for their love and support.

I knew from the beginning that undertaking a doctoral study is a difficult and challenging task, especially as a mother of three children. Therefore, sincere thanks and appreciation go to my parents and family for their emotional support. Saving the most important for last, my special warm acknowledgement and highest gratitude is to my Husband, Ismaeil Algneness, for his endless support, understanding, quiet patience, sacrifice and unconditional love throughout all the years of my study, which enabled me to complete my Ph.D. Last but not least, I am very thankful to the beloved kids, Rahaf, Lyth, and Rafeef, who have given me much happiness and allowed me to remain hopeful, their eyes and joy are the sources of my inspiration. They

have prayed all the time for me to finish my PhD so we can do special things together, and I hope we have not lost too much of this during my study.

# Contents

CHAPTER 1 LITERATURE REVIEW .....	21
1.1 Introduction .....	21
1.1.1 Discolouration and aesthetic issues.....	22
1.1.2.1.2 The effect of biofilms on Fe and Mn concentrations in water .....	30
1.2 Elemental regulatory and guidelines.....	39
1.3 Drinking water treatment plants .....	43
1.4 Inductively coupled plasma (ICP) for metal analysis.....	46
1.4.1 Inductively coupled plasma (ICP) .....	47
1.4.2 ICP advantages and disadvantages .....	49
1.4.3 Inductively coupled plasma optical emission spectrometry (ICP-OES) .....	50
1.4.4 Inductively coupled plasma mass spectrometry (ICP-MS).....	55
1.5 Fe and Mn analysis and elemental speciation .....	67
1.5.1 Elemental speciation.....	67
1.5.2 Analytical techniques used for elements speciation.....	68
1.5.3 Analytical methods for Fe and Mn determination.....	70
1.5.3.1 Mn speciation.....	71
1.5.3.2 Fe speciation .....	72
1.6 High performance liquid chromatography HPLC and ICP-MS .....	73
1.7 Aim and objectives .....	77

CHAPTER 2 THE DEVELOPMENT OF AN ICP-OES METHOD TO ANALYSE FE AND MN IN WATER SAMPLES .....	78
2.1 Introduction .....	78
2.2 Experimental .....	79
2.2.1 Reagents and materials .....	79
2.2.2 Samples .....	81
2.3 Instrumentation .....	83
2.4 The Optimisation of ICP-OES conditions .....	84
2.5 Results and discussion .....	85
2.5.1 ICP-OES optimisation .....	85
2.5.1.1 The determination of the optimum nebulizer gas flow .....	86
2.5.1.2 The determination of the optimum pump rate .....	88
2.5.1.3 The determination of the optimum auxiliary gas flow .....	90
2.5.1.4 The determination of the optimum coolant gas flow .....	91
2.5.2.5 The determination of the optimum RF power .....	94
2.6 Optimal parameters and determination of LoD and LoQ .....	95
2.7 Analytical figures of merit and method validation .....	99
2.7.1 Wavelength selection .....	101
2.7.2 Linearity and range .....	104
2.7.3 Accuracy and Precision .....	105
2.7.4 Spike recoveries .....	109
2.7.5 Selection of optimal internal standards .....	111
2.8 Analysis of United Utilities' treatment water samples .....	114



3.4 Validation using recovery studies .....	140
3.5 Sample collection and analysis .....	141
3.6 Results and discussion .....	142
3.6.1 Optimisation of ICP-MS and assessment of analytical figures of merit .....	142
3.6.2 Major parameter optimisation .....	143
3.6.2.1 The optimum conditions for the standard mode.....	144
3.6.2.2 The determination of the optimum D1.....	144
3.6.2.3 The determination of the optimum Extraction .....	146
3.6.2.4 The determination of the optimum nebulizer.....	149
3.6.2.5 The determination of the optimum Focus .....	151
3.6.2.6 The determination of the optimum Hexapole .....	152
3.6.2.7 The determination of the optimum sample depth.....	155
3.6.3 Minor parameters.....	156
3.6.3.1 The determination of the optimum Lens2 .....	156
3.6.3.2 The determination of the optimum Forward Power.....	157
3.6.3.3 The determination of the optimum Horizontal .....	159
3.6.3.4 The determination of the optimum Vertical .....	160
3.6.3.5 The determination of the optimum D2.....	161
3.6.3.6The determination of the optimum Auxiliary.....	163
3.6.3.7 The determination of the optimum DA .....	165
3.6.3.8 The determination of the optimum Coolant.....	166
3.6.3.9 The determination of the optimum Lens2 and L3.....	167
3.6.3.10 Optimisation of Add Gas parameters.....	169

3.6.3.11 The effect of ICP-MS modes.....	171
3.6.4 Analytical performance.....	175
3.6.4.1 Limits of detection and quantification.....	176
3.6.3.2 Figures of merit.....	177
3.6.4 Sample analysis.....	186
3.7 Conclusion .....	192
CHAPTER 4 SPECIATION ANALYSIS BY HIGH PERFORMANCE LIQUID CHROMATOGRAPHY INDUCTIVELY COUPLED PLASMA MASS SPECTROMETRY (HPLC-ICP-MS) .....	194
4.1 Introduction .....	194
4.2 Experimental .....	197
4.2.1 Chemicals and Reagent .....	197
4.2.2 Mobile Phase Preparation .....	197
4.2.3 Preparation of the standards for the analysis .....	198
4.2.4 Instrumentation.....	199
4.3.2 Spike recovery .....	199
4.3 Analytical figures of merit.....	203
4.3.1 The limits of detection and quantification.....	203
4.4 Sample collection and preparation.....	203
4.5 Results and discussion .....	204
4.5.1 The determination of Fe and Mn species.....	204

4.5.2 Testing the separation efficiency of different mobile phases .....	205
4.5.2.1 Mobile phase and column .....	205
4.5.2.3 pH Optimisation .....	208
4.5.2 Interferences .....	212
4.5.3 Validation .....	215
4.5.3.1 The limit of detection and quantification LOD and LOQ .....	218
4.5.4 Water processing sample analysis for Fe and Mn species in drinking water using HPLC-ICP-MS .....	220
4.5.4.1 Water analysis at different locations .....	220
4.5.4.2 Fishmoore Mn <sup>2+</sup> concentrations for each stage of the treatment process. ....	224
4.6 Conclusion .....	227
CHAPTER 5 OVERALL CONCLUSION AND FUTURE WORK .....	230
5.1 Overall conclusion.....	230
5.2 Future work.....	233
References.....	235

## List of tables

Table 1-1 Dietary allowances for iron in infants, children, and adults (Institute of Medicine Food and Nutrition Board (93).....	37
Table 1-2 Recommended Dietary Allowances for manganese for Infants, Children, and Adults (Institute of Medicine Food and Nutrition Board (93). .....	38
Table 1-3 Drinking water standards for Mn and Fe by selected organisations. .....	40
Table 2-1 List of samples and locations used in this study. ....	82
Table 2-2 ICP-OES operation conditions. ....	83
Table 2-3 The optimum parameters range for ICP-OES.....	85
Table 3-1 Instrumental parameters for ICP-MS. ....	129
Table 3-2 Ion optics parameters. ....	134
Table 3-3 Major parameters.....	135
Table 3-4 Minor parameters.....	136
Table 3-5 ICP-MS optimum con.....	173
Table 3-6 ICP-MS optimum conditions using CCT mode.....	174
Table 3-7 Analytical conditions for Fe and Mn. ....	175
Table 3-8 Parameters of the analytical calibration curves: linear range, correlation coefficient (R <sup>2</sup> ), average (RSD) for repeatability of calibration solutions measurements.....	180
Table 3-9 The certified and CCT mode found concentration (µg/mL) of the elements, in the certified reference material (SRM TMDA-70 and TMDA-64.2, river water). ....	181
Table 3-10 The LoD and LoQ for Fe and Mn in standard and CCT Mode. ....	183

Table 3-11 LoD and LoQ calculation using the above equation for Fe and Mn (ng/mL) using CCT Mode. ....	184
Table 3-12 Concentrations (ng/mL) of Fe and Mn from different locations of Northwest region of England. ....	187
Table 3-13 Spike and RSD of Fe and Mn from different locations of Northwest region of England. ....	188
Table 3-14 Concentrations (ng/mL) of Fe and Mn from different locations of Northwest region of England. ....	189
Table 3-15 Correlation coefficients ( $R^2$ ) and limits of detection (LoD) in ng/mL for Fe and Mn by ICP-OES and ICP-MS. ....	192
Table 4-1 Operation and acquisitions parameters of ICP-MS and HPLC. .	202
Table 4-2 TMDA-64 percentage recovery. ....	216
Table 4-3 LoD and LoQ for Fe and Mn using HPLC-ICP-MS. ....	220
Table 4-4 Metal contents of Wayoh water samples. ....	221
Table 4-5 Metal contents of Wybersley water samples. ....	222
Table 4-6 Metal contents of Sweet Loves water samples. ....	223
Table 4-7 Metal contents of Sutton Hall water samples. ....	223
Table 4-8 Metal concentration level of Fishmoore water by HPLC-ICP-MS. ....	225
Table 4-9 Metal concentration levels of Fishmoore water by ICP-MS. ....	225

## List of figures

Figure 1-1 EV-PH Pourbiax diagram for Fe oxides and hydroxides (31). ....	28
Figure 1-2 EV-PH Pourbiax diagram for Mn oxides and hydroxides (31).....	29
Figure 1-3 Schematic showing the common steps in water treatment used in drinking water processing plants. ....	44
Figure 1-4 Schematic of an ICP torch, adapted from Boss, 1977 (129).....	48
Figure 1-5 Diagram of sample introduction to ICP-OES, adapted from (M. Hieftije 1989) (130).....	50
Figure 1-6 Excited atom energy level adapted from (Charles B. Boss, 1997) (132).....	51
Figure 1-7 (A) Direct spectral overlap, (B) No overlapping, (C) Simple background shift, and (D) Wing overlapping interference shift. ....	54
Figure 1-8 The interface region of an ICP-MS adopted from PerkinElmer 2001 (137).....	57
Figure 1-9 Schematic diagram for the basic components of an ICP-MS system adapted from R. Thomas (140). ....	58
Figure 1-10 Schematic of the quadrupole mass filter adapted from PerkinElmer (137).....	61
Figure 1-11 A typical configuration for HPLC with an ICP-MS adapted from Michael (129).....	76
Figure 2-1 United Utilities water supply areas.....	81
Figure 2-2 The effect of nebuliser gas flow rates on signal intensity of Fe (A) and Mn (C) and signal to blank ratio of Fe (B) and Mn (D). ....	87

Figure 2-3 The effect of pump flow rate on the signal intensity of Fe (A) and Mn (C) and signal to blank ratio of Fe (B) and Mn (D).....	89
Figure 2-4 The effect of auxiliary gas flow rate on the signal intensity of Fe (A) and Mn (C) and signal to blank ratio of Fe (B) and Mn (D).....	91
Figure 2-5 The effect of coolant gas flow on the signal intensity of Fe (A) and Mn (C) and signal to blank ratio of Fe (B) and Mn (D).....	93
Figure 2-6 The effect of radio frequency on the signal intensity of Fe (A) and Mn (C) and signal to blank ratio of Fe (B) and Mn (D).....	94
Figure 2-7 Calibration graph of Mn recorded at 257.6 nm. ....	97
Figure 2-8 Subarray plots for Mn 257.6nm (A), Mn 279.4nm (B), Fe259.8nm (C) and Fe 238.2nm (D) respectively. ....	103
Figure 3-1 Skimmer and sampler cones before (left) and after cleaning (right) in an ultrasonic bath. ....	127
Figure 3-2 Schematic of X series ion optics.....	134
Figure 3-3 Signal and signal to blank ratio for D1 for <sup>55</sup> Mn (A), <sup>56</sup> Fe (B), <sup>57</sup> Fe (C) and <sup>58</sup> Fe (D).....	146
Figure 3-4 Signal and signal to blank ratio for extraction for <sup>55</sup> Mn (A), <sup>56</sup> Fe, <sup>57</sup> Fe and <sup>58</sup> Fe (B and C). ....	148
Figure 3-5 Signal and signal to blank ratio for nebuliser for <sup>55</sup> Mn (A), <sup>58</sup> Fe, <sup>56</sup> Fe, <sup>54</sup> Fe and <sup>57</sup> Fe (B and C). ....	150
Figure 3-6 Signal and signal to blank ratio for focus in standard mode for <sup>55</sup> Mn (A), <sup>56</sup> Fe (B), <sup>57</sup> Fe (C) and <sup>58</sup> Fe (D). ....	152
Figure 3-7 Signal and signal to blank ratio for hexapole for <sup>55</sup> Mn (A), <sup>56</sup> Fe, <sup>57</sup> Fe, <sup>54</sup> Fe and <sup>58</sup> Fe (B and C). ....	153

Figure 3-8 Signal and signal to blank ratio for pole bias for <sup>55</sup> Mn (A), <sup>56</sup> Fe, <sup>57</sup> Fe, <sup>54</sup> Fe and <sup>58</sup> Fe (B and C). .....	154
Figure 3-9 Signal and signal to blank ratio for sample depth for <sup>55</sup> Mn (A), <sup>56</sup> Fe, <sup>57</sup> Fe, <sup>54</sup> Fe and <sup>58</sup> Fe (B and C).....	155
Figure 3-10 Signal and signal to blank ratio for lens2 for <sup>55</sup> Mn (A), <sup>56</sup> Fe, <sup>57</sup> Fe, <sup>54</sup> Fe and <sup>58</sup> Fe (B and C). .....	157
Figure 3-11 Signal and signal to blank ratio for forward power for <sup>55</sup> Mn (A), <sup>56</sup> Fe, <sup>57</sup> Fe, <sup>54</sup> Fe and <sup>58</sup> Fe (B and C).....	158
Figure 3-12 Signal and signal to blank ratio for horizontal for <sup>55</sup> Mn (A), <sup>56</sup> Fe, <sup>57</sup> Fe, <sup>54</sup> Fe and <sup>58</sup> Fe (B and C).....	160
Figure 3-13 Signal and signal to blank ratio for vertical for <sup>55</sup> Mn (A), <sup>56</sup> Fe, <sup>57</sup> Fe, <sup>54</sup> Fe and <sup>58</sup> Fe (B and C). .....	161
Figure 3-14 Signal and signal to blank ratio for D2 for <sup>55</sup> Mn (A), <sup>56</sup> Fe, <sup>57</sup> Fe, <sup>54</sup> Fe and <sup>58</sup> Fe (B and C). .....	162
Figure 3-15 Signal and signal to blank ratio for Auxiliary gas flow for <sup>55</sup> Mn (A), <sup>56</sup> Fe, <sup>57</sup> Fe, <sup>54</sup> Fe and <sup>58</sup> Fe (B and C).....	164
Figure 3-16 Signal and signal to blank ratio for DA for <sup>55</sup> Mn (A), <sup>56</sup> Fe, <sup>57</sup> Fe, <sup>54</sup> Fe and <sup>58</sup> Fe (B and C). .....	165
Figure 3-17 Signal and signal to blank ratio for coolant gas flow for <sup>55</sup> Mn (A), <sup>56</sup> Fe, <sup>57</sup> Fe, <sup>54</sup> Fe and <sup>58</sup> Fe (B and C).....	167
Figure 3-18 Signal and signal to blank ratio for Lens2 for <sup>55</sup> Mn (A), <sup>56</sup> Fe, <sup>57</sup> Fe, <sup>54</sup> Fe and <sup>58</sup> Fe (B and C). .....	168
Figure 3-19 Signal and signal to blank ratio for lens3 for <sup>55</sup> Mn (A), <sup>56</sup> Fe, <sup>57</sup> Fe, <sup>54</sup> Fe and <sup>58</sup> Fe (B and C). .....	169

Figure 3-20 Signal and signal to blank ratio for CCT gas for $^{55}\text{Mn}$ (A), $^{56}\text{Fe}$ , $^{57}\text{Fe}$ , $^{54}\text{Fe}$ and $^{58}\text{Fe}$ (B and C).....	171
Figure 3-21 Calibration Curve for $^{55}\text{Mn}$ on standard mode. ....	177
Figure 3-22 Calibration curve for $^{55}\text{Mn}$ on CCT mode.....	177
Figure 3-23 Calibration curve for $^{56}\text{Fe}$ on Standard mode. ....	178
Figure 3-24 Calibration curve for $^{56}\text{Fe}$ on CCT mode.....	179
Figure 3-25 Calibration graph for $^{57}\text{Fe}$ on CCT mode. ....	179
Figure 3-26 Calibration graph for $^{55}\text{Mn}$ used for the calculation of LoD and LoQ. ....	183
Figure 3-27 Calibration graph for $^{56}\text{Fe}$ used for the calculation of LoD and LoQ. ....	184
Figure 4-1 Schematic diagram for HPLC-ICP-MS instrumentation (Thermo Fisher). ....	200
Figure 4-5 Chromatograms and the signal responses of 1 $\mu\text{g}/\text{mL}$ $\text{Mn}^{2+}$ , $\text{Fe}^{2+}$ and $\text{Fe}^{3+}$ at pH 3.3 using Dionex CG5A guard column (50 mm), PDCA acid mobile phase; .....	211
Figure 4-6 Calibration responses for $\text{Mn}^{2+}$ (A) and for $\text{Fe}^{2+/3+}$ (B and C respectively) using HPLC-ICP-MS. ....	213
Figure 4-7 Signal response of $\text{Fe}^{2+}$ and $\text{Mn}^{2+}$ standards solutions at the concentration of (A) 50 ng/mL (B) 100 ng/mL and (C) 1000 ng/mL using PDCA. ....	214
Figure 4-8 $^{55}\text{Mn}$ standard reference material (TMDA) peak. ....	217
Figure 4-9 $^{56}\text{Fe}$ standard reference material (TMDA) peak.....	217
Figure 4-10 1 ppm standard for SRM TMDA-64.2 for both $^{56}\text{Fe}$ and $^{55}\text{Mn}$ chromatograms. ....	218

Figure 4-11 All chromatograms for Fe <sup>3+</sup> calibration standard solutions. ....	219
Figure 4-12 All chromatograms for Mn <sup>2+</sup> calibration standard solutions.....	219
Figure 4-13 Chromatograms for Mn raw water. ....	226
Figure 4-14 Accelerator No1 water. ....	226

## List of abbreviations

Symbol	Full name
Ar	Argon gas
AEC	Anion Exchange Chromatography
ASV	Anodic stripping voltammetry
Conc	Concentration
CCT	Collision Cell Technology
DWI	Drinking Water Inspector
DI	Deionized Water
EV	Electron volt
Exp	Expansion pressure
EPA	The United States Environmental Protection Agency
FW	Forward Power
Fe	Iron
HNO <sub>3</sub>	Nitric acid
HCl	Hydrochloric acid
HCHO <sub>2</sub>	Formic acid
He	Helium
HPLC	High performance liquid chromatography
ICP	Inductively Coupled Plasma
LOD	Limit Of Detection
LOQ	Limit Of Quantification
LC-ICP-MS	Liquid Chromatography-Inductively coupled plasma Mass Spectrometry
L	Litter
MS	Mass Spectrometry
M	Molar
m	Milli
μ	Micro
Mn	Manganese
μg/mL	Microgram per milli
μg/L	Microgram per litre
mg/L	Milligram per litre
Min	Minute
mM	Millimolar
MW	Molecular weight
Mm	Millimetre
MΩ	Mega ohm
n	Nano
Nm	Nano meter
Neb	Nebuliser
OES	Optical Emission Spectrometry
ppm	parts per million
ppt	part per trillion
PH	Potential of Hydrogen
PVC	Poly Phenyl Chloride

<b>RF</b>	Radio Frequency
<b>R</b>	Correlation coefficient
<b>R<sup>2</sup></b>	Coefficient of determination
<b>RSD</b>	Relative Standards Deviation
<b>%R</b>	Percentage Recovery
<b>s</b>	Second
<b>S/b</b>	Signal-to- Background Ratio
<b>SRM</b>	Standard reference material
<b>T</b>	Temperature
<b>t</b>	time
<b>UPW</b>	ultrapure water
<b>V</b>	Volume
<b>WHO</b>	World Health Organization
<b>Wt</b>	Weight
<b>W</b>	Watt
<b>Y</b>	Yttrium
<b>λ</b>	Wavelength

---

## **Abstract**

Iron (Fe) has been indicated as the main cause of discoloration in drinking water. This normally takes the form of a yellow coloration. It is also known that manganese (Mn) can also lead to a similar yellow colour in solution. Hence, it is important to identify the source of discolouration in drinking water. To minimise the effect of these elements, the prescribed concentrations in drinking water have been set at 0.2 mg/L for Fe and 0.05 mg/L for Mn by the drinking water inspectorate (DWI-UK). The aim of this work was to optimise and validate different analytical methods for the determination of Fe and Mn simultaneously in water samples. It was also a purpose of the work to develop a robust methodology that would allow greater understanding of Fe and Mn speciation at different stages of water treatment and its relationship with governmental limits. The first two methods that were developed were inductively coupled plasma optical emission spectroscopy ICP-OES and inductively coupled plasma mass spectrometry ICP-MS. These two methods were validated using a standard reference material (SRM) and good accuracy was achieved with spiked addition methods. Further, The results showed good relative standard deviation (RSD) <5%, linearity  $R^2 > 0.996$ ), with spiked recovery between 95-105%. The limit of detection (LoD) and limit of quantification (LoQ) were found to 5 ng/mL and 12 ng/mL for Fe and 1.2 ng/mL and 6.7 ng/mL for Mn, respectively, using the optimum conditions for ICP-OES; and 0.6 ng/mL and 0.3 ng/mL, respectively, for ICP-MS using collision reaction cell (CCT) mode. United Utilities (UU) water was taken from, eight different locations and at different treatment stages: Huntington water, Fishmoore water, Wayho water, Wybesley water, Sweet loves water,

Oswestry and Sutton Hall. The samples were analysed to determine Fe and Mn levels using the developed ICP methods. These samples were analysed using an internal standard method and it was found to be good for the determination to minimise variation in the results obtained from the two ICP methods. The analytical method speciation was developed using cation exchange high performance chromatography ICP-MS (HPLC-ICP-MS) and this was optimized and validated for Fe and Mn species in the water processing samples. The soluble species forms of Fe<sup>3+</sup> and Mn<sup>2+</sup> were analysed using a chromatogram, the calibration graphs of both Fe and Mn had very good linearity ( $R^2 = 0.9995$  and  $0.9999$  for Fe and Mn species, respectively) in the range of 5 ng/mL to 1 µg/mL respectively. The percent recoveries were 95-105% with a RSD of <5% and spiked recoveries for both species were in the same range as the % recoveries. For the method, species were separated in three minutes with the cation-exchange capability of the IonPAC column CG5 ion pack and through using a guard column. The results showed that both Fe<sup>3+</sup> and Mn<sup>2+</sup> appeared at high concentrations during the addition of the coagulants in the water processing plant and the concentration was less at the final stages of the treatment. The HPLC-ICP-MS method indicates the benefit of using a Mn removal stage in the treatment works to ensure that less than 200 µg/L and 50 µg/L of soluble Fe and Mn are obtained in the final water supply.

## Chapter 1 Literature review

### 1.1 Introduction

All around the world, drinking water suppliers are responsible for providing safe and clean drinking water. An adequate, safe, and accessible supply of water should be available for both domestic and commercial use. Several elements and minerals are commonly found in water. Some of the elements are heavy metals like mercury, lead, chromium and arsenic and they can lead to acute toxicity and potential health risks, even at low concentrations. Many accidental poisoning incidents have been reported in different parts of the world including the USA, China, Turkey, Pakistan and Bangladesh as a result of heavy metals in water (1-4). In water, metals like iron (Fe) and manganese (Mn) can cause aesthetic problems at high concentration levels, such as an unpleasant metallic taste, discolouration and staining of laundry. Furthermore, Wassermann *et al.* (1) indicated that Mn in drinking water can cause more than aesthetic issues, and increased levels in drinking water can reduce intellectual function in children.

Fe and Mn are naturally occurring elements in groundwater (5) where both are present in anoxic environments (6). For a long period of time, Fe and Mn have been causing problems for regulatory authorities in connection to industrial and main water supplies. As a result, main water supply companies have experienced customer complaints, compliance failures, and a loss of custom (7). Although higher dissolved concentrations of Fe and Mn are not considered to have any serious harm to human or animal health (5), they can cause aesthetic problems. Therefore, the World Health Organization has approved

the treatment of water if concentrations of Fe and Mn are higher than 0.3 mg/L and 0.1 mg/L, respectively (8).

The water treatment processes for Fe include precipitation, oxidation with oxidants such as potassium permanganate, oxygen, chlorine, and other oxidant compounds. This is then followed by the removal of particles through clarification and filtration. In contrast, there are several processes for Mn removal that include adsorption of Mn on to manganese oxide coated media. This is continuously activated by the addition of chlorine as well as oxidation and precipitation by a strong oxidant such as permanganate followed by particle removal. These treatment processes for Fe and Mn involve removal of the metal. Drinking water systems use complexes of Fe and Mn to prevent precipitation and subsequent water quality problems, such as staining on clothes, colouration and turbidity (9).

### **1.1.1 Discolouration and aesthetic issues**

Water utility companies have struggled to prove the link between particles found in the distribution system in relation to the discolouration source. This is partly because controlling the amount of particles entering drinking water distribution systems is challenging. These particles from the water treatment plant represent the most important external source entering the distribution system; they can enter as dissolved inorganic and organic materials from the source.

It is believed that the most common cause of discolouration is the build-up of elements in the water distribution systems (10). Fe and Mn are usually the two elements responsible for the discoloration problem (11, 12) and have been

linked to both nuisance contaminants and aesthetic issues. As well as the staining of clothes and kitchen utensils due to discolouration of water, Fe and Mn can result in an unpleasant odor and taste in food (11). It is reported that the water industry receives over 50,000 customer contacts per year in England and Wales as a result of discoloured water (13).

#### **1.1.1.1 Sources of Fe and Mn**

Fe and Mn are common minerals that occur naturally in the Earth's crust (14). Although they are completely different elements, they can cause similar problems in water supplies (15). Pearson and Greenway (16) published a recent review about the developments in Mn speciation and found that Mn can cause severe disruption to the central nervous system. The exposure via inhalation resulted in the main cause of Mn toxicity. The Fe and Mn occurring chemical forms have different colours including yellow and dark brown, which adversely affect water aesthetic properties when present in high concentrations (15, 17-20).

The use of water for human consumption is obtained from two main sources, groundwater and surface water. Rivers, lakes, and reservoirs contribute to surface water supplies. When the groundwater is pumped up to the surface, it comes into contact with air allowing the oxidation of some elements and this is accompanied with release of carbon dioxide into the atmosphere. The dissolved oxygen is consumed by the decomposition of organic matter and microbes in the soil. This process reduces Fe and Mn from  $\text{Fe}^{3+}$  and  $\text{Mn}^{4+}$  to  $\text{Fe}^{2+}$  and  $\text{Mn}^{2+}$  respectively and the lack of oxygen also causes the pH value of water to be reduced due to microbial action. The soluble form of dissolved Fe is  $\text{Fe}^{2+}$  under the pH range of 5 to 8. After the oxidation process and carbon

dioxide release, the pH values are increased and hence the  $\text{Fe}^{2+}$  and  $\text{Mn}^{2+}$  are changed into the insoluble forms of  $\text{Fe}^{3+}$  and  $\text{Mn}^{4+}$ . If this is a source of drinking water, then the presence of Fe and Mn will require treatment to remove the colour, prior to distribution to customers.

### **1.1.2 Fe and Mn contamination in drinking water**

Water supply companies have faced two major problems. The first concerns drinking water discoloration and the second is compliance failures. They have attempted to eliminate these problems by cleaning, renewal and replacement of the mains distribution network (21).

It is therefore important to identify the source of discoloration and minimize the effect of these elements in the treatment system. Low concentrations of Fe and Mn can enter the distribution networks from the water treatment plants causing both elements to build up in the network (21). Although corrosion of cast Fe pipes was often regarded as the main source of the problem, particles originating from the water treatment plant played an important part in the generation of a discoloration in drinking water distribution systems (22). The deposits of both Fe and Mn depend on their chemical reactions, physical processes and microbiological activity within the network system (23-25).

Prescribed concentrations in drinking water in the UK are set at limits of 0.2 mg/L for Fe and 0.05 mg/L for Mn (26-29). The World Health Organization (WHO) guidelines (30) have set 0.4 mg/L for Mn and 0.3 mg/L for Fe in drinking water (28, 31) the different between these two guides because WHO based on the upper tolerable intake while DWI based on the avoidance of water discoloration and deposition. However, discoloration events are the

phenomenon that results in numerous complaints from customers to drinking water supply companies due to the visible deterioration of water quality leaving the tap. The two dominant processes that threaten tap water quality are particle accumulation (21) and microbial growth. These events can undermine customer confidence as well as causing nuisance such as staining of clothes. Further effects resulting from these problems are increased treatment costs and reduced treatment capacity, as well as increased pumping and rehabilitation costs, and a risk of health concerns. The process of deposition and release of these metals is highly complex and unpredictable.

Previous research has provided different methods to prevent the discolouration of water (10, 21). The work conducted by J.H.G. Vreeburget *al.* studied the prevention of the release of any matter into the distribution systems. Other research emphasised the importance of minimizing the settling of suspended solids, removing any sediments from the distribution systems in a timely way (21). The most important step was found to be the prevention of build-ups of the particle matter in distribution systems. (21). There was also extensive agreement that the ultimate objective of water utilities should be to offer good quality drinking water to customers (32). Indeed, there has been an urgent need for water companies to have a good understanding of the processes and mechanisms leading to water discolouration and to avoid compliance failures. In addition, there is a need for a comprehensive strategy in place to deal with such events. It has been suggested that water utility suppliers should focus on offering good quality drinking water at customers' taps instead of attempting to achieve this at the treatment plant (33).

Mn is one of the most abundant metals in the Earth's crust and exists in surface and ground water due to the erosion of rocks and soil and in air as dust particles. These dust particles settle to the ground within a few days. Mn is found in various oxidation states within several chemical compounds, usually in association with oxygen, chlorine, or sulphur. Principally it is found as pyrolusite ( $\text{MnO}_2$ ). Mn reacts with water and dissolves in diluted acids. The main mining areas for Mn ores are in Russia, South Africa, Gabon, Georgia and Australia. Industrial activities are also responsible for contaminating the environment with Fe and Mn. Elevated levels of Mn can cause lung, liver and vascular disturbances, declines in blood pressure, failure in development foetuses and brain damage in animals (34, 35).

Fe and Mn occur in dissolved forms as ions ( $\text{Fe}^{2+}$ ,  $\text{Mn}^{2+}$ ) and as undissolved higher forms as  $\text{Fe}(\text{OH})_3$  or  $\text{Mn}(\text{OH})_4$ , respectively. They can also bond to humic substances to produce colloid forms. This form depends on oxygen concentration, solubility of Fe and Mn compounds in water, redox potential, pH value, hydrolysis, the presence of complex forming organic and inorganic substances, water temperature and water composition ( $\text{CO}_2$ ).

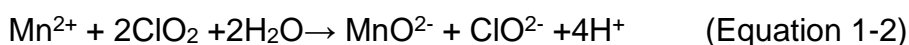
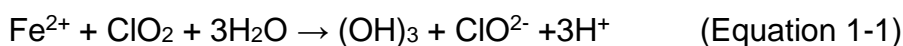
In the presence of oxygen in the water, the corrosion rate generally increases with dissolved oxygen forming hydrate oxides, which have a reddish-brown colour. Fe oxide and hydroxide are insoluble in water. At lower pH the water solubility of these compounds increases, as  $\text{Fe}^{3+}$  compounds are soluble in strongly acidic solutions (36)

### 1.1.2.1 Factors influencing Fe and Mn accumulation in the water network system

The link between particles found in the distribution system to the discolouration source has been found to be very difficult to prove for water utility companies. This is partly because control of the amount of particles entering drinking water distribution systems is a challenging task. These particles from the water treatment plant represent the most important external source entering the distribution system; dissolved inorganic and organic material from the source.

For water utilities, controlling the amount of sediment getting into drinking water from the distribution structures has been a major challenge (37). Typically, soluble  $\text{Fe}^{2+}$  / $\text{Mn}^{2+}$  is converted to an insoluble form at some point during water processing by making use of oxidants such as potassium permanganate, chlorine, ozone or chlorine dioxide (38). The redox chemistry of Fe and Mn plays a dominant role in their aquatic cycle, leading to transformations from their insoluble oxidized forms into their soluble reduced forms and vice-versa (39). These particles give the water a red tint from Fe and Mn leaves a black tint which is usually suspended in water. These soluble species and colloidal elements are responsible for the discolouration events (40).

Equations 1-1 and 1-2 show how chlorine dioxide oxidises  $\text{Fe}^{2+}$  and  $\text{Mn}^{2+}$  to insoluble  $\text{Fe}^{3+}$  and  $\text{Mn}^{4+}$ , respectively. Usually, the reaction takes place within two to three seconds (41).



The factors that influence the accumulation of Fe and Mn include complex chemical, physical/hydraulic and biological processes. From the water supply facilities or network, there are three possible causes of discolouration: (42);i) chemical reactions involved in water purification process, ii) biological parameters and iii) physical processes/forces inside the network.

### 1.1.2.1.1 The chemistry of Fe and Mn

Fe and Mn are abundant in the environment and present different oxidation states depending on the conditions in which they might be encountered. Different species of Fe and Mn are represented in Figures 1-1 and 1-2. The redox chemistry of Fe and Mn controls their aquatic cycle and the transformation from insoluble oxides to soluble reduced forms and vice-versa (43).

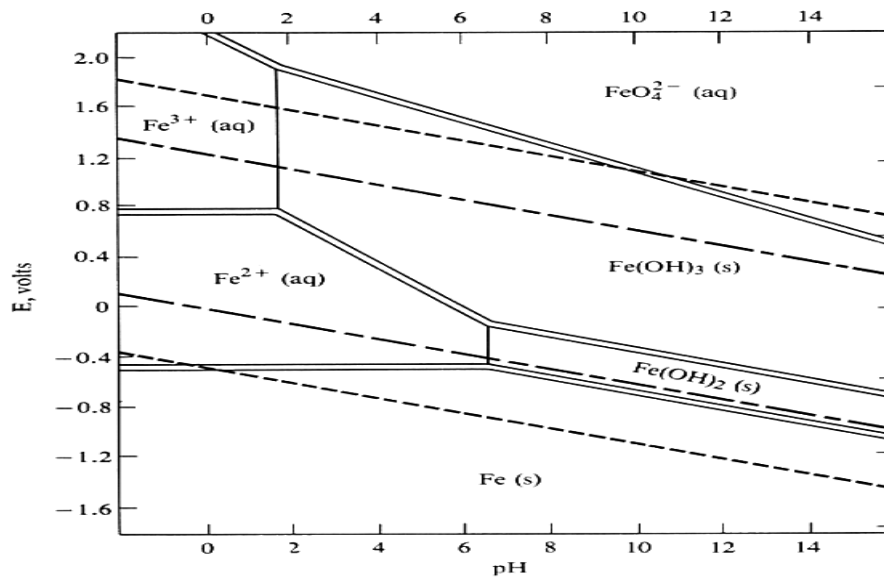
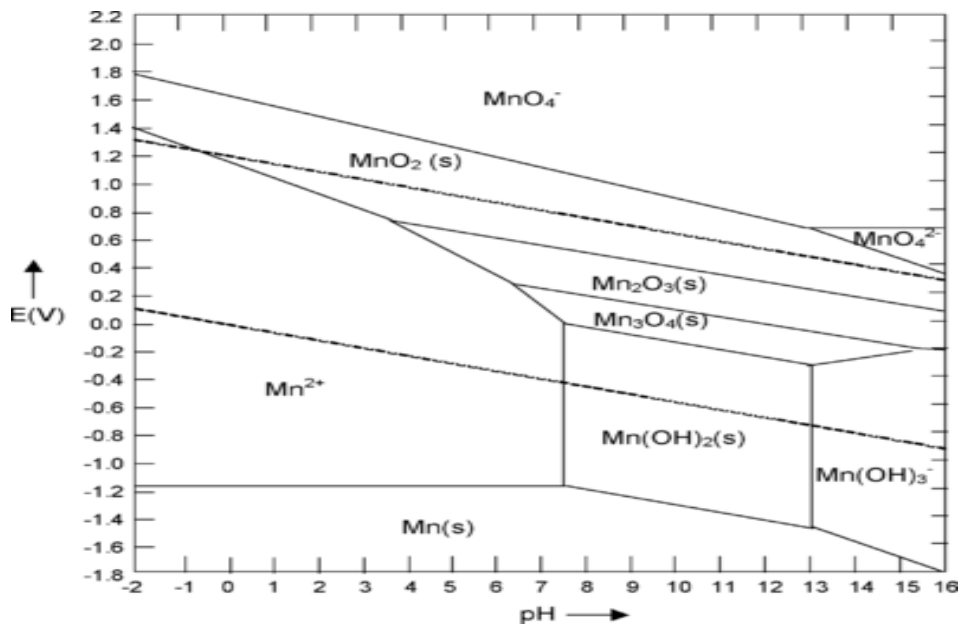


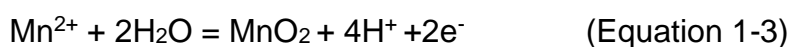
Figure 1-1 EV-PH Pourbiac diagram for Fe oxides and hydroxides (31).



**Figure 1-2** EV-PH Pourbiac diagram for Mn oxides and hydroxides (31).

Mn is similar to Fe as it is a transition metal. It occurs naturally, and the chemistry of Mn is complex. It exists in several species with different oxidation states between 0 to +7, with +2, +4, and +7 being environmentally and biologically important (44). The most chemically stable forms of Mn are +2 and +7 where both forms are soluble, whereas in contrast  $\text{Mn}^{4+}$  is insoluble. The most stable is  $\text{Mn}^{2+}$ , and it is this form that is the most naturally occurring dissolved form of Mn. In the presence of chlorine, bacteria, or dissolved oxygen the soluble  $\text{Mn}^{2+}$  is oxidized and precipitated as  $\text{MnO}_2$  in drinking water, causing a “black water” through home taps (45, 46). The pH medium also plays a role in determining the dominance of each form. For example, at pH less than 5, the soluble form dominates, while at a pH exceeding 5, the insoluble form is more dominant.  $\text{Fe}^{3+}$  is stable in oxygenated water but is usually insoluble forming solid particles. In contrast,  $\text{Fe}^{2+}$  is unstable under the same conditions but is generally soluble (47). The Mn species often occurs

with  $\text{Fe}^{3+}$  when the pH value is larger than 8, above this the stable form of  $\text{MnO}_2$  is found as shown in Equation 1-3.



Mn can also exist in the +3 state; however, this state is very unstable and usually reverts to the +2 state. Mn compounds in +5 states are not very common (48).

#### **1.1.2.1.2 The effect of biofilms on Fe and Mn concentrations in water**

The biofilms which can develop within the water distribution networks are composed of a number of bacteria held in the films. Biofilms are microorganisms that get attached to pipe walls and then multiply to form slime layers. Several definitions for biofilms have been published. USEPA (2002) (49) defines biofilms as a complex mixture of microbes and organic and inorganic material accumulated amidst a microbial-produced organic polymer matrix attached to the pipe wall. Biofilms that have Fe and Mn oxidising bacteria may contain high concentrations of inorganic content such as sediments, scales, and corrosion deposits (36). Trace amounts of some other nutrients are also required for the growth of biofilms, but these have not been investigated (50). As bacteria mainly consume organic carbons, reducing the concentration of this nutrient can limit biofilm growth. Such bacterial species have been identified by Sly *et al.* (51, 52). The bacteria that are released from biofilm in the distribution system are especially considered a major potential risk for drinking water. The bacteria can change Fe and Mn speciation and causes the precipitation of these metals in the distribution system.

The demand of biofilms for oxygen means that they may release, for example,  $\text{Fe}^{2+}$  during periods of extended anoxic conditions (53). Turbulent flow may cause shearing of biofilms from the pipe wall, causing bacteria to enter the water flow. Bacteriological regrowth is an issue of major concern for many water utilities and consumers. By consuming nutrients in the bulk water that bacteria grow in, the biofilms on the pipe are on the surface (10). Biofilms in the water distribution system contain a variety of microorganisms; however, only a few that oxidise Mn and Fe contribute to water discolouration. Such bacterial species have been identified by Sly *et al.* Biofilm detachment has important implications in distribution systems since this transport mechanism allows microorganisms or other chemicals of concern to be introduced into the bulk solution. Five categories of biofilm detachment processes have been identified: erosion, sloughing, human intervention, predator grazing, and abrasion (54, 55).

Chlorine, chlorine dioxide, and ozone are the three main primary disinfectants used by water companies to kill or prevent the growth of microorganisms in drinking water. It has been reported that increasing chlorine levels in the water distribution system reduces biofilm formation (56). Cerrato *et al.* (23) reported an increase in Fe and Mn deposition with the increase in microbial activity. This can affect the quality of water within the distribution systems and cause aesthetic and health problems (57). Biofilms in drinking water are relatively thin ( $10^7$  cells/cm<sup>2</sup>) and may have a more cohesive structure with fewer cells. As a result, it is more resistant to external shearing under turbulent flow conditions (57-60). However, the film can be released by changing the water

flow rates. This is advantageous because the metals that are covalently attached to the biofilm will be sheared away as well (61, 62).

There are a number of factors that may influence the formation and growth of biofilms on the pipe surfaces and these include disinfectant, temperature, water age, pipe material, availability of nutrients, concentration, disinfectant, flow parameters and form/concentration of organic carbon (63).

The microbial activity in distribution systems occurs in water, on pipe surfaces and in deposits which have accumulated in pipes and storage tanks causing water changes. Mn is oxidized to its insoluble form either by bacteria or by residual concentration of chlorine in the network and the insoluble form is deposited on the pipe walls (27). Peng and Korshin (64) discovered that Mn in drinking water was more mobile than chromium, cadmium, and arsenic and the metals are associated with organic fractions. The biofilms and natural organic matter in water distribution systems played an important role in the accumulation of Fe and Mn (64-69) and the observed changes in the water quality.

A recent study by Ginige and Wylie (70), also showed that seasonal influences may affect biofilm production because increases during the summer and autumn were found. This process, together with flow dynamics, may have some influence on increases in discoloured water by releasing Fe and Mn into the bulk flow (10). Particulate accumulations are known to be related to the biological activity (71), and up to 12% of organic matter in particulate accumulations may contain bacterial biomass (21).

Manganese oxidizing in drinking water systems was carried out (62), and this study showed that Mn was reduced by microorganisms even under oxidizing conditions. Accumulation of Mn oxides by microorganisms may lead to significant Mn deposition in natural environments. In pipelines and drinking-water distribution systems, deposition occurs where the build-up increases frictional forces at the surface, so causing a head loss at turbines, reduced flow in distribution systems and Mn-related dirty water (27, 72). Biochemical Mn oxidation and deposition occur in areas of the network where there is insufficient chlorination to control biofilm growth (72). This has the ability to oxidize manganese forms and then cause contamination to taste, odour, corrosion, and colour.

#### **1.1.2.1.3 Physical factors influencing the concentration of Fe and Mn in water**

Many water distribution networks are designed to target liquid velocities of 0.2–0.5 m/s, and in these systems, hydraulic stipulations range from laminar to turbulent flow (73). The parameters that have an impact on Fe and Mn deposition dynamics are grouped into two types: (i) pipe parameters such as pipe material, pipe age, and the pipe cleaning process; (ii) community hydraulic parameters such as the flow velocity, shear stress, diurnal variant and turbo apheresis turbulent transportation of particles from greater turbid areas to less turbid regions (21). Recent research (24) has also indicated that pipe material had a significant influence on deposition dynamics. For example, contrary to the common belief that networks with plastic pipes are less prone to discolouration, recent research indicates that deposits on plastic pipe walls

are loose and subject to sloughing under smaller shear forces compared to iron pipes (24). However, this research only reported on total Fe and Mn concentrations, and did not provide crucial information as to which species of Fe and Mn existed in the different pipes and under what hydraulic conditions. This information is necessary to understand, for example, the presence of insoluble  $Mn^{4+}$  and soluble  $Mn^{2+}$ , which will be crucial for understanding what conditions caused the change of concentration of species. Similarly, the type of pipe cleaning process employed may remove the corroded pipe wall material in the case of iron pipes, which may lead to further corrosion and scaling (74). Crane indicated (75) that shear stress was once the most important cause of sediment conditioning and re-release into pipe networks (74).

#### **1.1.2.1.4 Plastic pipes**

Fe and Mn both deposit in the water distribution system and this leads to clogged pipelines and decreased water pressure, thereby requiring more energy to pump water through the network (76). This problem can increase the cost of the pipe material (21), and many companies have attempted to reduce the discolouration of water by replacing iron pipes with those made from polyvinyl chloride (PVC). Clearly, PVC pipes are not as effective as first considered due to issues of cohesion and hydraulic events. Two types of pipe material have been studied; composite plastic (polyethylene, PE) and copper in a pilot scale water distribution network. They found that biofilms present in copper pipes decreased only at the beginning of the pipeline and chlorine concentration declined more rapidly in copper pipes than in PE. This

demonstrated that copper pipes required a higher chlorine dosage than plastic to achieve effective disinfection of the water.

The replacement has become important for these companies to reduce customer complaints and avoid excessive concentration of Fe and Mn.

Hydraulic and aesthetic effects, including water leaks, increase pumping costs, and corrosion products that can build up in the network iron and steel pipes (77). Fe corrosion forms a layer of Fe(2+), Fe(3+), and mixed (Fe(2+)/(3+)) oxides and oxy-hydroxides (78). Husband and Boxall (21, 79-81) focused on the corrosion of cast iron pipes and the dissolution of Fe through this process. As a result of this research, many cast iron pipes have now been replaced with (PVC) pipes. Currently about 54% of all pipes installed worldwide are plastic pipes, with up to 62% being PVC and approximately 33.5% polyethylene (PE) (82). The pipe material has a significant influence on deposition dynamics. Mn is much more of a problem than Fe, and investigations carried out to assess the potential effects of using PVC pipes indicated that drinking water extracted from them contained three times more soluble Mn, and 35 times more total Mn, than was present in drinking water transported by iron pipes (24).

Information provided according to customer black water problems, caused by insoluble Mn, were more noticeable where PVC pipes were used for distribution in system mains and house plumbing. Conversely where iron pipes were used, fewer complaints were reported in the affected areas (24). PVC pipes are problematic due to the detachment of Mn during flushing and therefore the infrastructure used for supplying water must be chosen with care,

as subtle reactions between water and the different materials (PVC and iron pipes) can affect the ultimate delivery quality (24). However, Husband and Boxall (83) recommended PVC pipes over iron due to the limited bacterial growth compared to iron pipes, in terms of safe drinking water. Research carried out confirmed that properties of synthetic plumbing materials (high-density polyethylene (HDPE) or chlorinated polyvinyl chloride (cPVC) (84) was important. Water quality changes were observed: a weak to moderate intensity of a “waxy/plastic/citrus” odor to the water from the HDPE pipes was found but not the cPVC-contacted water samples.

A large number of investigations have studied microbial Mn-oxidation in drinking water systems, mainly for its association with biological filtration (9, 85-87) ). A small number of studies have investigated microbial reduction and oxidation of Mn in drinking water distribution systems exposed to high levels of chlorine (23, 88). This study demonstrated that even under highly oxidative conditions (high chlorine and oxygen) microbes were capable of both Mn-oxidation and reduction, Mn reduction was assumed to be impossible under such conditions (23).

### **1.1.3 Health effects**

Fe and Mn in drinking water has long been considered to cause only aesthetic issues. In fact, low concentrations of Mn and Fe are known to be essential for human health (89). However, higher levels of Mn cause adverse health effects such as impaired motor skills and cognitive disorders (90). Fe intake allowances reported by the National Academy of sciences are displayed in Table 1-1.

**Table 1-1** Dietary allowances for iron in infants, children, and adults (Institute of Medicine Food and Nutrition Board (93).

<b>Age</b>	<b>Males (mg/day)</b>	<b>Females (mg/day)</b>	<b>Pregnancy (mg/day)</b>	<b>Lactation (mg/day)</b>
<b>7 to 12 months</b>	11	11	N/A	N/A
<b>1 to 3 years</b>	7	7	N/A	N/A
<b>4 to 8 years</b>	10	10	N/A	N/A
<b>9 to 13 years</b>	8	8	N/A	N/A
<b>14 to 18 years</b>	11	15	27	10
<b>19 to 50 years</b>	8	18	27	9
<b>51+ years</b>	8	8	N/A	N/A

Fe is present in the human body and is a dietary requirement for humans and other organisms, 70% of Fe in the human body is found in the blood cells. The body absorbs 25% of all Fe present in food, which may be increased by means of vitamin C tablets for someone who has Fe deficiencies because the vitamin reduces  $\text{Fe}^{3+}$  to  $\text{Fe}^{2+}$  (91).

Fe is an important element in haemoglobin, which binds and transports oxygen from the lungs to other body parts. Fe is also essential for enzymes, normal brain functions and is involved in DNA synthesis  $\text{Fe}^{2+}$  salts are used to treat young children, pregnant women and those who suffer from Fe deficits. In water, if Fe exceeds the permitted level it may cause toxic effects. Average adequate intake Mn concentrations are displayed in Table 1-2 (92).

**Table 1-2** Recommended Dietary Allowances for manganese for Infants, Children, and Adults (Institute of Medicine Food and Nutrition Board (93).

<b>Age</b>	<b>Males (mg/day)</b>	<b>Females (mg/day)</b>	<b>Pregnancy (mg/day)</b>	<b>Lactation (mg/day)</b>
<b>7 to 12 months</b>	0.6	0.6	N/A	N/A
<b>1 to 3 years</b>	1.2	1.2	N/A	N/A
<b>4 to 8 years</b>	1.5	1.5	N/A	N/A
<b>9 to 13 years</b>	1.9	1.6		N/A
<b>14 to 18 years</b>	2.2	1.6	2.0	2.6
<b>19 to 50 years</b>	2.3	1.8	2.0	2.6
<b>51+ years</b>	2.3	1.8	N/A	N/A

In one study, the health effects of high levels of Mn in drinking water were investigated and it was found that this can reduce the intellectual function of children (1). However, many researchers suggest that even low levels of Mn in drinking water may have adverse health effects (2, 93). A study conducted on 142 ten year old children in Bangladesh found that the exposure to Mn in drinking water was positively related to hyperactive classroom behaviours that was noticed in 46 children (93).

Mn has been identified as a potential threat to children’s health due to its associations with a wide range of outcomes including cognitive, behavioural and neuropsychological effects (94). In children’s hair samples, higher Mn concentrations compared to controls have also been linked to learning disabilities (95, 96) . The neurotoxicity of Mn after excessive work-related exposure by inhalation has also been studied (16), and Mn toxicity has caused

neurological symptoms comparable to Parkinson's disorder. This was first mentioned by Coupler (97), and the disorder is characterized by weakness, anorexia, muscle pain, apathy, slow speech, facial expressions, postural difficulties, rigidity, tremors, reduced intellectual status, and slow, disorientated actions of the arms and legs (28, 98). Both animal (99-101) and human (101, 102) records show that certain groups of individuals are predominantly susceptible to Mn intoxication.

Additionally, infants are more susceptible to Mn toxicity because their blood brain barrier is not fully matured (96, 103). In contrast to ingestion, inhalation is far more efficient at delivering Mn to the brain, as evidenced by inhalation being the most common route of exposure for toxic Mn in humans (104, 105).

## **1.2 Elemental regulatory and guidelines**

High concentrations of Fe and Mn in water distribution systems can lead to compliance failures. The Drinking Water Inspectorate (DWI) has set the maximum concentration levels of Fe and Mn in drinking water to 200 and 50 µg/L, respectively. In general, water companies set post-treatment targets of Fe and Mn to within 3% of those levels. They do so to reduce the concentrations of Fe and Mn entering the water distribution system, thereby leading to reduced deposition in the water system. However, irrespective of how effectively water is treated, very low concentrations of Fe and Mn may still enter the network from water treatment plants and gradually accumulate on the inner surface of pipe walls within the water distribution system. During hydraulic events, such as high flows created by bursts in water mains or high diurnal consumption of drinking water, these accumulated particles may be

dislodged from the pipe walls, cause discolouration, and subsequently end up at customers' taps, which cause problems drinking water.

**Table 1-3** Drinking water standards for Mn and Fe by selected organisations.

	<b>USEPA</b>	<b>DWI</b>	<b>WHO</b>
<b>Parameter(mg/L)</b>	Secondary Standard	Based on aesthetic of smell and taste	Health-based value
<b>Fe</b>	0.3	0.2	0.3
<b>Mn</b>	0.05	0.05	0.5

The UK Water Regulations regulate the quality of the quality of drinking water and are adhered to by the regulatory body for the UK water industry, the Drinking Water Inspectorate (DWI). This is a group appointed by the Secretary of State for the Environment, Food and Rural Affairs.

The Inspectorate has a duty to monitor the performance of water undertakers against the various regulations regarding drinking water quality. The reference document used by the DWI has come to be known as the Water Regulations document (106). This is a comprehensive text which includes all aspects of water quality from sampling and analysis to operational matters including procedures for when limits are exceeded. Each water company is visited annually and its compliance with the Water Regulations audited by the DWI. A variety of organisation and agencies has set drinking water standards for Fe and Mn concentrations Table 1-3. The limit of 0.05 mg/L for Mn has been set by the EU. The United States Environmental Protection Agency (US) health (24).

The regulations have not been mandated because Fe is not a direct cause of adverse health effects. However, the EPA has set a limit of 0.3 mg/L or greater for Fe in water treatment plants. Water with less than the concentrations stated in Table 1-3 should not exhibit any of the previously mentioned side effects. Thus if its concentrations are higher than these standards, then water must be treated before using it for drinking. Prof. J.N. Lester has studied the behaviour of heavy metals in waste water during treatment processes. It is apparent that the limitations on heavy metals in discharge from other particles and metals are more stringent in the US than the EU community. Lester's work concluded that the finite availability of unpolluted freshwater will result in greater water re-use and that appropriate standards are required to protect

potable supply, raw water and agricultural land from contamination by heavy metals (107).

### **1.2.1 Fe and Mn toxicity issues**

Fe and Mn are transition metals. It is this cohesive nature that is believed to be significant, as Mn is known to complex readily with Fe in water and to the pipe wall, so allowing Fe levels to increase (108). A very low level of Mn in the treated water entering the water network should greatly reduce the risk of Fe infringements and discoloured water complaints. However, the opposite of this is not always true i.e. higher levels of manganese do not necessarily lead to an increased risk. This can be explained by the fact that there are different oxidation states or species of Mn and that not all of them have an adverse effect on Fe infringement and discolouration rates.

Previous researchers (109-111) have discussed that the exposure of Mn can lead to a strain of Parkinson's disease called manganism, by using brain extracts section 1.1.3  $Fe^{2+}$  was seen to significantly relate to Mn concentration in the brain and showed that the level of  $Fe^{2+}$  was accompanied by higher Mn concentration because of the interaction of the different mechanisms of oxidative stress in the neural tissues.

### **1.3 Drinking water treatment plants**

There are several methods for Fe and Mn treatment in drinking water including oxidation, direct filtration and oxide filter media, sequestration, membrane filtration, and biological treatment. Figure 1-3 shows a schematic of a water treatment plant.

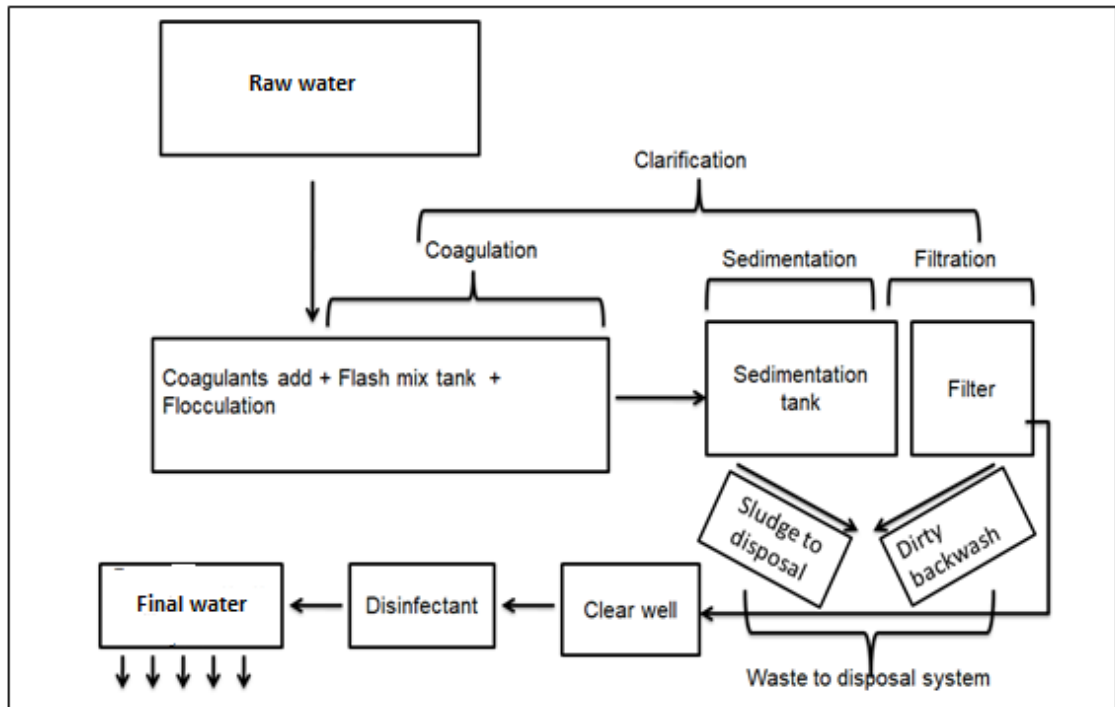


**Figure 1-3** Schematic showing the common steps in water treatment used in drinking water processing plants.

the water source which is raw water and the purification stage on the above diagram is the final water which is clean and go directly to the tap water as drinking water. Including the oxidation treatment process where the soluble Fe and Mn is oxidized prior to the addition of chemicals that lead the heavy particles to settle to the bottom of the water and then be removed. The oxidation process may be accomplished by different oxidation agents such as potassium permanganate, oxygen, chlorine, ozone, aeration, and chlorine dioxide (112).

Once soluble, Fe and Mn are oxidized into a particle form, they may be settled from solution. However, the settling velocity may be very slow, so to increase this settling velocity, coagulation agents are added to convert them into larger flocs that settle out more rapidly.

The water from the source is pumped and mixed with a coagulation reagent and salt such as aluminium sulphate or iron sulphate, or synthetic polymer is added during the mixing stage to attract any suspended particles. The selection of a suitable coagulation agent depends on each water company's regulations. The amount of the coagulants needed depends on the level of contaminating chemical compounds and solid present in the raw water. The water is then stirred to allow the particles to come together and form large particles (flocculation), which can then be removed by sedimentation and filtration.

Air can be used as a pre-oxidant for Fe, but for Mn, insufficient oxidation takes place. If Fe alone is present, aeration followed by filtration will be the best treatment without the need for permanganate or chlorine bleach. All these treatment technologies for Fe and Mn depend on raw water concentration levels and whether the minerals are dissolved. Finally, the purified water is pumped into the distribution system (21). Inadequate treatment of Mn at the water treatment plant can cause soluble Mn to enter the water distribution system where it is oxidized to an insoluble form either by chlorine or bacteria producing oxidized solids on the pipe surface (113).

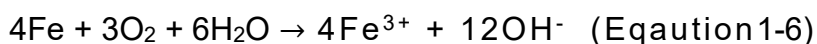
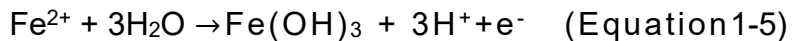
One goal of the water treatment process in drinking water was to minimize Fe uptake from the distribution system because of the corrosion of Fe and steel pipes (78). The application of filtration techniques has been used to remove Fe and Mn from drinking water after precipitation (Figure 1-3). Ultrafiltration membranes have been used to attempt to eliminate Fe and Mn by using small pore filtration, but this is not viable on a large water processing scale (114). It has been observed that Fe pipe material impacted on Mn deposition within the

drinking water distribution network, which resulted in discoloured water problems because of soluble Mn in the water surface (24, 115-117).

The source of Fe in drinking water is either from ferrous pipes in the distribution system or from the water supply after treatment (118, 119). The Fe (III) and Fe (II) ions present in river water precipitate as iron oxide and iron hydroxides such as goethite ( $\alpha$ -FeOOH), magnetite ( $\text{Fe}_3\text{O}_4$ ) and hematite ( $\alpha$ - $\text{Fe}_2\text{O}_3$ ). Iron can also adhere to the walls of drinking water pipes and is the most common reason for coloured water formation (120, 121). The oxidation process of  $\text{Fe}^{2+}$  to  $\text{Fe}^{3+}$  can be described as follows:



The full oxidation reduction-reaction equation for Fe is as follows:



In the next section accurate and reliable analytical methods that are needed to determine Fe and Mn in drinking water samples, such as the various ICP methods are discussed.

## **1.4 Inductively coupled plasma (ICP) for metal analysis**

In the field of environmental analysis, inductively coupled plasma optical emission spectrometry (ICP-OES) and inductively coupled plasma mass spectrometry (ICP-MS) have become the multi-element method of choice for low-level elemental determinations (122). In 1983 ICP-MS became commercially available, resulting in significantly lower limits of detection (123),

and the capability of the ICP-MS to analyse concentration down to ng/mL is very attractive in elemental analysis. The ICP is widely used as an ionization source in mass spectrometry (MS) and in optical emission spectrometry (OES). These techniques are broadly applied in analysis of a wide range of samples in several fields (25, 124).

### **1.4.1 Inductively coupled plasma (ICP)**

Inductively Coupled Plasma (ICP) is an analytical technique used for trace metal determination and was first employed in the early 1960s. ICP is self-sustained, since the ionization and collision mechanism is continuous because of several unique advantages including essential plasma characteristics leading to high electron density and temperature, high excitation and ionization capability, and high gas temperature. The ICP source allows the atomization and excitation of almost all elements. The plasma is an ionic gaseous mixture which occurs inside the torch containing cations and electrons.

ICP is characterized by a very high temperature of around 8000 to 10000K, which gives it the capability to efficiently desolvate, vaporize, excite and ionise atoms. This requires the elements to be analyzed in solution and aqueous solutions are preferred over organic solutions because the latter require special manipulation prior to injection in the ICP source. The advantages of ICP compared to AAS are greater precision, speed, and sensitivity. The high temperature results in the presence of no or few molecular species, and the relatively long residence time causes few ionization interferences (125, 126).

The sample is introduced into the system by the spray chamber and is carried by the Ar gas into the torch Figure 1-4. The torch plays a different role in ICP-OES than it does in ICP-MS.

Ar flows inside the concentric channels of the ICP torch to generate the plasma where the sample is nebulized and entrained (127). The torch consists of three concentric tubes with a 3 mm outer diameter within a copper induction coil of a radio frequency generator. The power is supplied to the load coil which surrounds the torch, transmitting a 40 or 27 MHz radio frequency (RF) field.

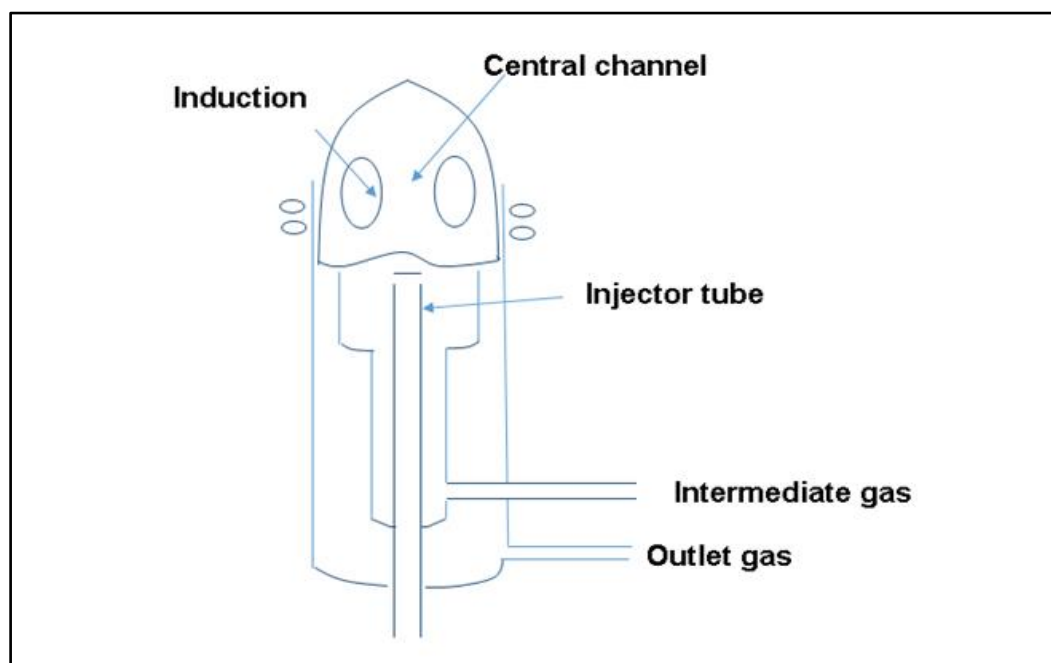


**Figure 1-4** Schematic of an ICP torch, adapted from Boss, 1977 (129).

An intensive magnetic field around the coil is developed and spark from a tesla coil is used to produce electrons and ions in this region. The oscillating RF field causes electrons injected from a tesla coil to oscillate and gain energy. This induced current flowing in a closed circular path, results in heating of the Ar gas, and ions are produced. The high temperatures necessitate cooling, which is applied using Ar to the outer tubes, the sample, preferably as an

aqueous solution, is introduced to the ICP via a nebulizer. This converts the solution into an aerosol, which is introduced through the inner tube. The light emitted by the atoms and ions of a metal in the plasma is converted to an electrical signal and is most frequently quantitatively measured (this is for ICP-OES, for ICP-MS ratio is measured).

In the ICP-MS, the plasma torch is positioned horizontally, and is used to generate positively charged ions. In the ICP-OES, the plasma, usually oriented vertically, is used to generate photons of light by the excitation of electrons of a ground state to a higher energy level of each atom. These electrons transfer back to the ground state, wavelength specific photons are emitted that are characteristics of the element of interest. Photomultiplier tubes are used to measure the light intensity at specific wavelengths for each element line. This intensity is compared to previous intensities of known concentrations of the element.

### **1.4.2 ICP advantages and disadvantages**

The ability of the ICP to identify and quantify all the elements with the exception of Ar is a major advantage over atomisation methods at lower temperatures. Also, ICP is suitable for all concentrations from ultra-trace levels to major components; the detection limits for most elements are very low. Another advantage of employing ICP is the capability of multi-element analysis and quite rapidly in a period as short as 30 seconds with low consumption of 0.5 ml of sample. However, ICP has difficulty handling halogens; specific optics for the transmission of the very short wavelengths become necessary.

### 1.4.3 Inductively coupled plasma optical emission spectrometry (ICP-OES)

ICP-OES is one of the most popular analytical techniques for the determination of trace metals in different samples. ICP-OES is based on the measurement of the light emitted by elements and ions in the sample, where the measured emission intensities are then compared to the intensities of known concentration to obtain the concentration in the unknown sample Figure 1-5.

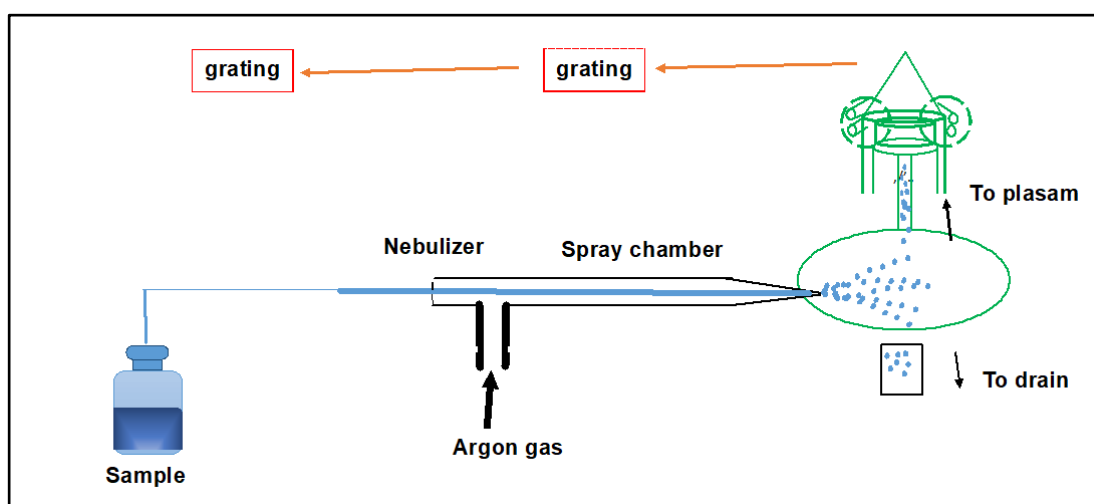


**Figure 1-5** Diagram of sample introduction to ICP-OES, adapted from (M. Hieftije 1989) (130).

The light emitted from ICP in the ICP-OES can be viewed radially which results in the highest upper linear ranges. Alternatively, it can be viewed axially, in which the background from the ICP is reduced and the sample path is maximised, thus providing better detection limits than the radial viewing by as much as a factor of 10. Most systems allow the plasma to use both views in a single analysis to provide the best detection and wide working ranges.

The ICP-OES has a spectrometer that separates the individual wavelengths of the light and focuses the other wavelengths onto the detector such as

photomultiplier or charge coupled devices (CCDs) which both convert photons to electric current. CCD is a highly sensitive photon detector which has a surface divided up into a large number of light sensitive small area (pixels), which can be used to build up an image of the scene of interest. The intensity is related to different color in the colours spectrum for each wavelength. After the atoms or ions are excited by the absorption of energy, they decay back to a lower energy, and a more stable state, by emitting a light of specific wavelength as shown in Figure1-6 (128).

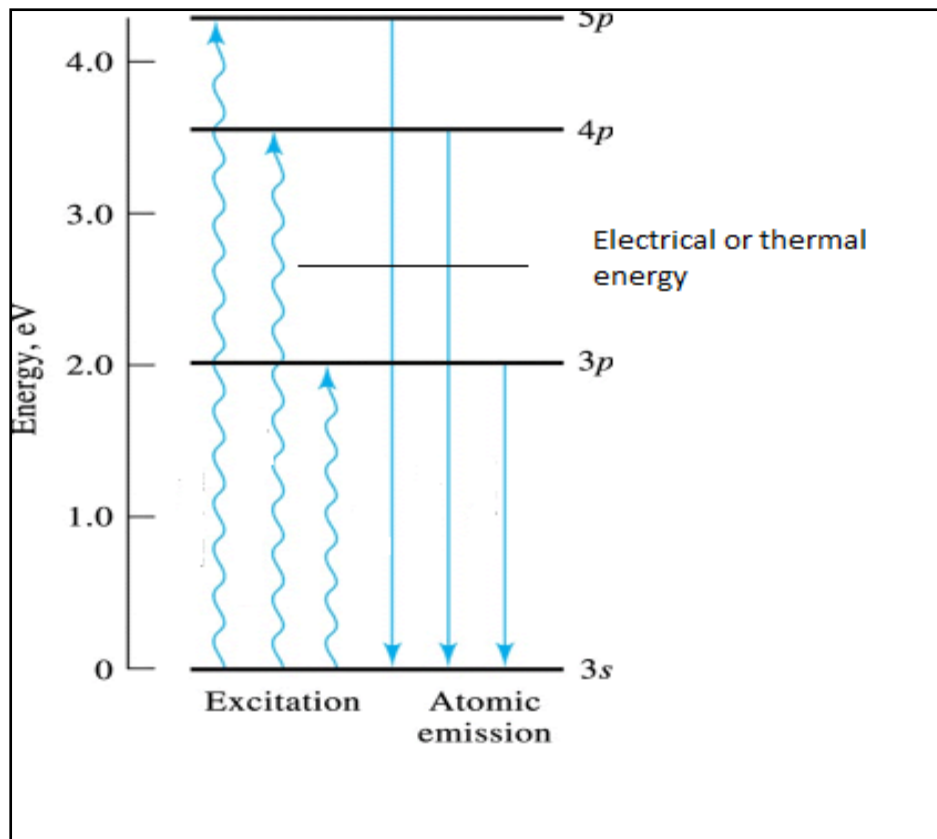


**Figure 1-6** Excited atom energy level adapted from (Charles B. Boss, 1997) (132).

The ICP-OES instrument allows the simultaneous analysis of about 60 elements. When the light intensity is calibrated against standards, the technique provides a quantitative analysis of the original sample (129, 130).

### 1.4.3.1 ICP-OES Interference

The interferences encountered using ICP-OES for multi-element analysis are spectral, physical and/or chemical in nature. The matrix effects can be divided into three types of interference.

**Chemical interference:** This type occurs when a compound is formed, which prevents the quantitative atomization of the element. In ICP-OES this type does not play a major effect because of the high temperature conditions in the plasma.

**Ionization interference:** This interference affects sensitivity and depends on the following factors: temperature, ionization potential, and concentration of the analyzed element.

Ionization interferences show a change in emission intensity by causing a shift in the Ar ionization. This is caused by easily ionizable elements such as alkali metals including K, Na, Cs, and Rb, which result in the greater intensity of the neutral lines to reduce the intensity of ionic lines because the changes of the emission intensity caused the ionization of equilibrium to shift. The ICP instruments have the capability to avoid these interferences by choosing different emission lines because modern instruments use simultaneous measurements of the analytes at the same time.

**Physical interference:** This occurs when the changes in the sample solution content cause changes in the nebulization rate due to the change of viscosity, matrix and density of the solution. These interferences can change the size of the droplets, which then have an influence on the sensitivity of the measurement. This type of interference can be overcome by matching of the sample's and standard's matrix and by the use of a suitable internal standard.

An internal standard usually consists of the addition of a known concentration of an element that is not present or is undetectable in the sample. It is added to all standard solutions and samples at the same concentration. If a rise or fall in the signal obtained for the internal standard is detected the final determination can be adjusted in accordance with the change in signal. Selection of the correct internal standard is important, as it must model the chemical behaviour of the analyte and be in the mass range of the analyte

#### **1.4.3.1.1 Spectral interferences**

This interference is one of the biggest problems of ICP-OES and is difficult to correct. The high temperatures produce emission from a wide range of elements with a higher risk of interference. These interferences alter the analyte's signals, and thus negative or positive signals result which affect the accuracy and precision of the method. Figure 1-7 A to D shows the different spectral interferences (131). Examples of spectral interferences are:

**Direct spectral overlap:** This occurs when two elements emit light at the same wavelength.

**Background shift:** This interference is visible on the smoothed subarray display and is identified by the distortion of the lines. The use of two background points to extend the width of the subarray helps to alleviate the problem(132).

**Wing spectral overlap:** This occurs when the high temperature of the plasma causes Doppler broadening of the spectral lines which leads to wing overlap where another analyte contributes to the signal of the others, but the peaks for

both analyte are separated. Also, the presence of an interfering element in very high concentration in the sample can cause wing overlap (133, 134).

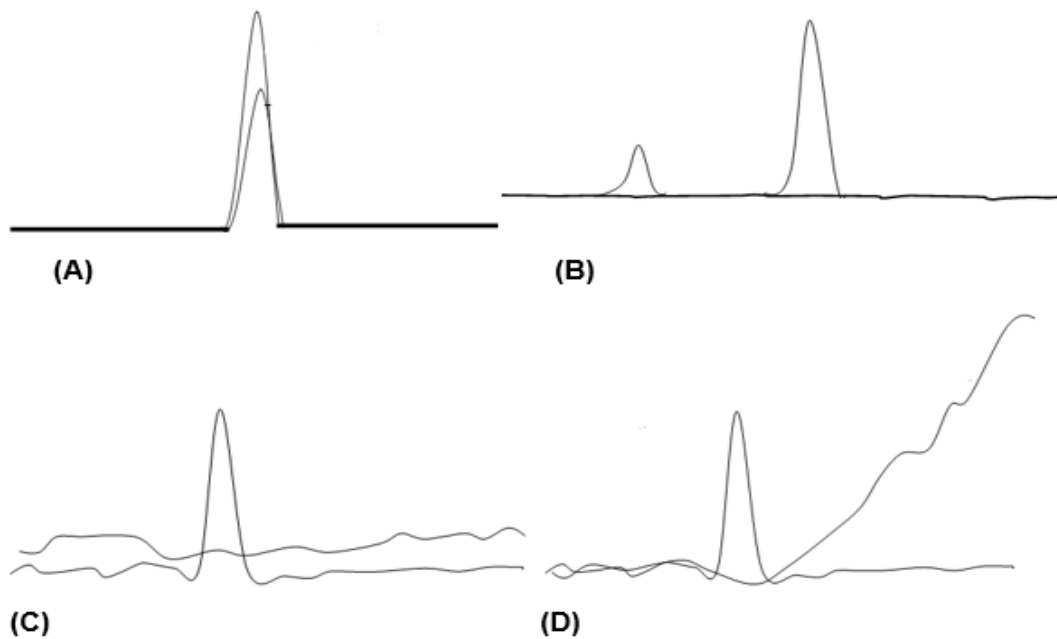


**Figure 1-7** (A) Direct spectral overlap, (B) No overlapping, (C) Simple background shift, and (D) Wing overlapping interference shift.

#### **1.4.4 Inductively coupled plasma mass spectrometry (ICP-MS)**

This instrument was developed in the late 1980s (135) to offer high sensitivity for the determination of a wide range of elements, the sample is introduced in the same way as in ICP-OES. It provides quick analysis, and low detection limits. This development has increased the use of a number of isotopes that are available for routine analysis and the number of applications as a routine technique (136).

The major reason for this instrument's unparalleled growth is its ability to carry out rapid multi-element determinations at the ultra-trace level ng/L. Even though it can be used to determine the same elements as other atomic spectroscopic techniques such as (GFAA) graphite furnace atomic absorption, (flame atomic absorption (FAA), and ICP-OES, ICP-MS has the advantages of multi-element characteristics, detection limits, isotopic capabilities, and speed of analysis. ICP-MS is able to extract the sample ions from the ion source because the plasma is analyzed with these ions in a high vacuum in the detector. The ICP-MS combines a high temperature ICP source with a mass spectrometer, the atoms are converted into the ions. These ions are then separated and detected by the mass spectrometer.

##### **1.4.4.1 Sample introduction**

Typically, the sample is introduced into the ICP plasma as an aerosol. Therefore, the samples must be introduced to the nebulizer in either liquid or as a dissolved solid sample. This liquid sample is pumped from a vial, via a peristaltic pump, through the spray chamber into the nebulizer that creates an

aerosol of fine droplets (the larger droplets going down to the drain). The small droplets enter the torch then the plasma generated in the ICP torch by passing Ar gas through the ICP tubes. The liquid droplets containing the sample matrix and the elements to be determined and through the high temperature undergo atomization. These atoms continue their travel through the plasma, they absorb more energy until they release an electron, becoming ionised. The ions formed by the ICP are typically positive ions,  $M^{1+}$  or  $M^{2+}$ . Once the ions are formed they travel out of the torch and come to the interface.

#### **1.4.4.2 The ICP-MS sampling interface**

Figure 1-8 illustrates a typical sampling interface used to extract ions from the ICP into the MS. The interface system consists of a sampling cone and skimmer cone; ion lenses; a quadrupole mass spectrometer and detector. The ions produced by the ICP are introduced to the MS through the orifice cones (sampler and skimmer cones are metal disks with hole about 1mm diameter).

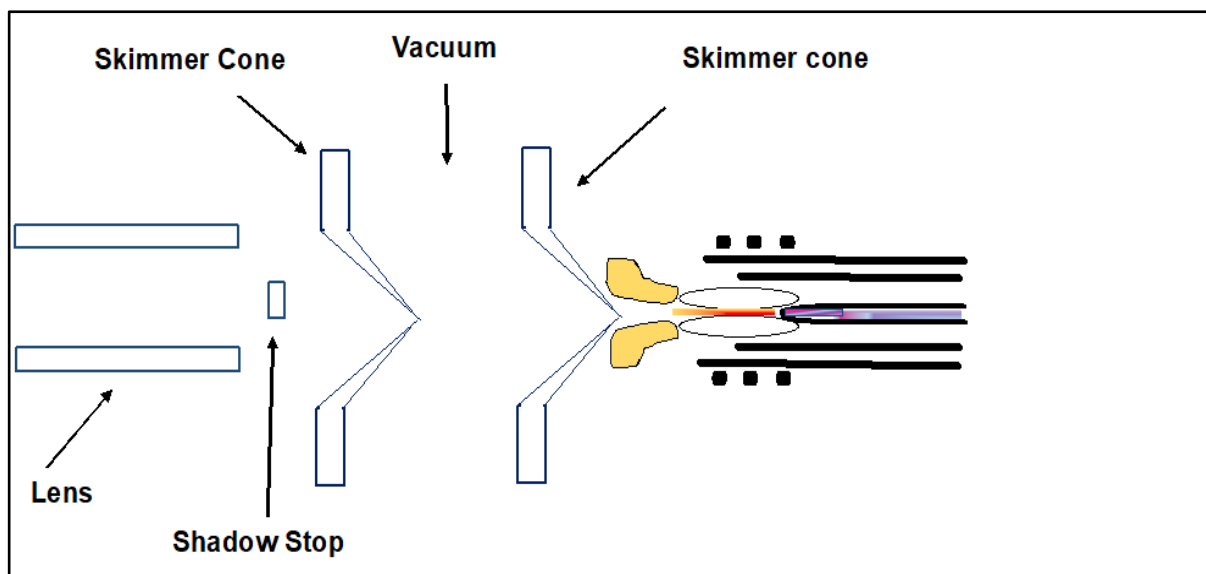


**Figure 1-8** The interface region of an ICP-MS adopted from PerkinElmer 2001 (137).

The interface can be described as a portion of the instrument that serves to allow the ICP and MS to be coupled at the point in which the sample from the ICP portion is introduced to the MS. The ions travel in the Ar stream at atmospheric pressure (1-2 torr) into the low pressure of the MS ( $< 1 \times 10^{-5}$  torr). This transmission takes place through the intermediate vacuum region created by the interface cones. The purpose of these cones is to sample the centre portion of the ion beam coming from the ICP torch. These cones are often produced from nickel or platinum where they later provide longer life and are more resistant to some acids, while nickel cones have a lower purchase price. The ions from the ICP source are then focused by the lenses in the system. These lenses are an essential part because of their function of separating the ions from the photons and residual neutral material. Different types of ICP-MS systems have different types of lens systems. The ions pass through a charged metallic cylinder, which keeps the ion beam from diverging. The ion optic separates electrons from analyte ions, resulting in a positive ion beam

as they pass through the vacuum system to the final chamber containing the MS and detector. Once these ions enter the MS analyzer chamber, they are separated by their mass-to-charge ratios  $m/z$  (Dalton) to create the mass spectrum.

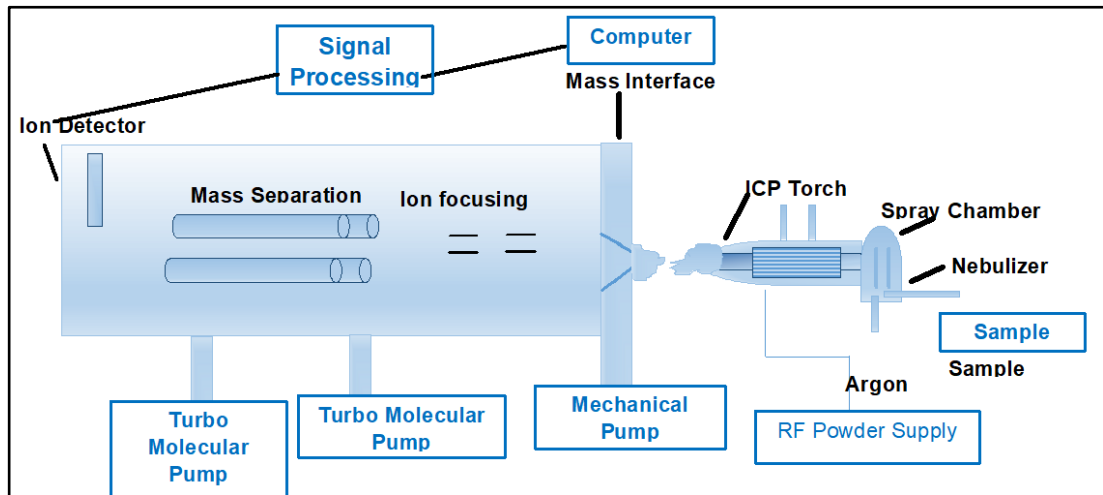


**Figure 1-9** Schematic diagram for the basic components of an ICP-MS system adapted from R. Thomas (140).

### 1.4.4.3 ICP-MS mass analyser

There are different types of mass analysers that have been used on ICP-MS; these are quadrupole, time-of-flight, and magnetic sector analysers (138). The quadrupole mass spectrometer by far is the most common type of analyzer used in ICP-MS due to its ease of use, mass range, robustness, and high scanning speed and relatively low cost. A quadrupole is a mass filter of four parallel cylinder rods serving as electrodes, which uses a combination of electrical fields of direct current (DC) and alternating current (AC) to separate ions based on their  $m/z$  values. Ions that are not of the correct  $m/z$  collide with the rods or exit the path between the rods and are rejected and then pumped out of the system.

The quadrupole ICP-MS is becoming the workhorse of trace metal analysis and is very reliable, even with unattended operation overnight. In addition, it can scan the mass spectrum from 3-250 amu in just a few seconds because of its speed which depends on the instrument settings. ICP-MS with quadrupole analyser is considered a routine, high-throughput, mature analytical tool. Furthermore, it has high sensitivity, being able to detect many metals at trace levels well below part per trillion (ppt) or ng/mL. It still has disadvantages in comparison with the high-resolution mass spectrometers such as the sector mass spectrometer. For example, strong backgrounds are linked to the sample ions being at much higher atmospheric pressure in the Ar stream, but then travelling into the low pressure high vacuum region of the spectrometer, at approximately  $1 \times 10^{-5}$  torr.

#### 1.4.4.3.1 Quadrupole mass filter

There are the two main tasks of the mass filter: the separation of ions according to their mass-to-charge ratio, and to measure the relative abundance of ions at each mass. This effectively separates each element present according to its mass as the charge is normally a single positive charge. Different elements have different masses and can be separated accordingly. The quadrupole mass filter is the most common choice of mass sorter for ICP-MS. Its main advantages are that it exhibits high sensitivity and can cope with large volumes of solvent. The use of a quadrupole mass analyser also has the advantage of less tendency to drift than magnetic sector instruments but has lower resolution. For example, certain polyatomic and isobaric interference's such as  $\text{ArO}^+$  on  $^{56}\text{Fe}^+$  cannot be resolved. Polyatomic and isobaric interferences can be resolved in specialised high-resolution double focussing or magnetic sector instruments. However, instruments are expensive in comparison to quadrupole instruments and this has limited their use.

The quadrupole mass filter is established so that only single  $m/z$  ratios pass through to the detector, the mass analyser can move to any  $m/z$  for any element of interest. For example, to measure sodium, which has a single isotope at mass 23, the spectrometer can be set to allow ions with  $m/z = 23/1$  to pass. This is why under the control of the instrumental software all elements can be analysed, even though only one mass passes through the analyser at a time sequentially to the electron multiplier (EM) detector. This is also the reason ICP-MS can determine so many different elements quickly, jumping between each measured mass to reduce measurement time. Since different

isotopes of the same element have different masses, ICP-MS can supply isotopic information.

The quadrupole mass analyser consists of four parallel rods arranged symmetrically. Opposite rods are connected, and parallel rods are supplied with a direct current (DC) voltage; one pair being held at the positive voltage and the other set at the negative voltage. The quadrupole ions of a certain mass will undergo stable oscillation, while others collide with the rods, as shown in Figure 1-10.

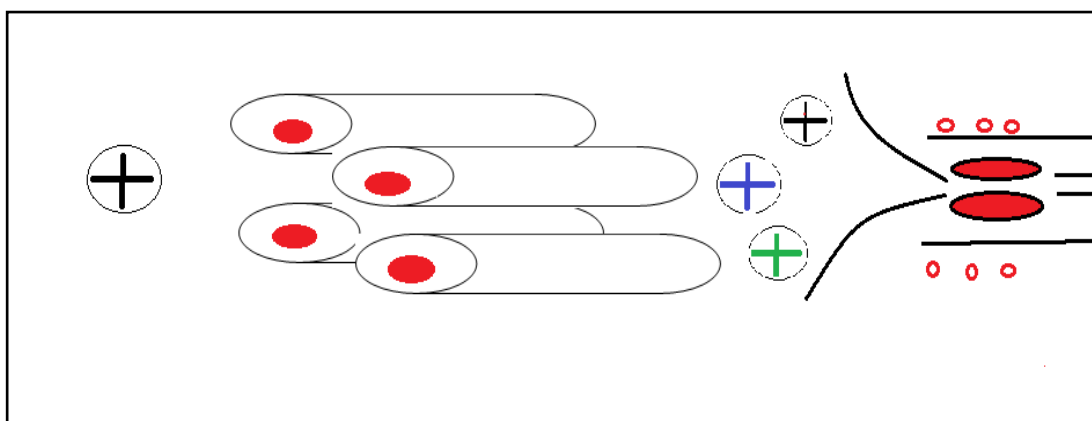


**Figure 1-10** Schematic of the quadrupole mass filter adapted from PerkinElmer (137).

The scanning process is repeated for another analyte at a completely different  $m/z$  until all the analytes in a multi-element analysis have been detected. Although quadrupole scan rates are typically in the order of 2500 atomic mass units (amu) per second and can cover the entire mass range of 0-300 amu in about 0.1 s, real-world analysis speeds are much slower than this, and in practice 25 elements can be determined in duplicate with good precision in 1-2 minutes (139).

#### **1.4.4.3.2 Ion detection on the detector**

In the final process, the ions exit the mass analyzer and enter the detector, where they strike the active surface of the detector and generate a measurable electronic signal. The detector converts the ions into electrical signal. The active surface on the detector is known as a dynode (a discrete dynode contains a series of metal dynodes along the detector) which is the most-common design used today. The dynode type detector can also be run in two modes, pulse-counting and analogue, which further extends the instrument's linear range and can be used to protect the detector from excessively high signals.

The released electrons are repelled from the high negative voltage at the front and strike the next dynode, electron multiplication takes place, amplifying the signal. This step is the basic principle of an electron multiplier, which detects all the ions as they exit from the quadrupole. By the time these electrons reach the final dynode, multiplication continues until a measurable pulse is created as an ion count. The detector creates the mass spectrum and provides a simple and accurate qualitative measurement of the sample. This electronic signal is then processed by the data handling system in the conventional way and converted into analyte concentration using ICP-MS calibration standards. The most important specifications of the detector performance in an ICP-MS system are high sensitivity, wide dynamic range and low random background (which is affected by the design of the plasma generator and ion lens configuration), as well as the analyser vacuum and the quality of the detector electronics.

#### **1.4.4.4 ICP-MS interferences**

The interferences in ICP-MS can be categorized into two main types: non spectral and spectral interferences (140).

##### **1.4.4.4.1 Non-spectral interference**

This is characterised by the suppression or enhancement in an analyte signal due to matrix-induced changes in sample transport efficiency; ionisation in the plasma, extraction; and transfer of ions in the mass analyser region. Furthermore, the nature and concentration of the sample matrix can have a direct effect on this, which is also known as “matrix effects”. The sample matrix effects depend on the analyte, as well as physical properties of the sample; matrix composition; and instrumental conditions. Internal standardization is routinely used in almost all ICP-MS applications because it is not only a remedy for matrix effects, but it also compensates for instrumental drifts (140, 141). This type of interference can often be reduced by diluting the sample properly.

Internal standards have been frequently used to overcome interference effects (142-144). The use of internal standards can reduce errors due to instrumental drift and some non-spectral interferences. Internal standards can also reduce dilution errors if added before sample dilution. The internal standard must also ionise to a similar extent as the sample and must be of a similar concentration. Two commonly used internal standards are indium and rhodium.

An ideal internal standard would model the behaviour of the analyte exactly. The closest we can get to this ideal internal standard is to use another isotope of the analyte as the internal standard. This is known as isotope dilution. When

this technique is used there is the possibility to account for secondary charging, refractory oxide formation and matrix suppression and enhancements. However, polyatomic and isobaric interferences cannot be accounted for using this technique. The use of isotope dilution analysis has been reported with improved precision and accuracy (145). Laser ablation ICP-MS has also been reported to use isotope dilution to overcome matrix effects. This technique enables the vaporisation of specific elements to be internally standardised more closely. In this technique, it is important that the internal standard is ablated at the same rate as the analyte.

#### **1.4.4.4.2 Spectral interferences**

##### **A) Polyatomic interference or molecular spectral interference:**

Polyatomic interference is the most significant interference concerning ICP-MS, which is produced by the combination of two or more atoms having the same mass-to-charge ratio as the analyte. It is usually associated with the plasma and nebulizer gas, and the components of solvent and samples. They are caused by the generation of other ions which are polyatomic, and are not the isotope of interest, but have the same  $m/z$  (138).

For example, in the case of  $^{56}\text{Fe}$ , Ar heated to plasma in the torch and oxygen leakage into the instrument from the air, as well as from elements from the cones and glassware, react to form the  $^{40}\text{Ar}^{16}\text{O}^+$  ion and  $^{40}\text{Ca}^{16}\text{O}^{56}\text{Fe}$ . This provides a large background signal compared to the  $^{56}\text{Fe}$ . Ar can also form polyatomic interferences with any element found in the acids used for the sample preparation. For example, using hydrochloric acid allows the formation

of  $^{40}\text{Ar}^{35}\text{Cl}$  due to the combination of the most abundant chlorine isotope  $^{35}\text{Cl}$  with  $^{40}\text{Ar}$  and this interferes with the only arsenic isotope  $^{75}\text{As}$ .

## **B) Hydroxides, oxides, and doubly charged species**

This type of spectral interference is produced by elements in the sample, water or air. This occurs at mass 1, 16 and 17 as  $^1\text{H}$ ,  $^{16}\text{O}$ , or  $^{16}\text{O}^1\text{H}$  form a molecular hydride, oxide, and hydroxide.

With doubly charged ions resulting from ions created by the loss of two electrons instead of just one, because the quadrupole separates ions based on  $m/z$ , a doubly charged ion ( $\text{M}^{2+}$ ) will appear at mass  $m/2$ . An example of this interference is  $^{36}\text{Ba}^{2+}$  overlap on  $^{68}\text{Zn}^+$ .

## **C) Isobaric interference**

This type of interference is produced by different isotopes of the elements in the sample having the same mass-to-charge ratio as the analyte. e.g.  $^{204}\text{Pb}$  and  $^{204}\text{Hg}$  (146);  $^{114}\text{Sn}$  and  $^{114}\text{Cd}$ . There are several ways to remove or correct all these spectral interferences. The easiest way is to choose another isotope (interference free) of the element of interest to avoid a direct isobaric overlap. For example, the resolution of the isobaric overlapping of  $^{114}\text{Sn}$  overlap on  $^{114}\text{Cd}$  can be carried out by using  $^{111}\text{Cd}$  which has no isobaric overlap. However, the detection limit will be lower because of the low abundance of this isotope (12.80%) whereas  $^{114}\text{Cd}$  is (28.73%).

The other type of interference such as mono and doubly charged species can be reduced through the proper tuning of the plasma and torch conditions. It has been demonstrated that the mono-charged  $\text{MO}^+$  level is proportional to

other matrix-based interferences especially those using chloride and sulfate matrices. The CeO ratio is referred to as a measure of plasma robustness in ICP-MS (at lower CeO/Ce level) and this makes the other removal interference techniques more efficient such as collision reaction cells.

Another solution is the use of high-resolution mass analyses. Collision/reaction cells have been developed to allow the spectral interferences to be removed before they reach the spectrometer (147) and different types of cells are used (quadrupole and hexpole, and octopole). The ions enter the interface in the normal way, where they are extracted into an off-axis, collision/ reaction cell under vacuum. He or H<sub>2</sub> is used as the gas blend in the cells operated using radio frequency (Rf) power only. This power field focuses the ions but does not separate the masses like the normal quadrupole which then react with molecules of the collision/reaction cells gas. Also, Rf power can be used to systematically bring back ions to the center of the rods, even if they were deflected by a collision. The gas interacts with the ion beam to remove polyatomic interferences in different ways. In collision mode, the gas collides with the polyatomic interference causing it to lose energy. These polyatomic interferences are large, and they undergo more collision than the analytes which lose more energy. The lower energy interference isotope is then separated from the higher energy one by kinetic energy discrimination (KED). The other mode is reaction mode where the gas reacts with an interference to convert it to a different species.

## **1.5 Fe and Mn analysis and elemental speciation**

This part discusses the elemental speciation and a comprehensive review that shows the analytical methods used for the determination of Fe and Mn species. In this chapter, the Fe and Mn speciation that lead to the increase in discolouration and customer complaints are discussed along with the HPLC-ICP-MS work that was developed for this purpose. Finally, a summary of the aims and objectives of this project is given.

### **1.5.1 Elemental speciation**

Chemical speciation of the elements is defined as the specific form of an element such as the concentration, isotopic composition, and oxidation state of each of the chemical forms of an element present in a sample. Most studies to date have looked at the total concentration of these elements or sequential extraction methods, which determine the total element rather than individual species. Currently, there are few research studies that focus on the speciation of Fe and Mn in drinking water distribution systems.

Element speciation is gaining more interest recently, because the species may differ in their biological activity, bioavailability and toxicity, and evaluation of bio-availability, aids in identification of Mn species involved in transportation across the blood-brain barrier (148-150). Element speciation also provides greater knowledge of what environmental conditions have created this species, which may lead to a solution as to how to deal with it.

### 1.5.2 Analytical techniques used for elements speciation

Many different techniques have been applied for elemental speciation in environmental samples. These include atomic absorption spectrometry (AAS), spectrophotometry, neutron activation analysis (NAA), ICP-OES and ICP-MS (151, 152).

An early example of Mn speciation was carried out using gel filtration chromatography (153). In order to select the appropriate treatment, Mn speciation provided essential information for the regulatory authorities. Also understanding of the treatment process involved in the water contamination by Mn revealed the usefulness of the speciation of this element, and this can reduce the environment effect on the organic matter (154). Recent work has been published on the application of cloud-point extraction to allow the use of flame atomic absorption spectroscopy (FAAS). This work required the pre-concentration of Mn to allow its detection by FAAS. The limits of detection (LoD) obtained for Mn was 0.28 ng/mL and it was achieved through the extraction of an insoluble complex (152, 155). FAAS is a simple and sensitive method of detection and a study was described for the separation of Mn<sup>2+</sup> and Mn<sup>4+</sup> in environmental water samples. However, there was a problem reported in this study in relation to its application to real water samples. For example, Mn<sup>2+</sup> concentration was determined via oxidation to Mn<sup>7+</sup> and was followed by determination of the total Mn concentration and a subtraction technique used to obtain the species (156).

De Munari *et al.*, represented in his paper that the addition of the metal has implications for Fe and Mn displacement to pore water. The literature

described physical separation techniques, which allowed the separation of soluble and insoluble forms of the elements to be identified, these techniques used ultrafiltration (157). Studies of the analysis of drinking water were highlighted because of the importance of the connection between speciation and pollution by Fe and Mn. A decrease of dissolved oxygen in the groundwater was one condition that caused  $Mn^{4+}$  reduction both chemically and bacterially to the  $Mn^{2+}$  soluble form (158).

Another technique that was applied to Mn speciation was electrochemical stripping analysis which is one of the most sensitive analytical methods available with a detection limit of sub ng/mL (159). In 1984 anodic stripping voltammetry (ASV) was applied to the analysis of water samples from rivers and streams(160). In diluted water at different pH values, differential pulse anodic stripping voltammetry (DPASV) was used to investigate Mn species (161). In order to fully evaluate the species, several Mn speciation methods were combined including square wave voltammetry and cyclic voltammetry along with ASV and DPASV (16, 162, 163). However, these methods suffer from interference and limit their ability to speciate Mn (164).

Despite the advantages of these techniques, including low cost, sensitivity and the separation, many problems arise with real samples using electrochemical methods (165, 166). ASV suffers from low solubility of Mn in mercury, and so in the mercury electrode used in ASV under negative potentials  $Mn^{2+}$  is directly reduced. The development of different techniques for Mn speciation has involved the combination of analytical methods (e.g. chromatographic, electrochemical and elemental analysis methods) (167). The hyphenated

techniques such as chromatographic separation with specific detection of ICP-MS are a powerful tool for elemental speciation (6, 120).

The previous studies prove that Mn and Fe exist in certain forms in water, but they have never been identified using chromatographic methods. There is a lack of research that focuses on speciation of both Fe and Mn in drinking water distribution systems, and which focuses on the water sampling source for customer use.

One of the important techniques that has been used in the extraction of trace metals from water is Solid Phase Extraction (SPE) which is based upon ion exchange. SPE and ICP-OES were used together as a flow injection analysis method for Mn speciation in milk (27). The species of Mn were analysed as cationic, neutral and anionic species and there were no specific interferences reported. Many studies have used different chelating agents for Mn extraction (26).

### **1.5.3 Analytical methods for Fe and Mn determination**

The analytical techniques used for the analysis of inorganic Fe and Mn in water may measure concentration directly or, if the concentration is too low, pre-concentration steps may be necessary. In all cases, the adsorption and precipitation of Mn to the walls of the sample container may occur and for this reason acid is added to prevent these problems.

The main techniques that have been used for the determination of total Fe and Mn, such as spectrophotometry, neutron activation analysis (NAA), polarography, AAS and ICP-OES, ICP-MS, provide high selectivity, good repeatability, low detection limits and accuracy (16). Pre-concentration and

separation techniques are often necessary for the determination of trace and complex matrices of Fe and Mn in biological and environmental samples. The multi-elemental techniques have been widely used to detect more than one analyte, including liquid-liquid extraction, precipitation and solid phase extraction. Also, chromatography techniques have been used for speciation analysis when it connects with other techniques (168).

The online coupling of chromatographic techniques (HPLC, SAX-HPLC, SEC-HPLC, GC) or electrophoresis systems (CE, CZE) with selective detectors (ICP-MS, ICP-OES) are the most popular techniques to identify Fe and Mn species. In this technique, no additional sample pre-concentration is required when the ICP instrumentation is used for water analysis because of the ability to handle complex sample matrices.

### **1.5.3.1 Mn speciation**

The limit of detection of 280 ng/L Mn has been achieved using FAAS with cloud point (CPE) for separation and pre-concentration of Mn (16, 168). In addition, CPE also has been applied for the pre-concentration of  $Mn^{2+}$  prior to detection by GFAAS and the LoDs were 20 ng/L of  $Mn^{2+}$ . In a separate study, 400 ng/L for Fe has been detected, while the concentrations of Mn was above the maximum level (169).

In a study using pre-concentration and acid digestion with ICP-OES for the evaluation and quantification of trace elements in drinking water in Saudi Arabia (169), the results showed that the concentration for most elements was below the maximum levels in well water samples, while the concentrations of Mn was above the maximum level recommended by WHO. Kondakis,

Xenophon G *et al.*, reported and investigated the possible correlation between long-term Mn exposure from water and neurological effects in elderly people with more than 10 years exposure in Greece (170).

In the last decade, researchers have developed a reliable method for the analysis of trace metals in seawater using on-line pre-concentration by coupling flow injection (FI) analysis with ICP-MS (5)(6). However, it was not possible to separate the polyatomic interference signal from that of the trace metal. ICP-MS has been used for trace metal determination in seawater at sub mg/l level but suffered from easily oxidized elements in the plasma and the accumulation of the salts on the ICP-MS cones and lenses which affect signal drift (171). A study was conducted using online pre-concentration (chelex -100column) with ICP-MS to address the challenge of trace metal levels and the LoD for Mn was 5 ng/L (171, 172).

Others have shown that here is no need for the pre-concentration method (173-176). A flow injection inductively coupled plasma magnetic sector mass spectrometry (FI-ICP-MS) method has been developed for the analysis of Mn and other metals in estuarine waters. The limits of detection for Mn using this method were 86 ng/l.

### **1.5.3.2 Fe speciation**

Most methods for the determination of the oxidation state of Fe in different samples are based on colorimetric measurement of the Fe<sup>2+</sup>, followed by a separation technique after reduction of Fe<sup>3+</sup> which is achieved by complexation with specific chelating agents (4, 177). These methods lack sensitivity for Fe determination on water samples at mg/l. Furthermore, most

of the methods required pre-concentration and separation techniques before any analysis. Xiu-ping yan (2000) developed a sensitive method for Fe speciation in water by on-line coupling of flow injection separation and pre-concentration with ICP-MS. The method was successfully applied to the determination of trace dissolved  $\text{Fe}^{3+}$  and  $\text{Fe}^{2+}$  in local tap water, river water, and groundwater samples (4, 172).

The use of efficient separation techniques such as chromatography with selective and sensitive detectors has successfully reduced the detection limit analysis for metal species. For this reason, high performance liquid chromatography (HPLC) with ICP-MS is the best technique for separation. There is no need for pre-concentration using these combined instruments (173). A recent study was performed for the speciation of  $\text{Mn}^{2+}$  and  $\text{Mn}^{7+}$  in water by reverse-phase ion pair chromatography with the determination of Mn by ICP-MS with the use of EDTA for the separation. The detection limit for  $\text{Mn}^{2+}$  was 0.22  $\mu\text{g/L}$ . Evaluation of  $\text{Mn}^{2+}$  and  $\text{Mn}^{7+}$  speciation in water samples by ion pair high-performance liquid chromatography-inductively coupled plasma mass spectrometry has been described in several reviews (164, 178-180). This work is needed to provide methods development as robust methodology which would allow greater understanding of Fe and Mn speciation at different stages of water treatment and its relationship with governmental limits.

### **1.6 High performance liquid chromatography HPLC and ICP-MS**

ICP-MS in general, is a powerful technique for trace metal determination. Its high sensitivity lends itself for use as a chromatographic detector. Such an approach would allow speciation to be carried out and hence its application to

the current issue of Mn and Fe oxidation would seem like an ideal solution. In this case, the analytes would be dissolved in the mobile phase and separated based on their interaction with the stationary phase, in the form of a column, and mobile phase. This mechanism of separation depends on the chromatography being used, such as in a normal phase or reverse phase or in ion exchange chromatography (IEC).

HPLC-ICPMS allows the detection of metal and non-metals in a wide variety of samples because of its sensitivity and selectivity (181). ICP-MS offers advantages as a liquid chromatography (LC) detector because of its element specificity, low detection limits, and wide linear range (182). This coupled technique often used in speciation analysis, in which both techniques are coupled online, and the sample introduced from the HPLC to ICP-MS by the nebulizer. Michalke focuses on the most important elements in speciation analysis and problems in his recent publications (181), which show particular importance to Mn.

Although the detector on the ICP-MS makes it the ideal detection method for speciation, difficulties arise because the detector needs to be coupled to selective separation techniques rather than the analysis of the element itself. Since the early 1990s, separation techniques such as chromatography (HPLC and gas chromatography) have been coupled to ICP-MS as specific detection methods (183). The ICP-MS detector allows the optimal detection conditions of elements simultaneously with mass ranges 7 to 250 amu and sometimes higher and this capability for multi-elemental determination of metals made it possible to apply ICP-MS as a detector for HPLC in speciation analysis (184).

Nevertheless, a number of problems associated with sample introduction of HPLC eluent into the ICP-MS have been reported depending on the selected mode of separation such as using organic solvents that may contain high fractions, salt concentrations in buffered solutions or high amounts of ion pairing reagents. For these reasons ICP-MS has a limited tolerance toward these constituents of HPLC mobile phases (185, 186). Various problems have been observed, such as short-term signal suppression or nebuliser blockage, and the erosion of the sampling and skimmer cones (181). Also, high loads of organic solvents which are required for the reverse phase chromatography led to decreased plasma stability and analytical performance. In addition, these solvents were reported to give rise to formation of carbon based interferences (e.g.  $\text{ArC}^+$  on  $^{52}\text{Cr}^+$ ) and this resulted in deposition of carbon on the torch and the sampling cone (187). Recent research has reported the importance of ICP-MS for element speciation analysis and will be used in the future for all the elements which are not associated with ICP-MS such as non-metals, sulphur, chlorine phosphorous and fluorine (184, 188).

The use of HPLC-ICP-MS techniques have been reviewed also by Bloxham (189) and Byrdy and Caruso (190). The techniques work by retaining each metal species for different periods of time on a column consisting of a stationary phase to which metal species are attracted. Figure 1-11 shows the direct connection of the LC system with the ICP-MS through the nebulizer and the spray chamber.

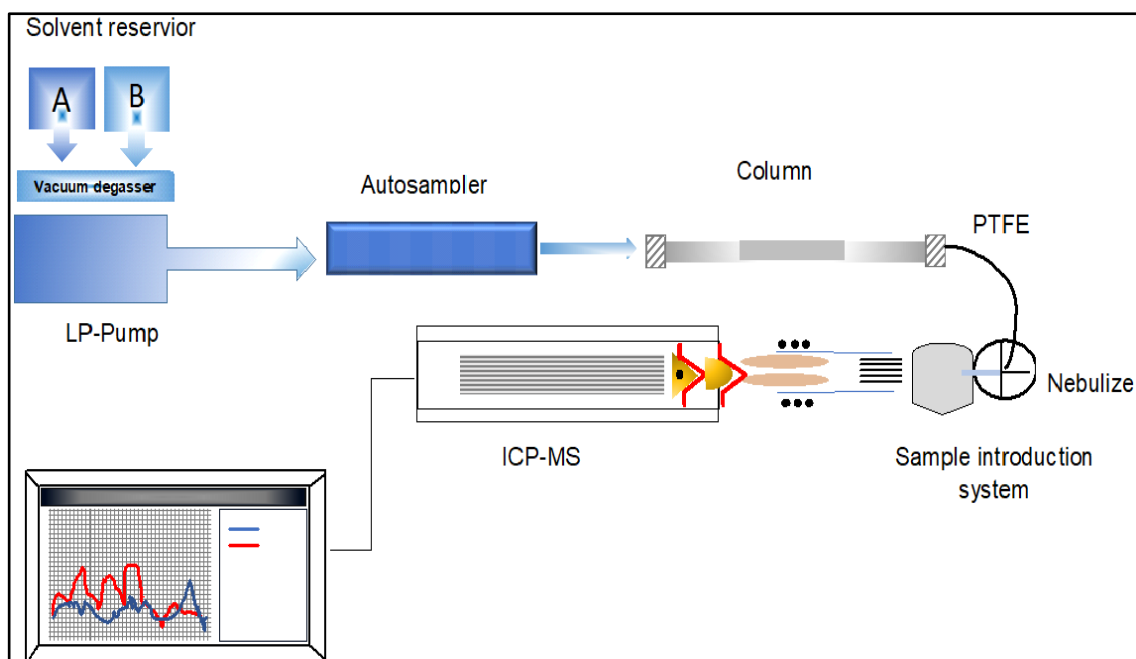


**Figure 1-11** A typical configuration for HPLC with an ICP-MS adapted from Michael (129).

The connection between the LC column and the ICP-MS sample introduction system is made with a simple PEEK or PTFE tubing transfer line. The length must be kept to a minimum between 20-50 cm, to avoid peak broadening (126). There are many factors that contribute to peak broadening as it travels through the chromatographic system. The column is the biggest contributor to this broadening and the determination of the column efficiency depending on the quality of the column packing, dimensions, the particle size. The most important thing of the HPLC separation is to obtain the good resolution in the minimum time.

## 1.7 Aim and objectives

The aim of this project was the development of a method using ICP for analysis of Fe and Mn in drinking water. The target was the determination of the species of inorganic Fe and Mn in drinking water during different purification stages. The treated water from different purification stages was obtained from treatment plants in the Northwest region of England. The aim was accomplished using the following specific objectives:

- Optimisation of an analytical method using ICP-OES for the determination of Fe and Mn in water treatment plant samples.
- Development and validation of a highly sensitive method using ICP-MS for the determination of Fe iron and Mn in water treatment plants.
- Validation of the optimised ICP-OES and ICP-MS analytical techniques using river water SRM.
- Development and validation of a method for the speciation of inorganic Fe and Mn in water using HPLC-ICP-MS.
- To analyse samples from different stages of water plant treatment for Fe and Mn speciation.

## **Chapter 2 The development of an ICP-OES method to analyse Fe and Mn in water samples**

### **2.1 Introduction**

ICP-OES is a well-established method and widely recognised as a powerful technique for the determination of elements because of its capability for multi-element analysis with simultaneous determination. Environmental water samples are one of the major applications for this technique (191, 192). ICP-OES has become one of the most used techniques for elemental determination, due to its advantages for metal analysis in a large variety of sample types. This method has been applied for the determination of total Fe and Mn in water samples. For this purpose, several research groups have measured trace metal analysis in different water samples using ICP-OES as the method of determination (192-197).

Several ICP-OES standard procedures, such as ISO 11885 (198) and USE-EPA method 200.7 (199) have been reported. These papers describe the ICP-OES method for the analysis of drinking water, including the sensitivity, selectivity, and all figures of merit. Mocak *et al.* (200) studied the metrological determination of Fe and Mn in surface water in the Malopolska rivers region in Poland. This study measured the variability of uncertainties of these metals corresponding to their concentration in real water using ICP-OES with a high level of accuracy. It also enabled the attainment of low levels of measurement for these metals for routine analysis in water samples. Abdalla *et al.* conducted

the evaluation of trace metals in drinking water in Saudi Arabia by ICP-OES using pre-concentration and acid digestion methods, and found most of the metals were below the recommended levels by WHO, whilst the concentration of Mn was above this level.

The ICP-OES method has also been applied to treatment water samples to check its applicability (201). It was found to be very useful to determine both Mn and Fe simultaneously because of their connection to discoloration of drinking water and aesthetic issues.

The present study aimed to develop and determine the Fe and Mn content in water treatment plant samples from different locations of the Northwest region of England by using ICP-OES, and compare the obtained values with those recommended by WHO and DWI.

## **2.2 Experimental**

### **2.2.1 Reagents and materials**

Ultrapure water with a resistivity of 18.2 M $\Omega$  (0.05  $\mu$ S cm<sup>-1</sup>) was obtained using a Triple Red water purification system (Triple Red Laboratory technology, UK) and was used to prepare all standards and reagents. Single-element stock solutions for ICP-OES containing 1000  $\mu$ g/mL of each Fe and Mn (SCP Science, QMx Laboratory UK) were used to prepare the calibrations in the concentration range between (20-1000 ng/mL). All the solutions were acidified for all experiments with 2% (v/v) nitric acid (HNO<sub>3</sub>), trace metal grade acid (67-69 % HNO<sub>3</sub>) was purchased from Fisher (TraceMetal Grade Fisher Scientific, UK). The accuracy and precision of the analytical method were validated using standard reference material SRM TMDA-70 trace elements in river water

Canada (LGC Standards, UK). Water samples were collected from different locations in the Northwest region of England, then followed by spiked samples and sample analysis. For sample preparation, 0.45  $\mu\text{m}$  filters were used. The internal standard was prepared from 1000 mg/L of Y and Sc single stock solution, by dilution of the stock into 2%  $\text{HNO}_3$  to yield a final concentration of 100 ng/mL. The internal standard was added to the solutions in order to reduce the adverse effects from the differences in viscosities and diluted to a final volume of 10 mL with DW (Triple Red, UK). Each sample was analyzed in triplicate. The plot of the ratio of the signal to the internal standard signal was used to account for any variability of the experimental conditions.

### 2.2.2 Samples

The water samples were collected from several United Utilities (UU) water processing locations across the Northwest region of England Figure 2-1.



**Figure 2-1** United Utilities water supply areas.

UU provide services to around seven million people. It was formed in 1995 and now has the UK's largest water operation system delivering 2,000 million litres of water a day to 2.9 million householders. The analysed samples locations and given names are listed in Table 2-1.

**Table 2-1** List of samples and locations used in this study.

<b>Sample name</b>	<b>purification stages</b>	<b>Abbreviation</b>
Fishmoore water	Raw water	RW
	First stage filter	FSF
	Fishmoore second water	FSS
	Accelator1	ACC1
	Accelator 2	ACC2
	Final water	FIN
Oswestry water	Raw water	
	Oswestry RGF	
	Slow common	
	Sand filter	
	Pilot	
	Final water	
Huntington water	Raw water	RW
	First stage filter	FSF
	second stage filter	SSF
	Post clarifier 1	PCF1
	Post clarifier 2	PCF2
	Second stage combined	SS combined
	Final water 1	Fin 1
Final water 2	Fin 2	
Wayoh water	Wayoh plant inlet	
	Wayoh clarified filter steam 1	
	Wayoh combined filtered	
	Wayoh actiflo combined outlet stream	
	Wayoh Wayoh secondary filtered stream 1	
	Wayoh final water	
Wybersley water	Wybersley combined raw water stream1	
	Wybersley combined raw water stream2	
	Wybersley clarified water stream 1	
	Wybersley clarified water stream 2	
	Wybersley combined primary filter 1	
	Wybersley combined primary filter 2	
	Wybersley combined 2nd filtrate	
	Wybersley 24 inch main	
	Sweet Loves water	Sweet loves raw water inlet
	Sweet loves clarified water	

	Sweet loves combined primary filtrate
	Sweet loves combined secondary filtrate
	Sweet loves final water
Sutton Hall water	Sutton Hall inlet to plant

## 2.3 Instrumentation

Elemental analysis was performed using a Thermo ICP-OES Model iCAP 6500 Duo (Thermo, UK). This instrument was equipped with a standard Meinhard nebulizer and cyclonic spray chamber and fittings. The samples were analysed using a Cetac ASX 510 autosampler held inside an ENC500 containment system (Cetac, UK). Signals were obtained using axial viewed plasma. High purity Ar gas (Air Products, CryoEase Services, UK) was used for plasma generation, nebulization and as an auxiliary gas. Prior to analysis, the operational conditions were optimised to give the highest signal and signal to blank ratio to obtain the settings with the greatest sensitivity for the analysis of Fe and Mn. The remaining operational conditions and the elements studied are shown in Table 2-2.

**Table 2-2** ICP-OES operation conditions.

<b>Components/parameter</b>	<b>Type/Value/Mode</b>
Plasma Spectrometer	ICAP 6500Duo Thermo fisher
Nebulizer	Meinhard glass Concentric
Optical view	Axial
Solution uptake	1mL/min
Internal standard	Sc
Pump speed	80
Replicate	3
Spray Chamber	Glass Cyclonic

---

## 2.4 The Optimisation of ICP-OES conditions

A full optimization of the measurement conditions (RF power, nebuliser gas flow, coolant gas flow, auxiliary gas flow and pump rate) was carried out in order to obtain the optimum signal and signal to blank ratio. All Fe and Mn wavelengths were used for the optimization method and the most sensitive wavelength was selected for analysis depending on the amount of spectral interferences.

In this work, the ICP-OES was applied to Fe and Mn determination in drinking water. Hence, a full optimisation of each variable used to generate the plasma was required to obtain the maximum sensitivity for each element. This required the optimisation of power, coolant flow, auxiliary flow, nebuliser flow etc. This optimisation considered raw signal but also signal-to-blank ratio.

The optimization process was carried out using three replicates of a 500 ng/mL (0.5 mg/l (ppm) Fe and Mn solution in 2% HNO<sub>3</sub>. The following characteristics were optimized: radio frequency power 750-1350 W; auxiliary gas flow (0.2 L/min - 2L/min); coolant gas flow (10 L/min to 20 L/min); nebulizer gas flow (0.3 L/min to 1.45 L/min); and pump rate (30-130 rpm). The experimental data was processed using iTeva software (Thermo Fisher, UK) and exported to an Excel spreadsheet (Microsoft, UK) for the preparation of all the graphs. These conditions were applied for the determination of both elements as shown in Table 2-3 and step size on Table 2-4.

**Table 2-3** The optimum parameters range for ICP-OES.

---

<b>The optimum parameter</b>	<b>Abbreviation</b>	<b>Range of optimum</b>
<b>Radio frequency Power</b>	RF	750-1350 W
<b>Nebulizer Gas Flow</b>	NB	0.35 to 45 L/min
<b>Auxiliary Gas Flow</b>	AUX	50 L/min to 2 L/min
<b>coolant gas flow</b>	Coolant	10 L/min to 20 L/min
<b>Pump Rate</b>	PR	30-130 rpm

---

**Table 2-4** Step sizes for each parameters

---

<b>Step sizes</b>	<b>Nb</b>	<b>RF</b>	<b>Aux</b>	<b>PR</b>	<b>Coolant</b>
0.3		750	0.2	30	12
0.35		800	0.4	40	13
0.4		850	0.6	50	14
0.45		900	0.8	60	15
0.5		950	1	70	16
0.55		1000	1.2	80	17
0.6		1050	1.4	90	18
0.65		1100	1.6	100	19
0.7		1150	1.8	110	20
0.75		1200	2	120	
0.8		1250			
0.85		1300			
0.9		1350			
0.95					
1					

---

## **2.5 Results and discussion**

### **2.5.1 ICP-OES optimisation**

All Fe and Mn wavelengths were optimised using the ICP-OES and the most sensitive lines for both elements were selected for the analysis.

The correlation coefficient was very similar at some wavelengths, but the decision was made depending on the most sensitive results based on strength of signal and minimal interferences. If the wavelength does not have any interference from other elements then that wavelength was selected for the analysis. The most sensitive wavelengths (Fe 238.2 nm and Mn 257.6 nm) were then used for the rest of the method development and sample analysis.

#### **2.5.1.1 The determination of the optimum nebulizer gas flow**

The optimum values for the instrument were determined by identifying the optimum signal/blank ratio. These conditions were assessed across the range of elements and wavelengths. The optimum value was selected from the highest value gained from the signal to blank ratio. Figure 2-2 illustrates the greatest signal and signal to blank ratio for the nebuliser gas flow. It can be seen that the increase in the nebuliser flow rate can affect each wavelength, therefore a compromise had to be made and the nebuliser was set at 0.8 L/min.

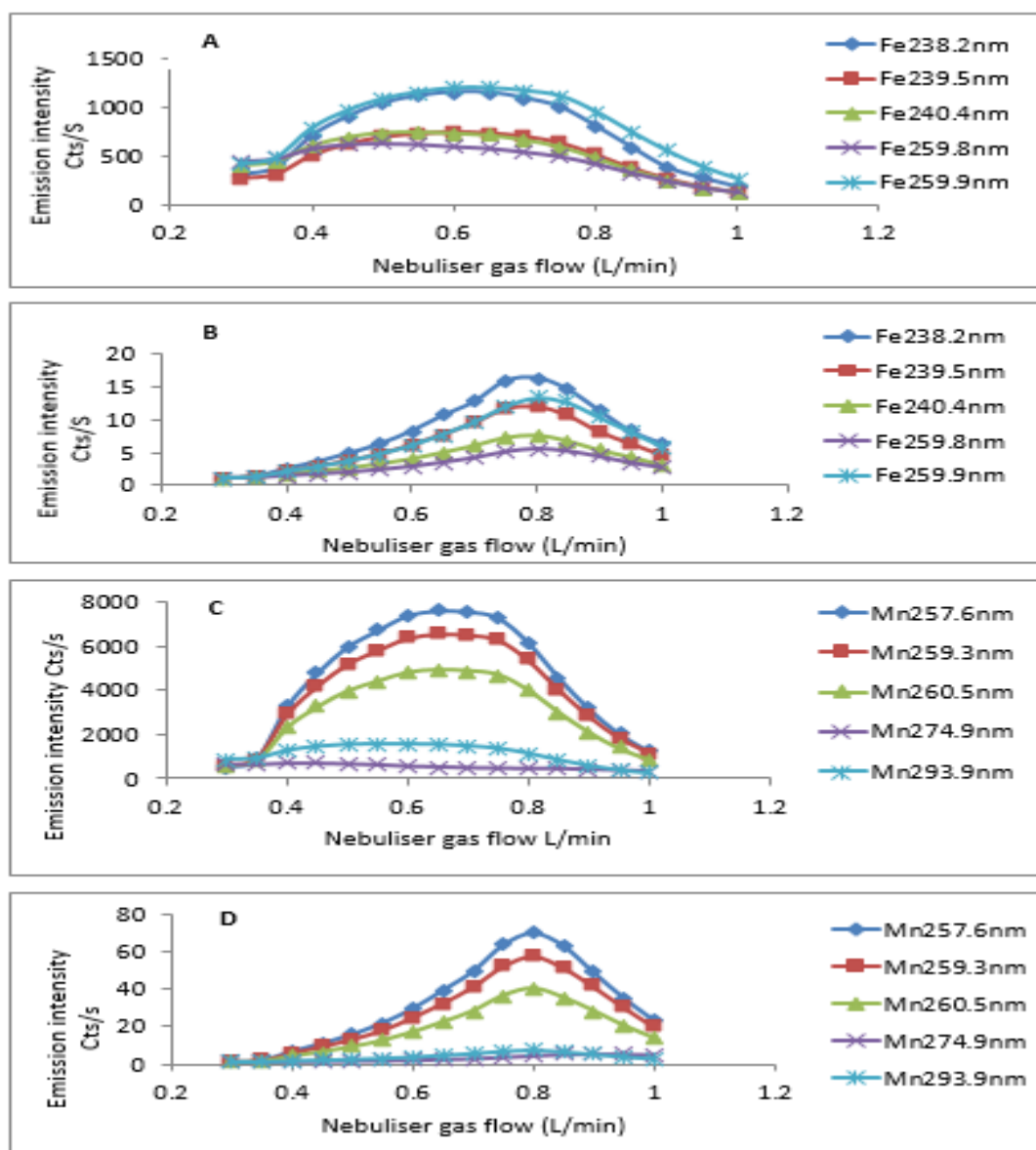


**Figure 2-2** The effect of nebuliser gas flow rates on signal intensity of Fe (A) and Mn (C) and signal to blank ratio of Fe (B) and Mn (D).

The sample is introduced into the nebulizer and range of small and large droplets are formed. Only the small droplets are transported to the plasma and so conditions which promote small droplet formation are required. A decrease in signal can be seen where large droplet formation was promoted by the conditions used. This is best considered in relation to the background signal and resulted in the decision to use a 0.8 L/min as the flow rate based on the data presented in Figure 2.2 B and D for Fe and Mn respectively.

### **2.5.1.2 The determination of the optimum pump rate**

Figure 2-3 illustrates the signal and signal to blank ratio obtained for different pump rates. The pump rate of 80 rmp was chosen for Fe and Mn. This pump rate was used, as although the signal and signal-to-blank ratio are approximately the same for Fe, using higher pump rates will produce further bigger droplets and this will slow the small droplet's access to the nebulizer, and reduce the sensitivity of the instrument. As can be seen, a variation in the pump speed did not improve the signal, but working at a pump rate of 60 rpm, the background signal was slightly lower for Mn but not for Fe.

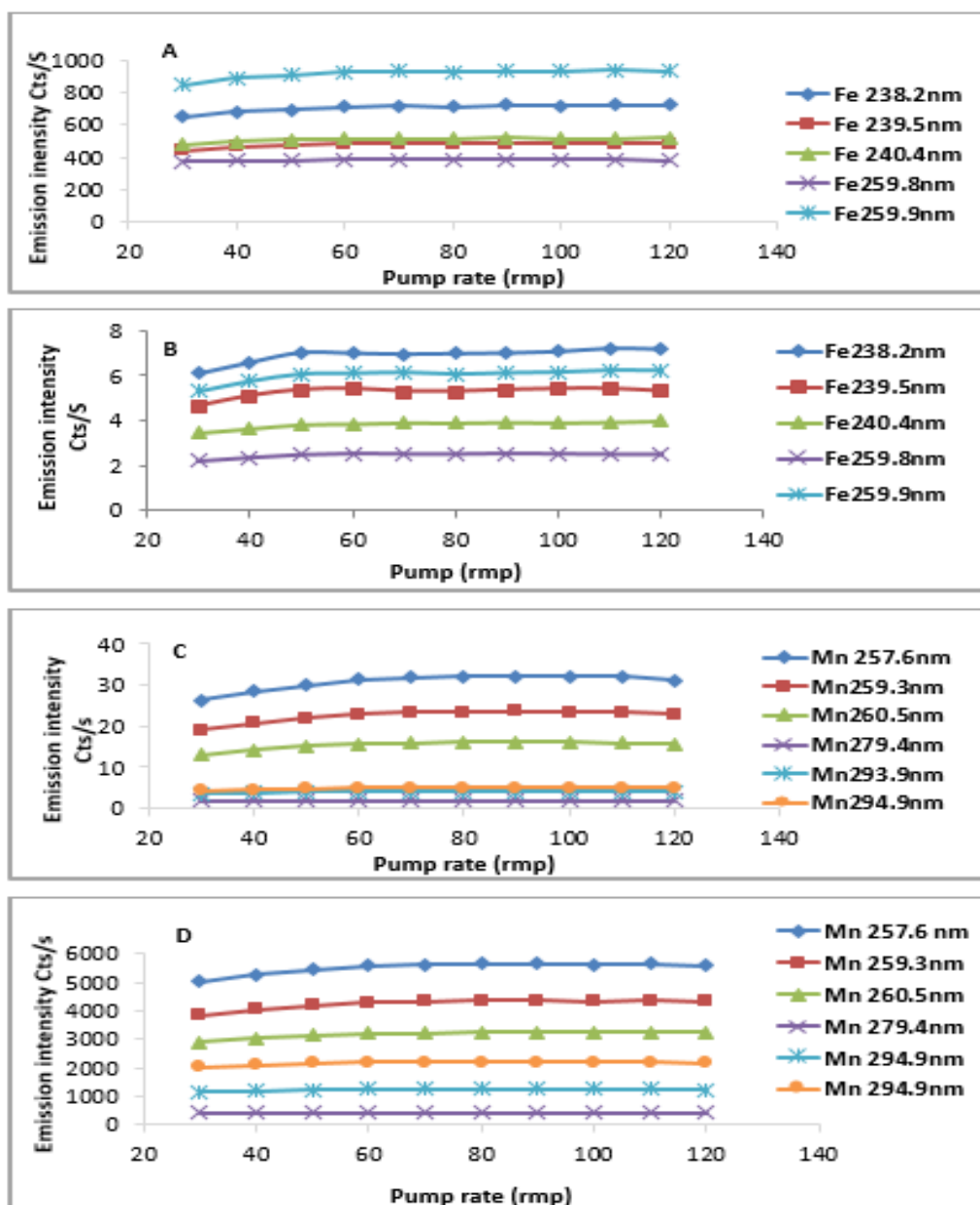


**Figure 2-3** The effect of pump flow rate on the signal intensity of Fe (A) and Mn (C) and signal to blank ratio of Fe (B) and Mn (D).

### **2.5.1.3 The determination of the optimum auxiliary gas flow**

Figures 2-4 (A and B) illustrate the best signal and signal to blank ratio obtained for the auxiliary gas flow. The auxiliary gas flow on the ICP-OES is used to elevate the bottom of the plasma away from the sample injector tube. It can be seen that the auxiliary gas flow exerts a much greater effect on plasma properties compared to the other parameters analysed. The auxiliary was set at 1.5 L/min for the standards parameters of measurement based on the improved signal to blank ratio because when a flow more than 1.5 was used the sensitivity dropped for each analyte.

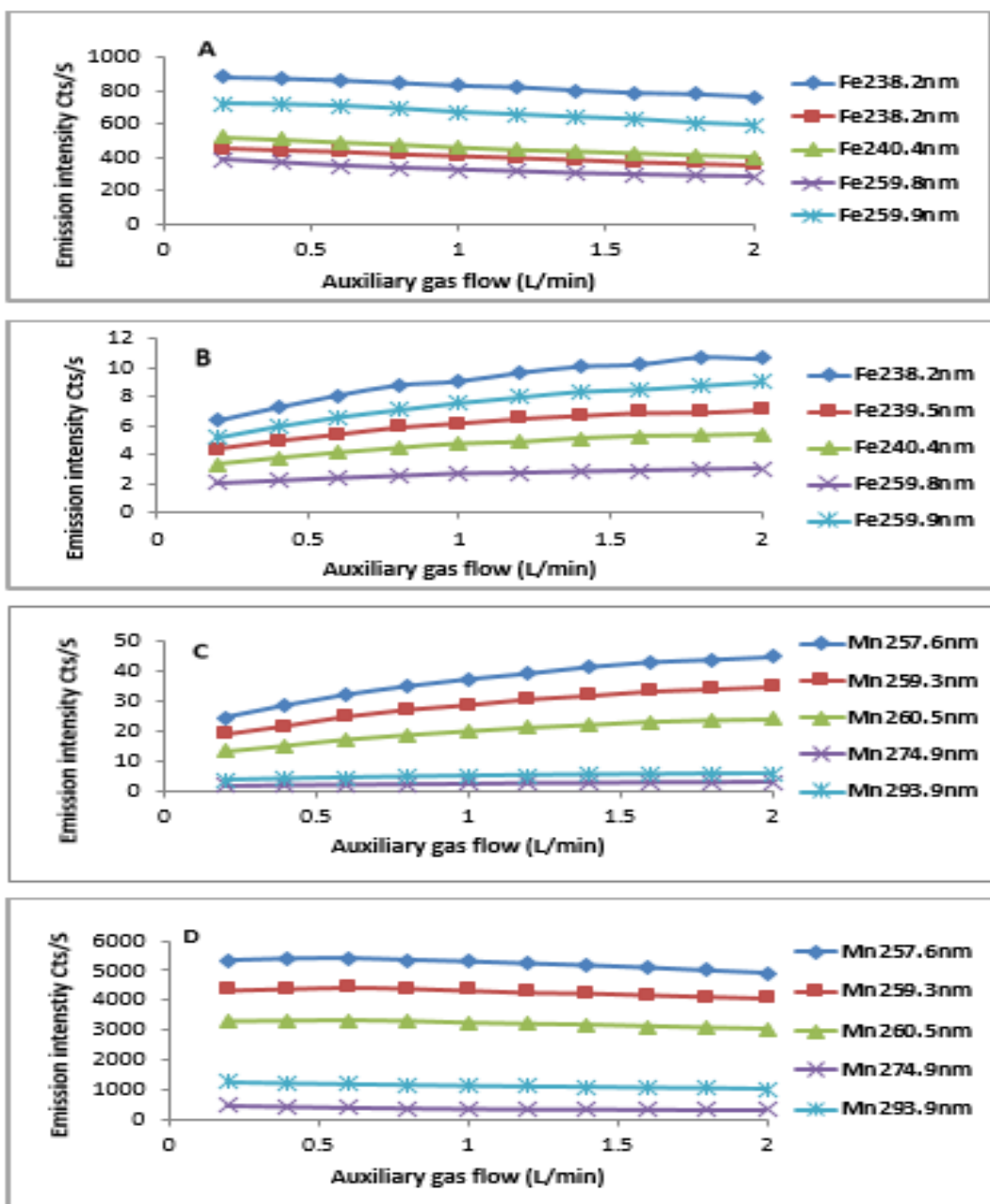


**Figure 2-4** The effect of auxiliary gas flow rate on the signal intensity of Fe (A) and Mn (C) and signal to blank ratio of Fe (B) and Mn (D).

#### 2.5.1.4 The determination of the optimum coolant gas flow

The coolant gas flow is used on the ICP-OES between the outer tube and auxiliary of the torch (Chapter1, section 1.4.1.), to keep the torch from melting and needing to be replaced. Figures 2-5 (A and B, C and D) illustrate the best signal and signal to blank ratio obtained for coolant gas flow to be 14 (L/min) for Fe and Mn, respectively, using the ICP-OES optimal conditions. The emission intensity was not very sensitive to the coolant gas flow. It was decided to use 14 (L/min) because this limited the amount of Ar used, which is very expensive.

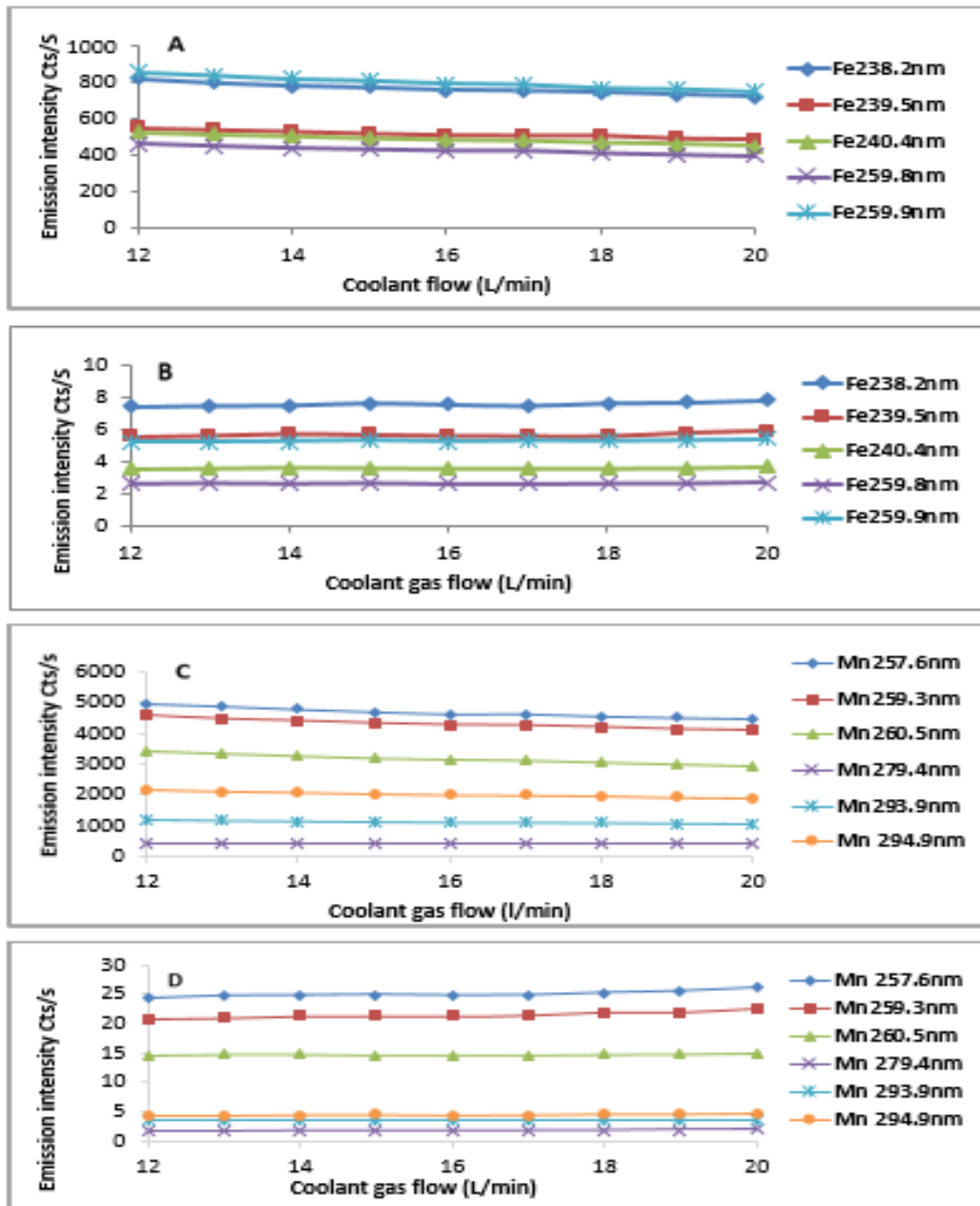


**Figure 2-5** The effect of coolant gas low on the signal intensity of Fe (A) and Mn (C) and signal to blank ratio of Fe (B) and Mn (D).

### 2.5.2.5 The determination of the optimum RF power

The optimum parameters were used to obtain emission intensity values using different RF powers, as shown in Figure 2-6. The optimal value of 750 W was chosen.

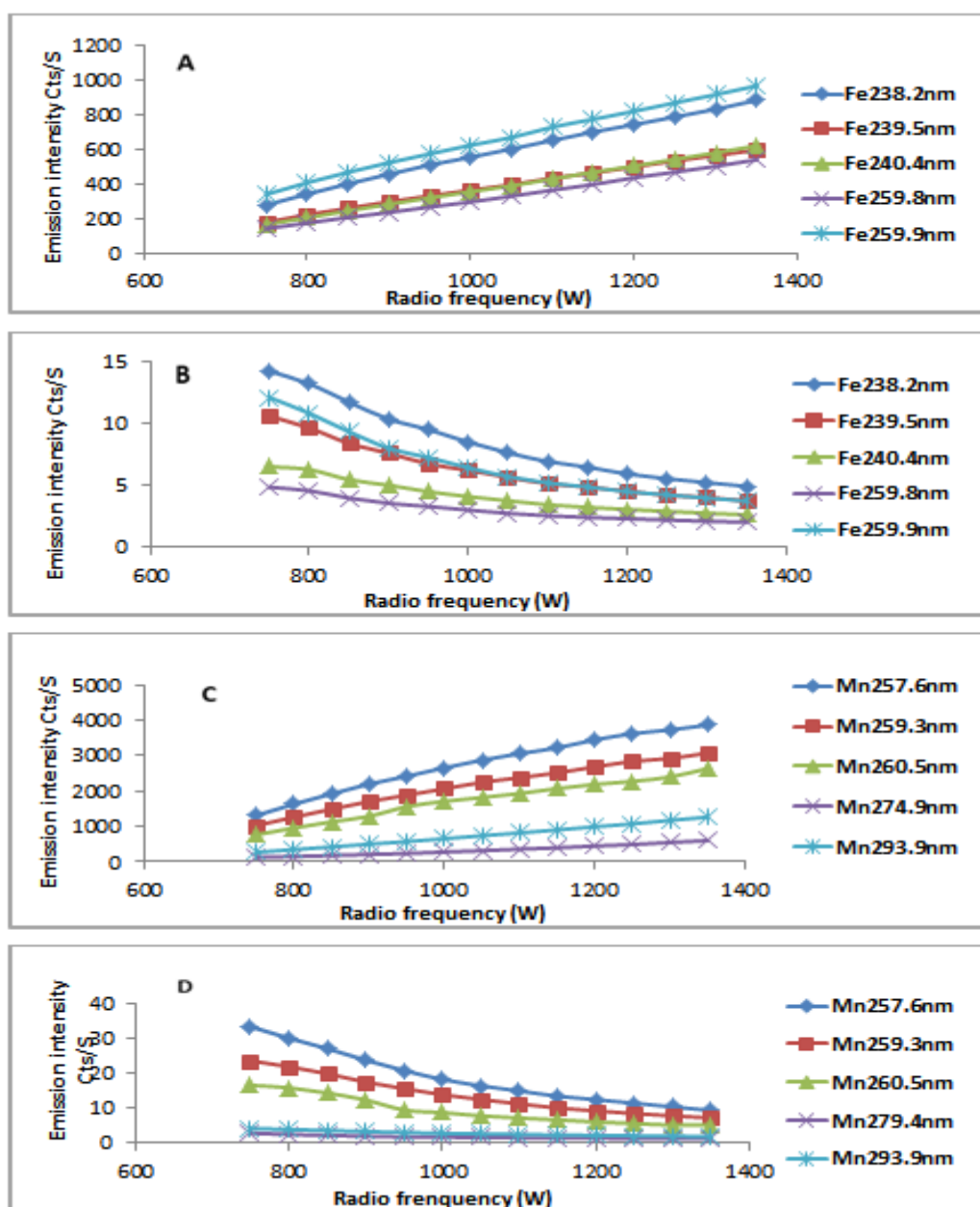


**Figure 2-6** The effect of radio frequency on the signal intensity of Fe (A) and Mn (C) and signal to blank ratio of Fe (B) and Mn (D).

## 2.6 Optimal parameters and determination of LoD and LoQ

A summary of the optimal parameters is displayed in Table 2-5.

**Table 2-5** Optimum Parameter values for ICP-OES.

Parameter	Optimum Value
Radio Frequency Power (W)	750
Coolant Gas Flow (L/min)	14
Auxiliary Gas Flow (L/min)	0.5
Nebuliser Gas Flow (L/min)	0.8
Pump Rate (rpm)	80

The optimum values were selected from the highest value gained from the signal /blank ratio. These values were initially used to obtain LoD and LoQ values. However, it was observed that the optimum radio frequency power of 750 W was insufficient to produce repeatable results and reliable values. It was found that a very large reduction in the blank signal caused a corresponding increase in the ratio intensity producing a high false reading for the power at 750 W. It was thought that this was due to the low plasma temperatures at this power. High temperatures must be reached before the

gas transforms into the plasma, which is needed to sustain ionisation that leads to higher sensitivity.

Consequently, the optimisation of the ICP-OES was repeated to obtain LoD and LoQ values with radio frequencies of 750 W, 1150 W and 1350 W. The determination of LoD and LoQ values allowed the assessment of the instrument's sensitivity and lowest possible calibration point. Using the optimum values obtained, LoD and LoQ data were calculated according to the Miller and Miller (202) method using  $3\sigma$  of the blank for LoD and  $10\sigma$  of the blank for LoQ.

For each element and wavelength, calibration standards using a linear series of Fe and Mn standards solutions were prepared in the concentration range from 0.1 ppm to 1 ppm. A blank solution was also prepared of 2% HNO<sub>3</sub>. For each run, the calibration standards and samples were composed of the same concentration of matrix. The blank solution was run 10 times and from the values the standard deviation could be calculated. From the linear solutions, the slope and R<sup>2</sup> value were greater than 0.995 and thus the LoD and LoQ values were obtained and no elements were calculated below this limit. The LoD and LoQ were determined at 750 W, 1150 W and 1350 W. This showed 1150 W to be the setting of power which produced the most sensitivity, and this dramatically improved the sensitivity for the calibrations and results (Table 2-6). Figure 2-7 uses Mn 257.6 nm as a continued example. The predicted LoD and LoQ were verified and validated for the required precision (Acceptance criteria % RSD is not more than 5%).

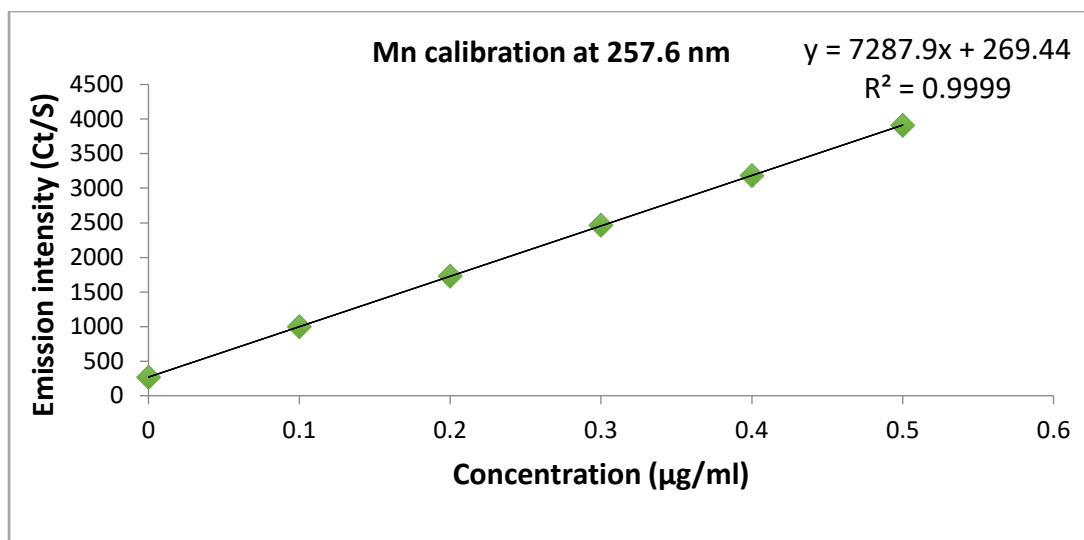


**Figure 2-7** Calibration graph of Mn recorded at 257.6 nm.

Figure 2-7 displays the calibration line equation and  $R^2$  value for Mn 257.6 nm at 1150 W. The LoD and LoQ were calculated for Mn. The average of the 10 blanks reading was 269.2 counts/second (Cts/S) with  $\sigma$  of 3.8 from the obtained calibration linear line equation, the slope = 7287.9x and the intercept = 269.44.

LoD and LoQ were calculated using Equations 3.1 and 3.2.

$$LoD = \frac{(average\ blanks\ reading + 3\sigma) - Intercept}{Slope} \dots \text{Equation 3.1}$$

$$LoQ = \frac{(average\ blanks\ reading + 10\sigma) - Intercept}{Slope} \dots \text{Equation 3.2}$$

$$LoD = \frac{(269.2 + (3 \times 3.8)) - 269.44}{7287.9} = \frac{(269.2 + 11.4) - 269.44}{7287.9} = \frac{11.16}{7287.9}$$

$$= 0.00153 \mu\text{g/mL} = 1.53 \text{ ng/mL}$$

$$LoQ = \frac{(269.2 + (10 \times 3.8)) - 269.44}{7287.9} = \frac{(296.63 + 38) - 269.44}{7287.9} = \frac{37.76}{7287.9}$$

$$= 0.00516 \mu\text{g/mL} = 5.16 \text{ ng/mL}$$

**Table 2-6** LoD and LoQ ( $\mu\text{g/mL}$ ) calculated using different RF powers.

<b>RF Power</b>	<b>750 W</b>		<b>950 W</b>		<b>1150 W</b>		<b>1350 W</b>	
<b>Element</b>	LoD	LoQ	LoD	LoQ	LoD	LoQ	LoD	LoQ
<b>Fe 283.2 nm</b>	0.035	0.0704	0.0116	0.027	0.003	0.0029	0.012	0.0025
<b>Mn 257.9 nm</b>	0.002	0.0091	0.002	0.0081	0.0014	0.0087	0.0052	0.0094

Consequently, the instrumental conditions chosen for the determination of Fe and Mn were established and are the same as displayed in Table 3.5; the only difference is that of RF power.

## **2.7 Analytical figures of merit and method validation**

All the parameters of the figure of merit of the analytical calibration curve were found such as linear range, correlation coefficient R<sup>2</sup>, average RSD for the repeatability of the solution (n = 5), LoD and LoQ. These limits were calculated (see Section 2.5.2.5) for all chosen analytes which were below those set by the regulations to ensure accurate analysis of those levels. In order to establish the analytical performance, drinking water SRM was analysed as per the developed method and the results are presented in Table 2-7.

**Table 2-7** limits of detection and Limits of quantification for Mn and Fe.

Element (λ-nm)	Blanks Av.*	Σ	Slope	Intercept	Av.+3σ	Av.+10σ	LoD μg/mL	LoQ μg/mL	LoD ng/mL	LoQ ng/mL
<b>Fe 238.2</b>	163.25	3.12	1157.3	159.21	163.25+3*3.12	163.25+3*3.12	0.01158	0.0308	11.58	30.8
<b>Mn 257.6</b>	296.63	3.8	7287.9	269.44	296.6 +3*3.8	296.6 +10*3.8	0.00153	0.005	1.43	8.6

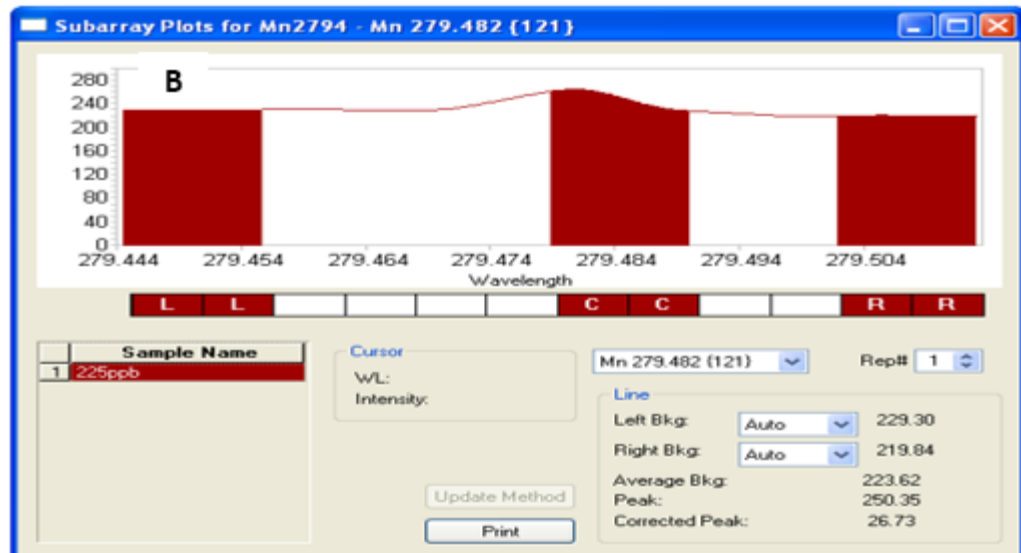
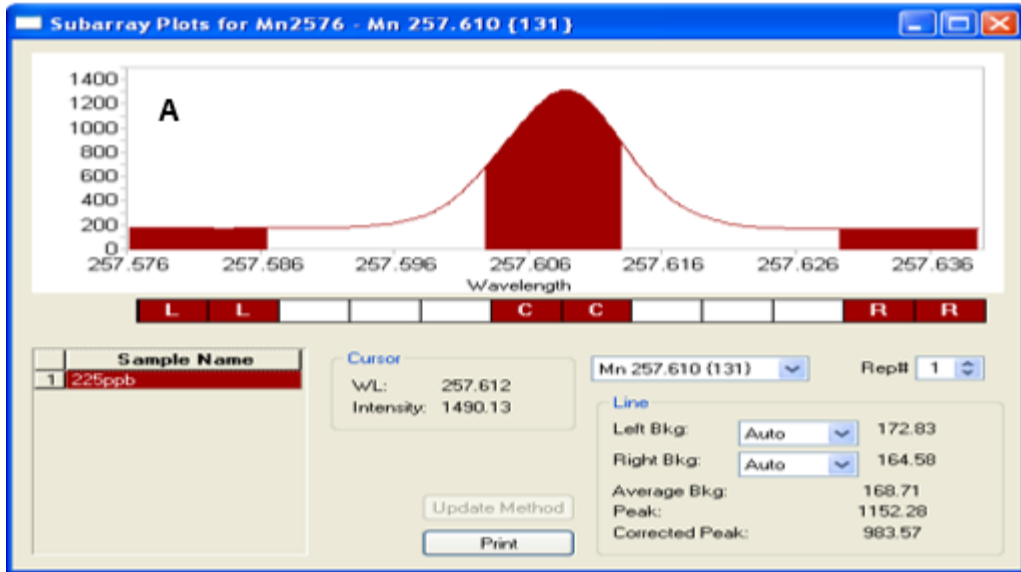
Wavelengths were selected for Fe and Mn in agreement with the requirements of the U.S. EPA7 Method 200.7 and ISO regulation 11885 and the Table 2-8 lists the selected analytical wavelengths. The selectivity of this method is based on accurately quantifying the analyte in the presence of interferences. The different sensitivities for each line at specific wavelengths were taken into consideration before selection. This selection was based on the interferences and baseline signal on the ICP-OES subarray on the software. The wavelengths in red were selected.

### 2.7.1 Wavelength selection

**Table 2-8** Spectral lines used for all the analytes.

Element	Wavelength/ nm
Fe	238.2
Fe	239.5
Fe	240.4
Fe	259.8
Fe	259.9
Mn	257.6
Mn	259.3
Mn	260.5
Mn	279.4
Mn	293.9
Mn	294.9
Y	371.0
Sc	255.2
Sc	424.3
Sc	361.3

The calibration for elements at different wavelengths were calculated using the ITIVA software provided by the instrument manufacturer. The results shown in Figure 2-7 illustrate the subarray plots for Fe and Mn lines and the selection of the lines was based on the lowest LoQ obtained.



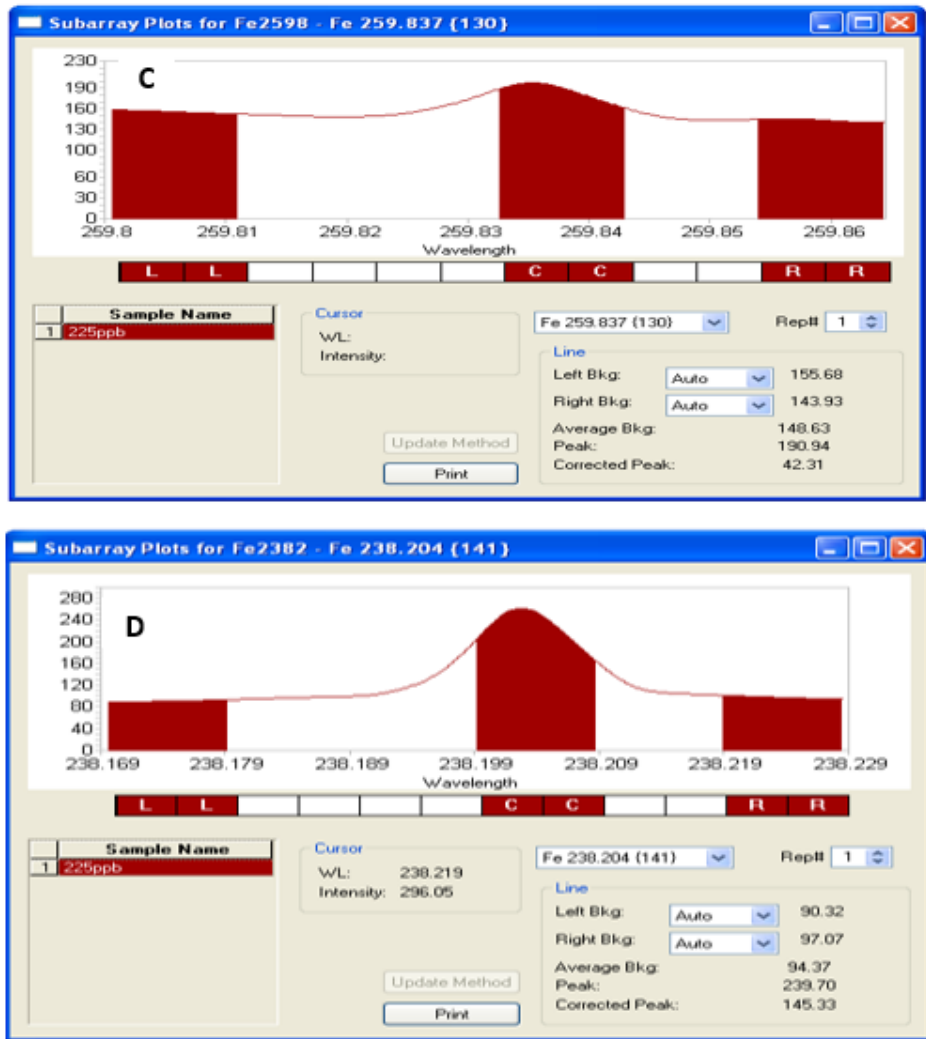


**Figure 2-1** Subarray plots for Mn 257.6nm (A, Mn 279.4nm (B), Fe259.8nm (C) and Fe 238.2nm (D) respectively.

### **2.7.2 Linearity and range**

The linear range is the working range of Fe and Mn concentrations over which the method is linear. The LoQ is the lowest end of this concentration range and the linearity was evaluated from the calibration using different standards, the lowest concentration close to the LoQ and the others were prepared according to Section 2.5.2. The lowest working range was selected to be between the LoQ and 1 µg/mL using the optimal conditions shown in Table 2-9.

**Table 2-9** Linearity results for Mn and Fe elements using ICP-OES.

<b>Element</b>	<b>Range (µg/mL)</b>	<b>Calibration equation</b>	<b>R<sup>2</sup> Value</b>
<b>Mn</b>	500	$y = 1217.9x + 457.84$	0.9999
<b>Fe</b>	1000	$y = 1083.3x + 227.97$	0.9998

### **2.7.3 Accuracy and Precision**

The accuracy and precision of the method were verified by analyzing river water SRM TMDA-70. Intra-laboratory reproducibility was used: A determination of the extent that qualified people within the same laboratory can successfully replicate results using a specific protocol at different times as opposed to using different laboratories (inter). The trueness of this method was estimated using the SRM analysis where six parallel samples of river water TMDA-70 were analysed. The recovery of Fe and Mn was calculated to be between 98-107 % showing agreements with the acceptance criteria (95-105 %) as listed in Table 2-9. The precision of the method is the repeatability and reproducibility within and between days, respectively. This was checked by analysing six replicates of two different SRM; high purity trace metal in TMDA-70 and TMDA-62.4 water samples. The measured values and the certified values using the same instrument were in good agreement and the % RSD was found to be within the specification of the method's accuracy; an RSD less than 5% was required for acceptable precision as shown in Table 2-10. The intra reproducibility was expressed as the coefficient of variability

(precision); calculated as the standards deviation of a set of measurements divided by the mean of the set. Less than 10% is acceptable.

**Table 2-10** Analysis of SRM TMDA-70 (4x dilution) using ICP-OES.

<b>Analyte</b>	<b>Certified value (µg/mL)</b>	<b>Average measured value (µg/mL)</b>	<b>Recovery (%)</b>	<b>RSD</b>
<b>Fe</b>	0.092	0.087	95.8	2.4
<b>Mn</b>	0.075	0.073	97.1	1.6

The recovery percentage was calculated as follow: (Spiked Sample Concentration – Non-Spiked Concentration)/Spike Concentration x 100.

The concentrations were obtained from six SRM samples after a four-fold dilution. The standard deviation, % RSD, was obtained to judge the precision of this method. These results show repeatability of SRM analysed and all the samples were run on the same day.

**Table 2-11** Analysis of SRM TMDA-70 neat sample using ICP-OES on the same day.

Analyte	Certified value (µg/mL)	Average measured value (µg/mL)	Recovery (%)	% RSD
<b>Fe</b>	0.368	0.359±3.3	97.5	2.5
<b>Mn</b>	0.302	0.301±2.7	99.6	1.9

The result obtained showed that the method is accurate, selective and validated. The results are in good agreement considering the confidence level between 95-105%. The evaluated data showed a good level of precision with the average RSD for repeatability of 5 measurements varying from 2.5% for Fe and 1.9% for Mn.

**Table 2-12** shows the concentrations that were obtained from six SRM samples after four-fold dilution. These results show repeatability of SRM analysed on six different days.

Element	R1	R2	R3	R4	R5	R6	Average	Certified SRM (µg/mL)	Recovery (%)	RSD (%)
<b>Mn</b>	0.301	0.304	0.306	0.303	0.305	0.301	0.303	0.302	97.6	3
<b>Fe</b>	0.361	0.376	0.361	0.364	0.365	0.361	0.364	0.368	99.4	4

#### **2.7.4 Spike recoveries**

Spike recovery was assessed by additions of Fe and Mn standard to final volume of 0.05 and 0.1  $\mu\text{g/mL}$   $\mu\text{g/mL}$  to water samples from the treatment plants. This method was used to ensure that the matrix does not significantly reduce or enhance the percentage recovery of the analyte. The spike recoveries should be within the acceptance recovery range 95-105% and RSD less than 5%. The results from the spike recovery of drinking water samples are presented in Table 2-13.

**Table 2-13** Results for water samples with spike recovery concentration of 0.05 µg/mL of Fe and Mn, n = 5 on the same day.

<b>Sample name</b>	<b>Analyte</b>	<b>Unspiked sample (µg/mL)</b>	<b>Spiked sample (µg/mL)</b>	<b>Recovery (%)</b>
<b>A</b>	Fe	0.0033	0.0536	100.6
	Mn	0.0338	0.0854	102.4
<b>B</b>	Fe	-0.0002	0.0484	97.2
	Mn	0.0257	0.0759	100.4
<b>C</b>	Fe	0.0007	0.0536	105.8
	Mn	0.0267	0.0768	100.2
<b>D</b>	Fe	0.0007	0.0536	105.8
	Mn	0.0267	0.0768	100.2
<b>E</b>	Fe	0.0004	0.0515	102.2
	Mn	0.0003	0.0507	100.8
<b>F</b>	Fe	0.0249	0.0763	102.8
	Mn	0.0001	0.0502	100.2
<b>H</b>	Fe	0.0003	0.0511	101.6
	Mn	-0.0001	0.0502	100.6
<b>I</b>	Fe	0.0054	0.0554	100.8
	Mn	0.0332	0.0836	100.5
<b>J</b>	Fe	0.0027	0.0543	102.6
	Mn	0.0237	0.0758	104.2
<b>K</b>	Fe	0.0004	0.0529	105.6
	Mn	0.0007	0.0516	101.8

## 2.7.5 Selection of optimal internal standards

Internal standards were chosen for the analysis to evaluate and identify the analytical problems that could influence the emission signals, such as the matrix composition. Acid effects were included in this procedure and nitric acid was used for the analysis. Spike recovery results for nitric acid, *aqua regia* (3 parts of HCl to 1 part of HNO<sub>3</sub>) and reverse *aqua regia* (1 to 3 of the HCl to HNO<sub>3</sub>) are presented in Tables 2-14 to 2-16. The results were obtained using different acid matrixes by spiking five syntactic samples and calculating the percentage recovery of each sample on different days to see how the acid affects results. Nitric acid was selected to use during the sample analysis of this method, because from the table below it can be seen that using different acids, the one with the best recovery is nitric acid.

**Table 2-14** Spike recovery (%) for Fe and Mn wavelengths (nm) in synthetic samples using 2% nitric acid on different days.

Element	Nitric acid							
	Day 1		Day 2		Day 3		Day 4	
	Fe	Mn	Fe	Mn	Fe	Mn	Fe	Mn
<b>sample1</b>	102.4	102.8	100.6	103	96.2	103	99.6	101.8
<b>sample2</b>	104.2	100.4	97.2	100.4	104	104.2	102.6	104.4
<b>sample3</b>	103.8	101.8	102.8	100.4	99.8	100.2	102.8	100.2
<b>sample4</b>	95.4	98.8	105.8	100.2	97.4	104.8	105.8	100.2
<b>sample5</b>	102.3	101.5	102.2	100.8	98.6	101.2	102.8	103

**Table 2-15** Spike recovery (%) for Fe and Mn wavelengths (nm) in synthetic samples using *aqua regia* acid 3 parts HCl to 1 part of HNO<sub>3</sub>.

<b>Aqua Regia</b>								
	<b>Day1</b>		<b>Day2</b>		<b>Day3</b>		<b>Day4</b>	
<b>Sample</b>	Fe2	Mn	Fe	Mn	Fe	Mn	Fe	Mn
	38.2	257.6	238.2	257.6	238.2	257.6	238.2	257.6
<b>sample1</b>	109	100.4	95.4	98.6	105.4	98.6	103.2	100.4
<b>sample2</b>	90.6	96.6	95.6	100.4	88.4	98.8	94.4	101.6
<b>sample3</b>	83.8	99	80.4	97.8	93.8	97.6	105.4	97.8
<b>sample4</b>	93.6	103.2	91.8	97.8	103.2	99.4	96.6	97.8
<b>sample5</b>	96.4	99	109	98.8	94.4	98.2	99	98.8

**Table 2-16** Spike recovery (%) for Fe and Mn wavelengths (nm) in synthetic samples using reverse *aqua regia* acid 1 parts HCl to 3 part of HNO<sub>3</sub>.

<b>Reverse aqua</b>								
	<b>Day1</b>		<b>Day2</b>		<b>Day3</b>		<b>Day4</b>	
<b>Sample</b>	Fe	Mn	Fe	Mn	Fe	Mn	Fe	Mn
	238.2	257.6	238.2	257.6	238.2	257.6	238.2	257.6
<b>sample1</b>	93.2	96.8	95.2	98.2	116.4	99	97	97.4
<b>sample2</b>	92.4	95.6	110.6	100.4	106.6	99.4	111	98.4
<b>sample3</b>	97.8	99.8	102.6	101.6	109.4	99.8	108.8	100.4
<b>sample4</b>	106.6	90.6	99	101.2	109.2	96.8	107	99.4
<b>sample5</b>	99	98.8	93.2	99.4	108.2	95.6	103	98

Yttrium and scandium were tested as internal standard for the determination of Fe and Mn in water samples using ICP-OES. This was carried out to improve precision to reduce the matrix induced signal variations. All the samples were referencing to the same state of element (atomic lines are better corrected by atomic lines, and ionic lines by ionic lines) to ensure they are of the same energy and react in the same way in the plasma.

Sc 255.2 nm was chosen for the method because it ensures a better improvement in the precision for the method than other wavelengths for both Sc and Y. Table 3-17 displays the corrected results obtained using iTEVA software after analysing the reference water compared with those obtained without IS correction for the same samples. The recovery value using the Sc 255.2 was close to the certified value, suitable IS because they had recoveries between 95-105% and RDS <5 %. The concentration of the Sc was set as 1 µg/mL, which provided the accurate results.

**Table 2-17** Concentrations ( $\mu\text{g/mL}$ ) obtained with and without the use of Sc 255.2 nm and Y 371.029 nm as internal standards, (mean  $\pm$   $\sigma$ , n = 3), (R) % recovery.

Element (nm)	Recovery & RSD with Sc 255.2 nm	Recovery & RSD with Y 371 nm	Recovery & RSD without IS	Reference (SRM certificate)
<b>Fe</b> <b>238.2</b>	102.6 $\pm$ 2.8	104.4 $\pm$ 3.2	108.4 $\pm$ 3.3	101.4 $\pm$ 2.1
<b>Mn</b> <b>257.6</b>	99.6 $\pm$ 1.2	103.6 $\pm$ 2.6	95.6 $\pm$ 2.6	99.3 $\pm$ 1.9

It can be seen that adding the same concentration of IS to all samples including the unknown samples improved the %RSD values. Sc was chosen because it produced results very close to the SRM in both % recovery and RSD. Thus, using Sc as IS in the analysis of the samples improved the precision of the results, removed all matrix effects and any drift of the instrument.

## 2.8 Analysis of United Utilities' treatment water samples

Finally, an analysis of the United Utilities water samples was undertaken to assess accuracy of the determination of Fe and Mn levels. Prescribed concentrations in drinking water in the UK are set at 200  $\mu\text{g/L}$  (0.2 mg/mL) for Fe and 50  $\mu\text{g/L}$  (0.05 mg/mL) for Mn (DWI, 2011) and recently confirmed with the inspector's report for drinking water in England and Wales July 2017. The

World Health Organization (WHO) guidelines (30) has set 400 µg/L for Mn and 300 µg/L for Fe in drinking water (28, 31).

By examining all the results obtained for Fe and Mn in drinking water in this analysis some of the water samples from individual processing stages were below the LOD stated determined in this work on this section. These levels were below the limits proposed by European DWI of 0.2 mg/mL and 0.05 mg/mL for Fe and Mn, respectively. Higher levels of Mn and Fe were seen in the stages after the coagulation agent was added which was after the filtration stages.

This clearly indicates that the coagulation agent itself contributes to the additional Mn and Fe levels. These results were obtained at different water processing plants but showed similar results. The Oswestry water had less Mn than the Fishmoore water. Although the treatment stages used at Oswestry are different to Fishmoore, there was a consistent decrease in the concentration level of Fe and Mn. In the UK, the water supply from companies have had occurrences of both Fe and Mn at higher levels than expected and if these levels are above the DWI standards of 50 µg/L and 200 µg/L, respectively, then the treatment plants have to put in place measures to lower these concentrations in the final water. Some of the treatment water methods used on the water from the pilot plant have been analysed in this study such as oxidation to insoluble Mn<sup>4+</sup> rapid gravity filtration (RGF) in the Oswestry water followed by a chlorination stage.

Table 2-18 displays Fe and Mn concentrations in Fishmoore and Oswestry water samples where there is variation in levels of both metals at different

stages of treatment but some stages of the treatment lead to higher Mn than Fe at FSF and Oswestry RGF. In addition, Fe seems to be higher than Mn at other stages such as, raw water, ACC1, ACC2 in Fishmoore and Oswestry raw water samples.

**Table 2-18** Metal content in Fishmoore water samples. The values are metal concentration ( $\mu\text{g}/\text{mL}$ ), percentage recoveries and RSD for Fe and Mn.

Wavelength/nm	Raw	FSF	FSS	ACC1	ACC2	Final
<b>Fe 238.2</b>	0.0631	0.0034	0.0022	0.0477	0.0417	<LoD
<b>Spike recovery (%)</b>	105	107	100.9	102	96.6	90.6
<b>RSD (%)</b>	5.3	3.2	4.5	2.8	5.1	3.1
<b>Mn 257.6</b>	0.023	0.0135	0.0001	0.0119	0.013	<LoD
<b>Spike recovery (%)</b>	96.7	104.5	99.7	102.3	98.4	100.6
<b>RSD (%)</b>	5.1	3.7	3.2	4.8	2.8	3.4

**Table 2-19** Metal contents in Oswestry Water Samples. The values are metal concentration ( $\mu\text{g}/\text{mL}$ ), percentage recoveries and RSD for Fe and Mn.

Wavelength/nm	Oswestry RGF	Final	Slow common	Pilot	Sand filter	Raw
<b>Mn 257.6</b>	0.0219	0.0012	0.0008	0.0009	0.0006	0.0012
<b>Spike recovery (%)</b>	101.3	102.8	97.4	99	96.8	95.8
<b>RSD (%)</b>	4.1	2.8	3.2	3.5	4.5	5.1
<b>Fe 238.2</b>	0.001	<LOD	0.0011	0.001	0.0011	0.004
<b>Spike recovery (%)</b>	102.4	99.8	102.1	99.9	103.8	100.6
<b>RSD (%)</b>	2.5	3.4	5.1	3.7	5.2	2.8

**Table 2-20** Metal contents in Huntington Water Samples. The values are metal concentration ( $\mu\text{g /mL}$ ), percentage recoveries and RSD for Fe and Mn.

<b>Wavelength/nm</b>	<b>Raw Huntington</b>	<b>FSF</b>	<b>SSF</b>	<b>PCF1</b>	<b>PCF2</b>	<b>SS (combined)</b>	<b>Final1</b>	<b>Final2</b>
<b>Fe 238.2</b>	0.0144	< LOD	< LOD	0.0477	0.0417	0.019	< LOD	<LOD
<b>Spike recovery (%)</b>	99.4	100.2	100.5	102.1	97.4	99.5	100.4	99.2
<b>RSD (%)</b>	5.1	3.3	4.5	2.9	3.7	3.9	5.4	3.4
<b>Mn 2576</b>	0.017	0.0135	0.0045	0.011	0.013	0.0048	0.0045	< LOD
<b>Spike recovery (%)</b>	101.6	96.8	95.8	104.7	99.7	102.3	97.2	102.3
<b>RSD (%)</b>	5.1	3.1	3.7	3.2	1.9	4	2.9	4.2

High concentrations of Mn occurred at the PCF (1 and 2) stages, giving 11 and 13 ppb for Mn at Huntington water. The level for Fe showed a higher concentration during the PCF stages. The Mn concentration level presented in Huntington raw water has a lower concentration of Mn than Fishmoore and Oswestry water. This may have related to the treatment process being different from one location to another. However, at all stages of the water treatment works, it has become an evident that Mn and Fe concentrations increase compared to the raw water during the Post clarified stages at Huntington water. Aluminium sulphate is used at Huntington whilst potassium permanganate is applied at Fishmoore. The increase in these concentrations of both Fe and Mn may be due to addition of the coagulants. For a more complete understanding, these coagulants need to be tested in the future with sulphuric acid samples from the water industry. The results will indicate how much amount of these reagents and materials are added. The sulphuric acid is usually added into the water just before filtration process to maintain the pH level to allow the filtration of un-precipitated material to go through. Also, this acid as part of the acidification process reduced the bicarbonate and avoids the precipitation of some metals.

These results are in line with the research undertaken by United Utilities (UU) in the past few years. One of the key challenges over the past 20 years for water companies has been the renewal and cleaning of water because of the high number of customer complaints which they receive every year. However, internal research groups of UU have shown that the key cause of the discolouration is the amount of Mn in the water entering supply. It is clear that

treatment solution to this problem has to cover a wider area than just cleaning the mains. Cleaning and renewal has improved the water quality from UU (106). In these water samples the relationship between Fe and Mn levels has shown that it is rare to have a sample with Fe level greater than the regulatory limit when the Mn level is less than the maximum level. A study of UU analysed random customer samples between 2007 and 2011 showed that about half of the samples had a Mn level above the LoD during the treatment stages of the exceeded limits on the regulatory for Fe and Mn level 50 µg/L and 200 µg/L respectively.

## 2.9 Conclusion

This study carried out the optimisation and development of ICP-OES method to determine Fe and Mn levels in different treatment plants from UU water samples. This will benefit the water industry since the discolouration of water is one of the main causes of customer contacts with over 50,000 customer contacts per year in England and Wales (DWI Chief Inspector's Reports 2012).

According to the WHO and DWI, the concentrations obtained from the Fishmoore water samples are below the maximum level recommended by the WHO.

In this work, the optimisation and validation of the ICP-OES demonstrated that a simple, robust and reliable analytical method for simultaneous determination of Fe and Mn in water samples was possible. The optimization of the parameters was essential for the determination of Fe and Mn using 11 wavelengths for both elements. Under the optimum conditions, ICP-OES was able to effectively measure low concentrations of Fe and Mn in drinking water. This was shown by obtaining LoD and LoQ values; found to be 5 ng/mL and 12 ng/mL for iron and 1.2 ng/mL and 6.7 ng/mL for Mn, respectively.

The percentage recovery (95-105%) for both SRM and water samples. The high amounts of Mn show that the water discoloration may not be related to the occurrence of Fe in water.

Generally, all the water treatment met the DWI of Fe and Mn. However, an increase of Fe and Mn removal is essential at many water treatment plants to meet most regulations because both metals change into insoluble forms of Fe and Mn, which then stick to water pipes as yellow and black colours under

sudden changes in physiochemical parameters such as velocity. Therefore, the water industry needs to minimize the discolouration occurrence by cleaning and removal processes depending on treatment plants.

Higher levels of Mn do not necessarily lead to an increased risk of discoloration of drinking water and this can be explained by the fact that there are different oxidation states or species of Mn. For example, the Pourbaix diagram (Figure 1-1) showed the different species of Mn that are formed at different pH levels (X-axis) and oxidation levels (Y-axis).  $Mn^{2+}$  is a soluble form of Mn and the normal treatment process is to oxidize the water (normally using chlorine) and raise the pH of the water in order to change it to a particulate form, which is then removed by the final filter stage (23).

This problem will be tackled in more detail in the next chapters in terms of speciation analysis. What is more important is the species of Mn that is present. In the case of Mn (IV), this presents little risk because the species normally occurs as a black solid ( $MnO_4$ ) which can be easily separated by filtration. In contrast,  $Mn^{2+}$  does present a risk of discoloration since it is a soluble, yellow coloured ion. It has been noted that different reagents are used to achieve coagulation stages at the water treatment works. Different coagulants are used for each location, and the increase in Mn concentration may be due to the addition of the coagulants. It is proposed that the concentration should be known to avoid increasing the levels of Mn through the treatment process. This method of ICP-OES analysis allowed the successful assessment of the presence of both elements in water samples. More sensitive techniques are required to verify the findings of the total concentration and species of Fe and Mn. ICP-MS will be considered for

analysis with its increased sensitivity and therefore lower detection limits; it has higher sensitivity and lower concentrations of the elements in water can be detected as low as ppt levels.

## **Chapter 3 Optimisation and development of inductively coupled plasma mass spectrometry (ICP-MS) for the analysis of Fe and Mn in drinking water**

### **3. Introduction**

This chapter describes the development, optimisation and validation of a method for the measurement of Fe and Mn concentration in drinking water by inductively coupled plasma mass spectrometry (ICP-MS). This technique simultaneously and rapidly processes samples so that the entire analytical spectrum within this range of elements can be recorded in every analysis. This differs from atomic absorption spectroscopy; which can only determine the quantity of a single element at a time. This feature, coupled with the ability to do multi-element analysis, makes ICP-MS a very attractive analytical technique. Thus, this has led to its wide scale use in the certification of reference materials (15). Boasting similar or better detection limits to that of electrothermal vaporization atomic absorption spectrometry, but also having the ability to do multi-element analysis simultaneously; ICP-MS is now increasingly used for performing low level environmental analysis (203, 204). Methods have been published for the determination of trace metals in water samples by the US environmental protection agency by ICP-MS (Method 200.8 Revision 5.4).

Recently, most research has focused on the determination of trace metal's concentration at low levels simultaneously, accurately and precisely using different techniques. ICP-MS is considered to be a highly sensitive detection

instrument and is being used in many different areas such as food, pharmaceuticals and environmental science (205, 206). Several environmental studies have reported the relationship between Fe and Mn levels and human health effects. For example, Bouchard *et al.* (207), identified a significant positive relationship between Mn concentration and classroom behaviours in a study on children in Quebec. Mn exposure in drinking water was also shown to be significantly negatively related to intellectual function of 10 year old children in Bangladesh. In a study by Wasserman *et al.* (208) of water with Mn concentration, below the WHO limits, (0.004 - 3.91 mg/l), it was shown there is a relationship between the exposure to Mn and human neurotoxic effects.

The work in this chapter describes the development and validation of a procedure for trace Fe and Mn determination in water treatment samples by ICP-MS. In this validation method, the analytical figures of merit calculated have not been determined before to the best of our knowledge for Fe and Mn in water treatment samples at different stages of the water treatment process. The following parameters were optimised and assessed: linearity, LoD, LoQ, repeatability and precision. There are many standards such as the USEPA method 200.8 which is used to assess for trace metals in water samples in United States and several other countries (209). The validation of the analytical method was carried out according to the ISO guide and was applied to the SRM and water samples. Therefore, the developed method for the validation and precision was carried out according to the USPE guide (28). The ICP-MS obtained complete information on trace metals in water in sub -

µg/L ranges. This capability of the instrument could be used for the simultaneous routine analysis in water treatment plants.

### **3.1 Experimental**

#### **3.1.1 Reagents and Materials**

Ultrapure water with a resistivity of 18.2 MΩ (0.05 µS cm<sup>-1</sup>) was obtained using a Triple Red water purification system (Triple Red Laboratory Technology, UK) and used to prepare all solutions. Single-element stock solutions for ICP-MS containing 1000 µg/mL of Fe and Mn were purchased from (SCP Science, QMx Laboratory UK) and were used to prepare the calibration solutions. All working solutions and standards were prepared weekly and acidified daily in 2% (v/v) nitric acid (HNO<sub>3</sub>). Trace metal grade acid (69 % HNO<sub>3</sub>) was purchased from Fisher (TraceMetal Grade Fisher Scientific, UK).

A tuning solution containing the elements Ce, Co, In, Ba, Tl, U, Li, Be, and Bi, in 2 % HNO<sub>3</sub> was employed. Firstly, daily performance reports were performed to evaluate the tuning criteria for precision and sensitivity that allowed the sweeping of a wide range of mass with final concentration of 10 ng/mL solution. A cross calibration was performed daily using a 50 ng/mL solution of the elements above. Three internal standards were added to the solutions; these were prepared from 1000 mg/L of Y, Sc and Rh single stock solution.

A stock solution of 500 ng/mL was prepared once a week, and this was used to prepare solutions, daily by diluting with 2% HNO<sub>3</sub> to yield the final concentration of 10 ng/mL. The three internal standards were tested and added to all samples and solution to obtain any changes in sensitivity in

different mass regions. Argon (Ar) and helium (He) high purity carrier gases (99.9995 %) were used (Air Products, CryoEase Services, UK).

### **3.1.2 Glassware and cone cleaning**

To avoid contamination, all labware was washed and soaked overnight in 5% (v/v) HNO<sub>3</sub> solution, and triple rinsed thoroughly with deionized water prior to use. The instrument components were cleaned daily as follows: The nebulizer was soaked in 5% nitric acid for 10 minutes. The spray chamber was soaked in Decon-90 phosphate free detergent (In-Situ Europe Ltd Decon, Laboratories limited, Uk) overnight and then rinsed, allowed to dry, then refitted into the instrument. The torch was soaked in *aqua regia* (1:3 HNO<sub>3</sub>: HCl) overnight. It was also necessary to clean the interface sampler and skimmer cones due to the build-up of deposits on the orifice and the cone, which appeared to become discoloured from the heat required for plasma generation. This deposit reduced the sensitivity of the instrument. In addition, it can also affect the quality of the analysis and the stability of the instrument. The interface cones were simply cleaned with deionised water, in an ultrasonic bath for at least 10 minutes. Afterwards, the cones were retrieved using the removal tools, and refitted back into the instrument. Figure 3-1 shows the cone torch before and after cleaning.



**Figure 3-1** Skimmer and sampler cones before (left) and after cleaning (right) in an ultrasonic bath.

### **3.1.3 Reference materials and samples**

The accuracy and precision of the analytical method were validated using standard reference material SRM TMDA-70 trace elements in Canada river water (LGC Standards, UK). Water samples were collected from different locations in Northwest region of England, and the all sample were analysed using different techniques. For sample preparation, 0.45  $\mu\text{m}$  filters were used. The metal contents of both elements of these samples were used for the method validation and determined by ICP-MS. Each sample was analyzed in triplicate.

## **3.2 ICP-MS determination procedure**

### **3.2.1 Instrumentation**

The samples were analysed using the Thermo Fisher Scientific X-series ICP-MS, which was equipped with a quadruple mass spectrometer. Two modes were used for the study. In standard mode, sample solutions were pumped via a peristaltic pump from a CETAC ASX 520 (Thermo UK) series auto sampler. The torch position, gas output, ion lenses, resolution, and background were

optimised daily. Short-term stability performance tests of the instrument using tuning solution were also performed daily, to verify that the resolution and mass calibration for the ion species of interest were of the required standard. Further ICP-MS operating conditions are summarised in Table 3-1. The conditions were optimised to obtain the highest signal to blank ratio for  $^{56}\text{Fe}$ ,  $^{57}\text{Fe}$ ,  $^{58}\text{Fe}$  and  $^{55}\text{Mn}$ ; the highest sensitivity and maximum interference resolution were obtained.

**Table 3-1** Instrumental parameters for ICP-MS.

<b>Operating conditions</b>	<b>Parameter range and type</b>
Nebulizer nebulizer)	concentric nebulizer (Meinhardt)
Spray chamber:	Cyclonic Spray chamber
Sample cone:	nickel
Skimmer cone:	nickel
Standard mode	adjusted daily
Plasma RF power	1400
Plasma gas flow:	0
Nebulizer gas flow	0.89
Auxiliary gas flow	0.8
Sample depth	160
Collision gas	He Gas
Flow:	l min <sup>-1</sup> , 0–10
Mass range:	(uma) 7–208
Number of channels:	300
Number of channels per peak:	3
Dwell time: s	160
Number of sweeps:	500

### 3.2.2 Instrumental performance

Single-elemental stock solutions for ICP-MS containing (1000 µg/mL) of each element studied (SCP Science, QMx Laboratory UK) were used to prepare analytical standards for Fe and Mn. This involved sequential dilution of the stock solutions in 2% (v/v) HNO<sub>3</sub> to yield a final concentration of 25 ng/mL and this solution was used for all the optimization analyses. The internal standard method used a solution prepared from 1 µg/mL of Rh, Y and Sc stock solution, by dilution of 1 mL of the stock into 100 mL of 2% HNO<sub>3</sub> to yield a final concentration of 10 ng/mL.

The performance test for standard mode of operation was performed, and if the instrument passed, He was pumped into the instrument for 1 hour if the CCT mode was being used for analysis. Thereafter, the CCT mode performance test was performed, and then if the instrument passed the tests in this mode, the instrument was used for the experiment. For this purpose, solutions were prepared by using 1 µg/mL stock solution, to obtain 50 mL each of tune and X-cal solutions in 2% HNO<sub>3</sub>. The final concentration of tune solution was 10 ng/mL, and 50 ng/mL for the X-Cal solution. The X-cal was used to calibrate the two detectors used in the ICP-MS, which were the pulse counter and analogue detector. The pulse counter was used to measure the signal at lower concentrations, below 50 ng/mL, and the analogue detector was used to measure higher signals at concentrations above 50 ng/mL. To evaluate whether the coefficients for the instrument relating to oxides and doubly charged ions were acceptable, the ratio of net isotope signals observed for a standard solution needed to be determined daily. This test allowed

maximization of the ion signals and minimization of the interference effects due to high oxide levels, ( $\text{Ce O/Ce} < 0.0200$ ). If the  $\text{CeO/Ce}$  oxide ratio was below 0.02 or 2%, it was assumed the oxide formation was at a minimum. Once the instrument passed the performance assessment then the analysis of Fe and Mn was assessed by the selected isotopes  $\text{Fe}^{56}$ ,  $\text{Fe}^{54}$ ,  $\text{Fe}^{57}$ ,  $\text{Fe}^{58}$  and  $\text{Mn}^{55}$  as analytical mass in ICP-MS with standard solutions using both the standard and CCT mode of operation. This ensured that reliable data was achieved.

After the performance test had been passed all of the experimental samples were prepared for analysis, as described above (3.1.1). The calibration blank and standards were prepared in 2% nitric acid in concentrations ranging between (2- 50 ng/mL in 100 mL) for all experiments, except for those used to determine the limit of detection limits which were in the range of 5-100 ng/mL for Fe and Mn. The instrument was then optimized for several parameters to obtain the best settings for each, for sample determination. RSD less than 5 was achieved for all experiments. The signal for both elements and the ratio of selected masses were calculated for each sample with three readings to obtain the best precision and accuracy of these results.

### **3.2.3 Collision cell technology mode**

The second mode employed in the experiments made use of collision cell technology (CCT). The instrumentation used was the same as described in Section 3.2.1, with the exception of the collision cell. The instrument passes the sample into a collision cell where a non-reactive gas, such as helium, is added. Interferences can occur when polyatomic ions have the same mass-

to-charge ratio as the species of interest. Polyatomic ions formed in the ionisation chamber have a larger cross-sectional area than the single atom analyte ions, and thus are more likely to collide with the reaction gas in the reaction cell. In the collision cell, two main processes occur; chemical reactions between the polyatomic ion species and the added gas, and charge transfer from the polyatomic ion species to the added gas. These processes together remove many of the solvent and Ar polyatomic spectral interferences. Also, a CCT mode configuration is used that reduces Fe by the matrix into the collision cell. Due to this there is a loss of sensitivity in the instrument over time. Therefore, the use of both standards and CCT modes to find analyte concentrations in the sample offers a good combination of performances and simplicity of the sample matrices.

### **3.3 Analytical figures of merit**

#### **3.3.1 The optimisation of ICP-MS conditions**

The operation parameters of the ICP-MS affect the analytical results by influencing sensitivity, signal, and type of interference, etc. The setting of these parameters must be independently optimised to obtain the maximum signal and signal to blank ratio of each selected isotope. The optimisation of ICP-MS appeared in the 1990's in several papers (210, 211); one of these papers reported the optimisation of the ICP-MS plasma and ion optics parameters using 10 elements and measured the signal-to-blank ratio. The other papers focused on different parameters and settings using standard or collision reaction cell mode and were applied to the determination of specific elements.

The ICP-MS instrument parameters were fully optimised to determine the best signal- and signal-to-blank ratio in order to achieve the maximum sensitivity. The optimization process was carried out using three replicates of a 25 ng/mL Fe and Mn solution in 2% HNO<sub>3</sub>. The parameters themselves were divided by the Plasma lab software (Thermo, UK) into four groups; Major, Minor, Global and Add Gas. The optimum conditions for parameters were optimised depending on their purpose on the instrument including the nebuliser; auxiliary and coolant which are related to the gas flow rate parameters; the torch position parameters (horizontal, vertical and sampling depth); the quadrupole and acquisition parameters (forward power, pole bias, standard resolution, sweeps, Dwell time) and the focusing parameters which related to the lenses position, ion flow and deflectors. Figure 3-2 and Table 3-2 show the individual components and the settings for the mass spectrometer, respectively. The parameters were determined to assess their potential to achieve maximum sensitivity. The major and minor parameters are the most common ones used for tuning, and these have the greatest effect on signal sensitivity and stability, and are changed by adjusting the voltage for every single parameter individually. The global parameters (standard resolution, high resolution, analogue detector, PC detector) relate to the detector. These conditions were applied for the determination of both elements as will be described in the coming sections. The short-term stability test for the instrument was carried out by optimizing the ion lenses, torch position and gas flow. All were optimized daily with the tuning solution. This test was used to minimize interference effects from doubly charged ions and to maximise ion signals

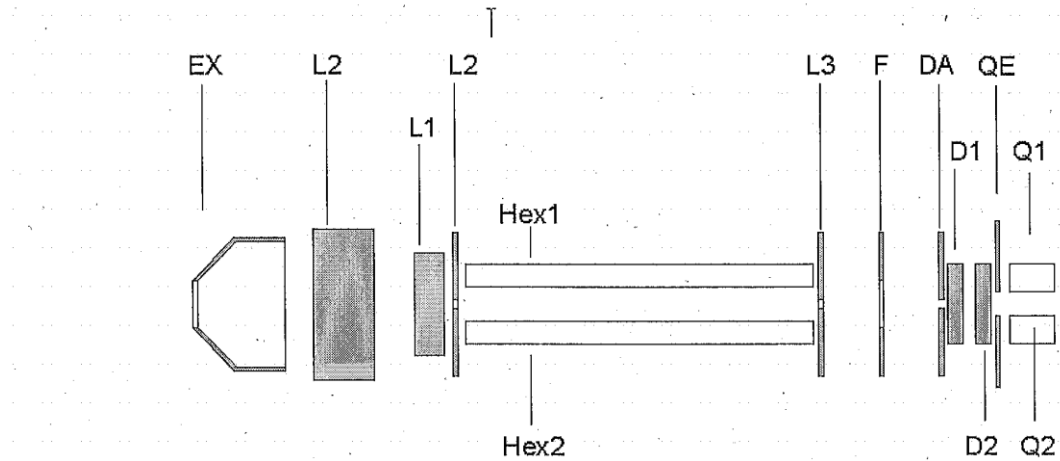


**Figure 3-2** Schematic of X series ion optics.

**Table 3-2** Ion optics parameters.

Abbreviation	Parameters
Ex	Extractor
L1	Lens 1
L2	Lens 2
L3	Lens 3
Hex	Hexapole RF
Hex2	Hexapole Rf
F	Focus
DA	Differential aperture
D1	Deflector
D2	Deflector
QE	Quadrupole entrance
Q1	Quadrupole RF
Q2	Quadrupole RF

### 3.3.1.1 The optimum conditions for the standard mode

The determination of the optimum conditions for standard mode was divided into two stages as follows.

#### 3.3.1.1.1 The determination of the major optimum parameters

All the optimisation procedures were carried out as previously described in section 3.2.5 using the same preparation methods. The major parameters optimised were as follows; extraction (0-1000), D1 (0 to -80), focus (0-50), hexapole (10 to -10), lens (24 to -200), nebulizer gas (0.5-1.0), pole bias (10 to -10) and sample depth (50-600). The experimental data were processed by using Plasma software (Thermo Fisher UK), and the data was exported to an Excel (Microsoft, UK) spreadsheet for the preparation of all the graphs. The counts per second (CPS) for the signal- and the signal to blank ratio were plotted against the adjustment range for each parameter, and the graphs were used to obtain the optimum conditions for the ICP-MS analysis. Table 3-3 shows the steps for each major parameter.

**Table 3-3** Major parameters.

<b>sample dep</b>	<b>PB</b>	<b>Neb</b>	<b>Hex</b>	<b>Ext</b>	<b>F</b>	<b>D1</b>	<b>L1</b>
50	10	1.5	10	0	0	0	24
100	8	1.45	8	-50	10	-20	-50
150	6	1.35	6	-100	20	-40	-100
200	4	1.25	4	-150	30	-60	-150
250	2	1.12	2	-200	40	-80	-200
300	0	1	0	-400			
350	-2	0.9	-2	-600			
400	-4	0.8	-4	-800			
450	-6	0.7	-6	-1000			
500	-8	0.6	-8				
550	-10	0.5	-10				
600							

### 3.3.1.3 The determination of the minor optimum parameters

All the optimisation procedures were carried out as previously described in Section 2.1.3.3 using the same preparation methods, but with adjustments to the minor parameters as follow: lens 3 varied between (0 to-200), forward power (800 to 1600), horizontal (0-160), vertical (0-811), D2 (0 to -400), auxiliary (0-1.5), DA (0 to-200), coolant (8-20), lens 2 (0 to-200) and Add Gas (3.3-10). The experimental data were processed using Plasma software (Thermo Fisher UK), and the data was exported to an Excel (Microsoft, UK) spreadsheet for the preparation of all the graphs. The counts per second (CPS) for the signal, and the signal to blank ratio were plotted against the adjustment range for each parameter, and the best optimum conditions were chosen at the greatest signal to blank ratio for Fe and Mn. Table 3-4 shows the steps for each of the minor parameters.

**Table 3-4** Minor parameters.

<b>L3</b>	<b>L2</b>	<b>Aux</b>	<b>He</b>	<b>Ver</b>	<b>Hor</b>	<b>D2</b>	<b>cool</b>	<b>DA</b>	<b>FW</b>
0	0	0	3.3	0	0	0	8	0	750
-20	-20	0.2	3.5	100	20	-50	10	-50	800
-40	-40	0.4	4	200	40	-100	12	-100	1000
-60	-60	0.6	4.5	300	60	-150	14	-150	1200
-80	-80	0.8	5	400	80	-200	16	-200	1400
-100	-100	1	6	500	100	-250	18		1600
-120	-120	1.1	7	600	120	-300	20		
-140	-140	1.2	8	700	140	-350			
-160	-160	1.3	9	800	160	-400			
-180	-180	1.4	10	811					
-200	-200	1.5							

#### **3.3.1.4 The determination of the add gas parameters optimum parameters**

The maximum signal and signal to blank ratio for each analyte ion was obtained after passing of the ions through the reaction cell, using He as a collision gas. The flow rate of the gas was varied between 0-10 mL per minute. The experimental data were processed using Plasma Lab software (Thermo Fisher UK), and the data was exported to an Excel (Microsoft, UK) spreadsheet for the preparation of all the graphs. The counts per second (CPS) for the signal and the signal to blank ratio were plotted against the adjustment range for each parameter, and the graphs were used to obtain the optimum conditions for the ICP-MS analysis.

The most suitable conditions for analysis in standard mode and for CCT mode were selected for each element on the basis of sensitivity.

### **3.4 Analytical figures of merit**

The analytical figures of merit were calculated in both standard and CCT modes. Prior to analysing unknown samples and the method validation, LoD, LoQ, linearity, and percentage recovery were established for each analyte at the optimum set of conditions determined above. The LoD and LoQ were calculated using the method suggested by Miller and Miller (202). This involved the calibration of the instrument and then the measurement of a blank ( $n = 10$ ). The blank solution of 2% nitric acid was prepared and was analyzed as an unknown sample using ten replicate measurements. From this result,

the LoD was calculated for Fe and Mn using Excel software. For LoD, the average corrected mass for the blank was added to three times the standard deviation of the blank signal (212). For LoQ the same calculation was used except 10 times the standard deviation of the blank was used. In both cases, the equation of the calibration line was used to convert the obtained signal into a concentration value.

The accuracy and precision of this method were evaluated using the analysis of Canadian River Water (TMDA-70 and TMDA 62.4) as standard reference materials purchased from LGC Standards, UK. The accuracy was assessed by using a similar matrix to the samples with a known composition. The analysis of replicates of such samples provide data on repeatability and accuracy. The percentage recoveries were calculated for both water samples and certified reference material.

### **3.4.1 Isotope selection**

The calibration included a number of different isotopes for Fe and one Mn isotope for both analytes, these isotopes may suffer from interferences in ICP-MS depending on sample preparation and matrix. Some of these interferences can be overcome by choosing a different isotope or correction, but for Mn an alternative is not available because it is a monoisotopic element ( $^{55}\text{Mn}$ ). Fe isotopes are subjected to critical interference by ArO and ArN ions for  $^{56}\text{Fe}$  with 92% abundance and  $^{54}\text{Fe}$  with 6%. The optimisation of different instrument parameters verified that a less abundant isotope was selected,  $^{57}\text{Fe}$  with 2.2% abundance because ArO interference is much less than with other isotopes. With this experiment it was possible to choose the greatest sensitivity of each

isotope and the signal to blank ratio for both elements used for quantification measurements.

A benefit to using CCT mode was that the LoD and LoQ was lower than when the standard mode was used for Fe and Mn by ICP-MS. The results from the analysis of SRM (TMDA) and spike recovery study of diluted and undiluted drinking water SRM is shown in the results section. Finally, drinking water spike recovery data were obtained from United Utilities water samples and are shown in the results section (3.6). It can be seen that almost all the spike recoveries and SRM values are within the drinking water criteria  $\pm 10\%$ . Measured values and spike recoveries of trace elements in Standards Trace Metals in Drinking Water (TMDW) SRM using ICP-MS (data for both the neat sample and a 10-x dilution of the sample) were calculated.

### **3.4.2 Linearity**

Although ICP-MS is a well-known technique for the determination of a wide range of concentrations, the linearity was evaluated by checking the linear correlation coefficient ( $R^2$ ) of the calibration obtained for the standards. The  $R^2$  value and the linearity of the calibration were acceptable when  $R^2 > 0.995$ . The linearity was verified by the calibration standards; prepared from 1000 mg/mL Fe and Mn using a series of concentrations ranging from 0.5 ng/mL-1000  $\mu\text{g/mL}$  in water with 2% nitric acid. A blank was made in the same matrix. LoD was calculated for Fe and Mn using the same approach as previously described in Chapter 2, Section 2.7.1.

### **3.4.3 Precision**

Six spiked samples were measured on different days. The final Fe and Mn masses were obtained by the spiked method as well as the repeatability and precision. The repeatability of the method was calculated by evaluating the RSD.

### **3.4 Validation using recovery studies**

The validation and accuracy of the method used for this study were verified using standard reference materials SRM TMDA-70 and TMDA64.2 (trace elements in River Water). In addition, spiked samples with known concentration (30-50 ng/mL) of Fe and Mn were tested. The results were evaluated by calculating the percentage recovery of the signal for both the water samples tested and certified reference material, after spiking. The method was considered valid when the recovery percentage calculated achieved a range between 95-105%, using the average measurements for SRM over 5 days. The recovery percentage was calculated using the following equation (3.1).

$$\frac{(\text{Spiked Sample concentration} - \text{No spiked concentration})}{\text{Spike concentration}} \times 100 \quad (\text{Equation 3-1})$$

The variability of the results that described the precision of this method was evaluated by the determination of each sample with ten repeats using relative standard deviation. SRM and River Water (TMDA62.4) was analysed for the determination of both Fe and Mn by ICP-MS. The spike recovery experiment

was used to verify the analytical method using 30 mg/mL of both selected elements.

### **3.5 Sample collection and analysis**

The method was evaluated by the analysis of water processing samples from different locations across the Northwest region of England, to ensure that the methodology functioned appropriately with real samples. The sample location has been provided previously in Section (1.10) with a map showing the location in Figure 2-2. These were collected from the local water supplier, UU. Prior to analysis, these samples were stabilized with (2%) nitric or hydrochloric acid. All the samples sources, and analytical results obtained from these samples are presented in the results section (3.6). The samples were placed in disposable sterile polypropylene (50 mL) centrifuge tubes (Fisher Scientific) and transported to the lab, where they were kept frozen until analysis to prevent the oxidation of the minerals in the sample.

To determine the Mn and Fe contents of the water samples, the samples were filtered through filter membranes (PTFE) with pore sizes of 0.45  $\mu\text{m}$ . Thereafter, 4 mL of each sample was prepared to obtain final concentrations of 2%  $\text{HNO}_3$  and 0.1  $\mu\text{g/mL}$  of the internal standard Rh and/or 10 ng/mL of Sc. The internal standard was added in order to reduce any adverse effects due to differences in viscosities of the sample solutions and easily ionisable element concentrations such as Na and K. The samples were then diluted to a final volume of 10 mL with DW (Triple Red, UK).

## **3.6 Results and discussion**

### **3.6.1 Optimisation of ICP-MS and assessment of analytical figures of merit**

A new method for the determination of Fe and Mn in water samples was developed and validated. The following parameters to allow analysis of the water treatment samples were obtained: figure of merit, linearity, accuracy, precision, LoD and LoQ.

ICP-MS was optimised under different conditions, as listed previously in Tables 3-3 and 3-4, for standard and CCT modes, respectively. The use of the collision cell technology also required the optimisation of the parameters associated with the flow rate, the pole bias, and hexapole bias voltages. These were then applied to the collision cells before ion separation at the quadrupole. These parameters enabled the achievement of the best sensitivity and quantitation of both the Fe and Mn in the water processing samples and have been detailed in the ICP-OES section 2.11. The signal to blank ratio and CCT were used since the signals for different isotopes could not be used because of the interferences.

A performance test in the standard mode with 10 ng/l of tuning solution was used daily to optimise the torch position and the ion lenses, in order to maximize the ion signals, oxide levels and stability of the ICP-MS. This test was followed by flushing of the collision cell with collision gases (He) for one hour after the standard test was performed as described in section 3.2.3. Tuning solutions used for the test and the optimisation of these parameters

were explained in Section 2.2.3. The mass to charge ratio, ( $m/z$ ), of  $^{55}\text{Mn}$  was used to monitor Mn and the two major iron isotopes  $^{57}\text{Fe}$  and  $^{56}\text{Fe}$  with relative abundances of  $^{56}\text{Fe}$  – 91.72% and  $^{57}\text{Fe}$  – 2.2%, were monitored in both standard and CCT mode.  $^{58}\text{Fe}$  was removed because of sensitivity issues. 10 ng/mL of  $^{103}\text{Rh}$  solution was used as an internal standard in initial investigations.

### **3.6.2 Major parameter optimisation**

The major parameters are the most common ones for tuning and have the greatest effect on signal stability and sensitivity. These parameters were optimised for both Fe and Mn to obtain the best signal and signal to blank ratio for each isotope. Mn, has only one isotope;  $^{55}\text{Mn}$ ; and thus, is easy to select the most abundant isotope of this element. In contrast, Fe has four isotopes; with the abundances being in the order of  $^{56}\text{Fe}$ , followed by  $^{58}\text{Fe}$ ,  $^{57}\text{Fe}$  and  $^{54}\text{Fe}$  (213). The calibration response for all the analytes is presented below. The major parameters were optimised, and the best signal-to-blank ratio was selected after plotting the calibration curves for each single parameter, using the solution prepared as detailed in sections 3.2.1 and 3.2.2. The torch was generally centred on the sample cone, starting with D1, followed by Extraction, Lens 1, Focus, then Pole Bias, monitoring how the signal changed with each adjustment. Each of the lenses was adjusted in sequence until the optimum signal was obtained. All the parameters were optimised before the analysis, as changing any of them during the analysis would have affected the signal and the sensitivity of the ICP-MS.

### **3.6.2.1 The optimum conditions for the standard mode**

The goal of the optimisation requires both lenses (L1 and L2, Figure 3-2) to be varied to determine the true maximum over a wide enough range because both lenses interact. These lenses retain the negative ions or neutral species in the system. A smaller value of L2 gives a lower signal while setting a larger value will increase the signal. The hexapole bias (HB) will normally be set slightly lower in the CCT mode and must be at the negative value. This is because when the cell is pressurised the ions tend to adopt the bias potential and then they leave the collision cell with the same ion energy as HB.

F and DA (Figure 3-2) also interact, so DA was set, and F tuned to maximise the signal. D1 and D2 also interact, and again D1 was set and D2 tuned and optimised. The deflectors may optimise at a lower or higher voltage. The extractor accelerates ions from the beam when it passes through the skimmer and focuses them towards the axis. The voltages depend on the operating mode applied. In all modes, over time the optimum voltage gradually changes. This is often caused by sample deposition on the skimmer that contains a high matrix concentration, if this matrix concentration remains the same substantially, the tuning will stabilise as the cones become conditioned to the matrix. This voltage was usually low with a new cone, but it increases as the cone ages. These are deflectors of the ionic flow retaining the photons generated from plasma from reaching the detector.

### **3.6.2.2 The determination of the optimum D1**

Figure 3-3 displays the optimisation of sensitivity and signal response for the major parameters: D1 for  $^{55}\text{Mn}$  and  $^{56}\text{Fe}$ ,  $^{57}\text{Fe}$  and  $^{58}\text{Fe}$  presented by the

double Y axes of signal and signal to blank ratio plotted against the values for D1. These calibrations were examined and the best sensitivity for the instrument was assessed as being when the D1 value was set at -40. For  $^{55}\text{Mn}$  the signal and *signal to blank ratio* were high at -40. Fe isotopes were varied in the results on each graph so that the greatest signal and signal to blank ratio were for D1 for  $^{57}\text{Fe}$ .

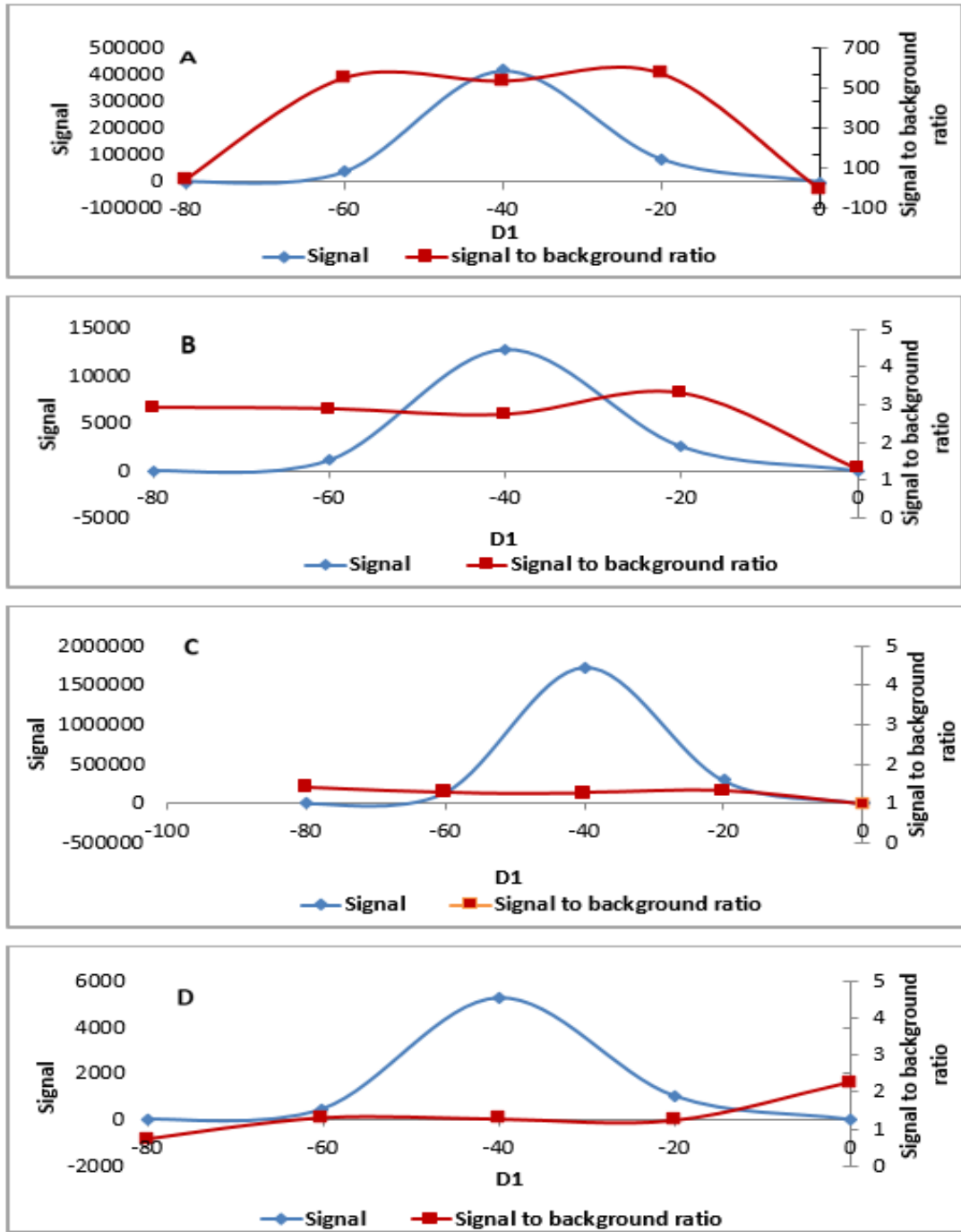


**Figure 3-3** Signal and signal to blank ratio for D1 for  $^{55}\text{Mn}$  (A),  $^{56}\text{Fe}$  (B),  $^{57}\text{Fe}$  (C) and  $^{58}\text{Fe}$  (D).

### 3.6.2.3 The determination of the optimum Extraction

The optimisation of sensitivity and signal response for the extraction voltage used for  $^{55}\text{Mn}$  and  $^{56}\text{Fe}$ ,  $^{57}\text{Fe}$  and  $^{58}\text{Fe}$  are represented in Figure 3-4 for both signal and the signal to charge ratio. It can be seen that the optimal greatest

signal is for  $^{54}\text{Fe}$  (blue). Looking at the optimal signal to blank ratio from the graph, the optimum signal for the extraction is -200 V. This gives the most sensitive signal. The extraction voltage attracts the ions from the plasma and is negatively charged as the ions are positively charged. The optimum voltage will be related to the mass of the ions. Here the ions studied are similar in mass and hence the optimum is similar. As the extraction researches over -200 V the signal and signal to blank ratio drops down because of the sensitivity of the instrument. The dip at -50 V (orange) is due to a change of background signal. For  $^{55}\text{Mn}$ , which is the only isotope for Mn, the signal and signal to blank ratio were high at -200.

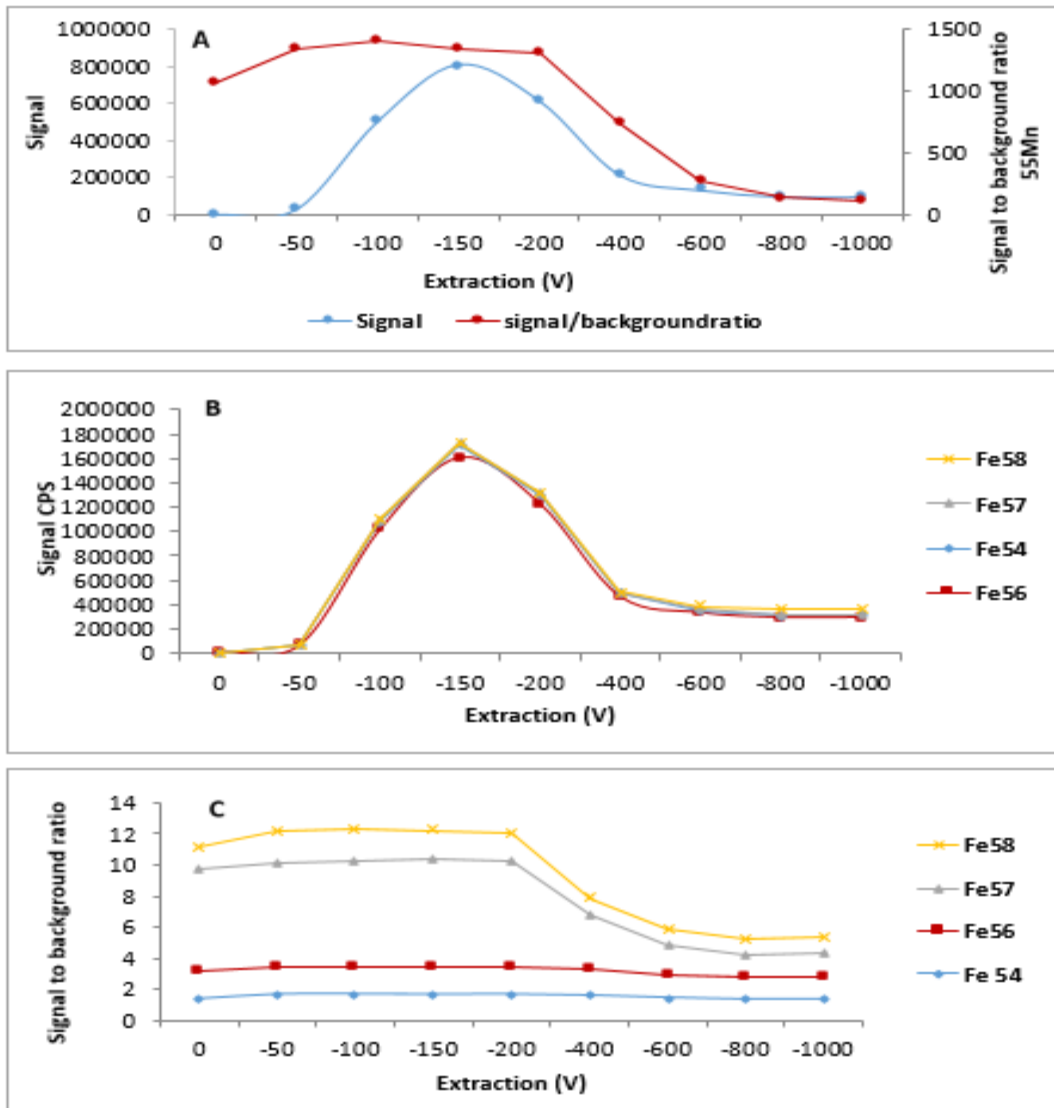


**Figure 3-4** Signal and signal to blank ratio for extraction for <sup>55</sup>Mn (A), <sup>56</sup>Fe, <sup>57</sup>Fe and <sup>58</sup>Fe (B and C).

### **3.6.2.4 The determination of the optimum nebulizer**

The nebulizer flow rate was varied for  $^{55}\text{Mn}$  and the Fe isotopes and the results are shown in the Figure 3-5. These response plots were examined and the best sensitivity for the instrument was assessed as being when the nebulizer flow rate value was set at 0.89 - 1.5 L/min. The nebuliser is used to form a consistent sample aerosol that mixes with the Ar gas, which is then sent to the ICP. The changes in Ar flow rate in the nebuliser affect droplet formation. For example, at lower flow rates, few small droplets are formed and hence lower signals. As flow rate increases, smaller droplets increase to an optimum. After this point, the higher flow rates reduce the formation of small droplets causing the signal to decrease. For  $^{55}\text{Mn}$  the signal and signal to blank ratio were largest at 0.8 – 0.9. Results for Fe isotopes were varied and the flow rate was adjusted based on the signal and signal to blank ratios shown in Figure 3-5.

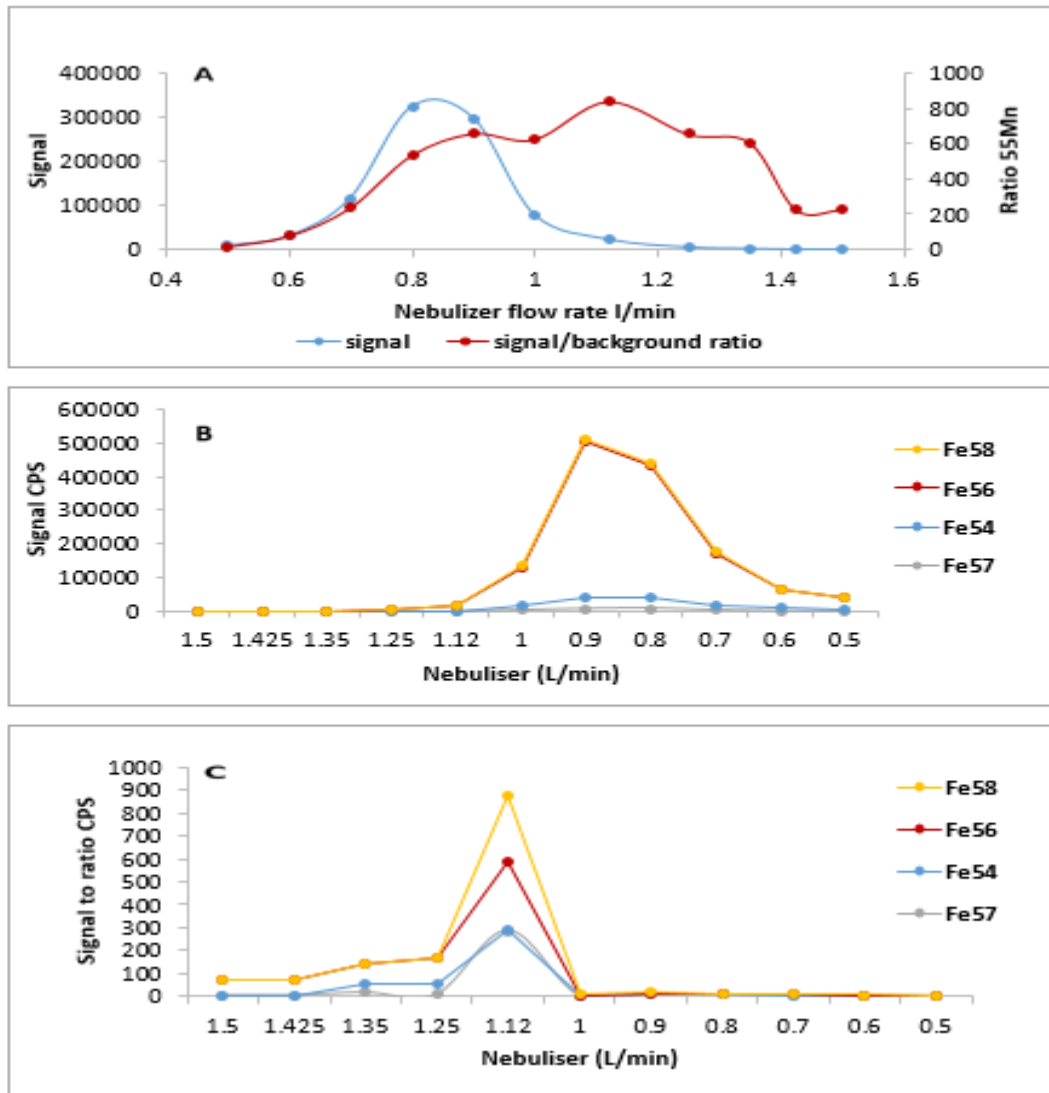


**Figure 3-5** Signal and signal to blank ratio for nebuliser for  $^{55}\text{Mn}$  (A),  $^{58}\text{Fe}$ ,  $^{56}\text{Fe}$ ,  $^{54}\text{Fe}$  and  $^{57}\text{Fe}$  (B and C).

### 3.6.2.5 The determination of the optimum Focus

The Focus is used in standard mode for removing Ar based interferences. Measurements of signal with different values of  $^{55}\text{Mn}$  and  $^{56}\text{Fe}$  are shown in Figure 3-6. These calibrations were examined and the best sensitivity for the instrument was assessed as being when the Focus value was set at 10 in standard mode. Care must be taken because increase of the signal of the blank will change the optimum result. For  $^{55}\text{Mn}$  the greatest signal and signal to blank ratio were observed for a value of 10. The value of ten was also optimum for  $^{57}\text{Fe}$  and  $^{58}\text{Fe}$ , however, not for  $^{56}\text{Fe}$ , which needed higher flow rates. Overall, the value of ten was used to cover as many isotopes as possible.

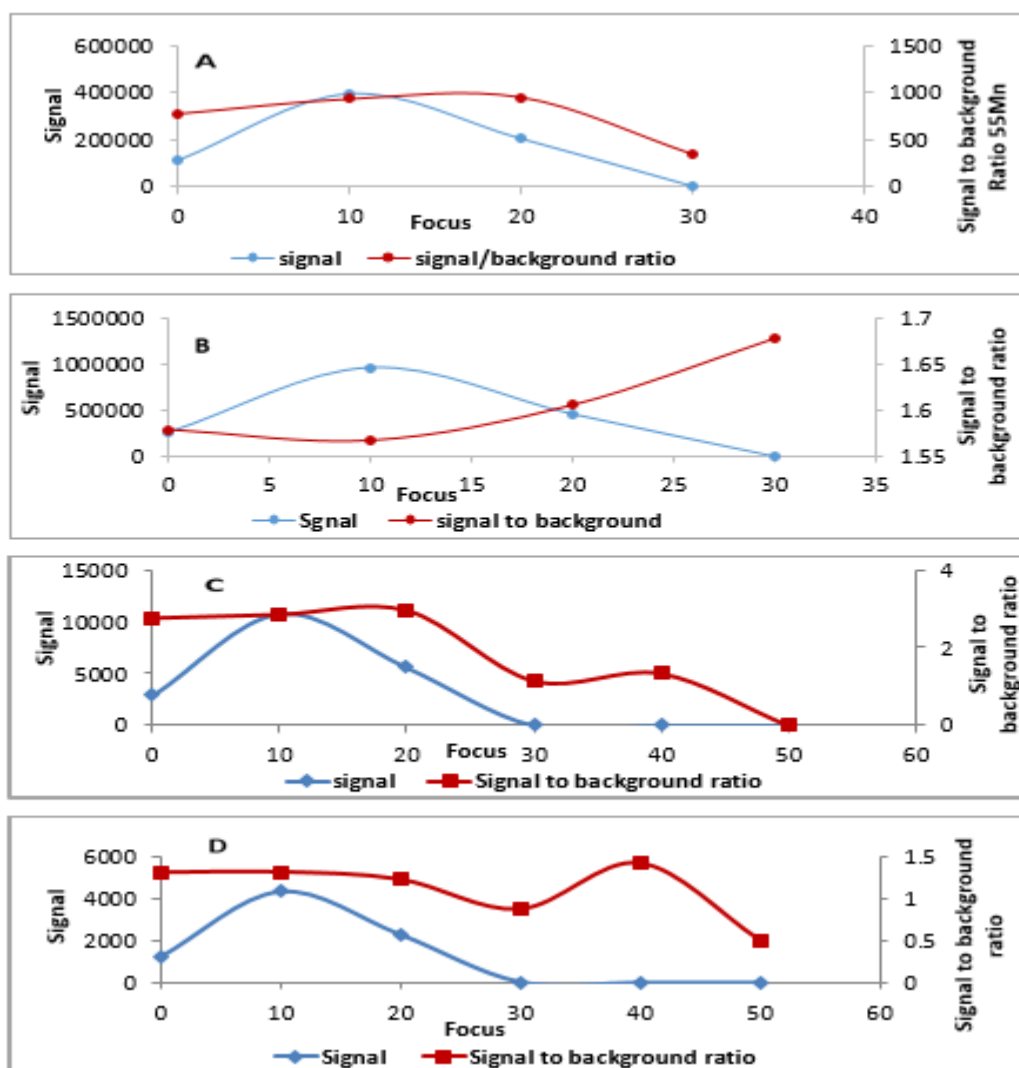


**Figure 3-6** Signal and signal to blank ratio for focus in standard mode for  $^{55}\text{Mn}$  (A),  $^{56}\text{Fe}$  (B),  $^{57}\text{Fe}$  (C) and  $^{58}\text{Fe}$  (D).

### 3.6.2.6 The determination of the optimum Hexapole

The role of the Hexapole is to reduce interferences due to polyatomic species. Figure 3-7 shows measurements of signal with different values of the Hexapole using the standard mode for  $^{55}\text{Mn}$  and the  $^{56}\text{Fe}$  isotopes. These graphs were examined and the best sensitivity for the instrument was assessed as being when the Hexapole value was set at -10 because of the high signal-to-noise values obtained for both Mn and Fe. The greatest signal

was observed for  $^{56}\text{Fe}$  and  $^{58}\text{Fe}$  which they were because of the weak background for this isotopes.

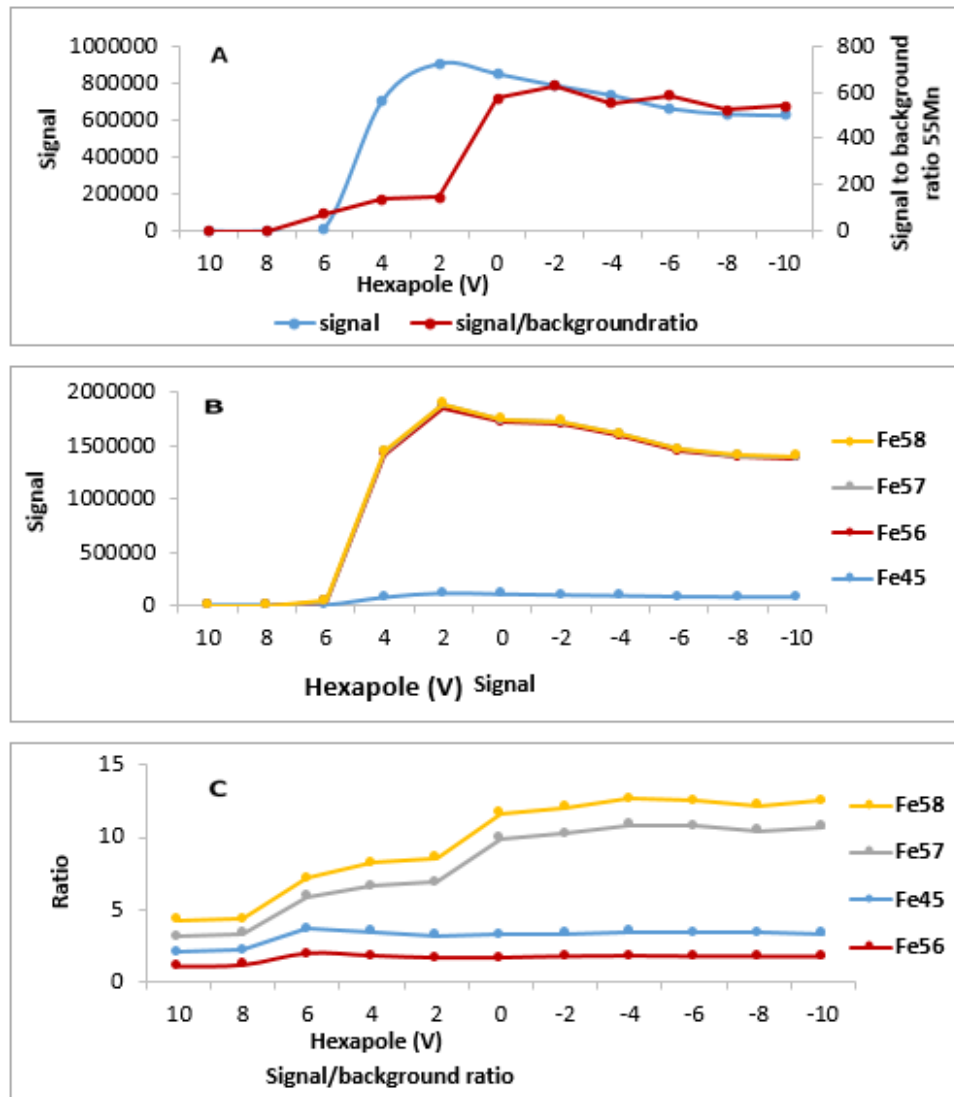


**Figure 3-7** Signal and signal to blank ratio for hexapole for  $^{55}\text{Mn}$  (A),  $^{56}\text{Fe}$ ,  $^{57}\text{Fe}$ ,  $^{54}\text{Fe}$  and  $^{58}\text{Fe}$  (B and C).

### 3.6.2.7 The determination of the optimum Pole Bias

The Pole Bias is used to obtain the optimum ion flight path through the system. Figure 3-8 shows the optimum Pole Bias study using the standard mode for  $^{55}\text{Mn}$  and  $^{56}\text{Fe}$ ,  $^{57}\text{Fe}$  and  $^{58}\text{Fe}$ . These calibrations were examined and the best sensitivity for the instrument was assessed as being when the Pole Bias value was set at -10.

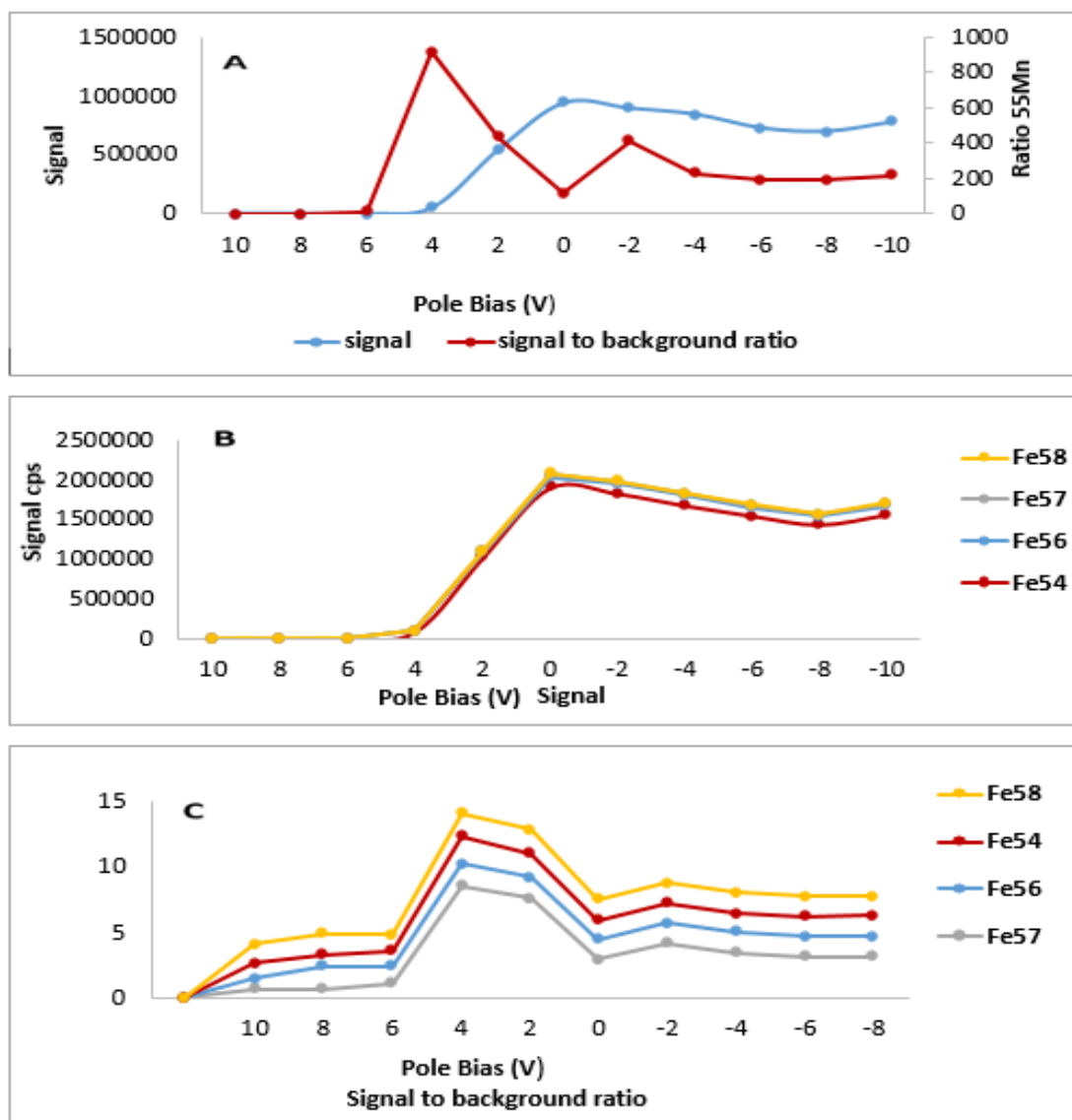


**Figure 3-8** Signal and signal to blank ratio for pole bias for  $^{55}\text{Mn}$  (A),  $^{56}\text{Fe}$ ,  $^{57}\text{Fe}$ ,  $^{54}\text{Fe}$  and  $^{58}\text{Fe}$  (B and C).

### 3.6.2.7 The determination of the optimum sample depth

Sample depths on the ICP-MS are defined as the distance between the end of the torch and the sample cone. Figure 4-9 displays the double Y axes of signal and signal to blank ratio plotted against the values for sample depth for  $^{55}\text{Mn}$  and  $^{56}\text{Fe}$ ,  $^{57}\text{Fe}$  and  $^{58}\text{Fe}$ . These calibrations were examined and the best sensitivity for the instrument was assessed as being when the sample depth value was set at 160.

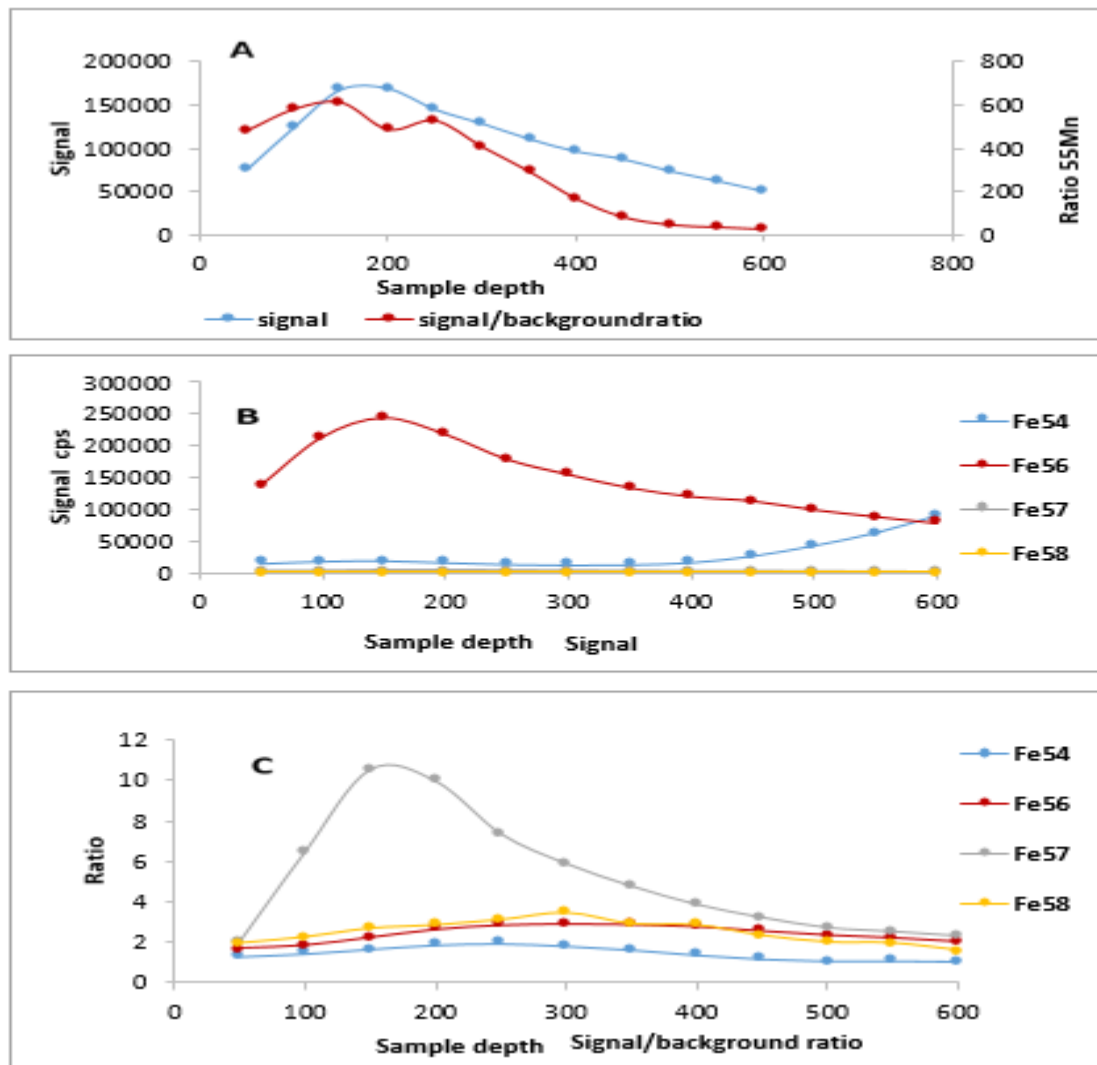


**Figure 3-9** Signal and signal to blank ratio for sample depth for  $^{55}\text{Mn}$  (A),  $^{56}\text{Fe}$ ,  $^{57}\text{Fe}$ ,  $^{54}\text{Fe}$  and  $^{58}\text{Fe}$  (B and C).

### **3.6.3 Minor parameters**

All the optimisation procedures were carried out as previously described in Section 3.2.2 using the same preparation method. However, with adjustments to the minor parameters as follows: Lens 3 varied between (0 to -200), Forward power (800 to 1600), Horizontal (0-160), Vertical (0-811), D2 (0 to -400), Auxiliary (0 to 1.5), DA (0 to-200), Coolant (8 to 20), Lens 2 (0 to -200) and Add Gas (3.3 to 10). After determination of both the Fe and Mn signals on the ICP-MS instrument using these conditions; full optimisation of the parameters was performed in a univariate manner. The experimental data were processed using Plasma software (Thermo Fisher UK), and the data was exported to an Excel (Microsoft, UK) spreadsheet for the preparation of all the graphs. The counts per second (CPS) for the signal and the signal-to-blank ratio were plotted against the adjustment range for each parameter, and the graphs were used to obtain the optimum conditions for the ICP-MS analysis.

#### **3.6.3.1 The determination of the optimum Lens2**

The lens2 is used to direct the ion beam into the collision cell. The lenses are tuned together for maximum signal. The lens2 for  $^{55}\text{Mn}$  and  $^{56}\text{Fe}$  are shown in Figure (3-10). These calibrations were examined and the greatest sensitivity for the instrument was assessed as being when the lens2 value was set at -40.

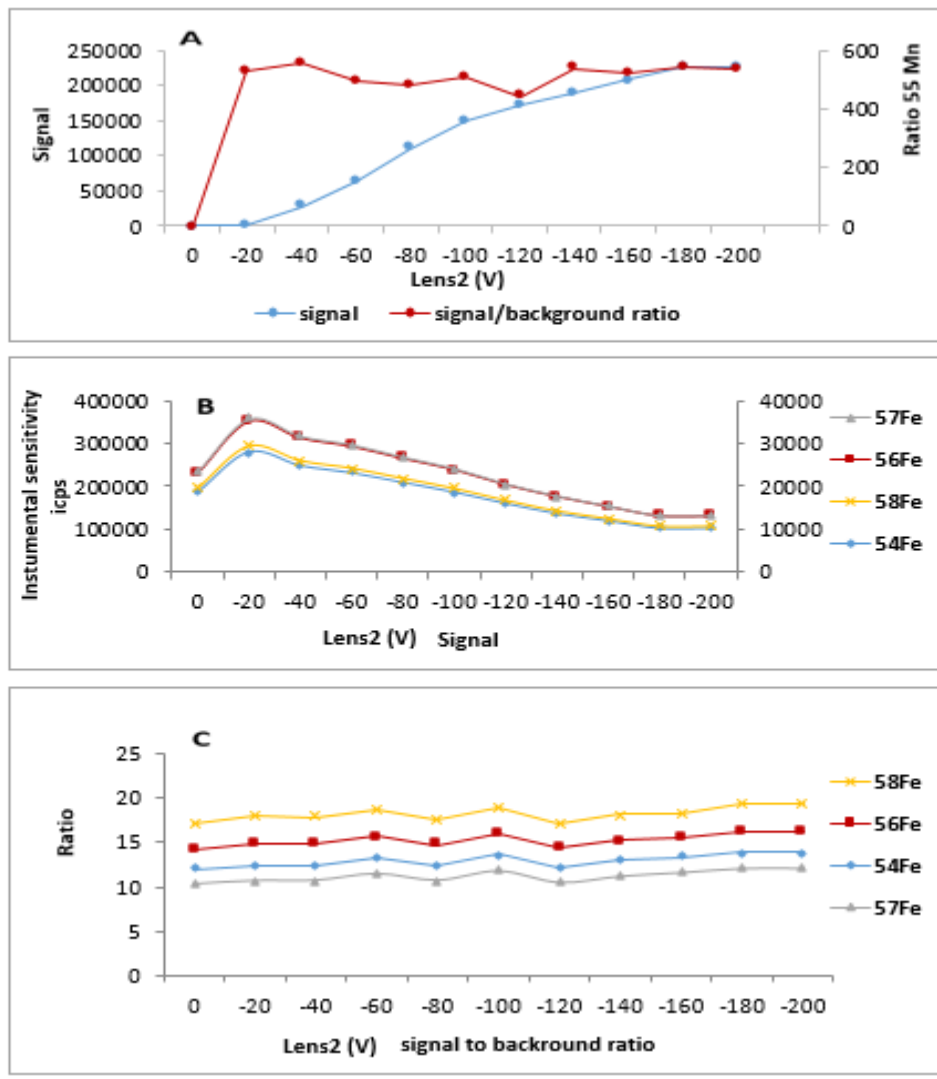


**Figure 3-10** Signal and signal to blank ratio for lens2 for <sup>55</sup>Mn (A), <sup>56</sup>Fe, <sup>57</sup>Fe, <sup>54</sup>Fe and <sup>58</sup>Fe (B and C).

### 3.6.3.2 The determination of the optimum Forward Power

The forward power is used to ignite and sustain the plasma during the analysis.

The number of Watts may vary depending on different sample and matrixes.

The Forward Power analysis is displayed for <sup>55</sup>Mn and <sup>56</sup>Fe in Figure 3-11.

These graphs were examined and the best sensitivity for the instrument was assessed as being when the Forward power value was set at 1400 W, which represented the greatest signal to blank ratio for all analytes.

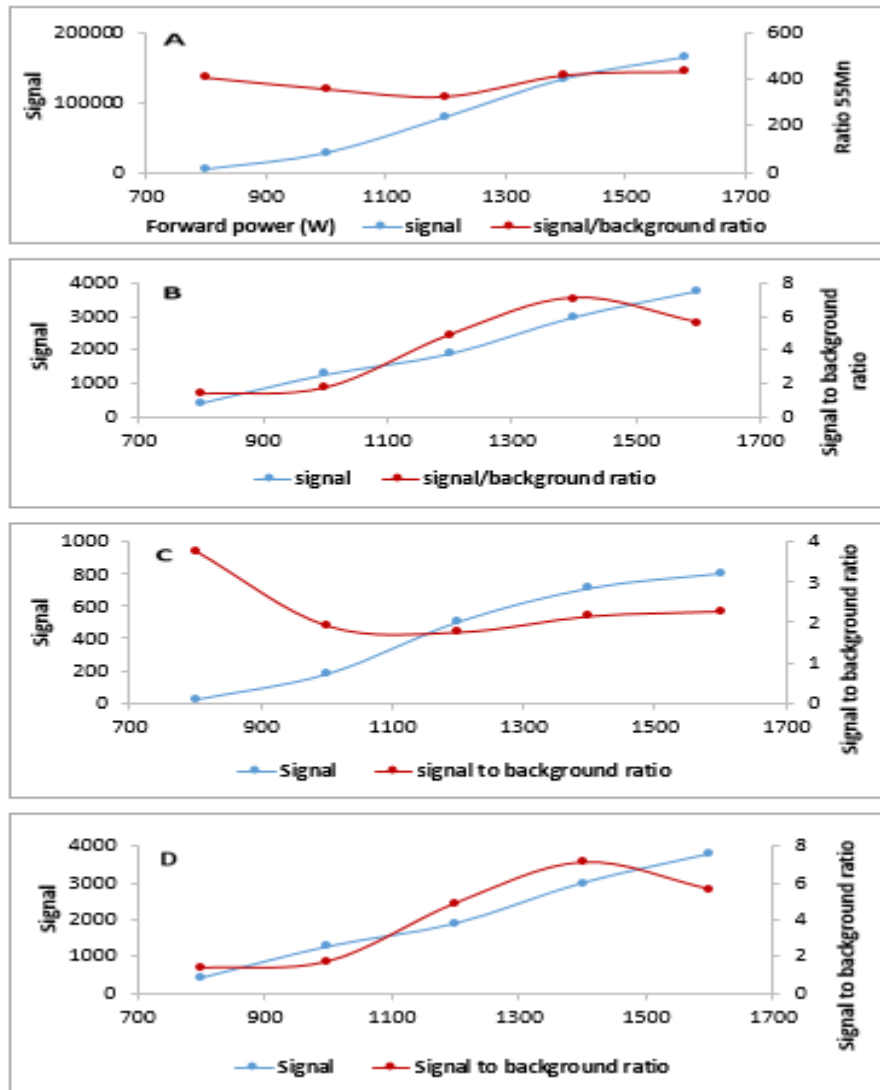


**Figure 3-11** Signal and signal to blank ratio for forward power for  $^{55}\text{Mn}$  (A),  $^{56}\text{Fe}$ ,  $^{57}\text{Fe}$ ,  $^{54}\text{Fe}$  and  $^{58}\text{Fe}$  (B and C).

### **3.6.3.3 The determination of the optimum Horizontal**

The optimum Horizontal concerns the orifice in the sampler cone and the position is related to where the ions move through the cone. Horizontal values for  $^{55}\text{Mn}$  and Fe isotopes are shown in (Figure 3-12). These graphs were examined and the best sensitivity for the instrument was assessed as being when the Horizontal value was set at 60.

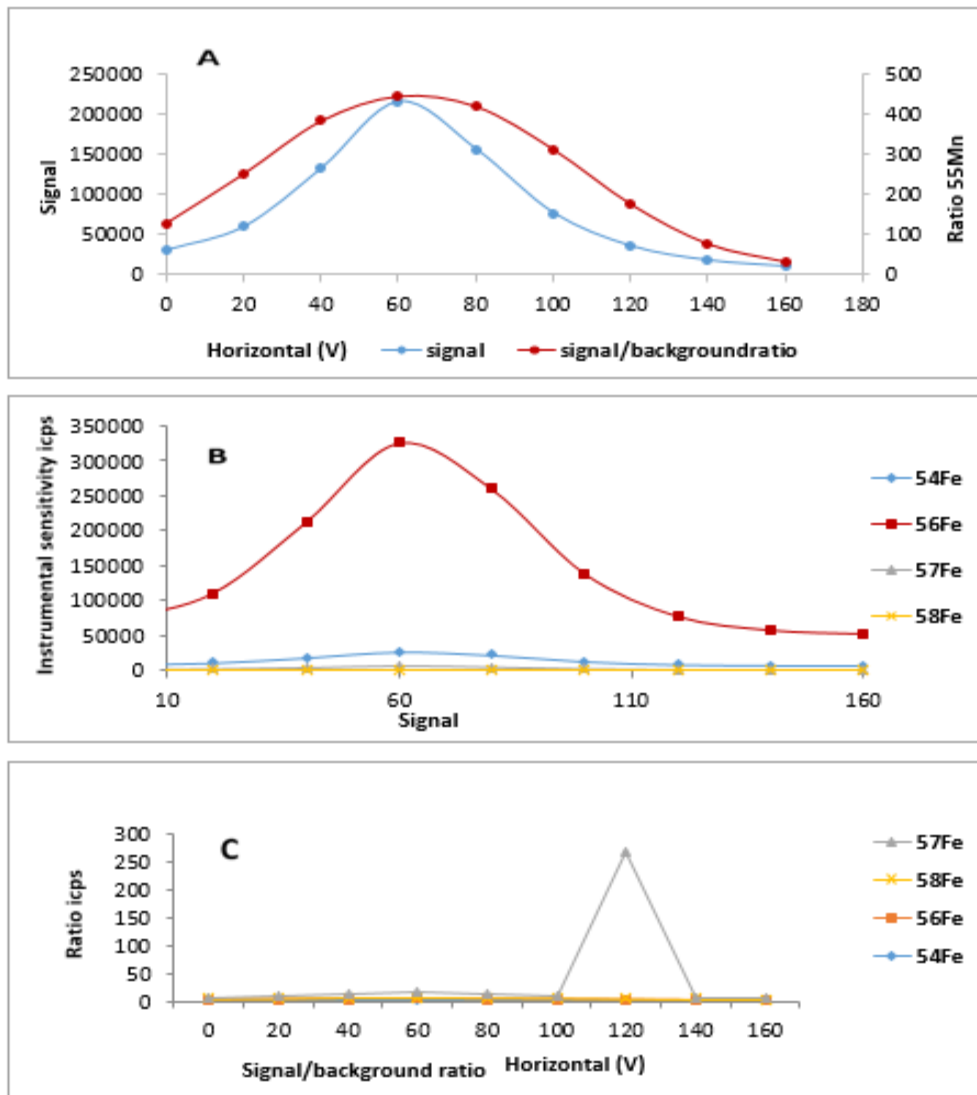


**Figure 3-12** Signal and signal to blank ratio for horizontal for  $^{55}\text{Mn}$  (A),  $^{56}\text{Fe}$ ,  $^{57}\text{Fe}$ ,  $^{54}\text{Fe}$  and  $^{58}\text{Fe}$  (B and C).

### 3.6.3.4 The determination of the optimum Vertical

Similarly, to the optimum Horizontal the optimum Vertical determines the position of the orifice in the sampler cone which determines where the ions move through the cone. Vertical for  $^{55}\text{Mn}$  and the  $^{56}\text{Fe}$  represented by the double Y-axes of signal and *signal to blank ratio* plotted counts is shown in Figure (3-13). These graphs were examined and the best sensitivity for the instrument was assessed as being when the Vertical value was set at 484. The

ratio for  $^{56}\text{Fe}$  was very low at a value of less than 3 because the background for Fe was very high giving rise to poor sensitivity due to the presence of interferences in the standard mode.

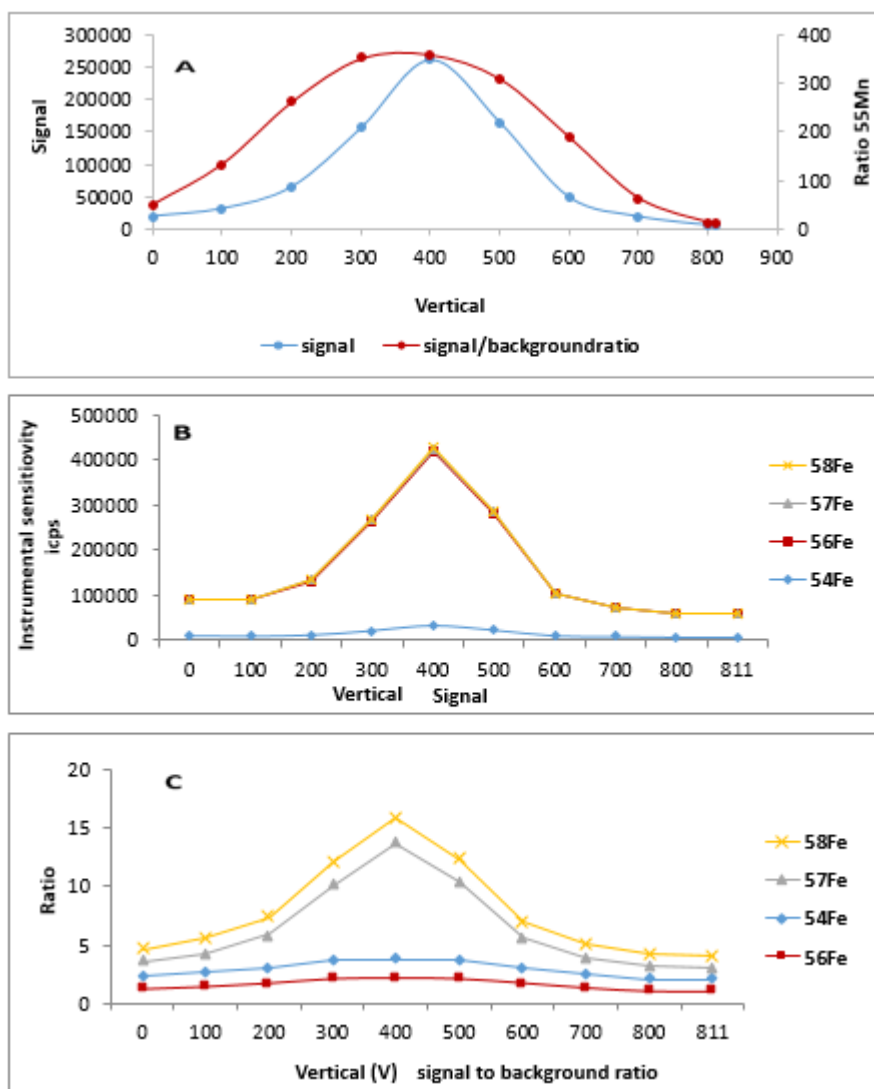


**Figure 3-13** Signal and signal to blank ratio for vertical for  $^{55}\text{Mn}$  (A),  $^{56}\text{Fe}$ ,  $^{57}\text{Fe}$ ,  $^{54}\text{Fe}$  and  $^{58}\text{Fe}$  (B and C).

### 3.6.3.5 The determination of the optimum D2

D2 deflectors direct the ions into the quadrupole. Using D1 set at -40 and D2 set at -130 there was enough signal to operate the instrument. Figure 3-14) shows typical tuning for D2. The graphs were examined and the best sensitivity for the instrument was assessed as being when the D2 value was set at -130. The value of -100 was also considered but the chosen value was judged the best compromise for all isotopes.

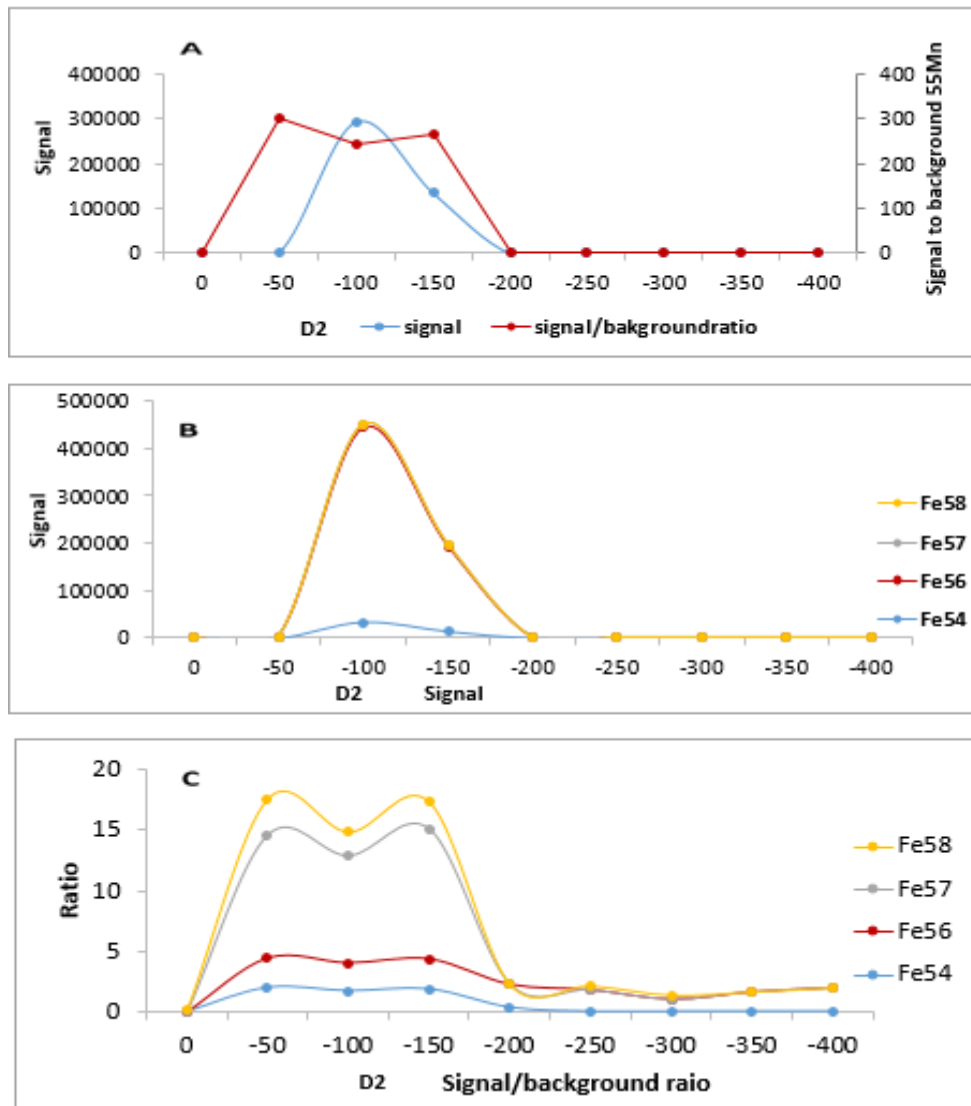


**Figure 3-14** Signal and signal to blank ratio for D2 for  $^{55}\text{Mn}$  (A),  $^{56}\text{Fe}$ ,  $^{57}\text{Fe}$ ,  $^{54}\text{Fe}$  and  $^{58}\text{Fe}$  (B and C).

### **3.6.3.6 The determination of the optimum Auxiliary**

The auxiliary gas moves the plasma position; hence, higher flow rates cause the plasma to move forward. The gas is also used to lift the plasma off the surface of the torch. The auxiliary then prevent melting of the intermediate tube, and the formation of carbon and the salt deposits on the inner tube. The Auxiliary optimisation for  $^{55}\text{Mn}$  and the  $^{56}\text{Fe}$  is displayed in Figure (3-15). The graphs were examined and the best sensitivity for the instrument was assessed as being when the Auxiliary value was set at 0.8.

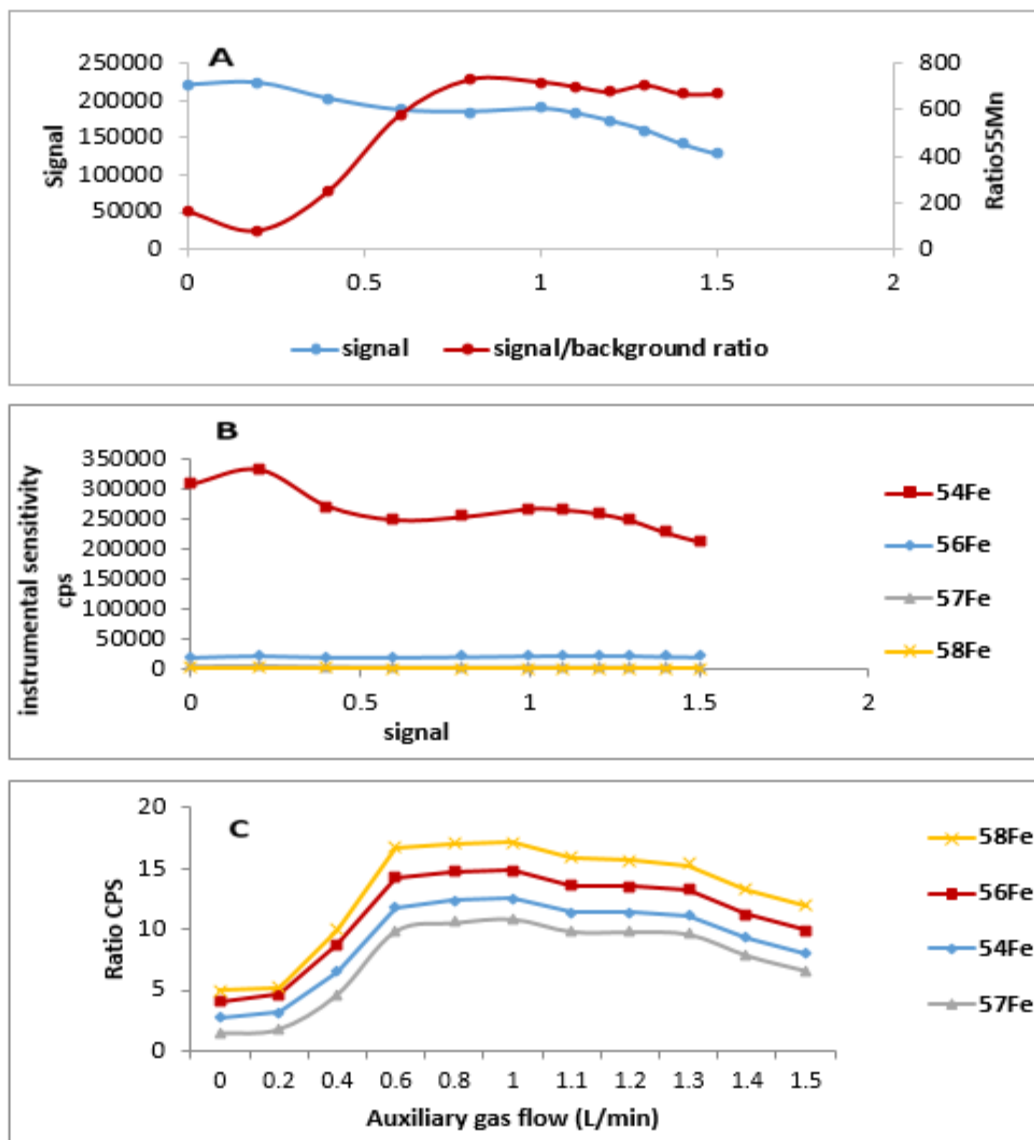


**Figure 3-15** Signal and signal to blank ratio for Auxiliary gas flow for  $^{55}\text{Mn}$  (A),  $^{56}\text{Fe}$ ,  $^{57}\text{Fe}$ ,  $^{54}\text{Fe}$  and  $^{58}\text{Fe}$  (B and C).

### 3.6.3.7 The determination of the optimum DA

Differential aperture (DA) used to sustain the pressure differential between the intermediate chambers. DA for  $^{55}\text{Mn}$  and the  $^{56}\text{Fe}$  represented by the double Y-axes of signal and signal to blank ratio plotted against the values for DA is shown in Figure (3-16). These graphs were examined and the greatest sensitivity for the instrument was assessed as being when the DA value was set at -37.6 where DA voltage applied was not critical.

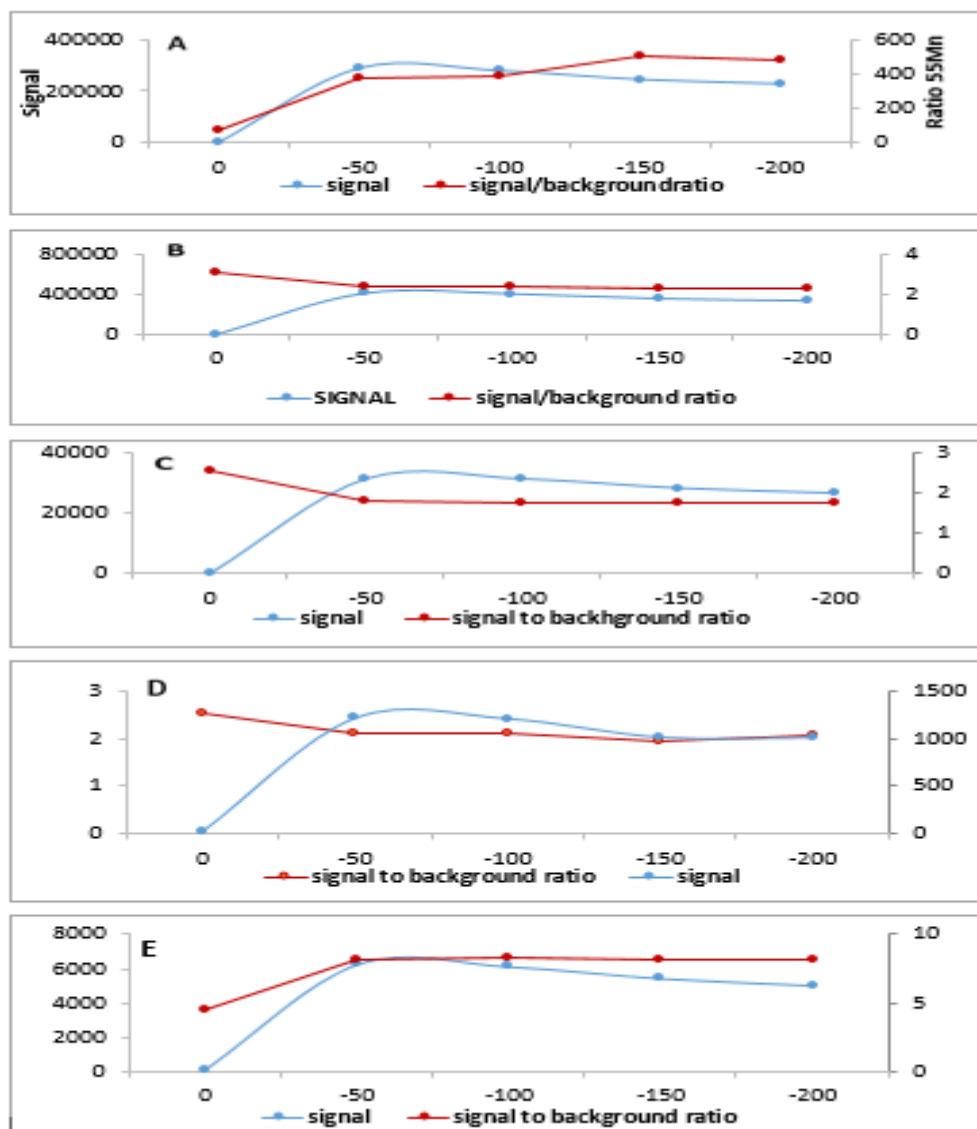


**Figure 3-16** Signal and signal to blank ratio for DA for  $^{55}\text{Mn}$  (A),  $^{56}\text{Fe}$ ,  $^{57}\text{Fe}$ ,  $^{54}\text{Fe}$  and  $^{58}\text{Fe}$  (B and C).

### **3.6.3.8 The determination of the optimum Coolant**

The coolant provides the plasma gas as well as cooling the torch. Coolant for  $^{55}\text{Mn}$  and the  $^{56}\text{Fe}$  represented by the double Y-axes of signal and signal to blank ratio plotted against the values for coolant is shown in Figure (3-17). These graphs were examined and the best sensitivity for the instrument was assessed as being when the coolant value was set at 14 depending on signal and signal to blank ratio.

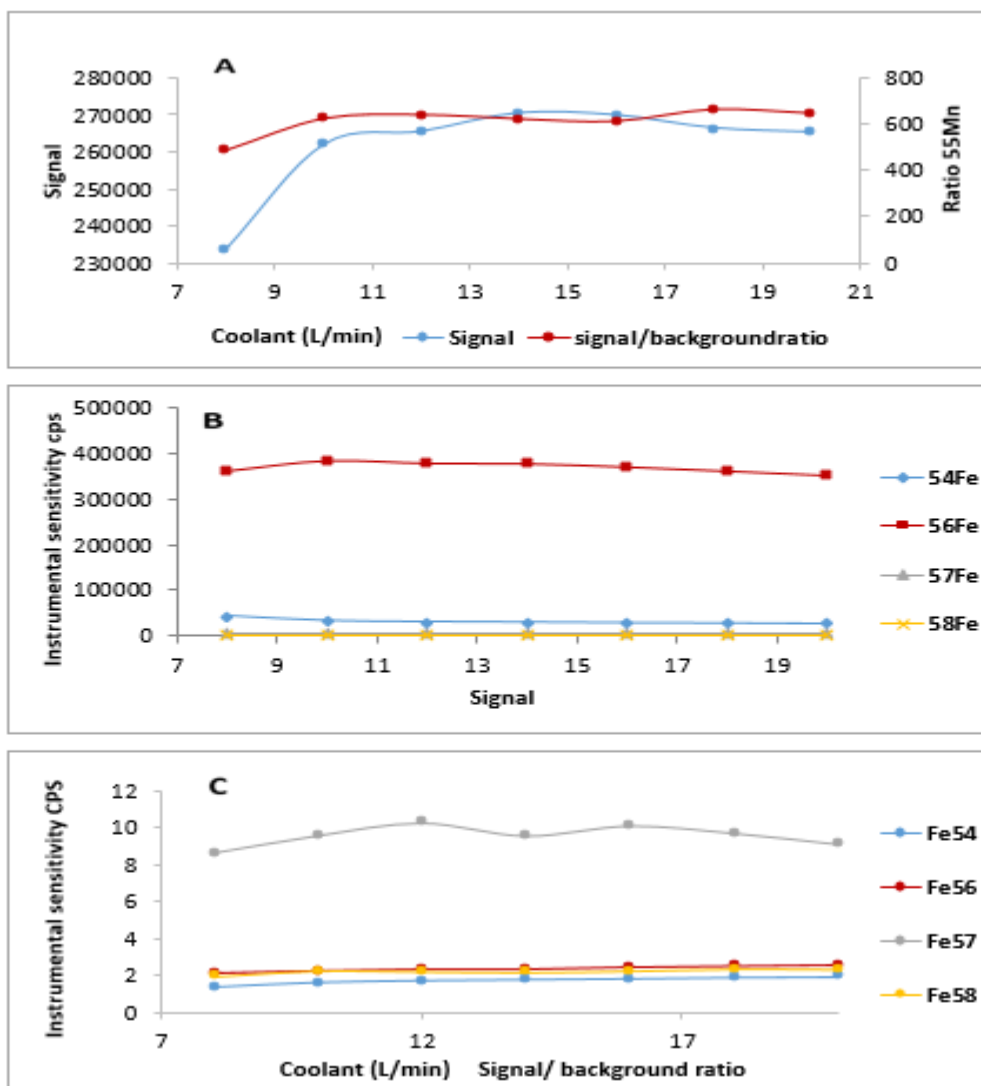


**Figure 3-17** Signal and signal to blank ratio for coolant gas flow for  $^{55}\text{Mn}$  (A),  $^{56}\text{Fe}$ ,  $^{57}\text{Fe}$ ,  $^{54}\text{Fe}$  and  $^{58}\text{Fe}$  (B and C).

### 3.6.3.9 The determination of the optimum Lens2 and L3

The lens2 is used to direct the ion beam into the collision cell. They are tuned together for maximum signal. Lens3 is used to accelerate the ion beam out of the collision cell. The optimisation of sensitivity and signal response was investigated: Lens2 for  $^{55}\text{Mn}$  and the Fe isotopes represented by the double Y axes of signal and signal to noise plotted against the values for Lens2 (Figure 3-18) and (Figure 3-19) for Lens3. These graphs were examined and the best

sensitivity for the instrument was assessed as being when the Lens2 value was set at -36.9 and Lens3 value was set at -150.

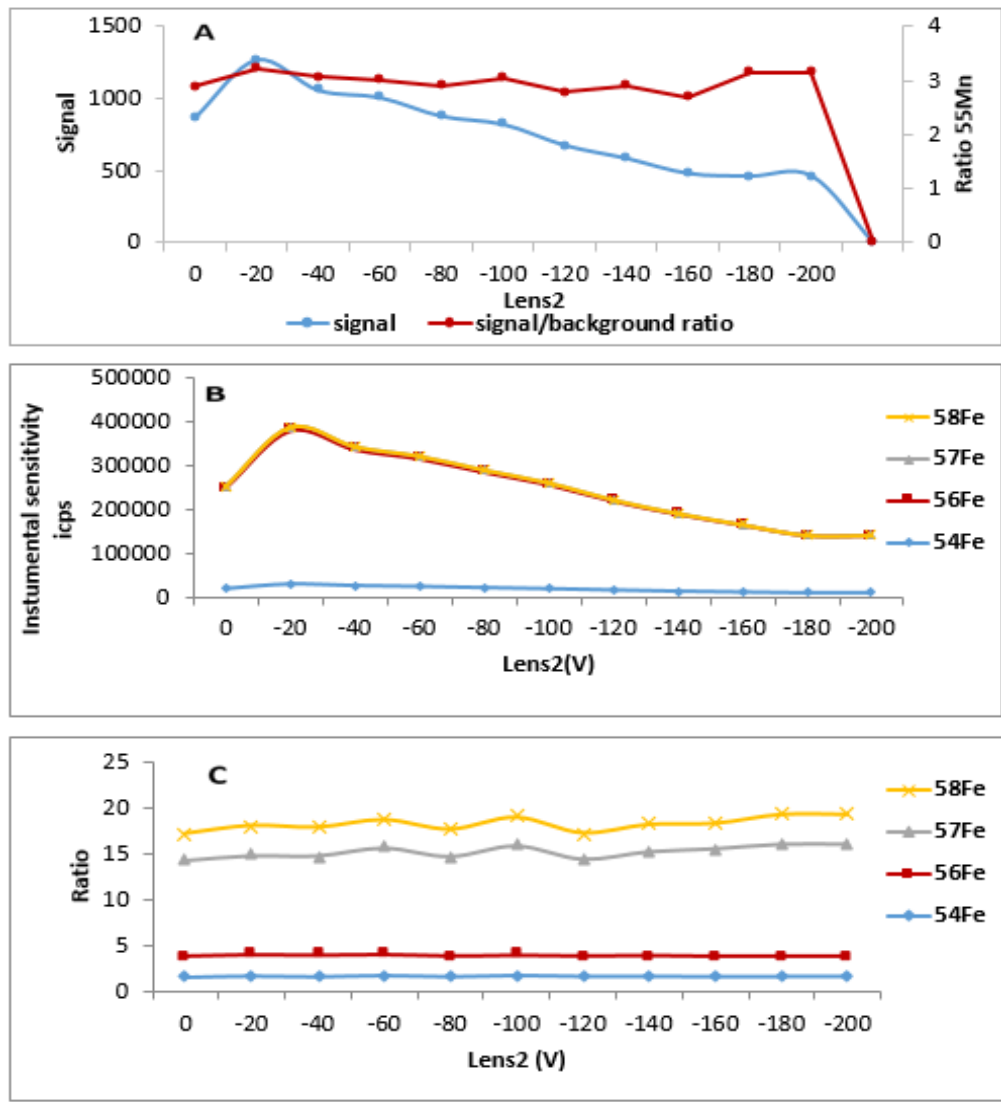


**Figure 3-18** Signal and signal to blank ratio for Lens2 for  $^{55}\text{Mn}$  (A),  $^{56}\text{Fe}$ ,  $^{57}\text{Fe}$ ,  $^{54}\text{Fe}$  and  $^{58}\text{Fe}$  (B and C).

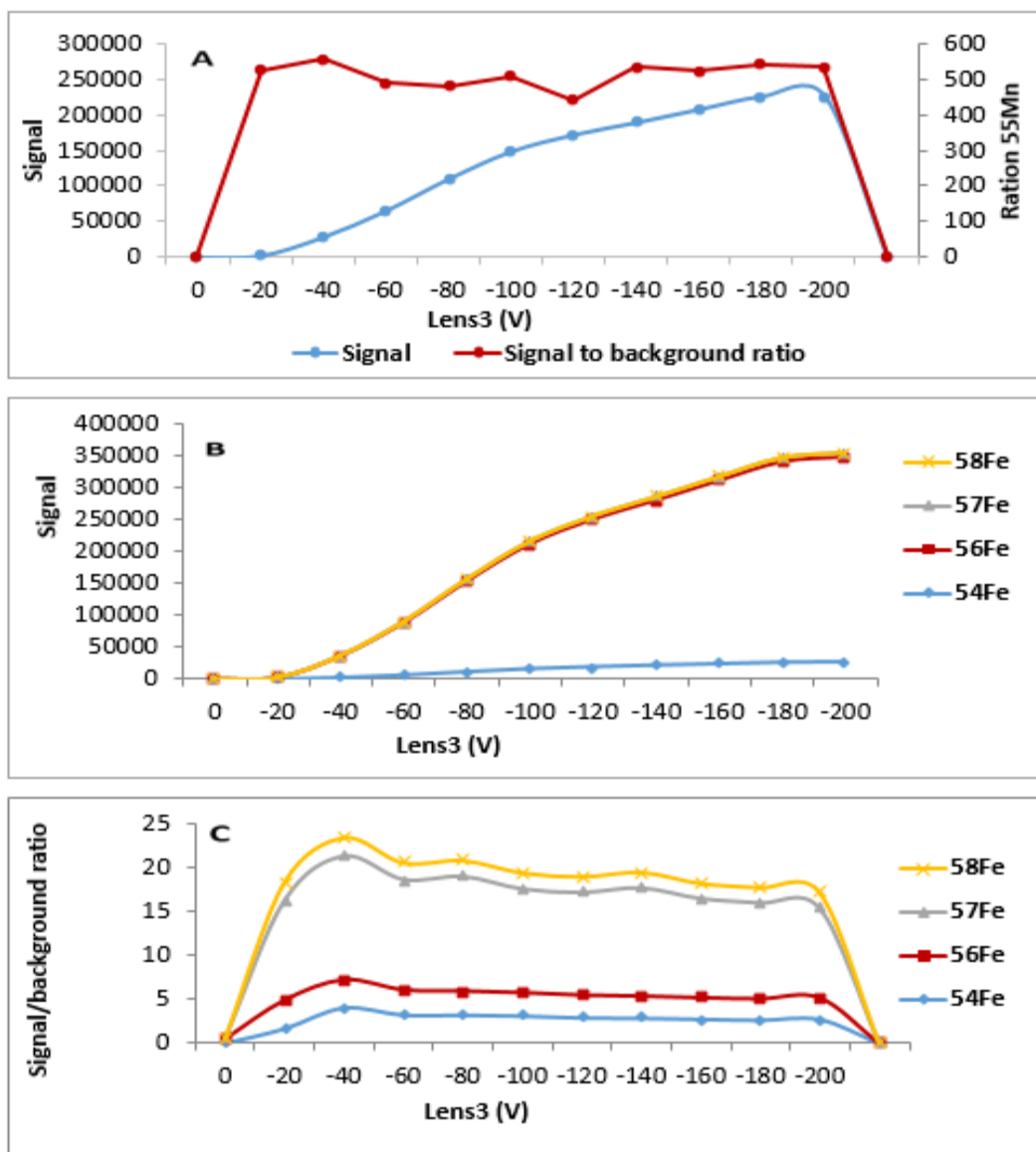


**Figure 3-19** Signal and signal to blank ratio for lens3 for  $^{55}\text{Mn}$  (A),  $^{56}\text{Fe}$ ,  $^{57}\text{Fe}$ ,  $^{54}\text{Fe}$  and  $^{58}\text{Fe}$  (B and C).

### 3.6.3.10 Optimisation of Add Gas parameters

Using most of the parameters obtained using Standard Mode, the Add Gas parameters were obtained for CCT mode. The main differences between standard mode and CCT tuning are that for the Pole Bias optimum it is set to negative (usually -0.7 V), D1 is -100 and focus is 0, advised by the manufacturer. Also, the Focus drops depending on the type of interface cones

being used for each set up. The maximum signal for each analyte ion was obtained after passing of the ions through the reaction cell, using He as a collision gas. The flow rate of the gas was varied between 0-10 mL per minute. Afterward the calibration graphs produced for both Fe and Mn were used in the drinking water analysis.

The carrier gas affects the transport and extraction of vapor from the gas–liquid separator in the chemical vapor generation system. The Ar flow rate used to transport Fe and Mn volatile compounds into the gas–liquid separator and then into the plasma torch was varied over the range 0.10 to 1.0 l min<sup>-1</sup>. The most suitable He flow rate was about 3.5 l min<sup>-1</sup> in this system. Above or below this value, the Fe and Mn signals decreased. The reduction of ArO and CaO was observed; hence, why <sup>57</sup>Fe works better in standard Mode and <sup>56</sup>Fe is better in CCT.

As the sensitivity of the instrument varies the best signal to blank ratio for each element needed to be identified. It was found that for both isotopes of Fe and Mn, the sensitivity decreased with the addition of the He gas. Hence, the minimum flow rate that provided better sensitivity for both isotopes by optimisation was selected, i.e. 3.5 mL/minute, as shown in Figure 3-20.

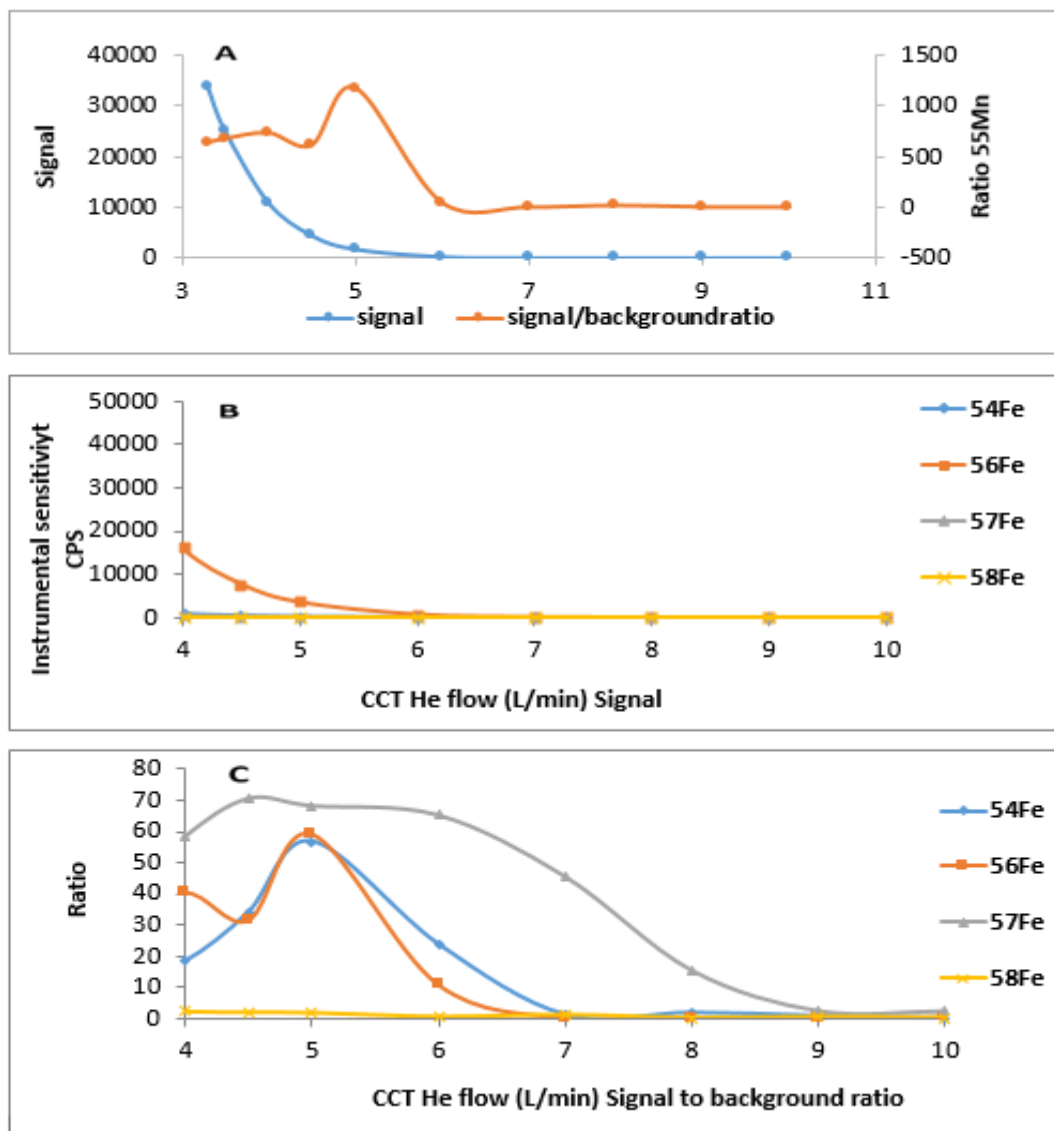


**Figure 3-20** Signal and signal to blank ratio for CCT gas for  $^{55}\text{Mn}$  (A),  $^{56}\text{Fe}$ ,  $^{57}\text{Fe}$ ,  $^{54}\text{Fe}$  and  $^{58}\text{Fe}$  (B and C).

### 3.6.3.11 The effect of ICP-MS modes

Both standard and CCT modes were used to determine the best conditions for a reduction in Ar interference. Optimising the CCT conditions led to reduced

main Ar interferences at the mass to charge ratio ( $m/z$ ) of  $^{56}\text{Fe}$  ( $^{40}\text{Ar}^{16}\text{O}$ ). Furthermore, polyatomic interferences due to other species such as  $^{40}\text{Ar}^{16}\text{O}$  and  $^{40}\text{Ca}^{16}\text{O}$  were also reduced. The results for the most sensitive isotopes at 92% abundance are presented in Table 3-5 and 3-6, for both standards and CCT mode of operation of the instrument. Following the abundance determination, some performances of the instrument under these optimised conditions were evaluated, and thereafter these were used for the drinking water analysis. Several parameters were found to have a significant effect on the sensitivity and performance of the ICP-MS signal. These included the nebulizer flow rate, Extraction Voltage, Pole Bias, Focus, He flow rate, Horizontal and Vertical rates. The changes in these parameters led to a change in the instrument's sensitivity when the reading for each parameter was either increased or decreased. However, other parameters did not have a significant effect.

TABLE 3-5 ICP-MS optimum con

<b>Major Parameters</b>	<b>Optimum</b>	<b>Minor Parameters</b>	<b>Optimum3</b>	<b>Global</b>	<b>Optimum2</b>	<b>Add. Gas</b>	<b>Optimum5</b>
<b>Extraction</b>	-200	Lens2	-36.9	Standard Resolution	125	CCT1 7% H2- He	0
<b>Lens1</b>	-1.5	Lens3	-150	High Resolution	125	CCT2 He	0
<b>Focus</b>	10	Forward power	1400	Analogue Detector	1900		
<b>D1</b>	-40	Horizontal	60	PC Detector	3550		
<b>Pole Bias</b>	10	Vertical	484				
<b>Hexapole</b>	-10	D2	-130				
<b>Nebulizer</b>	0.89	DA	-37.6				
<b>Sample Depth</b>	160	Cool	14				
		Auxiliary	0.8				

**Table 3-6** ICP-MS optimum conditions using CCT mode.

<b>Major Parameters</b>	<b>Optimum</b>	<b>Minor Parameters</b>	<b>Optimum3</b>	<b>Global</b>	<b>Optimum2</b>	<b>Add. Gas</b>	<b>Optimum5</b>
<b>Extraction</b>	-200	Lens2	-36.9	Standard Resolution	125	CCT1 7% H2-He	0
<b>Lens1</b>	-1.5	Lens3	-150	High Resolution	125	CCT2 He	4
<b>Focus</b>	0	Forward power	1400	Analogue Detector	1900		
<b>D1</b>	-36.9	Horizontal	60	PC Detector	3550		
<b>Pole Bias</b>	-0.7	Vertical	484				
<b>Hexapole</b>	-10	D2	-100				
<b>Nebulizer</b>	0.89	DA	-37.6				
<b>Sample Depth</b>	160	Cool	14				
		Auxiliary	0.8				

### 3.6.4 Analytical performance

All the experiments were performed with standard solutions, as previously detailed in Section 2.4. The linearity of this calibration curve was satisfied in the range of 0-100 ng/mL, with a correlation coefficient of  $R^2 > 0.995$ . The analytical conditions obtained for the developed method are presented in Table 3-4.

**Table 3-7** Analytical conditions for Fe and Mn.

Isotope	Analysis mode	Internal standard	Concentration range ( $\mu\text{g/L}$ )
<sup>55</sup> Mn	CCT and Standard	<sup>103</sup> Rh and <sup>45</sup> Sc	0-100
<sup>56</sup> Fe	CCT and Standard	<sup>103</sup> Rh and <sup>45</sup> Sc	0-50
<sup>57</sup> Fe	CCT and Standard	<sup>103</sup> Rh and <sup>45</sup> Sc	0-50

Before validation of the method for Fe and Mn analysis; the range of linearity for both Fe and Mn was obtained. Furthermore, the limit of quantification (LoQ), limit of detection (LoD) and specificity were all evaluated by analysing the measurements using 12 blanks. The LoD and LoQ were estimated at 3SD, and 10SD, of the average blank concentration, respectively. The details for these measurements are provided below.

The specificity of this method was determined and checked, to ensure lack of interferences by other species. This involved measuring the recoveries of the calibration curves for spiked solutions of drinking water samples taken from

different locations in the Northwest of England. These samples were spiked with a known Fe and Mn standard to obtain final concentrations varying between 30 and 50 ppb. In addition, some samples were analysed without the spiking with Fe and Mn. HNO<sub>3</sub> was used as a matrix, diluent and in the rinse solution for the ICP-MS instrument, as most metals are soluble in this acid, and it does not introduce matrix components such as C, S, Cl to the analyte, which can cause polyatomic interferences. However, operating the instrument in CCT can eliminate these interferences. The specificity was within the acceptable range, and the quantitative determination of both elements in drinking water was validated. Five rounds of validation were performed on different days, and the validation methods used were the spike response method (SRM) and spike method for the water samples. All the validation and figures of merit for these are presented in the next section.

#### **3.6.4.1 Limits of detection and quantification**

The LoD and LoQ were determined for Fe and Mn; as the lowest concentration measurable in both the standard and CCT modes. These were 16 ng/mL for Fe, and 0.7 ng/mL for Mn. It was established that LoQ was improved in CCT mode for both Fe and Mn; with values being 0.6 ng/mL and 0.3 ng/mL respectively; when compared to the standard mode, and this is presented in Table 3-5. The most abundant isotope was selected to be used for the analysis. Both LoD and LoQ were calculated as the blank signal plus three or ten standard deviations, respectively, using 10 blank measurements for the calculation as previously in Section 3.6.2.3.

### 3.6.3.2 Figures of merit

The analytical figures of merit were estimated after the optimisation of every single parameter. The results obtained in the standard mode of operation were compared to the results obtained in CCT mode. When using CCT mode, with He as the collision gas at a flow rate of 4 mL/min, a greater than a 10-fold drop in the Fe background counts per second was found. This is illustrated in the Figures 3-21 and 3-23 for both Fe and Mn. The calibration was successful in achieving linearity in the range of concentrations indicated.

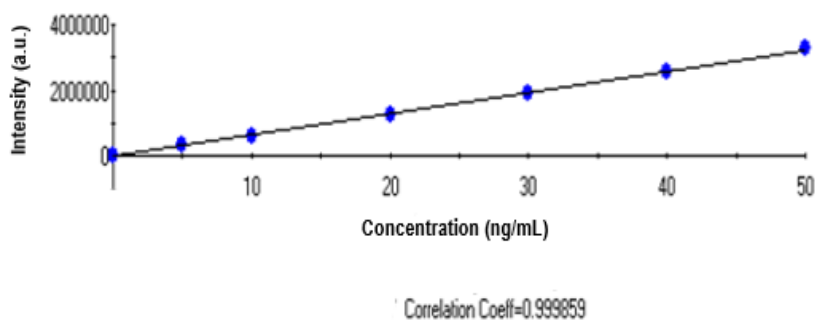


**Figure 3-21** Calibration Curve for  $^{55}\text{Mn}$  on standard mode.

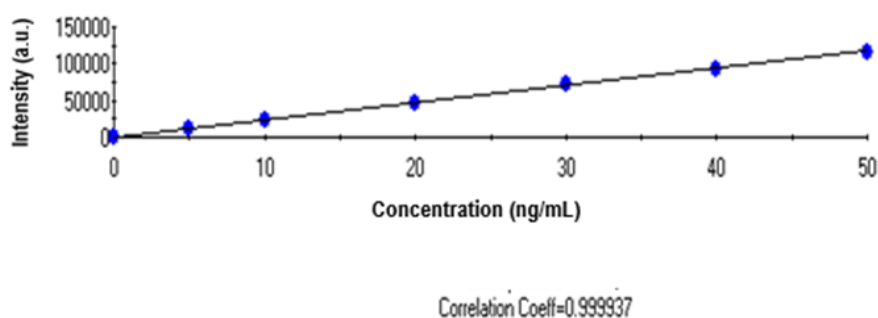


**Figure 3-22** Calibration curve for  $^{55}\text{Mn}$  on CCT mode.

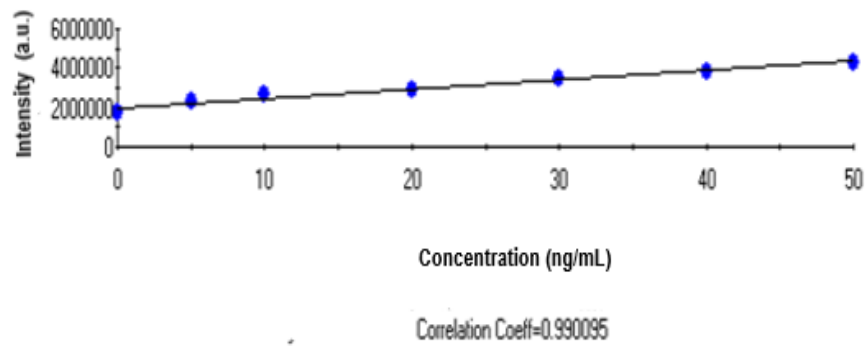


**Figure 3-23** Calibration curve for  $^{56}\text{Fe}$  on Standard mode.

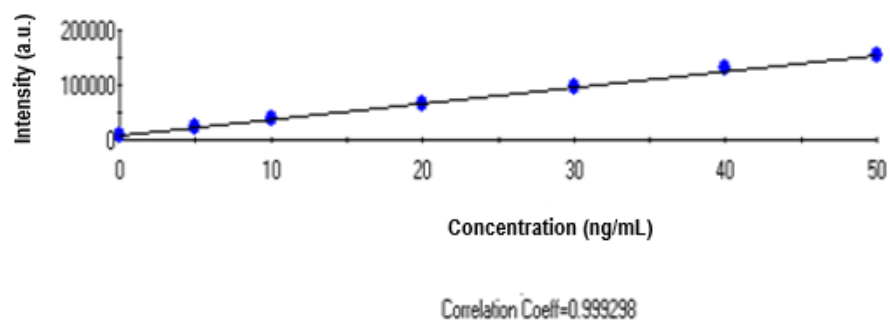


**Figure 3-24** Calibration curve for  $^{56}\text{Fe}$  on CCT mode.

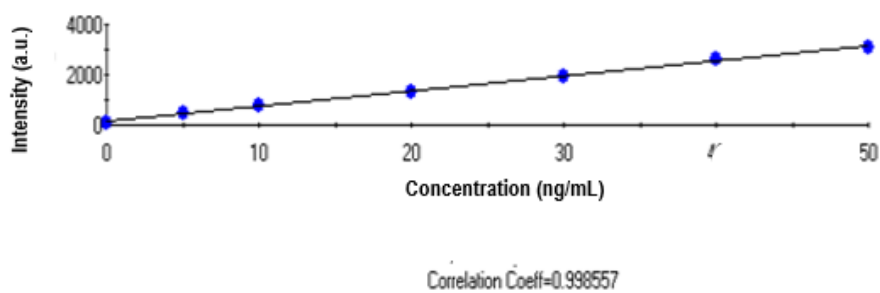


**Figure 3-25** Calibration graph for  $^{57}\text{Fe}$  on CCT mode.

**Table 3-8** Parameters of the analytical calibration curves: linear range, correlation coefficient (R<sup>2</sup>), average (RSD) for repeatability of calibration solutions measurements.

Isotope	Analysis mode	Internal standard	Concentration range(mg/l)	RSD% <sup>a</sup>	R <sup>2</sup>
<sup>55</sup> Mn	Std	<sup>103</sup> Rh and <sup>45</sup> Sc	0-100	5.36	0.9985
<sup>56</sup> Fe	Std	<sup>103</sup> Rh and <sup>45</sup> Sc	0-100	4.56	0.9992
<sup>57</sup> Fe	Std	<sup>103</sup> Rh and <sup>45</sup> Sc	0-100	5.12	0.9988

<sup>a</sup> n=5 , Std =Standard mode

**Table 3-9** The certified and CCT mode found concentration ( $\mu\text{g/mL}$ ) of the elements, in the certified reference material (SRM TMDA-70 and TMDA-64.2, river water).

Element	Certified value ( $\mu\text{g/l}$ )	Found value ( $\mu\text{g/l}$ )	% Recovery
TMDA-64.2 Fe	306	310 $\pm$ 3	102.3
Mn	295	297 $\pm$ 4	100.8
TMDA-70 Fe	368	370 $\pm$ 3	100.5
Mn	302	305 $\pm$ 5	101.9

As it can be noted from Table 3-10, CCT mode worked well and provided a better result compared to standard mode especially for  $^{56}\text{Fe}$ , because the percentage recovery was greater. Furthermore, all the Fe and Mn results obtained by CCT were within the range of the certified value, indicating good agreement with the true value.

In the CCT mode,  $^{40}\text{Ar}^{16}\text{O}$  and  $^{40}\text{Ca}^{16}\text{O}$  species were removed from ions reaching the detector. Examining the results for  $^{56}\text{Fe}$  there is a large background, which was removed when CCT mode was used.  $^{57}\text{Fe}$  provides the best sensitivity using standard mode because of the much smaller background signal caused by  $^{40}\text{Ar}^{16}\text{O}^{1}\text{H}$ . The isotope abundance of  $^{56}\text{Fe}$  rather than  $^{57}\text{Fe}$  led to a significant improvement in sensitivity and hence the attempt to remove the background from  $^{56}\text{Fe}$ . The results demonstrated that the method is more accurate and sensitive for the determination of Fe and Mn using ICP-MS in CCT mode compared to the standard mode. This improved the LoD and LoQ by a factor of 10 when using CCT compared to the results obtained using the standard mode. Moreover, the results obtained using two different certified reference materials gave percentage recovery values which agreed with the SRM. The relative standard deviation RSD for both elements was found to be less than <5%.

**Table 3-10** The LoD and LoQ for Fe and Mn in standard and CCT Mode.

Analyte-CCT	LoD (ng/mL)	LoQ (ng/mL)
<sup>56</sup> Fe	0.3	0.6
<sup>55</sup> Mn	0.09	0.3
<b>Analyte-Standard</b>		
<b>Analyte</b>		
<sup>56</sup> Fe	14	16
<sup>55</sup> Mn	0.2	0.7

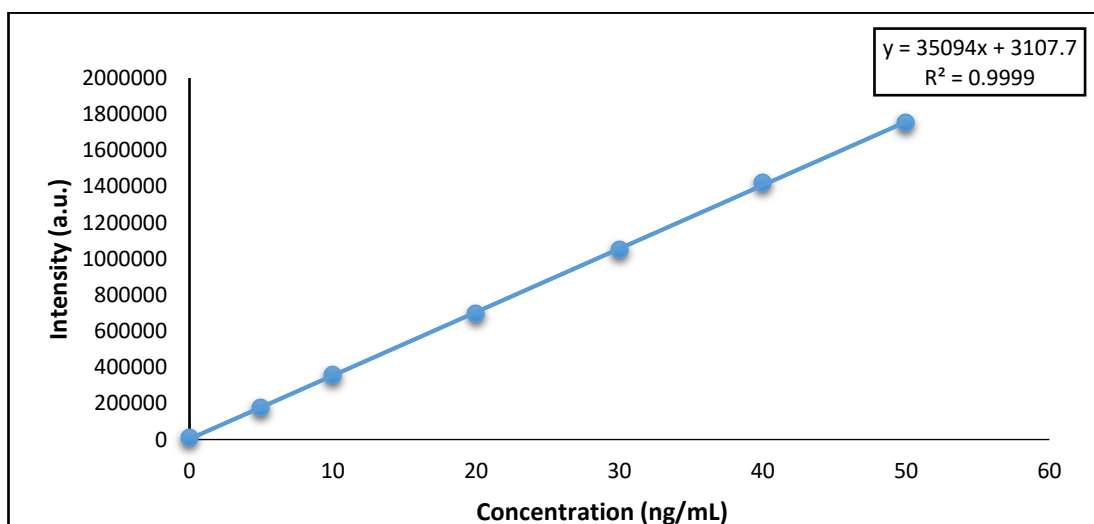


**Figure 3-26** Calibration graph for <sup>55</sup>Mn used for the calculation of LoD and LoQ.

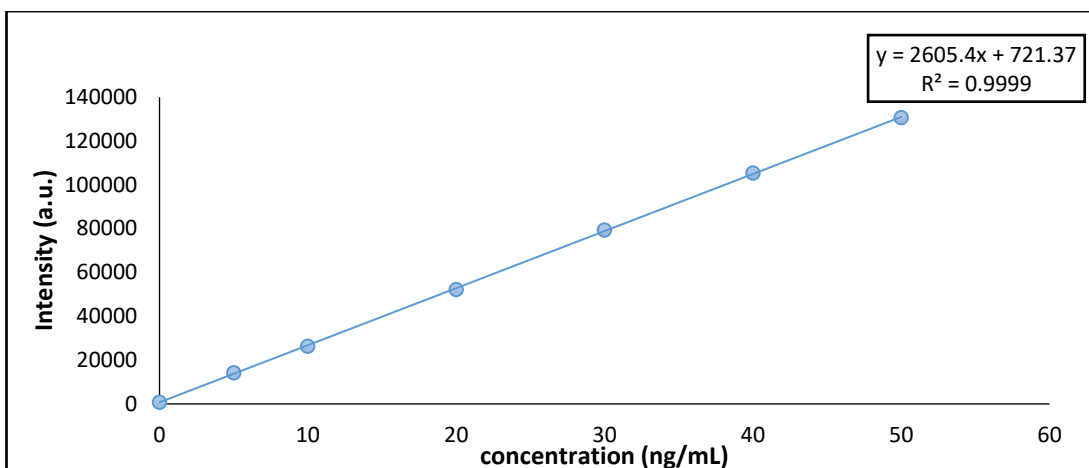


**Figure 3-27** Calibration graph for  $^{56}\text{Fe}$  used for the calculation of LoD and LoQ.

The LoD and LoQ results for ICP-MS showed greater sensitivity and better recovery than ICP-OES for the analysis of Fe and Mn in water samples. Table 3-9 shows certified values for both instruments and certified values with recovery %. Very good recovery values were obtained of 104% and 98% for Fe and Mn, respectively. Thus, ICP-MS may be applied with confidence for both Fe and Mn using simultaneous analysis as confirmed by the stated figures of merit.

**Table 3-11** LoD and LoQ calculation using the above equation for Fe and Mn (ng/mL) using CCT Mode.

Blank reading	$^{55}\text{Mn}$	$^{56}\text{Fe}$
Mean of 12 repeats	786.6343	5042.3993
SD	60.20545382	139.615934



### **3.6.4 Sample analysis**

After successful development and validation of the method for the determination of Fe and Mn metals, it was applied to the analysis of the water samples was taken from the Northwest region of England. This was in order to assess the quantity of Fe and Mn levels in the water treatment process which went on to be used for drinking water in this area. The water samples were obtained at different times of the year.

Water samples from two sites were analysed by ICP-MS using CCT mode (after tuning using standard mode) ; Fishmoore and Oswestry at different water processing treatment points starting with raw water before any treatment or adding of any coagulant to the final water which goes to the costumer tap. The results show that concentration of Fe and Mn was in ng/mL (Tables 3-12 to 3-14). This was within the allowed WHO limits for drinking water.

**Table 3-12** Concentrations (ng/mL) of Fe and Mn from different locations of Northwest region of England.

<b>Water stages</b>	<b>Mn</b>	<b>Fe</b>
<b>Raw water</b>	7.33	26.28
<b>First stage filter outlet</b>	13.53	4.3
<b>Second stage filter outlet</b>	0.73	0.2
<b>Accelerator No.1</b>	13.6	32.8
<b>Accelerator No.2</b>	38.9	62.61
<b>Final water</b>	0.5	0.65

**Table 3-13** Spike and RSD of Fe and Mn from different locations of Northwest region of England.

<b>Isotope</b>	<b>Raw</b>	<b>FSF</b>	<b>FSS</b>	<b>ACC1</b>	<b>ACC2</b>	<b>Final</b>
<b><sup>56</sup>Fe Spike recovery (%)</b>	96	97	96.5	96	98	105
<b>RSD (%)</b>	5.4	4.3	5.6	3.6	5.5	4.7
<b><sup>55</sup>Mn Spike recovery (%)</b>	98	95	96	99	98	103
<b>RSD (%)</b>	5.3	4.5	4.4	5.4	3.5	4.6

**TABLE 3-14** Concentrations (ng/mL) of Fe and Mn from different locations of Northwest region of England.

<b>Isotope</b>	<b>Oswestry RGF</b>	<b>Final</b>	<b>slow common</b>	<b>Pilot</b>	<b>sand filter</b>	<b>raw</b>
<b><sup>55</sup>Mn</b>	0.03	0.0012	0.00072	0.0005	0.00045	0.0042
<b>Spike recovery (%)</b>	100.3	103.5	97.6	98.5	99.8	95.8
<b>RSD (%)</b>	4.5	3.8	3.6	4.3	4.5	5.3
<b><sup>57</sup>Fe</b>	0.002	<lod	0.0016	0.003	0.015	0.007
<b>Spike recovery (%)</b>	104.5	99.7	100.5	98.9	102.8	100.4
<b>RSD (%)</b>	4.5	5.3	4.6	4.3	3.5.	2.8

Studying each Table of results, it is likely that the key risk for the discolouration is Fe and Mn levels in the final water of each region which is above 50 µg/L for Mn and 200 µg/L for Fe (regulation limit).

It can be seen that the Fishmoore raw water has more Fe and Mn present than Oswestry water, giving 0.059 and 0.029 ppb for Fe and Mn in Fishmoore water, respectively, and for Oswestry water, the level was 0.007 and 0.0042 ppb, respectively. These all vary in concentration in the different regions and the Fe concentration increased during the treatment process. Generally, the raw water is at the highest level of Fe and Mn concentration for the water stages (accelerator stage), such as Huntington water in the ICP-OES chapter. This is likely to be due to the adding of a coagulant such as Fe phosphate or  $\text{KMNO}_4$ . These coagulants increase the level of Fe or Mn during the treatment process as displayed in Tables 3-12 and 3-14. However, at all water treatment works, it has become evident that during the post clarifier and the accelerating in different stages, Mn concentration increases compared to the raw waters and this agrees with the results obtained using ICP-OES (Section 2.8). As, mentioned previously, in different regions aluminium sulphate is used as coagulant. Ferral coagulation applied at different locations may be one of the reasons why Mn concentration increased during the treatment process.

The results indicated that a number of analyte determinations provided negative element concentrations in the samples below the LoD. For Mn, these values are within the margin of error. However, for Fe, these results can be attributed to decreased sensitivity in the concentration determination at the lower end of the calibration range.

In the UK, drinking water standards follow guidelines provided by the Drinking Water Inspectorate (DWI) and determine acceptable levels according to prior research. These standards are legally enforceable. The national requirements are that the maximum concentration of Fe permissible is 200 µg/L, which is equivalent to 200 ng/mL, at the point of the consumers' tap. For Mn, the permissible concentration at the consumers' point of use is 50 µg/L; equivalent to 50 ng/mL and the analysis shows that the samples are within this range. The optimisation of the ICP-MS method is highly dependent on the plasma parameters and sample introductions. All these were successfully parameters optimised to provide the best signal.

### 3.7 Conclusion

The determination of Fe and Mn was successfully carried out by ICP-OES and ICP-MS. The elements were analysed and the measured concentrations were obtained for both standards and water samples. The results obtained by both instruments were satisfactory using the calibration samples. Comparing both techniques, the analytical figures of merit were obtained and all the results expressed as the correlation coefficients, which showed more than 0.995 for both Fe and Mn. The LoD were lower by ICP-MS than by ICP-OES as can be seen in Table 3-12. The ICP-MS had higher sensitivity and precision obtained by the relative standards deviation values than ICP-OES and allowed the determination of both Fe and Mn in concentrations of very low values. Thus, showing it to be a very powerful technique for the quality control of water determination.

**Table 3-15** Correlation coefficients ( $R^2$ ) and limits of detection (LoD) in ng/mL for Fe and Mn by ICP-OES and ICP-MS.

Analyte	ICP-OES		ICP-MS	
	$R^2$	LoD (ng/mL)	$R^2$	LoD (ng/mL)
Fe	0.9998	11.58	0.9999	0.3
Mn	0.9999	1.43	0.9999	0.009

This work has demonstrated the ability of both ICP-OES and ICP-MS to analyse elements present at trace metals levels (Fe and Mn) in drinking water samples. The analysis of Fe and Mn by ICP-MS was validated, and this method was simple, selective, accurate and precise to use in drinking water analysis. The method is linear and accurate where the percentage recovery of both metals was within 95-105%. The method was precise, and this was confirmed by the replication of the sample results with low RSD so that this method can be used for the determination of Fe and Mn in water samples. The capability of the ICP-MS for signal intensity and sensitivity using cell technology made the instrument more suitable to measure speciation with HPLC as a hyphenated technique. Although the results obtained for the samples were similar using ICP-OES and ICP-MS, it should be noted that these techniques are different because each one has its strengths and weaknesses for water samples and Fe and Mn levels. In general, both instruments were found to be good methods for the determination of Fe and Mn in water samples with satisfactory accuracy and precision but the ICP-MS was better. The determination was sufficiently a good linear range and sensitivity enabling to reach LoD and LoQ in water samples which is fully suitable for routine analysis of these metals in water treatment plants.

## **Chapter 4 Speciation analysis by high performance liquid chromatography inductively coupled plasma mass spectrometry (HPLC-ICP-MS)**

### **4.1 Introduction**

Spectrophotometry, AAS, LC-ICP-MS and LA-ICP-MS techniques are used or combined with extraction procedures such as cloud point extraction (CPE) and solid phase extraction (SPE) for Mn speciation in water (90). In addition, many different analytical techniques have been used for the determination of Fe speciation in water including UV-VIS spectrophotometry, flame (FAAS), ICP (ICP-AES, ICP-MS, and LC Methods), electrothermal atomic absorption spectrometry and ion chromatography (214). The present study has focused on the speciation of  $Mn^{2+}$ ,  $Fe^{2+}$  and  $Fe^{3+}$  using ICP-MS as a technique for identification of trace metal elements coupled with chromatographic separation using high performance liquid chromatography. The coupling of HPLC-MS is straightforward, however, there are some limitations of the analysis; for example, contamination can take place in the mobile and stationary phases, valves, and tubing on the chromatographic system inert pumps and valves. The stability of the plasma is also an issue especially concerning the use of organic mobile phases where in the process of desolvation, these organics pyrolyse in the plasma to carbon, which causes deposits in the sample injector tube which then affects the torch and the sample cones of the ICP-MS interface. The sample runs through the introduction system to the chromatography and can cause the orifices to become clogged, lowering overall sensitivity. Dispersion effects can also be a

problem, which effects the post column due to the sample introduction system used between the HPLC and ICP-MS.

Speciation analysis required the use of efficient separation techniques, such as electrophoresis and chromatography, with specific and sensitive detectors. ICP-MS is an excellent technique for speciation analysis, including element specific detection and excellent sensitivity with no need for a pre-concentration method, and reverse phase chromatography has been used for separation of charged species for both organic and inorganic species (215) (173). For charged ions separation, ion pair chromatography has been used with complexing agents; based on separation caused by differences in charges. The complexing reagents used for the separation of Mn species have been EDTA and 1-(2-pyridylazo)-2-resorcinol in two different studies (216, 217), and PDCA for Fe and Mn species with the formation of negatively charged complexes (218).

A  $Mn^{2+}$ ,  $Fe^{2+}$  and  $Fe^{2+}$  study was carried out by Michalke *et al.* (109), PDCA was used as a chelating agent and was found to be a good choice for the speciation of both elements using ion chromatography. Several projects have been carried out (219) related to Fe and Mn speciation as a means of elemental analysis of environmental samples using HPLC-ICP-MS.

The final stage of this work was to develop speciation methods for Fe and Mn and therefore determine what species of metal are present. In many cases, the chemical species of each element present is what defines the level of the water samples. In this work, it was important not only to assess the levels of both elements in water samples but also in which form they exist in the

samples. The combination and the application of HPLC and ICP-MS allowed the separation and analysis of individual species by ion exchange chromatography and then allowed the optimisation and application to water processing samples. The objective of this work was to perform speciation of both  $\text{Fe}^{3+}$  and  $\text{Mn}^{2+}$  in water by HPLC-ICP-MS using PDCA that was added to the mobile phase for the separation.

## 4.2 Experimental

### 4.2.1 Chemicals and Reagent

All standard solutions, reagents, and samples used for this study were as previously prepared in Chapters 2 and 3. These solutions were used to prepare  $Mn^{2+}$  and  $Fe^{3+}$  standards daily prior to analysis and 10 ng/l of an internal standard (Rh and Sc).

### 4.2.2 Mobile Phase Preparation

The mobile phase was made using 1.7 g of pyridine-2,6-dicarboxylic acid (PDCA) (Sigma- Aldrich.com, China), 7.5 mL of formic acid (Sigma- Aldrich.com, China), 3.8 g of potassium hydroxide (KOH,) and 0.98 g of potassium sulfate ( $K_2O_4S$ ) (Fisher Scientific) added to a 1 L bottle containing 900 mL of ultra-pure water. For PDCA to dissolve, the container was left in an ultrasonic bath for 20 minutes or until no PDCA residue was visible. A pH electrode was inserted into the mobile phase and formic acid was added dropwise with mixing to the solution until the pH of the solution dropped to 3.3. The mobile phase was then filtered through a PTFE filter (nylon membrane filter 0.45  $\mu m$ , diameter 47 mm), the solution was then degassed for 15 to 30 minutes in He gas. The composition of the mobile phase was optimised at different pH and the eluent compositions.

### 4.2.3 Preparation of the standards for the analysis

The acids used were of trace metal grade. Stock solutions of  $\text{Fe}^{3+}$  and  $\text{Mn}^{2+}$  standards (5, 10, 20, 50, 100, 200, 500 ng/mL - 1  $\mu\text{g/mL}$ ) were made, in 0.2% M  $\text{HNO}_3$ , from 1000 mg/L ICP stock solutions (SCP Science) of both Fe and Mn and 1 mL of (1 ppm Rh and Sc stock solutions, QMx Laboratory UK) added as an internal standard to all calibrations and blank solutions.  $\text{Fe}^{2+}$  standards were made from ferrous ammonium sulphate hexahydrate, known as Mohr's salt (ACS reagent 99%, Sigma-Aldrich) diluted in 0.1 M HCl. Rh (final conc. was 10 ng/mL) was added as an internal standard. In order to minimise oxidation of  $\text{Fe}^{2+}$  to  $\text{Fe}^{3+}$  samples were prepared in 0.1 M (8.6 mL) HCl when measuring for  $\text{Fe}^{2+}$ . The ICP-MS was performed using CCT mode for all analysis. Mohr's Salt 1000  $\mu\text{g/mL}$  was used as the stock solution to prepare  $\text{Fe}^{2+}$  in 100 mL. The standards calibration for  $\text{Fe}^{2+}$  had a range of 5 ng/mL – 1  $\mu\text{g/mL}$ . The standards were freshly prepared to avoid the oxidation of  $\text{Fe}^{2+}$ . 0.1 M sodium sulphate (analytical reagent grade Fisher Chemical, UK) was pumped, for ca.1 hour, through the column to remove oxygen.  $\text{Na}_2\text{SO}_3$  was prepared by dissolving 12.65 g in 1 L of deionised water to make a 0.1 M solution.

The standard reference material SRM TMDA-64.2 (LG Standards, UK) was used to assess the accuracy of the method. The SRM contained only  $\text{Fe}^{3+}$  and  $\text{Mn}^{2+}$  for the validation, but not  $\text{Fe}^{2+}$  because  $\text{HNO}_3$  was used in this reference which oxidizes  $\text{Fe}^{2+}$  to  $\text{Fe}^{3+}$

In order to assess the effect of  $\text{Ca}^{2+}$  ions on the samples, different levels of Ca (0-100  $\mu\text{g}/\text{mL}$ .) were spiked into a series of 100 ng/mL solutions chosen as the concentration of the mid calibration of the standards. The % recovery of Ca ion was calculated. All experiments used a flow rate of helium between 3 - 5 mL/min.

#### **4.2.4 Instrumentation**

#### **4.3.2 Spike recovery**

The validation and accuracy of the method used for this study was assessed by using certified reference material SRM TMDA64.2 (trace elements in water, river water, Canada), as well as samples spiked with known concentration (0.0375  $\mu\text{g}/\text{mL}$ ) using 75  $\mu\text{l}$  of 1  $\mu\text{g}/\text{mL}$  Fe and Mn solution in a 2 mL vial. The percentage recovery was calculated and achieved a range between 95-105%. The recovery percentage was calculated as previously described in section 3.4.

**Chromatography (HPLC):** A Spectra autosampler AS3000 and Thermo 4000 series HPLC pump (Thermo Fisher Scientific, USA) were used. The system consisted of an injector fitted with a 100  $\mu$ l PEEK injection loop. Fe and Mn speciation were performed using a Dionex CS5 (250 mm) & CG5 Guard column (50 mm) with diameter size 9. The flow rate of the mobile phase was 1 mL/min (Thermo Fisher Scientific, USA).

**The interface of HPLC-MS:** The HPLC column was directly connected to the ICP-MS impact bead nebuliser to enable transfer of the separated species to the ICP-MS for detection. These elemental species were then detected and quantified through the analysis of each ion according to the  $m/z$  ratio. The temperature not regulated by the HPLC.

Figure 4-1 illustrates the interface between HPLC-ICP-MS.

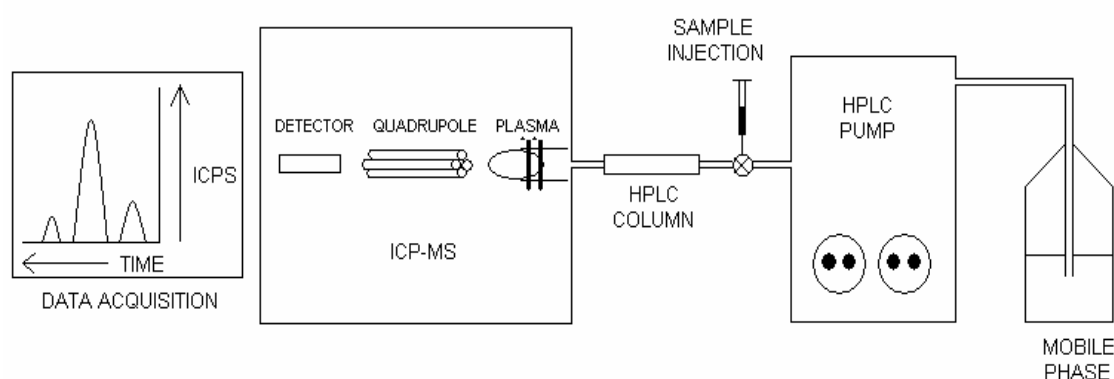


**Figure 4-1** Schematic diagram for HPLC-ICP-MS instrumentation (Thermo Fisher).

**ICP-MS:** ICP-MS Thermo X –series was used as a detector. It was equipped with a quadrupole mass spectrometer, with nickel sampler and skimmer cones (Thermo Scientific). The sample solution is pumped by a peristaltic pump from tubes. The torch (Thermo Scientific, Quartz-torch) position, gas output, ion lenses, resolution and background were optimised daily with the tuning

solution, which is discussed in section 3.2.1. The analysis was formed in CCT mode (collision cell technology) using He gas for reduction of polyatomic interfering ions. Table 4-1 presents the operating conditions and acquisitions parameters for the instrument.

**Table 4-1** Operation and acquisitions parameters of ICP-MS and HPLC.

	<b>Parameters</b>	<b>CCT Mode</b>
ICP-MS	RF Power	
	Nebuliser	Meinhardt nebulizer
	Spray Chamber	Cyclonic Spry chamber
	Extraction	-200
	Sample cone	Nickel
	Skimmer cone	Nickel
	Hexapole	-10
	Pole Bias	-7
	Analogue	$5-7 \times 10^{-7}$
	Expansion	$2.1 \times 10^{+0}$ mbar
	Helium flow rate	3.8 mL/min
HPLC	Flow rate	1 mL/min
	Run time	180 sec
	Mobile phase	PDCA
	Anionic-exchange columns	IonPac -Dionex CS5 (250 mm) and CG5 Guard (50 mm).
	Injection Volume	100 $\mu$ l

Instrumental conditions were tuned with the tuning solution as previously described in Sections 2.1.3.2 and 3.2.1. The calculation of peak area from the chromatograms was carried out by integrating the peak area using the Thermo-Plasma Lab software.

## **4.3 Analytical figures of merit**

### **4.3.1 The limits of detection and quantification**

Ten blank measurements were used for the determination of LoD and LoQ using Fe and Mn. Integrated areas of the peaks were used and the LoD and LoQ were calculated as previously described in Section 3.2 using the Miller and Miller method (202). The performance criteria of the method were assessed according to the IUPAC guidelines and according to the ICH Harmonisation Tripartite guideline validation of analytical procedure (220, 221) on different samples and with spiked samples. The spiked levels were comprised between the LoD and the most concentrated standard of the calibration curve.

## **4.4 Sample collection and preparation**

The water samples were collected from the Northwest region of England as previously shown on the map in Section 3.10. These samples were obtained from different locations and then they were collected from United Utilities (UU). These samples were placed in sterile disposable centrifuge tubes made of polypropylene (50 mL, Fisher Scientific) washed with hydrochloric acid and de-ionised water before use. These samples were acidified immediately after collection by addition of hydrochloric acid because acidification eliminates colloids and to avoid change of the low Fe oxidation state, Fe<sup>2+</sup> state (222). Then, all samples were kept frozen until analyzed to avoid oxidation of the minerals. Filtration was an essential step in the collection of this type of sample. All the preparation steps were carried out in a fume hood. For the

water analysis all samples were prepared in 2 mL HPLC vials (Agilent technology); 1.44 ml of sample was filtered (0.45 µm PTFE) to remove any particles in 0.18 mL of 2% HNO<sub>3</sub> and 0.18 mL of 100 ng/ml Rh solution as an internal standard. The solutions were then made up to a volume of 1.8 mL using ultra-pure water. The mobile phase was optimised using different pH values and the pH which gave optimum resolution of speciation was chosen for this method. Experimentally, a filtered sampling regime was designed in order to establish whether the Mn was soluble, colloidal or particulate. The water from each region was filtered through 0.45 µm, even though these samples had already been filtered during the UU treatment stages, and any Fe or Mn that passed through was classed as soluble. The filtration was required because of the solubility of both Fe and Mn according to the Pourbaix Diagram in Figures 1-2 and 1-3, which shows the different species of these metals formed at different pH levels (Section 1.1.2.1.1). The normal treatment process for soluble, Mn<sup>2+</sup>, is to oxidise the water (normally using chlorine) and raise the pH of the water in order to change it to a particulate form, which is then removed by the final filter stage.

## **4.5 Results and discussion**

### **4.5.1 The determination of Fe and Mn species**

The samples were collected from UU at different locations and treatments stages as described in Section (5.4).

#### **4.5.2 Testing the separation efficiency of different mobile phases**

Two mobile phases were tested systematically to obtain the final mobile phase after the optimisation of their compositions to change ionic strength and pH. Different columns were also tested as described below.

##### **4.5.2.1 Mobile phase and column**

In order to carry out Fe and Mn speciation by HPLC-ICP/MS, successfully, It was important to use the most effective mobile phase that was compatible with ICP-MS to maximize the long term stability and the sensitivity. The ICP showed a low tolerance for organic solvents due to the deposition of carbon into the torch. The optimization of the chromatographic method and the determination of Fe<sup>2+</sup>, Fe<sup>3+</sup>, and Mn<sup>2+</sup> was carried out using a using different mobile phase additives and the columns: Dionex CG5A guard column (50 mm) and Accucore C18 column (50 mm).

Two mobile phase additives, EDTA and PDCA, were tested with respect to time, pH and concentration; PDCA was chosen as a potential additive as it forms strong anionic complexes with most of the metal ions. Figure 4-2 shows that the peak for the standard 1 ppm sample gave different positions each run using EDTA. It was not stable using identical conditions.

The CG5A Guard (50 mm) column is an anion-exchange mixed bed columns containing anionic and cationic material and allows separation of Fe and Mn with PDCA (223). This column was previously used by Dionex for multi-element determination (224). Figure 4-3 (AB) shows the peak separation differences between the two column conditions that were optimized; Dionex CG5A guard column with PDCA; Accucore C18 with EDTA. The separation

using EDTA for Fe and Mn species was not very good at pH 6.8 using Accucore C18 with EDTA. The separation was found to be excellent using Dionex CG5A guard column, including separation of both ion species. No further conditions were optimized. The species of Fe can be influenced by pH and concentration of the eluent so further experiments were carried out.

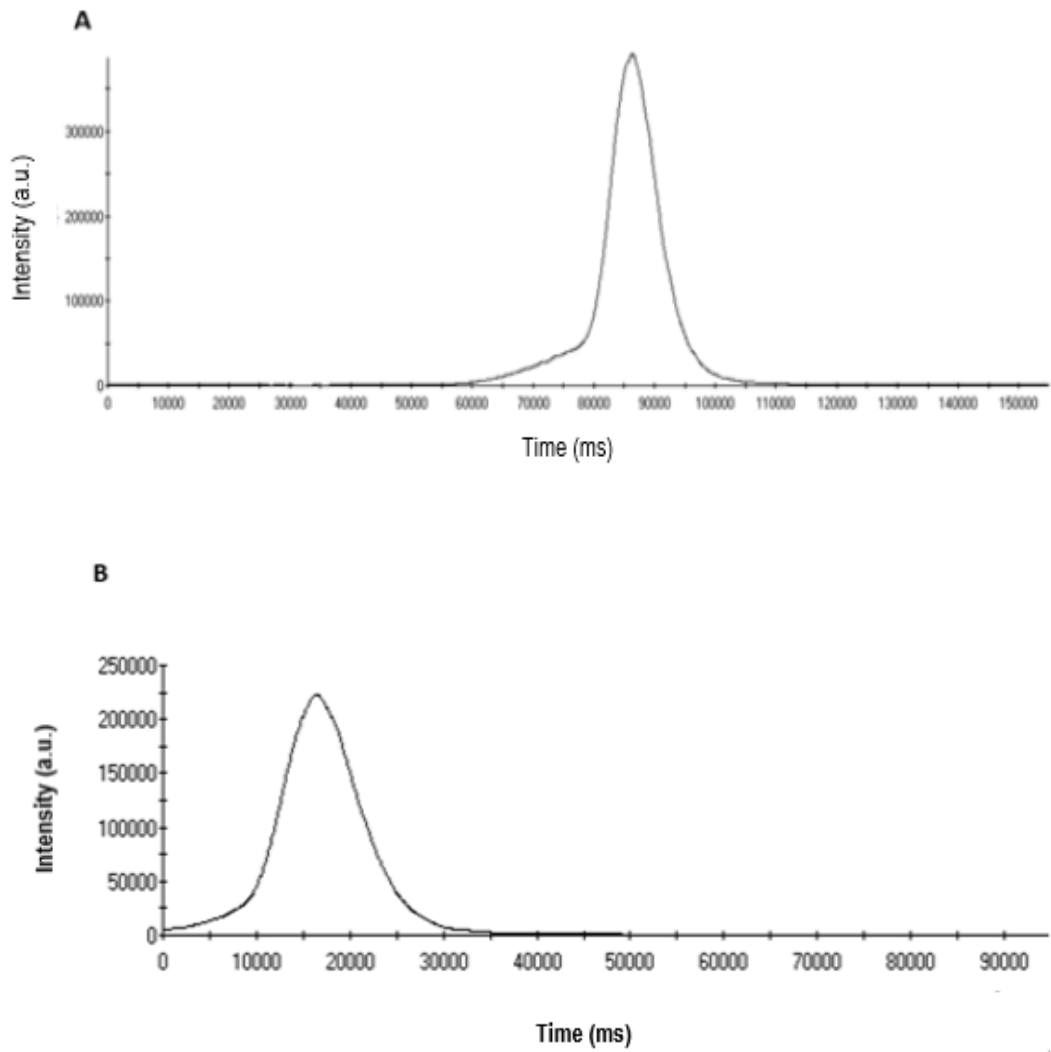


**Figure 4-2** 1 ppm Mn standard traces (A and B) using EDTA shifted after identical runs.

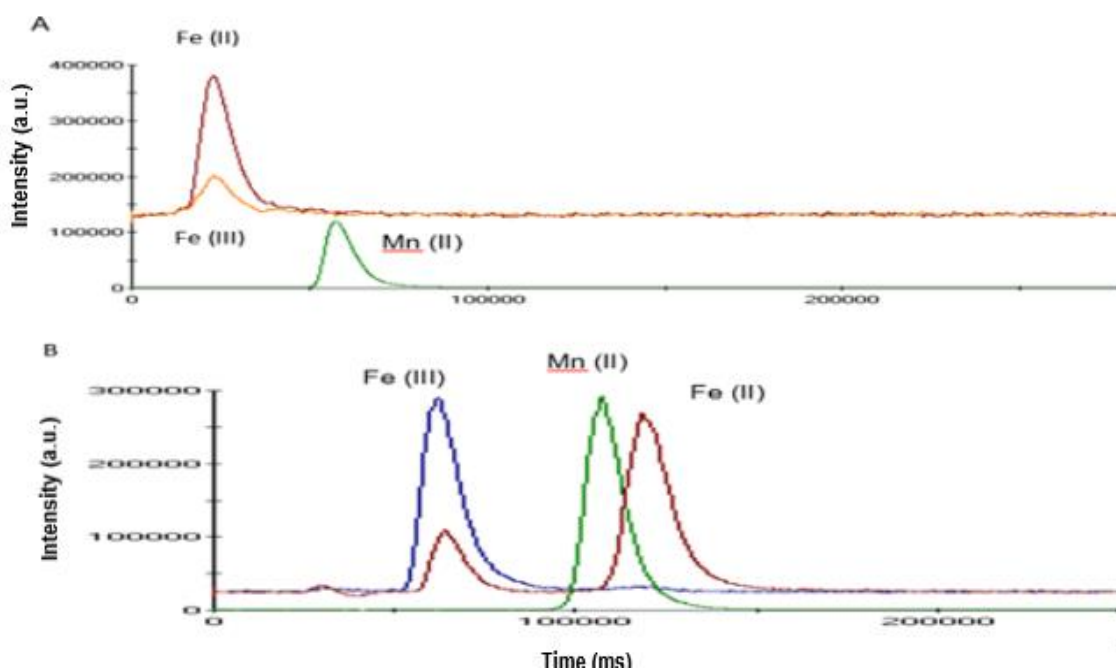


**Figure 4-3** The different mobile phases and peak separation for EDTA using ACCUCORE C18 column (A) and PCDA using Dionex CG5A guard column (B).

#### 4.5.2.3 pH Optimisation

A Pourbaix diagram shown in Section 1.1.2.1 shows how different species of Fe and Mn are formed at different pH levels and the associated oxidation levels for both elements. For example,  $\text{Mn}^{2+}$  is a soluble form of Mn and there are a number of treatment processes able to raise the pH of the water causing particles to form, which are then removed through the water treatment filter. It was important to optimise the pH of the mobile phase during the sample's analysis using HPLC- ICP-MS and then study the different levels to observe how pH affects the changes of the species of the elements, and therefore how pH can affect water treatment analysis. The optimisation studied the optimal pH range for speciation.

Figure 4-4 (A-E) shows the effect of pH on the peak separation of  $Mn^{2+}$ ,  $Fe^{2+}$  and  $Fe^{3+}$ . The aim was to avoid overlapping of peaks in the traces. A range of pH values were investigated using the same eluent. There was little effect on retention time for Fe and Mn separation. A small peak appeared before the major Fe and Mn peaks (Figure 4-3, A/B). The reason could be the presence of  $^{40}Ca^{16}O$ , but this should be removed by the CCT system.

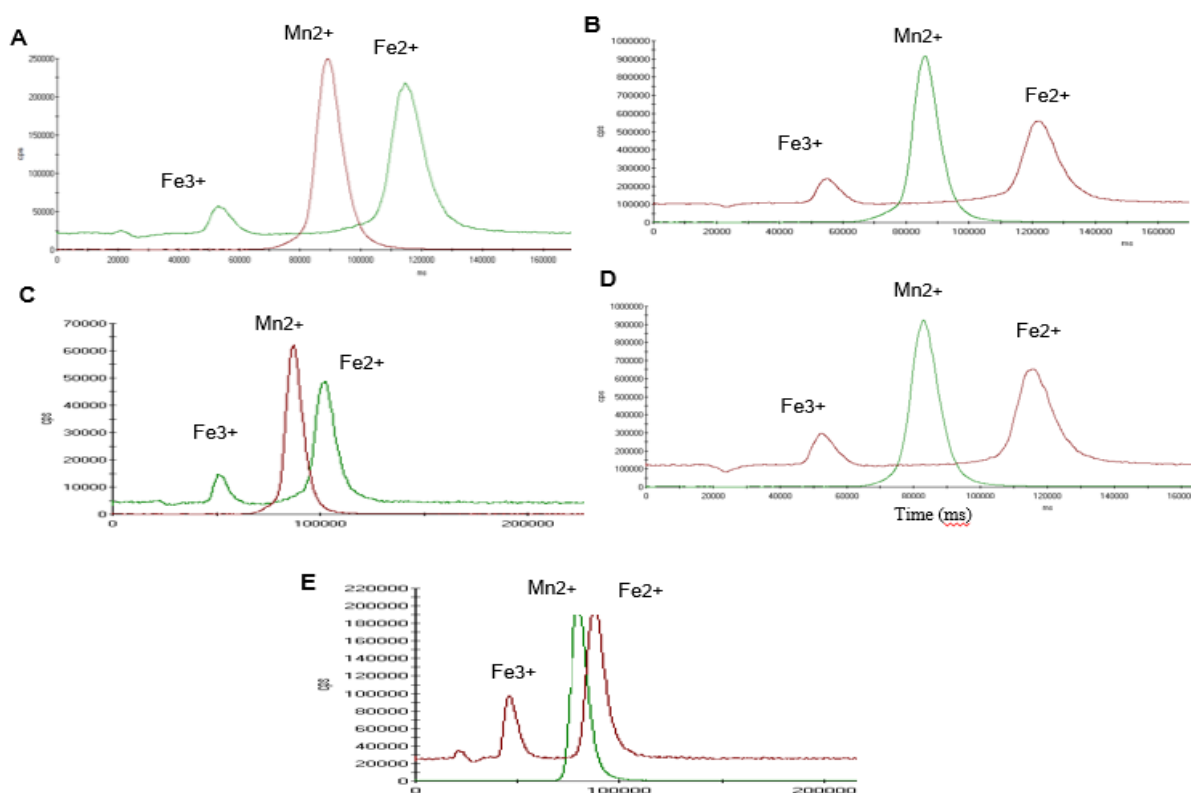


**Figure 4-4** The effect of mobile phase pH on the peak separation for Fe and Mn species using PDCA and CG5 Guard (50 mm) (pH; A = 3, B = 3.3, C = 3.6, D = 3.9 and E = 4.2).

Both Fe and Mn generated peaks at all pH values. For example, at pH 4.2, Mn had a retention time of 1.66 min with a peak height of 80000 cps, and Fe had a peak height of ~140000 cps and appeared at an earlier time than the Mn species. The optimal peak separation was observed at pH 3.3 where  $Mn^{2+}$ ,

$\text{Fe}^{3+}$  and  $\text{Fe}^{2+}$  were detected at retention times of 1.3, 0.66 and 2 minutes, respectively. Based on the results obtained, further experiments were performed at pH 3.3 using Dionex CG5A guard column (50 mm), with the mobile phase as reported in the experimental section.

The selectivity of this separation depends on the different binding between metal ions and chelating agents. Using the chelating agent, PCDA, it was possible to separate  $\text{Mn}^{2+}$ ,  $\text{Fe}^{3+}$  and  $\text{Fe}^{2+}$  in one single chromatogram run. The results showed that using the column and mobile phase stated above and through adjustment of the pH of the mobile phase that the amount of  $\text{Fe}^{3+}$  was considerably reduced.

The peak height was found to vary at different pH values as can be seen on the chromatograms of all species. Based on the investigation using the chromatograms, stability was found to be sufficient at pH 3.3. At the other pH values, greater instability was observed because of instrument sensitivity, which caused a shift of the retention times and poor Fe species resolution. This shift may have been the result of changes in flow rate and response of the HPLC at the different pH values. Figure 4-5 shows HPLC-ICP-MS chromatograms and the signal responses of 1  $\mu\text{g}/\text{mL}$   $\text{Mn}^{2+}$ ,  $\text{Fe}^{2+}$  and  $\text{Fe}^{3+}$  under the optimal conditions discovered as stated above. The speciation and use of PDCA as the complexing agent for seven transition metal ions was performed so that  $\text{Fe}^{3+}$  was eluted before  $\text{Fe}^{2+}$  as seen in the chromatograms (225).

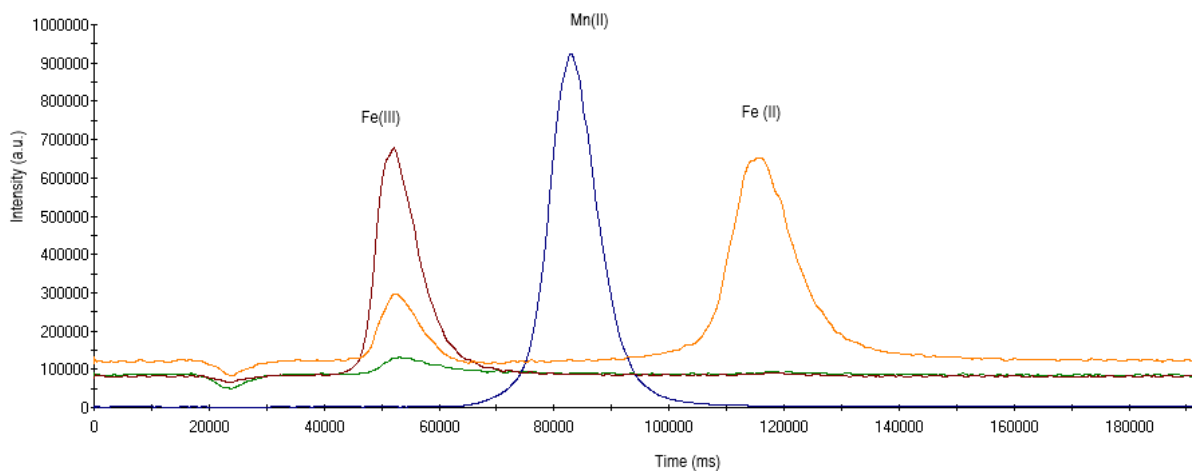


**Figure 4-2** Chromatograms and the signal responses of 1  $\mu\text{g/mL}$   $\text{Mn}^{2+}$ ,  $\text{Fe}^{2+}$  and  $\text{Fe}^{3+}$  at pH 3.3 using Dionex CG5A guard column (50 mm), PDCA acid mobile phase;

### 4.5.2 Interferences

The use of CCT mode and selectivity of the Dionex CG5A guard column was studied to avoid interferences in the water samples such as cationic components including alkali and alkali earth metals. Figure 4-6 shows the chromatograms for both metal ion analytes. All water samples were analysed using CCT. The helium flow rate obtained from optimisation work was 3.8 mL/min and resulted in more than a 10-fold drop in Fe background counts per second because of reduction of Ar based polyatomic interferences to  $^{56}\text{Fe}$  such as  $\text{Ar}^{40}\text{O}^{16}$  and  $\text{Ca}^{40}\text{O}^{16}$  derived from the plasma gas, reagents or sample matrixes. The use of an internal standard during the analysis by ICP-MS and method development was important to ensure that any cause of instrumental drift or enhancement of ICP-MS response that was caused by sample matrixes were corrected. This way of trying to achieve satisfactory instrument performance and obtaining the best reproducibility was the simplest and used the least resources to lower the interferences. Indeed, this method obtained a good calibration curve and the instrument performance was acceptable.

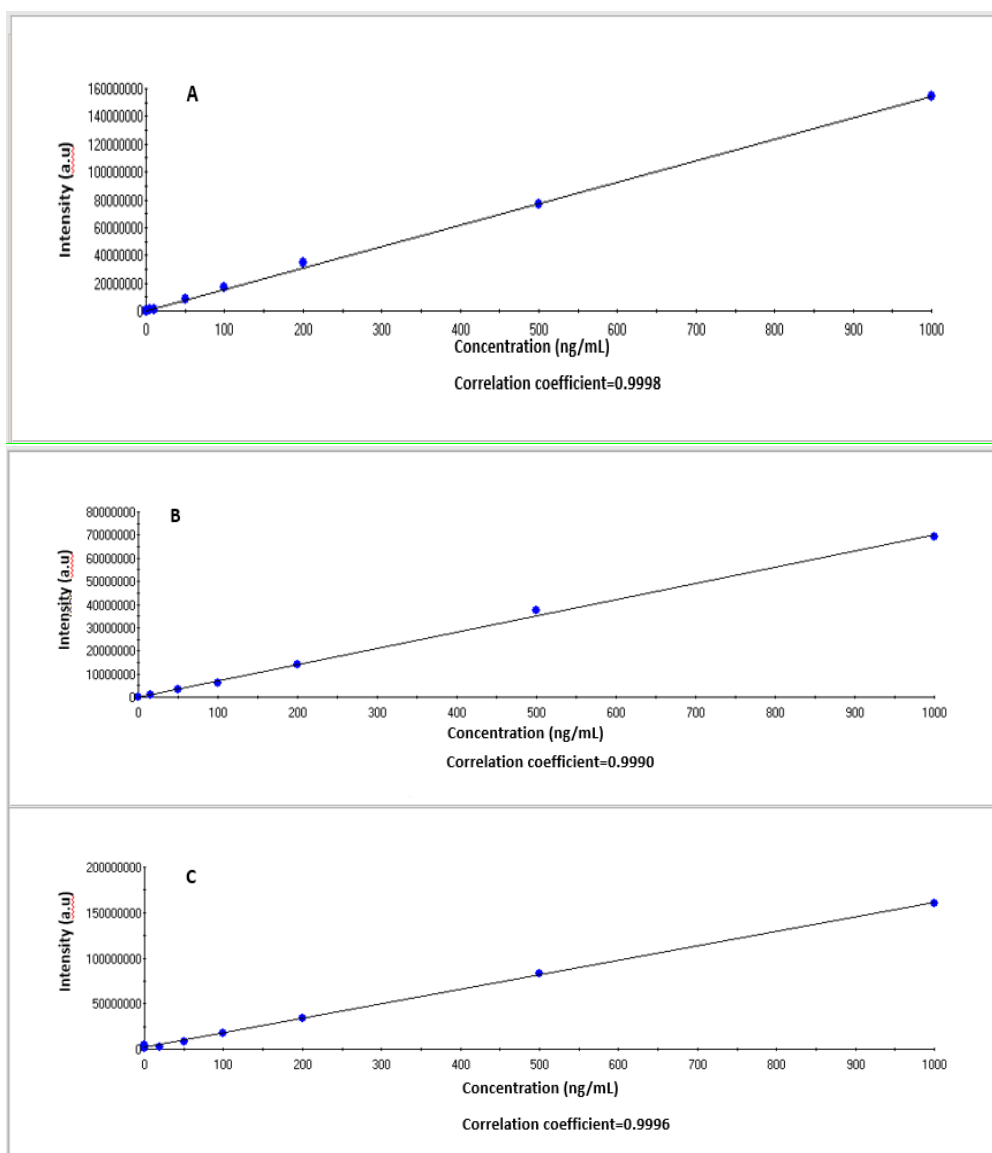


**Figure 4-3** Calibration responses for Mn<sup>2+</sup> (A) and for Fe<sup>2+/3+</sup> (B and C respectively) using HPLC-ICP-MS.

The calibration graphs of both Fe and Mn had very good linearity ( $R^2 = 0.9995$  for Fe and 0.9999 for Mn) as presented in Figure 4-6. There were some issues with the reproducibility of signal using HPLC-ICP-MS in both the Fe and Mn determinations. The chromatogram of Fe (1  $\mu\text{g/mL}$ ) and all standards of Mn using CCT had sufficient sensitivity for sample peaks to be observed in both chromatograms. The major problem interferences from the <sup>56</sup>Fe line (<sup>40</sup>Ar<sup>16</sup>O and <sup>40</sup>Ca<sup>16</sup>O,) during sample analysis was reduced through the use of helium

gas and HCl was used for the analysis of  $\text{Fe}^{2+}$  to avoid conversion of this element ( $\text{Fe}^{2+}$  to  $\text{Fe}^{3+}$ ). Signal response of  $\text{Fe}^{2+}$  and  $\text{Mn}^{2+}$  standard solutions at the concentration of 50 ng/mL, 100 ng/mL and 1000 ng/mL, respectively, using PDCA are shown in Figure 4-7.

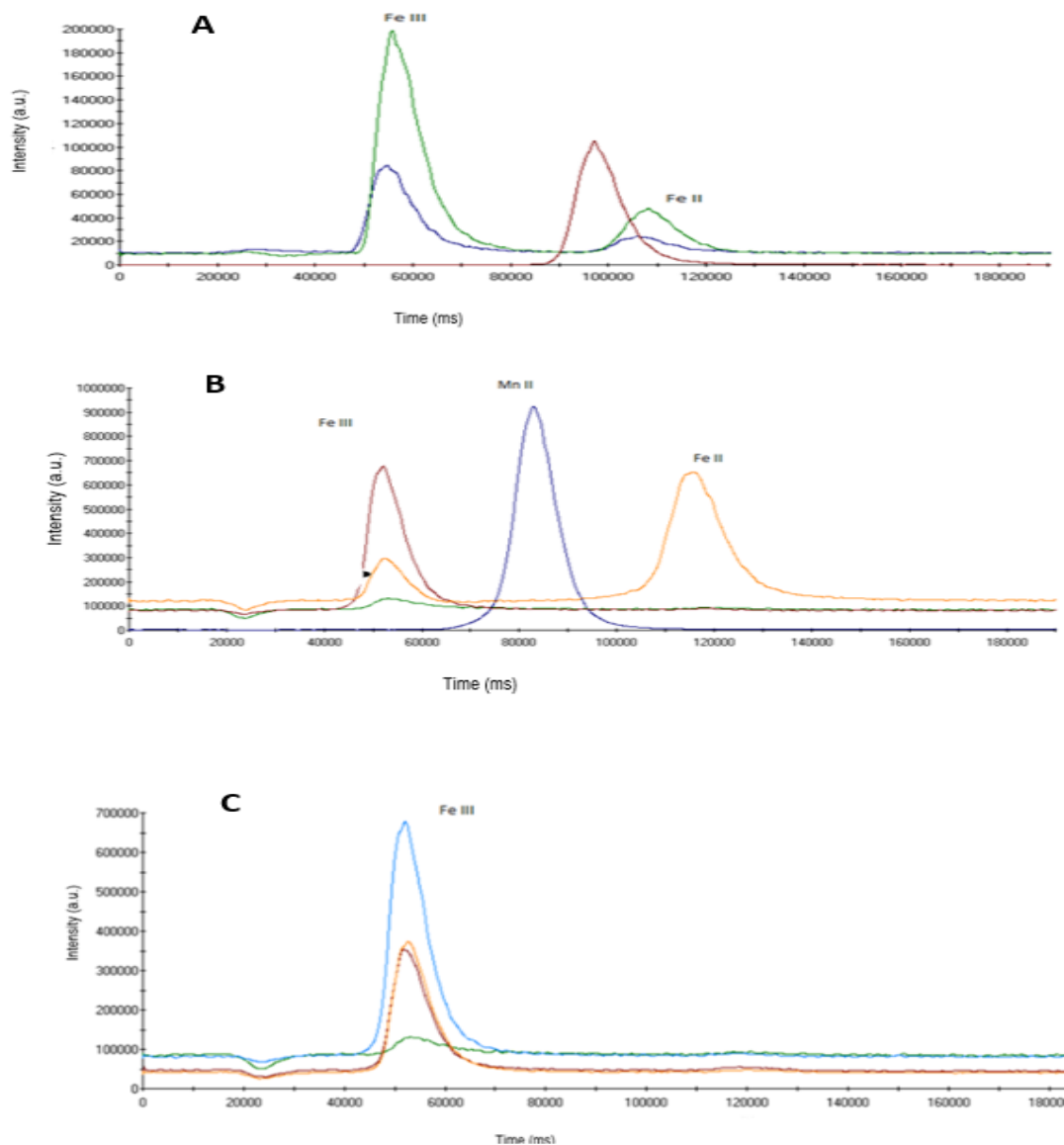


**Figure 4-4** Signal response of  $\text{Fe}^{2+}$  and  $\text{Mn}^{2+}$  standards solutions at the concentration of (A) 50 ng/mL (B) 100 ng/mL and (C) 1000 ng/mL using PDCA.

Daily CCT conditioning was performed to achieve low baselines counts for each of the ions monitored.  $\text{Fe}^{2+}$  standards were prepared from a working standard of 1000  $\mu\text{g}/\text{mL}$   $\text{Fe}^{2+}$  for this study. Figure 4-7 B shows the  $\text{Fe}^{2+}$

(monitoring at  $^{56}\text{Fe}$  and  $^{57}\text{Fe}$ ) peak with a small amount of  $\text{Fe}^{3+}$  indicated by the peak earlier in the chromatogram. This was likely caused during the preparation of the standards or other problems as described in Section 4.5.2.2.

Figure 4-4 shows the chromatograms of mixed standards of  $\text{Mn}^{2+}$  and  $\text{Fe}^{2+}$  using different calibration ranges for each standards. Compared to the 7000,000 cps background level for  $^{56}\text{Fe}$ , the background for  $^{55}\text{Mn}$  was only at about 800 cps, which indicated lower polyatomic interferences. This is a bigger problem for Fe because of the generation of ArO and CaO. The measurements of the  $\text{Fe}^{2+}$  standards indicated that the detection of  $\text{Fe}^{2+}$  species using the HPLC-ICP-MS method was dependant on the use of different standard solutions; 50 ng/mL for both Mn standards and 20 ng/mL and for Fe. Figure 5-7 (A-C). All the results show good chromatograms with reproducible retention times for  $\text{Fe}^{2+}$ ,  $\text{Fe}^{3+}$  and  $\text{Mn}^{2+}$  species. In addition, the  $\text{Fe}^{3+}$  peaks reached the level of 200,000 for all calibration standards of  $^{56}\text{Fe}$  and 100,000 cps for  $^{55}\text{Mn}$  (Figure 4-7 (A-C)). Sometimes a small peak appeared before the main Fe and Mn peaks and it was related to contamination of the salt used to manufacture the standard with  $\text{Fe}^{3+}$ .

### **4.5.3 Validation**

The accuracy of this method was determined using a river water certified reference material TMDA-64.2 containing a known concentration of Fe and Mn. The analysis was carried out four times with a triplicate reading taken in each case the sample were analysed on the same day to make sure of repeatability. The percentage recoveries were between 95-105%. Since the  $\text{Fe}^{2+}$  ion is easily oxidized to  $\text{Fe}^{3+}$ , oxygen must be removed from the column

using a solution of 0.1 M sodium sulphite (12.6 g/L Na<sub>2</sub>SO<sub>3</sub>) which was pumped, for ca.1 hour, through the column to remove oxygen. The measured results and % recoveries are presented in Table 4-4.

The precision was evaluated by analysing solutions containing Fe and Mn in at least 10 replicates. The repeatability and precision were expressed in the results as recoveries. The relative standard deviation for Fe and Mn were 5 and 4%, respectively. The precision was assessed by the analysis of 0.025 mg/mL of this solution over 5 different days. The value of the results obtained from Fe precision was higher than Mn and probably due to the instability of its species (3% for Mn and 6% for Fe).

**Table 4-2** TMDA-64 percentage recovery.

<b>Analyte</b>	<b>CRM<sup>a</sup> Recovery (%)</b>	<b>Certified value (µg/l)</b>	<b>Found value (µg/l)</b>	<b>Spiked Sample<sup>b</sup> Recovery (%)</b>
<b>Fe<sup>2+</sup></b>	N/A	N/A	N/A	102.5 ± 5.2
<b>Fe<sup>3+</sup></b>	98.2 ± 5.1	306	298.3	98.4 ± 5.5
<b>Mn<sup>2+</sup></b>	96.2 ± 4.1	295	294.2	96.5 ± 4.3

<sup>a</sup> TMDA-62.2 was used as Certified Reference Material.

<sup>b</sup> Mean of four replicates.

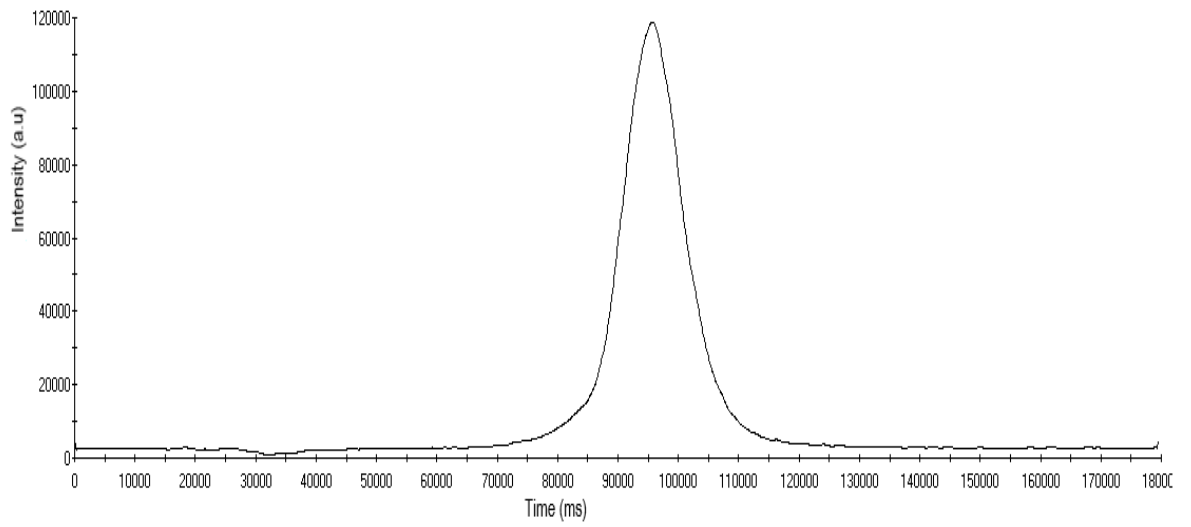


**Figure 4-5**  $^{55}\text{Mn}$  standard reference material (TMDA) peak.

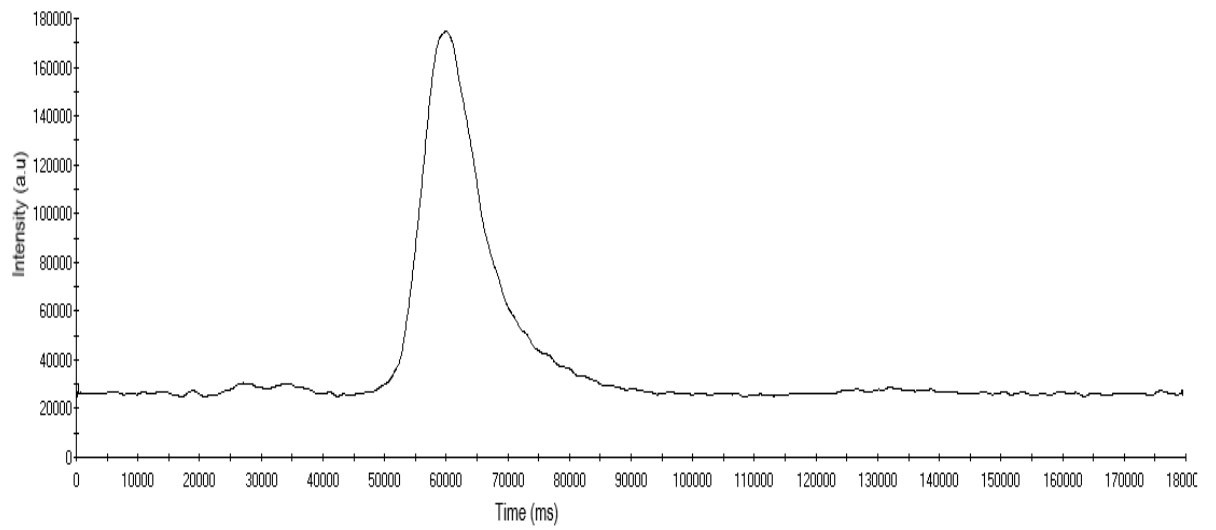


**Figure 4-6**  $^{56}\text{Fe}$  standard reference material (TMDA) peak.

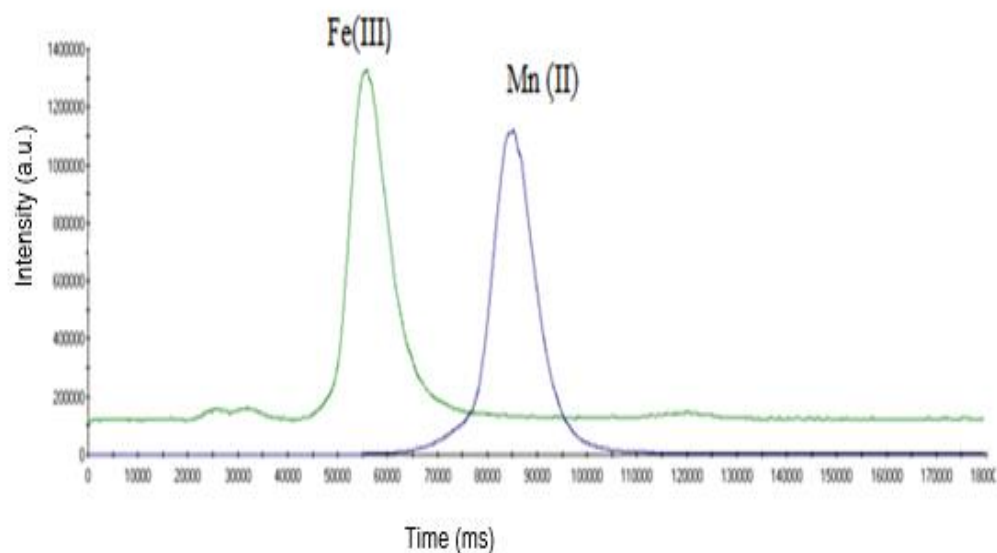


**Figure 4-7** 1 ppm standard for SRM TMDA-64.2 for both  $^{56}\text{Fe}$  and  $^{55}\text{Mn}$  chromatograms.

#### 4.5.3.1 The limit of detection and quantification LOD and LOQ

The detection using ICP-MS coupled to HPLC can be used without modification of the HPLC or ICP-MS conditions. The conditions for ICP-MS were checked to ensure the optimal conditions using CCT mode. In order to maximise sensitivity, no changes were made to the previous conditions and, with the exception of flow rate, the detection limits for Fe and Mn were as given in Table 4-3. Calibration graphs for both elements are shown in Figure 4-11 and 4-12 and the linearity obtained in both cases was greater than a  $R^2$  of 0.995. In order to improve reproducibility, Rh at 10 ng/mL as an internal standard. These results were compared to the LoD and LoQ obtained using CCT mode with ICP-MS as described in Section 3.6.3.2. The LoD and LoQ for

Fe and Mn were determined using x3 and x10 of the standards deviation of a blank which were 0.2 and 0.7 ng/mL for Mn, respectively, and 14 and 16 ng/mL for Fe, respectively.

The CCT conditions led to reduced Ar interferences at the mass to charge ratio ( $m/z$ ) of  $^{56}\text{Fe}$  ( $^{40}\text{Ar}^{16}\text{O}$ ). Furthermore, polyatomic interferences due to other species such as  $^{40}\text{Ar}^{16}\text{O}$  and  $^{40}\text{Ca}^{16}\text{O}$  were also reduced.

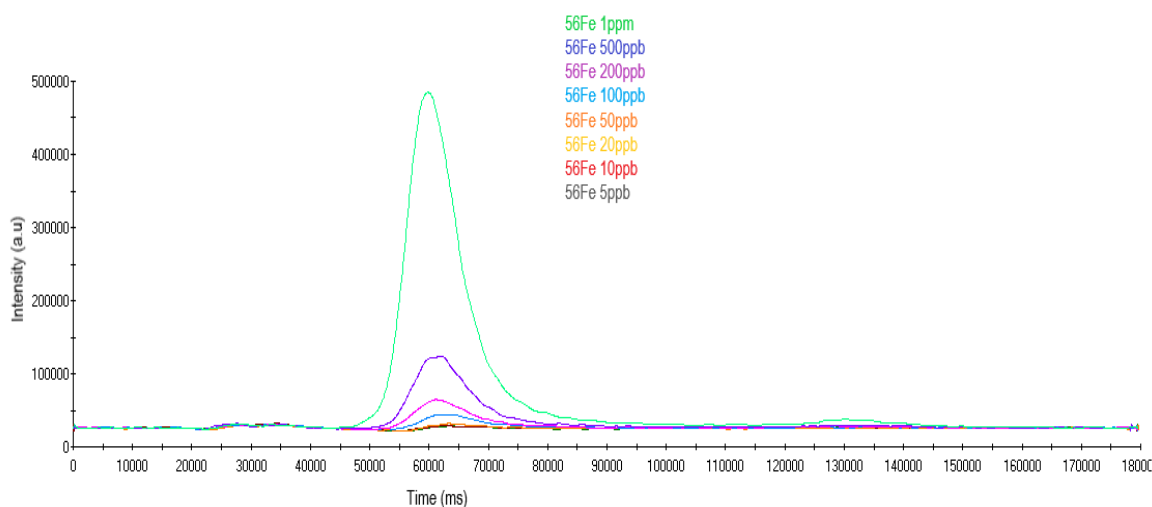


**Figure 4-8** All chromatograms for  $\text{Fe}^{3+}$  calibration standard solutions.

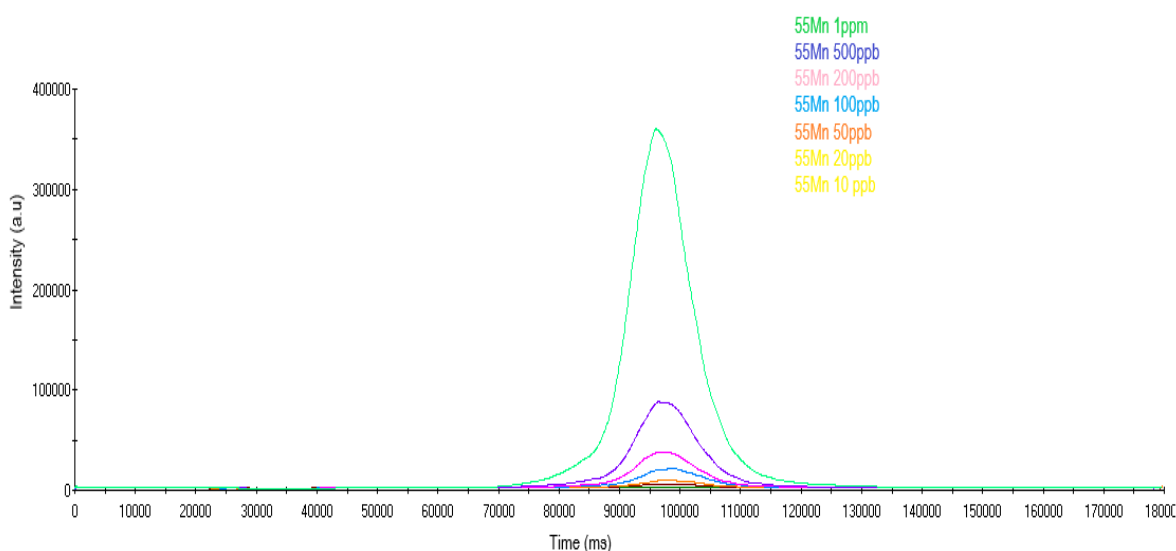


**Figure 4-9** All chromatograms for  $\text{Mn}^{2+}$  calibration standard solutions.

Analyte	LoD (ng/mL)	LoQ (ng/mL)
Fe <sup>2+</sup>	0.07	0.017
Fe <sup>3+</sup>	0.005	0.0014
Mn <sup>2+</sup>	0.0005	0.0018

**Table 4-3** LoD and LoQ for Fe and Mn using HPLC-ICP-MS.

#### **4.5.4 Water processing sample analysis for Fe and Mn species in drinking water using HPLC-ICP-MS**

##### **4.5.4.1 Water analysis at different locations**

The full results of the water processing samples are shown in Tables (4-4 - 4-7). Highest concentrations of Mn occurred at the post clarifier stages at the treatment works, giving 109.7 and 69.6 ng/mL for the Wayho water samples clarified stages (Table 4-4). The concentrations showed that more Mn than Fe was detected, particularly at the clarified water stream. The results show that for Wybersley, Sweet Loves and Sutton Hall, the Mn concentration increased during the clarified and combined stages as well. The concentration of Mn changed at the filtration stages to higher concentrations. This was particularly evident for Wayoh and Wayoh plants. This was because of the addition of coagulations at the clarification stages. For example, aluminium sulphate was used at Huntington and ferral coagulant sulphate applied at Sutton Hall, and

these compounds may have contained impurities. The various stages of filtration at the Wayoh plant (Table 4-4) appear to be successful in reducing the amount of Mn<sup>2+</sup>. The amounts of Fe and Mn concentrations at the final stages were shown to be less than at previous treatment stages and below the LoD and the excess limits.

The Fe level in 95% of the samples was below the permit level. The Fe concentration increased at the Wybersley “combined primary filtrate 2” only, but otherwise the level was less than the LoD. Interestingly, Sutton Hall, which used iron sulphate as a coagulant, showed very low levels of ion species.

**Table 4-4** Metal contents of Wayoh water samples.

<b>Water samples</b>	<b>Mn<sup>2+</sup></b> ng/mL	<b>Fe<sup>3+</sup></b> ng/mL
<b>Wayoh Plant inlet*</b>	1.6	< LoD
<b>Wayoh clarified water stream 1</b>	109.7	< LoD
<b>Wayoh combined filtered from filters</b>	69.6	< LoD
<b>Wayoh combined filtered from 5-8</b>	43.9	< LoD
<b>Wayoh actiflo combined outlet stream</b>	51.6	< LoD
<b>Wayoh secondary filtered stream 1</b>	< LoD	< LoD
<b>Wayoh final water</b>	<LoD	< LoD

**Table 4-5** Metal contents of Wybersley water samples.

<b>Water samples</b>	<b>Mn<sup>2+</sup> ng/mL</b>	<b>Fe<sup>3+</sup> ng/mL</b>
<b>Wybersley combined raw water stream 1*</b>	1.9	26.2
<b>Wybersley combined raw water stream 2*</b>	1.2	17.8
<b>Wybersley clarified water stream 1</b>	70.7	< LoD
<b>Wybersley clarified water stream 2</b>	21.9	6.1
<b>Wybersley combined primary filtrate 1</b>	78.8	< LoD
<b>Wybersley combined primary filtrate 2</b>	84.1	43.7
<b>Wybersley combined 2nd filtrate</b>	< LoD	< LoD
<b>Wybersley 24 Inch main</b>	0.4	< LoD

**Table 4-6** Metal contents of Sweet Loves water samples.

<b>Water samples</b>	<b>Mn<sup>2+</sup> ng/</b>	<b>Fe<sup>3+</sup> ng/mL</b>
<b>Sweet Loves raw water inlet*</b>	0.8	44.9
<b>Sweet Loves clarified water</b>	5.0	12.0
<b>Sweet Loves combined primary filtrate</b>	0.7	< LoD
<b>Sweet Loves combined secondary filtrate</b>	0.3	< LoD
<b>Sweet Loves final water</b>	<LoD	<LoD

**Table 4-7** Metal contents of Sutton Hall water samples.

<b>Water samples</b>	<b>Mn<sup>2+</sup> ng/mL</b>	<b>Fe<sup>3+</sup> ng/mL</b>
<b>Sutton Hall inlet to plant</b>	< LoD	< LoD
<b>Sutton Hall WTP raw water inlet</b>	1.4	14.5
<b>Sutton Hall combined clarified</b>	17.4	< LoD
<b>Sutton Hall combined 1st stage filter</b>	17.5	< LoD
<b>Sutton Hall 2nd stage B filtered</b>	1.4	< LoD
<b>Sutton Hall No.2 final water</b>	< LoD	< LoD
<b>Sutton Hall No.1 final water</b>	< LoD	< LoD

#### **4.5.4.2 Fishmoore Mn<sup>2+</sup> concentrations for each stage of the treatment process.**

For most water treatment works, it has become evident that during the Post Clarifier stage Mn concentrations increase compared to the raw water.

Fishmoore raw water (Tables 4-8 – 4-9) was found to have less Mn present than Wybersley, Wayoh, and Sweet Love water during the Clarifier stages. The chromatograms for Fishmoore water and changes that occur during different stages of the treatment plant clearly showed different levels of Mn. It has also been noted that different reagents were used to achieve coagulation at the treatment stages, so that the increase in Mn concentrations may be due to the addition of these coagulants. It was suspected that the Mn levels increased because of addition of ferric chloride (used as a coagulant) and H<sub>2</sub>SO<sub>4</sub>, which was used to adjust pH. It was also suspected that different species of Mn occurred at the different stages. This was significant because it makes it more likely that drinking water metallic concentrations in pipes could over time increase and lead to colouration.

Table 4-8 presents Fe and Mn species concentrations found for both Mn<sup>2+</sup> and Fe<sup>3+</sup> in Fishmoore raw water analysed by HPLC-ICP-MS and table 4-9 presents <sup>55</sup>Mn and <sup>56</sup>Fe using ICP-MS. Figure 4-13 and 4-14 show the Mn species as an example of the speciation on the HPLC-ICP-MS for raw water and accelerator water chromatograms in Fishmoore water. Studying the acc stages in both tables, the metals concentration is higher than the levels in the other stages which can be explained by the addition of the different coagulants at this stage.

**Table 4-8** Metal concentration level of Fishmoore water by HPLC-ICP-MS.

Water stages	Mn <sup>2+</sup>	Fe <sup>3+</sup>	Fe <sup>2+</sup>
Raw water	6.30	21.50	0
First stage filter outlet	12.49	0.00	0
Second stage filter outlet	0.60	0.00	0
Accelerator No.1	14.07	18.10	21.9
Accelerator No.2	30.58	37.30	65.4
Final water	0.25	0.65	0

**Table 4-9** Metal concentration levels of Fishmoore water by ICP-MS.

Water stages	<sup>55</sup> Mn	<sup>56</sup> Fe
Raw water	7.33	26.28
First stage filter outlet	13.53	4.3
Second stage filter outlet	0.73	0.2
Accelerator No.1	13.6	32.8
Accelerator No.2	38.9	62.61
Final water	0.5	0.65

The results clearly showed that both Fe and Mn appeared at high concentration during the addition of the coagulations in the Fishmoor water processing plant and the concentration was less at the final stages of the

treatment. The source of the Mn is thought to be due to  $\text{KMnO}_4$  used in the treatment process.

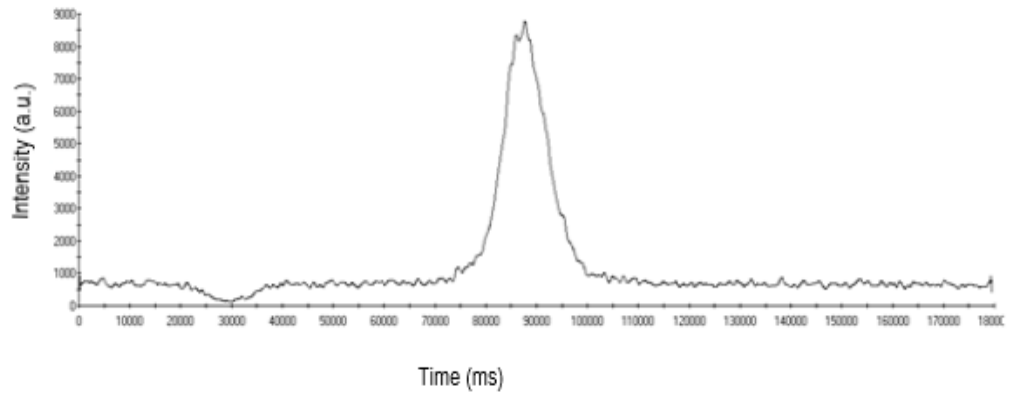


**Figure 4-10** Chromatograms for Mn raw water.

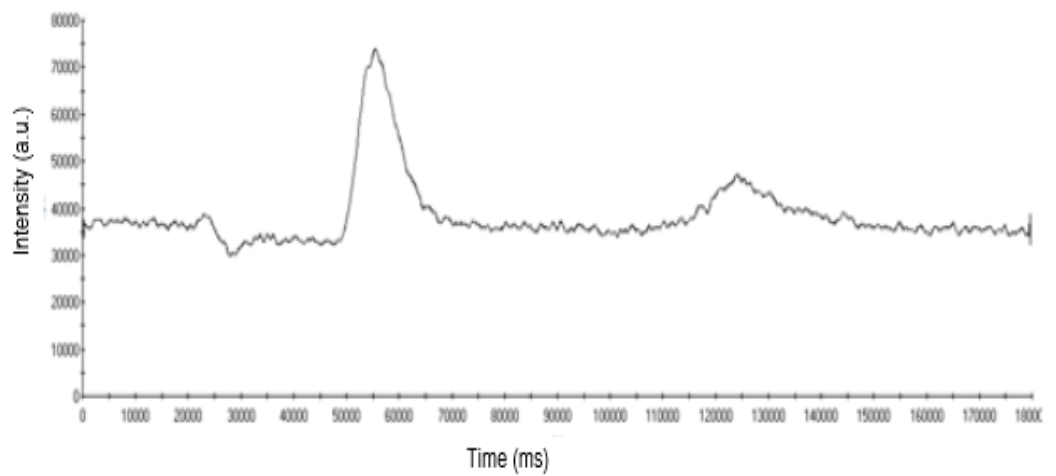


**Figure 4-11** Accelerator No1 water.

## 4.6 Conclusion

A HPLC-ICP-MS method has been successfully developed to determine the speciation of Fe and Mn at low levels in drinking water. HPLC-MS is a valuable speciation tool for the analysis of Fe and Mn in drinking water with a wide range of variability. This is important as it indicates more details about the metal compounds.

The results obtained above show that the use of HPLC-ICP-MS with a CS5 column is a rapid way of screening water plant samples to identify the cause of the problem in different locations at each stages of water treatment network. The use of the column was capable of separation of all species in a fast time (3 min). The separation of both Fe and Mn were possible through coupling of the HPLC mobile phase flow rate and the nebuliser flow of the ICP-MS.

The result showed that both Fe<sup>3+</sup> and Mn<sup>2+</sup> appeared at high concentration during the addition of the coagulations in the water processing plant and the concentration was less at the final stages of the treatment. The levels of Fe and Mn at the different removal stages such as post clarified, ACC (1 and 2), steam, clarified and inlet stages were seen to vary. These levels were higher at some point of the treatment than others. This information will be beneficial to the removal of discolouration through achieving very low levels of Fe and Mn and it is important as improvements of pipes to manage discolouration was only a temporary solution to this problem.

It has been noted that different reagents are used to achieve coagulation at the water treatment plants. For example, different coagulants applied during the treatment stages, such as aluminium sulphate used at Huntington and ferric coagulant sulphate applied at Sutton Hall. The increase in Mn concentrations may be due to addition of the coagulants. The results showed that both Fe and Mn appeared at high concentration during the addition of the coagulations in the water processing plants whereas, the concentration was less at the final stages of the treatment. Previously, water treatment issues have been implicated concerning Mn added during water processing as a disinfectant and Fe added at the coagulant agent stages lead to an increase of Mn concentration (226).

This resulted in the presence of higher concentrations of Mn in post treatment water samples. It is possible that the addition of ferric chloride as a coagulant and H<sub>2</sub>SO<sub>4</sub> which was used to adjust the pH during the water treatment process caused Fe and Mn to enter the network system and resulted in precipitation and caused the discolouration problem and customer's complaints. The treatment water issue that Mn being added during water processing, Fe coagulant agent stages the addition of it was increased soluble Mn concentration. It is likely that the soluble manganese (Mn<sup>2+</sup>) is the species that contributes to the cohesive material on the internal surface of pipes that leads to discolouration in the water supply.

Despite the large amount of the investment over the past 20 years in mains pipe renewal and cleaning, discoloration still remains one of the key challenges for the water industry. It is really important for these companies to

understand the mechanism of water treatment and how it affects speciation and to have a comprehensive strategy in place to deal with compliance. It can be concluded our HPLC-ICP-MS methodology, is an important, reliable, procedure for the multi-element speciation for the analysis of Fe and Mn in water samples.

## **Chapter 5 Overall conclusion and future work**

### **5.1 Overall conclusion**

Improvement of the quality of drinking water by minimization of the amounts of potential Mn and Fe ions is necessary. The aim of this work was to optimise and validate different analytical methods for the determination of Fe and Mn simultaneously in water samples. It was also a purpose of the work to develop a robust methodology that would allow greater understanding of Fe and Mn speciation at different stages of water treatment and its relationship with governmental limits. The first two methods that were developed were inductively coupled plasma optical emission spectroscopy ICP-OES and inductively coupled plasma mass spectrometry ICP-MS. This work has given a better understanding of the ion species by studying water from different treatment plants which will pass through into the water system and could potentially influence discoloration. Thus, the project makes a contributions towards the improvement of the aesthetic quality of water.

The methods of ICP-OES and ICP-MS were validated using TMDA as the standard reference material (SRM). It was found to be sufficient along with the spiked addition technique for the accuracy of the determinations. The samples were also analysed using the internal standard method and was found to be good for the determination to minimise variation in the results obtained from both methods. The results showed good relative standard deviation (RSD) <5%, linearity ( $R^2 > 0.996$ ), and spiked recovery between 95-105%. The low limit of detection (LoD) and limit of quantification (LoQ) were found to 5 ng/mL and 12 ng/mL for Fe and 1.2 ng/mL and 6.7 ng/mL for Mn, respectively, using

the optimum conditions for ICP-OES. These limits for the ICP-MS were found to be 0.6 ng/mL and 0.3 ng/mL, respectively, with collision reaction cell (CCT). Generally, all the water treatment met the DWI of Fe and Mn using the ICP-OES. However, an increase of Fe and Mn removal is essential at many water treatment plants to meet most regulations because both metals change into insoluble forms of Fe and Mn, which then stick to water pipes as yellow and black colours under sudden changes in physiochemical parameters such as velocity. Therefore, the water industry needs to minimize the discolouration occurrence by cleaning and removal processes depending on treatment plants.

One of the main finding of this work is the proposal of a need to test the coagulation reagents from water treatment works. Importantly, there is a need to know how much of these coagulant materials are added. However, it was not an aim of this study as the focus was on method development for the determination and the speciation of both Fe and Mn at different processing plants. In this way it is hoped the work could improve the quality and reliability of drinking water. It can be concluded that use of the coupled techniques is an efficient way to monitor both elements in drinking water, as a multi-element capability with low detection limits (ng/mL) which lower than then regulated levels of the water regulations. Results demonstrated the presence of higher concentrations of soluble  $Mn^{2+}$  in post-treatment water samples at the treatment works, indicating that a change in water treatment may reduce soluble manganese entering the water distribution network. It was found that addition of a coagulant during the water treatment process gave rise to higher concentrations of manganese in water samples compared to raw waters.

In this study, low levels of coloured water were observed at different water treatment plants, especially the raw water samples and during the treatment processing. In general, factors are known that influence accumulation of both Fe and Mn in drinking water such as chemical oxidation and this was the most important to investigate during the present work. Presently, most water companies test and monitor water discolouration in different water distribution networks by using either customer complaint data or selection made by the UU based on association of high levels of Mn and Fe to certain areas. The use of oxidation and coagulants to remove these elements from the water such as  $\text{KMnO}_4$  as an effective oxidant has been thought to improve the issue. However, overdose during treatment can cause the residual Mn to enter the distribution system. Similarly, for Fe coagulants in aiding of the flocculation of the particles in the water treatment process. There are a number of chemical, biological and physical processes that can lead to the formation of the discoloured water, as already explained in the introduction (Section 1.1). These change the water chemistry of the treatment processes caused through the interaction with the added chemicals, as well as changes in dissolved oxygen, temperature and pH. This, in turn, will influence the chemical oxidation within the pipes. This information will be beneficial to the removal of discolouration through achieving very low levels of Fe and Mn and it is important as improvements of pipes to manage discolouration was only a temporary solution to this problem

The comparison between differently developed ICP methods and understanding of Mn and Fe species for discoloured and non-discoloured

water samples is important to improve water quality. This will allow water companies to find possible solutions to poor water quality.

## **5.2 Future work**

Further studies for this project could focus on speciation of Fe and Mn in a water distribution network system that uses different filter sizes; this could be used to remove both elements from the network system by ensuring Fe and Mn levels are less than the regulated values in the final water. The aim should be to try and determine the species involved and how they change within a network over time, which will provide essential information as to their mobility, transformation and accumulation.

It is now widely accepted that the combination of chromatographic separation (HPLC) with element-specific detection (ICP-MS) is a powerful tool for chemical speciation studies (16). Homonick *et al.* (2010) reported that redox and pH conditions do not totally explain Mn distribution in groundwater, but a stronger influence of pH on Mn mobilisation exists. This study only attempted to focus on either Fe or Mn and did not consider speciation and all the variables that may affect the trace metals deposition or solubility. A significant step change is required towards solving this problem which is costing water companies billions of pounds each year. Further studies for this project would take about year to look at all the variation such as coagulants, oxidations and precipitation that may affect the trace metals deposition or solubility. The speciation of Fe and Mn at different stages during water treatment should be studied in more detail to provide essential information as to mobility, transformation and accumulation. In addition, future work needs to be carried out using hyphenated techniques with collision cell technology to determine all

oxidation states of the elements. Furthermore, work could also be extended to investigate the extent of organic compounds in the water and how this influences speciation.

## References

1. Wasserman GA, Liu X, Parvez F, Ahsan H, Levy D, Factor-Litvak P, et al. Water Manganese Exposure and Children's Intellectual Function in Araihasar, Bangladesh. *Environmental Health Perspectives*. 2006;114(1):124-9.
2. Mitchell E, Frisbie S, Sarkar B. Exposure to multiple metals from groundwater a global crisis: Geology, climate change, health effects, testing, and mitigation. *Metallomics*. 2011;3(9):874-908.
3. Tezcan S, Altıntaş H, Sönmez R, Akinci A, Doğan B, Çakır B, et al. Cardiovascular risk factor levels in a lower middle-class community in Ankara, Turkey. *Tropical Medicine & International Health*. 2003;8(7):660-7.
4. Yan X-P, Hendry MJ, Kerrich R. Speciation of Dissolved Iron(III) and Iron(II) in Water by On- Line Coupling of Flow Injection Separation and Preconcentration with Inductively Coupled Plasma Mass Spectrometry. *Analytical Chemistry*. 2000;72(8):1879.
5. Tredoux G, Engelbrecht P, Cavé L. Groundwater pollution: Are we monitoring appropriate parameters? *Water SA*. 2004;30(5):662-7.
6. Findings from University of Saskatchewan Update Knowledge of Water Quality Research [Biofiltration field study for cold Fe(II)- and Mn(II)-rich groundwater: accelerated Mn(II) removal kinetics and cold-adapted Mn(II)-oxidizing microbial ...].(Report). *Ecology, Environment & Conservation*. 2018:499.
7. World Health Organization. *Guidelines for Drinking-water Quality*. Geneva: World Health Organization; 2002.

8. Graham N. Guidelines for Drinking-Water Quality, 2nd edition, Addendum to Volume 1 – Recommendations, World Health Organisation, Geneva, 1998, 36 pages. *Urban Water*. 1999;1(2):183.
9. Katsoyiannis IA, Zouboulis AI. Biological treatment of Mn(II) and Fe(II) containing groundwater: kinetic considerations and product characterization. *Water Research*. 2004;38(7):1922-32.
10. Ginige MP, Wylie J, Plumb J. Influence of biofilms on iron and manganese deposition in drinking water distribution systems. *Biofouling*. 2011;27(2):151-63.
11. Al-Jasser AO. Chlorine decay in drinking-water transmission and distribution systems: Pipe service age effect. *Water Research*. 2007;41(2):387-96.
12. Peng CY, Hill AS, Friedman MJ, Valentine RL, Larson GS, Romero AMY, et al. Occurrence of trace inorganic contaminants in drinking water distribution systems. *Journal - American Water Works Association*. 2012;104(3):53-4.
13. Colbourne J. Parliamentary Under-Secretary for Natural Environment and Fisheries: Drinking Water Inspectorate; 2013 [
14. Rajmohan N, Elango L. Distribution of Iron, Manganese, Zinc and Atrazine in Groundwater in Parts of Palar and Cheyyar River Basins, South India. *Environ Monit Assess*. 2005;107(1):115-31.
15. El Araby R HS, El Diwani G. Treatment of iron and manganese in simulated groundwater via ozone technology. *Desalination*. 2009;249(3):1345-9.

16. Pearson GF, Greenway GM. Recent developments in manganese speciation. *TrAC Trends in Analytical Chemistry*. 2005;24(9):803-9.
17. Roels H, Meiers G, Delos M, Ortega I, Lauwerys R, Buchet JP, et al. Influence of the route of administration and the chemical form (MnCl<sub>2</sub>, MnO<sub>2</sub>) on the absorption and cerebral distribution of manganese in rats. *Archives of Toxicology*. 1997;71(4):223-30.
18. Jin P, Liang X, Xia L, Jahouh F, Wang R, Kuang Y, et al. Applied methodology: Determination of 20 trace elements and arsenic species for a realgar-containing traditional Chinese medicine Niu Huang Jie Du tablets by direct inductively coupled plasma–mass spectrometry and high performance liquid chromatography–inductively coupled plasma–mass spectrometry. *Journal of Trace Elements in Medicine and Biology*. 2016;33:73-80.
19. Cao X, Hao C, Wang G, Yang H, Chen D, Wang X. Sequential extraction combined with HPLC–ICP-MS for As speciation in dry seafood products. *Food Chemistry*. 2009;113(2):720-6.
20. Homoncik SC, MacDonald AM, Heal KV, Ó Dochartaigh BÉ, Ngwenya BT. Manganese concentrations in Scottish groundwater. *Science of The Total Environment*. 2010;408(12):2467-73.
21. Vreeburg IJHG, Boxall DJB. Discolouration in potable water distribution systems: A review. *Water Research*. 2007;41(3):519-29.
22. Vreeburg JHG, Schippers D, Verberk J, van Dijk JC. Impact of particles on sediment accumulation in a drinking water distribution system.
23. Cerrato JM, Falkinham Iii JO, Dietrich AM, Knocke WR, McKinney CW, Pruden A. Manganese-oxidizing and -reducing microorganisms isolated from

biofilms in chlorinated drinking water systems. *Water Research*. 2010;44(13):3935-45.

24. Cerrato JM, Reyes LP, Alvarado CN, Dietrich AM. Effect of PVC and iron materials on Mn(II) deposition in drinking water distribution systems. *Water Research*. 2006;40(14):2720-6.

25. Majestic BJ, Schauer JJ, Shafer MM. Development of a Manganese Speciation Method for Atmospheric Aerosols in Biologically and Environmentally Relevant Fluids. *Aerosol Science & Technology*. 2007;41(10):925-33.

26. Silva FV, Trevizan LC, Silva CnS, Nogueira ARA, Nóbrega JA. Evaluation of inductively coupled plasma optical emission spectrometers with axially and radially viewed configurations. *Spectrochimica Acta Part B: Atomic Spectroscopy*. 2002;57(12):1905-13.

27. Sly LI, Hodgkinson MC, Arunpairojana V. Deposition of manganese in a drinking water distribution system. *Applied and Environmental Microbiology*. 1990;56(3):628-39.

28. Frisbie SH, Mitchell EJ, Dustin H, Maynard DM, Sarkar B. World Health Organization Discontinues Its Drinking-Water Guideline for Manganese. *Environmental Health Perspectives*. 2012;120(6):775-8.

29. Gerke TL, Little BJ, Barry Maynard J. Manganese deposition in drinking water distribution systems. *Science of The Total Environment*. 2016;541:184-93.

30. World Health Organization. *Guidelines for Drinking Water Quality (Electronic resources)* 2006.

31. Nawab J KS, Ali S, Sher H, Rahman Z, Khan K, et al. Health risk assessment of heavy metals and bacterial contamination in drinking water sources: a case study of Malakand Agency Pakistan. *Environ Monit Assess.* 2016;188(5):286.
32. Braissant O, Bonkat G, Bachmann A. Do lymphocytes really like radix roots? A reality check of microcalorimetric data and a reply to Liu et al. (2013). *Thermochimica Acta.* 2014;580:63-5.
33. Liu R, Yu Z, Zhang H, Yang M, Shi B, Liu X. Diversity of bacteria and mycobacteria in biofilms of two urban drinking water distribution systems. *Canadian Journal of Microbiology.* 2012;58(3):261-70.
34. Rindernecht A, McGregor J, Rouse-Ho A, Kleinman M. Environmental air pollution and in utero brain damage: Maternal manganese (Mn) inhalation alters brain development and susceptibility to postnatal brain injury. *American Journal of Obstetrics and Gynecology.* 2005;193(6):S36-S.
35. Yokel RA, Crossgrove JS, Bukaveckas BL. Manganese distribution across the blood-brain barrier. II. Manganese efflux from the brain does not appear to be carrier mediated. *NeuroToxicology.* 2003;24(1):15-22.
36. Prasad TD, Danso-Amoako E. Influence of Chemical and Biological Parameters on Iron and Manganese Accumulation in Water Distribution Networks. *Procedia Engineering.* 2014;70:1353-61.
37. Soylak M AA. Determination of some heavy metals in food and environmental samples by flame atomic absorption spectrometry after coprecipitation. *Food and Chemical Toxicology.* 2011;49(6):1242-8.

38. Gantzer PA, Bryant LD, Little JC. Controlling soluble iron and manganese in a water-supply reservoir using hypolimnetic oxygenation. *Water Res.* 2009;43(5):1285-94.
39. Aller RC. Bioturbation and Manganese Cycling in Hemipelagic Sediments. 1990:51.
40. Albaiges J. *Environmental chemistry*, 9th edition.
41. Coffey BM, Knocke WR, editors. Evaluation and modeling of soluble manganese removal by oxide-coated dual media filtration. *National Conference on Environmental Engineering*; 1990.
42. Warnken J DR, Teasdale PR. Investigation of recreational boats as a source of copper at anchorage sites using time-integrated diffusive gradients in thin film and sediment measurements. *Marine Pollution Bulletin.* 2004;49(9–10):833-43.
43. Thakur V, Guptan RC, Hashmi AZ, Sakhuja P, Malhotra V, Sarin SK. Absence of hemochromatosis associated Cys282Tyr HFE gene mutation and low frequency of hemochromatosis phenotype in nonalcoholic chronic liver disease patients in India.
44. Gantzer PA, Bryant LD, Little JC. Controlling soluble iron and manganese in a water-supply reservoir using hypolimnetic oxygenation. *Water Research.* 2009;43(5):1285-94.
45. Peng H, Zheng X, Chen L, Wei Y. Analysis of numerical simulations and influencing factors of seasonal manganese pollution in reservoirs. *Environmental Science and Pollution Research International.* 2016;23(14):14362-72.

46. Napp J. Review of Water chemistry by Mark M. Benjamin. *Journal of Environmental Engineering*. 2002;128(4):395.
47. Bernier R, Locke A. New record of *Penilia avirostris* Dana, 1849 (Cladocera) in the Gulf of St. Lawrence.
48. Danso-Amoako E, Prasad TD. ANN Model to Predict the Influence of Chemical and Biological Parameters on Iron and Manganese Accumulation. *Procedia Engineering*. 2014;70:409-18.
49. Waller SA, Packman AI, Hausner M. Comparison of biofilm cell quantification methods for drinking water distribution systems. *Journal of Microbiological Methods*. 2018;144:8-21.
50. Norton CD, LeChevallier MW. Chloramination: Its effect on distribution system water quality. *Journal / American Water Works Association*. 1997;89(7):66-77.
51. Sly LI, Hodgkinson MC, Arunpairojana V. Effect of water velocity on the early development of manganese-depositing biofilm in a drinking-water distribution system. *FEMS Microbiology Letters*. 1988;53(3):175-86.
52. Bouchard MF, Surette C, Cormier P, Foucher D. Low level exposure to manganese from drinking water and cognition in school-age children. *NeuroToxicology*. 2018;64:110-7.
53. Sarin P, Snoeyink VL, Lytle DA, Kriven WM. Iron corrosion scales: Model for scale growth, iron release, and colored water formation. *Journal of Environmental Engineering*. 2004;130(4):364-73.
54. Cloete TE, Brözel VS, Von Holy A. Practical aspects of biofouling control in industrial water systems. *International Biodeterioration & Biodegradation*. 1992;29(3):299-341.

55. Bryers JD. Biofilms and the technological implications of microbial cell adhesion. *Colloids and Surfaces B: Biointerfaces*. 1994;2(1):9-23.
56. Gauthier V, Gérard B, Portal J-M, Block J-C. Organic matter as loose deposits in a drinking water distribution system. 1999;33:1014±26,.
57. Percival SL, Walker JT. Potable water and biofilms: A review of the public health implications. *Biofouling*. 1999;14(2):99-115.
58. Abe Y, Skali-Lami S, Block J-C, Francius G. Cohesiveness and hydrodynamic properties of young drinking water biofilms. *Water Research*. 2012;46(4):1155-66.
59. Manuel CM NO, Melo LF. Unsteady state flow and stagnation in distribution systems affect the biological stability of drinking water. *Biofouling*. 2009;26(2):129-39.
60. Melo LF BT. Biofouling in Water Systems. *Experimental Thermal and Fluid Science* 1997;14(4):375-81.
61. Nealson KH MC. Microbial Reduction of Manganese and Iron - New Approaches to Carbon Cycling. *Appl Environ Microb*. 1992;58(2):439-43.
62. Bratina BJ SB, Green WJ, . Manganese reduction by microbes from oxic regions of the Lake Vanda (Antarctica) water column. Schmidt TM *Appl Environ Microb*. 1998;64(10):3791-7.
63. Camper AK, Broadaway SC, LeChevallier MW, McFeters GA. Operational Variables and the Release of Colonized Granular Activated Carbon Particles in Drinking Water. 1987:70.
64. Peng C-Y, Korshin GV. Speciation of trace inorganic contaminants in corrosion scales and deposits formed in drinking water distribution systems. *Water Research*. 2011;45(17):5553-63.

65. Block JC HK, Paquin JL, Miazga J, Levi Y. . Biofilm accumulation in drinking water distribution systems. *Biofouling*. 1993;6(4):333-43.
66. LeChevallier WM. Conditions favouring coliform and HPC bacterial growth in drinking water and on water contact surfaces. In: Bartram J, Cotruvo J, Exner M, Fricker C, Glasmacher A, editors. *Heterotrophic Plate Counts and Drinking-water Safety*. London: IWA Publishing; 2003. p. 177-97.
67. van der Kooij D. Managing regrowth in drinkingwater distribution systems. In: Bartram J, Cotruvo J, Exner M, Fricker C, Glasmacher A, editors. *Heterotrophic Plate Counts and Drinking-water Safety*. London: IWA Publishing; 2003. p. 199-232.
68. Dukan S, Levi Y, Piriou P, Guyon F, Villon P. Dynamic modelling of bacterial growth in drinking water networks. *Water Research*. 1996;30(9):1991-2002.
69. van der Kooij D, Martijn B, Schaap PG, Hoogenboezem W, Veenendaal HR, van der Wielen PWJJ. Improved biostability assessment of drinking water with a suite of test methods at a water supply treating eutrophic lake water. *Water Research*. 2015;87:347-55.
70. Ginige MP, Wylie J, Plumb J. Influence of biofilms on iron and manganese deposition in drinking water distribution systems 2011.
71. Gauthier V, Gérard B, Portal J-M, Block J-C, Gatel D. Organic matter as loose deposits in a drinking water distribution system. *Water Research*. 1999;33(4):1014-26.
72. Sly LI AV, Hodgkinson MC. . *Pedomicrobium manganicum* from Drinking-Water Distribution Systems with Manganese-Related “Dirty Water” Problems. *Systematic and Applied Microbiology*. 1988;11(1):75-84.

73. Malato S, Blanco J, Alarcón DC, Maldonado MI, Fernández-Ibáñez P, Gernjak W. Photocatalytic decontamination and disinfection of water with solar collectors. *Catalysis Today*. 2007;122(1–2):137-49.
74. Blokker E VJ, Schaap P, van Dijk J. The Self-Cleaning Velocity in Practice. *Water Distribution Systems Analysis 2010*:. American Society of Civil Engineers. 2011: 187-99.
75. Crane M. Proposed development of Sediment Quality Guidelines under the European Water Framework Directive: a critique. *Toxicology Letters*. 2003;142(3):195-206.
76. Danso-Amoako E. Iron and manganese accumulation potential in water distribution networks. University of Salford; 2016.
77. Świetlik J R-SU, Piszora P, Nawrocki J. . Corrosion in drinking water pipes: The importance of green rusts. *Water Research*. 2012;46(1):1-10.
78. Pankaj Sarin JAC, Vernon L. Snoeyink, Waltraud M. Kriven. Iron release from corroded, unlined cast-iron pipe *Journal /American Water Works Association*. Nov 2003;95(11):12.
79. Husband PS BJ, Saul AJ. Laboratory studies investigating the processes leading to discolouration in water distribution networks. *Water Research*. 2008;42(16):4309-18.
80. Husband PS BJ. Asset deterioration and discolouration in water distribution systems. *Water Research*. 2011;45(1):113-24.
81. Zwart SJ BW. Review of measured crop water productivity values for irrigated wheat, rice, cotton and maize. . *Agricultural Water Management*. 2004;69(2):115-33.

82. Mukerjee D YL, Ong V, Denton CP, Howells K, Black CM, et al. The myth of pulmonary Raynaud's phenomenon: the contribution of pulmonary arterial vasospasm in patients with systemic sclerosis related pulmonary arterial hypertension. *Ann Rheum Dis*. 2004; 63(12):1627-31.
83. Niquette P SP, Savoie R. Impacts of pipe materials on densities of fixed bacterial biomass in a drinking water distribution system *Water Research*. 2000;34(6):1952-6.
84. Heim TH, Dietrich AM. Sensory aspects and water quality impacts of chlorinated and chloraminated drinking water in contact with HDPE and cPVC pipe. *Water Research*. 2007;41(4):757-64.
85. Burger MS MS, Shupe GD, Gagnon GA. Manganese removal during bench-scale biofiltration. *Water Research*. 2008;42(19):4733-42.
86. Linhardt P. Corrosion of metals in natural waters influenced by manganese oxidizing microorganisms. *Biodegradation*. 1997;8(3):201-10.
87. Vandenabeele J dBD, Germonpré R, Van de Sande R, Verstraete W. Influence of nitrate on manganese removing microbial consortia from sand filters. *Water Research*. 1995;29(2):579-87.
88. Petrunic BM MK, Al TA. . Reductive dissolution of Mn oxides in river-recharged aquifers: a laboratory column study. *Journal of Hydrology*. 2005;301(1-4):163-81.
89. Swistock BR, Sharpe WE, Dickison J. Educating Rural Private Water System Owners in Pennsylvania Using Satellite versus Traditional Programs. *Journal of Extension*. 2001;39(3).

90. Grygo-Szymanko E, Tobiasz A, Walas S. Speciation analysis and fractionation of manganese: A review. *Trends in Analytical Chemistry: TRAC*. 2016;80:112-24.
91. Hurrell R, Egli I. Iron bioavailability and dietary reference values. *The American Journal of Clinical Nutrition*. 2010;91(5):1461S-7S.
92. Bouchard MF. Manganese in Drinking Water: Bouchard Responds. 2011:A241.
93. Bouchard M. Hair manganese and hyperactive behaviors: Pilot study of school-age children exposed through tap water. *Epidemiology*. 2007;18(5):S164-S5.
94. Khan K, Wasserman GA, Liu X, Ahmed E, Parvez F, Slavkovich V, et al. Manganese exposure from drinking water and children's academic achievement. *Neurotoxicology*. 2012;33(1):91-7.
95. Collipp PJ, Chen SY, Maitinsky S. Manganese in infant formulas and learning disability. *Ann Nutr Metab*. 1983;27:488-94.
96. Elsner RJF, Spangler JG. Neurotoxicity of inhaled manganese: Public health danger in the shower? *Medical Hypotheses*. 2005;65(3):607-16.
97. Ellingsen DG, Hetland SM, Thomassen Y. Manganese air exposure assessment and biological monitoring in the manganese alloy production industry. *Journal of Environmental Monitoring*. 2003;5(1):84-90.
98. Bouchard MF, Sauve S, Barbeau B, Legrand M, Brodeur ME, Bouffard T, et al. Intellectual impairment in school-age children exposed to manganese from drinking water. *Environ Health Perspect*. 2011;119(1):138-43.

99. Deckwerth TL, Elliott JL, Knudson CM, Johnson EM, Snider WD, Korsmeyer SJ. BAX Is Required for Neuronal Death after Trophic Factor Deprivation and during Development. *Neuron*. 1996;17(3):401-11.
100. Knudson CM, Tung KSK, Tourtellotte WG, Brown GAJ, Korsmeyer SJ. Bax-Deficient Mice with Lymphoid Hyperplasia and Male Germ Cell Death. *Science*. 1995;270:96-9.
101. Newland MC. Persistent effects of manganese on effortful responding and their relationship to manganese accumulation in the primate globus pallidus. *Toxicology And Applied Pharmacology*. 1992;113(1):87.
102. Cawte J. Psychiatric Sequelae of Manganese Exposure in the Adult, Foetal and Neonatal Nervous Systems. *Australian and New Zealand Journal of Psychiatry*. 1985;19:211-7.
103. Bouchard MF. Manganese in Drinking Water: Bouchard Responds. *Environmental Health Perspectives*. 2011;119(6):a241-a.
104. Weber S, Dorman DC, Lash LH, Erikson K, Vrana KE, Aschner M. Effects of Manganese (Mn) on the Developing Rat Brain: Oxidative-Stress Related Endpoints. *NeuroToxicology*. 2002;23(2):169-75.
105. Khan M, Jung J, Stoyko SS, Mar A, Quetz A, Samanta T, et al. The role of Ni-Mn hybridization on the martensitic phase transitions in Mn-rich Heusler alloys. *Applied Physics Letters*. 2012;100(17):172403.
106. Drinking Water Inspectorate. Drinking water 2012: Private water supplies in England: Drinking Water Inspectorate; 2013 [Available from: <http://dwi.defra.gov.uk/about/annual-report/2012/>].

107. Kirk PWW, Lester JN. Significance and behaviour of heavy metals in wastewater treatment processes IV. Water quality standards and criteria. *Science of the Total Environment*. 1984;40(1):1-44.
108. Marsidi N, Abu Hasan H, Sheikh Abdullah SR. A review of biological aerated filters for iron and manganese ions removal in water treatment. *Journal of Water Process Engineering*. 2018;23:1-12.
109. Fernsebner K, Zorn J, Kanawati B, Walker A, Michalke B. Manganese leads to an increase in markers of oxidative stress as well as to a shift in the ratio of Fe(ii)/(iii) in rat brain tissue. *Metallomics*. 2014;6(4):921.
110. Michalke B, Fernsebner K. New insights into manganese toxicity and speciation. *Journal of Trace Elements in Medicine and Biology*. 2014;28(2):106-16.
111. Bowler RM, Koller W, Schulz PE. Parkinsonism due to manganese in a welder: Neurological and neuropsychological sequelae. *NeuroToxicology*. 2006;27(3):327-32.
112. Kim J. Manganese treatment to reduce black water occurrence in the water supply. *Environmental Engineering Research*. 2015;20(3):230-6.
113. Sarin P, Snoeyink VL, Bebee J, Jim KK, Beckett MA, Kriven WM, et al. Iron release from corroded iron pipes in drinking water distribution systems: effect of dissolved oxygen. *Water Research*. 2004;38:1259-69.
114. Choo K, Lee H, Choi S. Iron and manganese removal and membrane fouling during UF in conjunction with prechlorination for drinking water treatment. *Journal of Membrane Science*. 2005;267(1-2):18-26.

115. Wersin P CL, Karthein R, Stumm W. From adsorption to precipitation: Sorption of  $Mn^{2+}$  on  $FeCO_3(s)$ . *Geochimica et Cosmochimica Acta*. 1989;53(11):2787-96.
116. Peng C-Y, Hill AS, Friedman MJ, Valentine RL, Larson GS, Young AM, et al. Occurrence of trace inorganic contaminants in drinking water distribution systems. *Journal - American Water Works Association*. 2012;104.
117. Homoncik SC, Macdonald AM, Heal KV, Dochartaigh BE, Ngwenya BT. Manganese concentrations in Scottish groundwater. *The Science of the total environment*. 2010;408(12):2467-73.
118. Gupta VK, Dobhal R, Nayak A, Agarwal S, Uniyal DP, Singh P, et al. Advanced and Hyphenated Techniques for Nano-Level Analysis of Iron in Water. *Critical Reviews in Analytical Chemistry*. 2012;42(3):245-56.
119. Persson DP, Hansen TH, Laursen KH, Husted S, Schjoerring JK. ICP-MS and LC-ICP-MS for analysis of trace element content and speciation in cereal grains. *Methods in Molecular Biology*. 2012;860:193-211.
120. Sarin P, Snoeyink VL, Bebee J, Jim KK, Beckett MA, Kriven WM, et al. Iron release from corroded iron pipes in drinking water distribution systems: effect of dissolved oxygen. *Water Research*. 2004;38(5):1259-69.
121. Gerke TL, Maynard JB, Schock MR, Lytle DL. Physiochemical characterization of five iron tubercles from a single drinking water distribution system: Possible new insights on their formation and growth. *Corrosion Science*. 2008;50(7):2030-9.
122. Saitoh K, Sera K, Gotoh T, Nakamura M. Comparison of elemental quantity by PIXE and ICP-MS and/or ICP-AES for NIST standards. *Nuclear*

Instruments and Methods in Physics Research, Section B: Beam Interactions with Materials and Atoms. 2002;189(1-4):86-93.

123. Hu K, Houk RS. Inductively coupled plasma mass spectrometry with an electrically floating sampling interface. *Journal of the American Society for Mass Spectrometry*. 1993;4(9):733-41.

124. R. Bacon J, S. Crain J, Van Vaeck L, G. Williams J. Atomic mass spectrometry. *Journal of Analytical Atomic Spectrometry*. 1999;14(10):1633-59.

125. R. H. Wendt VAF. Induction-Coupled Plasma Spectrometric Excitation Source. *Anal Chem* 37 (7), pp 920–922. 1995(June 1965):920-2.

126. Shum SCK, Neddersen R, Houk RS. Elemental speciation by liquid chromatography-inductively coupled plasma mass spectrometry with direct injection nebulization. *Analyst*. 1992;117(3):577-82.

127. Turner J, J. Hill S, Hywel Evans E, Fairman B. The use of ETV-ICP-MS for the determination of selenium in serum. *Journal of Analytical Atomic Spectrometry*. 1999;14(2):121-6.

128. Skoog DA, West DM, Holler FJ. *Fundamentals of analytical chemistry*. 7th ed: Saunders; 1996.

129. Lichte F. *A handbook of inductively coupled plasma spectrometry*: Michael Thompson and J. Nicholas Walsh. Blackie Publishing Group, Glasgow, 1983, x + 273 pp., UK £ 35.00 (hardcover). *Chemical Geology*. 1985;51(1–2):153.

130. Federal Courts — Section 1983 Litigation — Fifth Circuit Equally Divides on Decision To Uphold Judgment Against District Attorney's Office for

Withholding Exculpatory Evidence. — Thompson v. Connick, 578 F. 3d 293 (5<sup>th</sup> Cir. 2009) (en banc). 2010:1019.

131. Fredeen KJ, Boss CB. Concepts, Instrumentation and Techniques in Inductively Coupled Plasma Optical Emission Spectrometry. Second Edition ed. U.S.A: Perkin Elmer 1997.

132. Overcoming Interferences with the Thermo Scientific iCAP 7000 Plus Series ICP-OES: Thermo Fisher Scientific; 2016 [Available from: <https://tools.thermofisher.com/content/sfs/brochures/TN-43332-ICP-OES-Overcoming-Interferences-iCAP-7000-Plus-Series-TN43332-EN.pdf>]

133. I. Stewart I, W. Olesik J. Transient acid effects in inductively coupled plasma optical emission spectrometry and inductively coupled plasma mass spectrometry. Journal of Analytical Atomic Spectrometry. 1998;13(9):843-54.

134. Todoli JL, Gras L, Hernandis V, Mora J. Elemental matrix effects in ICP-AES. Journal of Analytical Atomic Spectrometry. 2002;17(2):142-69.

135. Rettberg T. The Development of Inductively-Coupled Plasma Mass Spectrometry (ICP-MS). The Encyclopedia of Mass Spectrometry. Boston: Elsevier; 2016. p. 87-91.

136. Beauchemin D. Inductively coupled plasma mass spectrometry. Analytical Chemistry. 2002;74(12):2873-93.

137. PerkinElmer. PerkinElmer Instruments PerkinElmer Instruments2001 [Available from: <http://www.perkinelmer.co.uk/>].

138. Pröfrock D, Prange A. Inductively Coupled Plasma–Mass Spectrometry (ICP-MS) for Quantitative Analysis in Environmental and Life Sciences: A Review of Challenges, Solutions, and Trends. Applied Spectroscopy. 2012;66(8):843-68.

139. Begley IS. A study of isotope ratio measurement by inductively coupled plasma mass spectrometry. Loughborough University; 1996.
140. Bacon JR, Crain JS, Van Vaeck L, Williams JG. Atomic mass spectrometry.
141. Vanhaecke F, Vanhoe H, Dams R, Vandecasteele C. The use of internal standards in ICP-MS. *Talanta*. 1992;39(7):737-42.
142. Beary ES, Paulsen PJ, Jassie LB, Fassett JD. Determination of environmental lead using continuous-flow microwave digestion isotope dilution inductively coupled plasma mass spectrometry. *Analytical Chemistry*. 1997;69(4):758.
143. Hu Y-L, Chen Z-P, Chen Y, Shi C-X, Yu R-Q. Generalized multiple internal standard method for quantitative liquid chromatography mass spectrometry. *Journal of Chromatography A*. 2016;1445:112-7.
144. Gupta JGS, Bertrand NB. Direct ICP-MS determination of trace and ultratrace elements in geological materials after decomposition in a microwave oven. I. Quantitation of Y, Th, U and the lanthanides. *Talanta*. 1995;42(11):1595-607.
145. Montes Bayon M, Ignacio Garcia Alonso J, Sanz Medel A. Enhanced semiquantitative multi-analysis of trace elements in environmental samples using inductively coupled plasma mass spectrometry. *Journal of Analytical Atomic Spectrometry*. 1998;13(4):277-82.
146. Jeffrey RB, Kathryn LL, Randall RP, Luc Van V. Atomic spectrometry update. Atomic mass spectrometry. *JAAS (Journal of Analytical Atomic Spectrometry)*. 2008;23(8):1130-62.

147. McCurdy E, Woods G. The application of collision & sol reaction cell inductively coupled plasma mass spectrometry to multi-element analysis in variable sample matrices, using He as a non-reactive cell gas. *Journal of Analytical Atomic Spectrometry*. 2004;19(5):607-15.
148. Mutaftchiev K TK. Determination of manganese (II) in some medicinal plants and their decoctions by a kinetic spectrophotometric method. *Phytochem Anal*. 2003;14(3):160-3.
149. Michalke B. Manganese speciation using capillary electrophoresis–ICP-mass spectrometry. *Journal of Chromatography A*. 2004;1050(1):69-76.
150. Webb S, Bartos J, Boles R, Hasty E, Thuotte E, Thiex NJ. Simultaneous Determination of Arsenic, Cadmium, Calcium, Chromium, Cobalt, Copper, Iron, Lead, Magnesium, Manganese, Molybdenum, Nickel, Selenium, and Zinc in Fertilizers by Microwave Acid Digestion and Inductively Coupled Plasma-Optical Emission. *Journal of AOAC International*. 2014;97(3):700-11.
151. Normandin L ABL, Salehi F, St -Pierre A, Kennedy G, Mergler D, et al. Manganese distribution in the brain and neurobehavioral changes following inhalation exposure of rats to three chemical forms of manganese. *Neurotoxicology*. 2004;25(3):433-41.
152. Sanagi MM, Ling SL, Nasir Z, Hermawan D, Wan Ibrahim WA, Naim AA. Comparison of signal-to-noise, blank determination, and linear regression methods for the estimation of detection and quantification limits for volatile organic compounds by gas chromatography. *Journal of AOAC International*. 2009;92(6):1833-8.
153. Borg H. Trace metals in Swedish natural fresh waters. *Hydrobiologia*. 1983;101(1-2):27-34.

154. Hutchins CM, Teasdale PR, Lee SY, Simpson SL. The Effect of Sediment Type and pH-Adjustment on the Porewater Chemistry of Copper- and Zinc-Spiked Sediments. *Soil & Sediment Contamination*. 2009;18(1):55-73.
155. Burton A, Aherne J, Hassan N. Trace Metals in Upland Headwater Lakes in Ireland. *AMBIO*. 2013;42(6):702-14.
156. A. Tessier PGCC, M. Bisson. Sequential Extraction Procedure for the Speciation of Particulate Trace Metals. *Anal Chem* 1979;51(7):pp 920–2.
157. De Munari A, Schäfer AI. Impact of speciation on removal of manganese and organic matter by nanofiltration. *Journal of Water Supply: Research & Technology-AQUA*. 2010;59(2/3):152-63.
158. Jaudon P MC, Galea J, Rey J, Vacelet E. . Groundwater pollution by manganese. Manganese speciation: Application to the selection and discussion of an in situ groundwater treatment. *Science of The Total Environment*. 1989;84(169-83).
159. Michalke B, Caroli S. Speciation of Trace Elements. *Essentials of Medical Geology*. 2013:611.
160. Michalke B, Caroli S. Chapter 25: Speciation of trace elements. 2005. p. 609.
161. Michalke B. The coupling of LC to ICP-MS in element speciation – Part II: Recent trends in application. *Trends in Analytical Chemistry: TRAC*. 2002;21(3):154.
162. Gorny J DD, Lesven L, Noiriél C, Madé B, Billon G. Development and application of a HPIC-ICP-MS method for the redox arsenic speciation in river

sediment pore waters. JAAS (Journal of Analytical Atomic Spectrometry). 2015;30(7):1562.

163. Bruce D, Lazerte K. Manganese speciation in dilute waters of the Precambrian shield. Canada. 1990;24(1990):1097-101.

164. Chiswell B, Mokhtar MB. The speciation of manganese in freshwaters. Talanta. 1986;33(8):669-77.

165. Ljung K, Vahter M. Time to re-evaluate the guideline value for manganese in drinking water? Environmental Health Perspectives. 2007;115(11):1533-8.

166. Saterlay AJ, Foord JS, Compton RG. Sono-cathodic stripping voltammetry of manganese at a polished boron-doped diamond electrode: application to the determination of manganese in instant tea.

167. Boughriet A OB, Fischer JC, Wartel M, Leman G. Variability of dissolved Mn and Zn in the Seine estuary and chemical speciation of these metals in suspended matter. Water Research 1992;26(10):1359-78.

168. Liang P, Sang H, Sun Z. Cloud point extraction and graphite furnace atomic absorption spectrometry determination of manganese(II) and iron(III) in water samples. J Colloid Interface Sci. 2006;304(2):486-90.

169. Liang P, Sang H, Sun Z. Cloud point extraction and graphite furnace atomic absorption spectrometry determination of manganese(II) and iron(III) in water samples. Journal of Colloid and Interface Science. 2006;304(2):486-90.

170. Kondakis XG, Makris N, Leotsinidis M, Prinou M, Papapetropoulos T. Possible Health Effects of High Manganese Concentration in Drinking Water. Archives of Environmental Health. 1989;44(3).

171. Sondergaard J, Asmund G, Larsen MM. Trace elements determination in seawater by ICP-MS with on-line pre-concentration on a Chelex-100 column using a 'standard' instrument setup. *MethodsX*. 2015;2:323-30.
172. Measures CI, Yuan J, Resing JA. Determination of iron in seawater by flow injection analysis using in-line preconcentration and spectrophotometric detection. *Marine Chemistry*. 1995;50(1):3-12.
173. Heitkemper DT, Vela NP, Stewart KR, Westphal CS. Determination of total and speciated arsenic in rice by ion chromatography and inductively coupled plasma mass spectrometry. *Journal of Analytical Atomic Spectrometry*. 2001;16(4):299-306.
174. Maher WA, Ellwood MJ, Krikowa F, Raber G, Foster S. Measurement of arsenic species in environmental, biological fluids and food samples by HPLC-ICPMS and HPLC-HG-AFS. *J Anal At Spectrom*. 2015;30(10):2129-83.
175. Rekhi H, Rani S, Sharma N, Malik AK. A Review on Recent Applications of High-Performance Liquid Chromatography in Metal Determination and Speciation Analysis. Taylor & Francis; 2017. p. 524-37.
176. Barałkiewicz D, Pikoś B, Belter M, Marcinkowska M. Speciation analysis of chromium in drinking water samples by ion-pair reversed-phase HPLC–ICP-MS: validation of the analytical method and evaluation of the uncertainty budget. *Journal for Quality, Comparability and Reliability in Chemical Measurement*. 2013;18(5):391-401.
177. Hirayama K, Unohara N. Spectrophotometric Catalytic Determination of an Ultratrace Amount of Iron(III) in Water Based on the Oxidation of N,N-Dimethyl-p-phenylenediamine by Hydrogen Peroxide. *Analytical Chemistry*. 1988;60(23):2573-7.

178. Magdalena J-C. Arsenic, Antimony, Chromium, and Thallium Speciation in Water and Sediment Samples with the LC-ICP-MS Technique. *International Journal of Analytical Chemistry*. 2015;2015(2015).
179. Grygo-Szymanko E, Tobiasz A, Miliszkiewicz N, Dudek-Adamska D, Walas S. Evaluation of Manganese(II) and Manganese(VII) Speciation in Water Samples by Ion Pair High-performance Liquid Chromatography-inductively Coupled Plasma Mass Spectrometry. *Analytical Letters*. 2017;50(13):2147-60.
180. Grygo-Szymanko E, Tobiasz A, Walas S. Speciation analysis and fractionation of manganese: A review. *Trends in Analytical Chemistry*. 2016;80:112-24.
181. Michalke B. The coupling of LC to ICP-MS in element speciation: I. General aspects. *TrAC Trends in Analytical Chemistry*. 2002;21(2):142-53.
182. Sutton K, Sutton RMC, Caruso JA. Inductively coupled plasma mass spectrometric detection for chromatography and capillary electrophoresis. *Journal of Chromatography A*. 1997;789(1–2):85-126.
183. Grebe M, Profrock D, Kakuschke A, Estella del Castillo Busto M, Montes-Bayon M, Sanz-Medel A, et al. Comparison of different methods for the absolute quantification of harbour seal transferrin glycoforms using HPLC-ICP-MS. *Journal of Analytical Atomic Spectrometry*. 2012;27(3):440-8.
184. Marcinkowska M, Barańkiewicz D. Multielemental speciation analysis by advanced hyphenated technique – HPLC/ICP-MS: A review. *Talanta*. 2016;161:177-204.
185. Łobiński R. Speciation—targets, analytical solutions and markets. *Spectrochimica Acta Part B: Atomic Spectroscopy*. 1998;53(2):177-85.

186. Zhou YX, Yang WJ, Zhang LY, Wang ZY. Determination of Kanamycin A in Animal Feeds by Solid Phase Extraction and High Performance Liquid Chromatography with Pre-Column Derivatization and Fluorescence Detection. *Journal of Liquid Chromatography & Related Technologies*. 2007;30(11):1603-15.
187. Liquid column chromatography. *Journal of Chromatography A*. 1998;820(2):B105-B53.
188. Feldmann J, Raab A, Krupp E. Importance of ICPMS for speciation analysis is changing: future trends for targeted and non-targeted element speciation analysis. *Analytical and bioanalytical chemistry*. 2018;410(3):661-7.
189. Hill SJ, Bloxham MJ, Worsfold PJ. Chromatography coupled with inductively coupled plasma atomic emission spectrometry and inductively coupled plasma mass spectrometry: A review. *Journal of Analytical Atomic Spectrometry*. 1993;8(4):499-515.
190. Carey JM, Byrde FA, Caruso JA. Alternate methods of sample introduction for plasma mass spectrometry. *Journal of Chromatographic Science*. 1993;31(8):330-44.
191. Cui C, He M, Hu B. Membrane solid phase microextraction with alumina hollow fiber on line coupled with ICP-OES for the determination of trace copper, manganese and nickel in environmental water samples. *Journal of Hazardous Materials*. 2011;187(1):379-85.
192. Froes RES, Borges Neto W, Naveira RLP, Silva NC, Nascentes CC, da Silva JBB. Exploratory analysis and inductively coupled plasma optical

emission spectrometry (ICP OES) applied in the determination of metals in soft drinks. *Microchemical Journal*. 2009;92(1):68-72.

193. Yamini Y, Rezaee M, Khanchi A, Faraji M, Saleh A. Dispersive liquid-liquid microextraction based on the solidification of floating organic drop followed by inductively coupled plasma-optical emission spectrometry as a fast technique for the simultaneous determination of heavy metals. *Journal of Chromatography A*. 2010;1217(16):2358-64.

194. Yamini Y, Safari M. Modified magnetic nanoparticles with catechol as a selective sorbent for magnetic solid phase extraction of ultra-trace amounts of heavy metals in water and fruit samples followed by flow injection ICP-OES. *Microchemical Journal*. 2018.

195. Garbarino JR, Taylor HE, Batie WC. Simultaneous Determination of Major and Trace Elements by Inductively Coupled Plasma Mass Spectrometry/Optical Emission Spectrometry. *Analytical Chemistry*. 1989;61(7):793-6.

196. Ferreira L. Brazilian environmental sociology: A provisional review. *Ambiente & Sociedade*. 2002;10:27-43.

197. Saitoh K, Sera K, Gotoh T, Nakamura M. Comparison of elemental quantity by PIXE and ICP-MS and/or ICP-AES for NIST standards. *Nuclear Instruments and Methods in Physics Research Section B: Beam Interactions with Materials and Atoms*. 2002;189(1):86-93.

198. Eh. BS EN ISO 11885:1998, BS 6068-2.60:1998 - Water quality. Determination of 33 elements by inductively coupled plasma atomic emission spectroscopy 1998.

199. Martin TDMaER. <200\_7method validation drinking water oes.pdf>.

200. Aneta Chochorek AB, Zuzana Kiralyova, Jan Mocak. ICP-OES Determination of Select Metals in Surface Water – a Metrological Study. 2010;19:59-64.
201. Pancras JP, Norris GA, Landis MS, Kovalcik KD, McGee JK, Kamal AS. Application of ICP-OES for evaluating energy extraction and production wastewater discharge impacts on surface waters in Western Pennsylvania. Science of The Total Environment. 2015;529:21-9.
202. Miller JN, Miller JC. Statistics and Chemometrics for Analytical Chemistry. 6th ed. Harlow: Pearson; 2010.
203. Mahar M TJ, Neubauer K, Grosser Z. High throughput sample introduction system for the analysis of drinking waters and wastewaters by ICP-MS. Journal of Analytical Atomic Spectrometry. 2008;23(9):1204-13.
204. Cave MR BO, Cook JM, Cresser MS, Garden LM, Miles DL. Environmental analysis. Journal of Analytical Atomic Spectrometry. 2000;15(2):181-235.
205. Ammann AA. Inductively coupled plasma mass spectrometry (ICP MS): a versatile tool. Journal of Mass Spectrometry. 2007;42(4):419-27.
206. Yang X, Low G. Validation of a digestion procedure for ICP-AES and dynamic reaction cell ICP-MS for trace elemental analysis in environmental samples. Environmental Chemistry Letters. 2009;7(4):381-7.
207. Bouchard M, Laforest F, Vandelac L, Mergler D, Bellinger DC. Hair Manganese and Hyperactive Behaviors: Pilot Study of School-Age Children Exposed through Tap Water. Environmental Health Perspectives. 2006;115(1).

208. Wasserman GA, Liu X, Parvez F, Ahsan H, Levy D, Litvak-Factor P, et al. Water manganese exposure and children's intellectual function in Araihasar, Bangladesh.(Research / Children's Health). *Environmental Health Perspectives*. 2006;114(1):124.
209. Fernandez-Turiel JL, F Llorens J, López-Vera F, Gómez-Artola C, Morell I, Gimeno D. Strategy for water analysis using ICP-MS2000. 601-6 p.
210. Ford MJ, Ebdon L, Hutton RC, Hill SJ. Simplex optimization of the plasma parameters and ion optics of an inductively coupled mass spectrometer with pure argon and doped argon plasmas, using a multi-element figure of merit. *Analytica Chimica Acta*. 1994;285(1):23-31.
211. van Veen EH, Bosch S, de Loos-Vollebregt MTC. Precision-based optimization of multicomponent analysis in inductively coupled plasma mass spectrometry. *Spectrochimica Acta Part B: Atomic Spectroscopy*. 1996;51(6):591-608.
212. Gazulla MF, Rodrigo M, Vicente S, Orduña M. Methodology for the determination of minor and trace elements in petroleum cokes by wavelength-dispersive X-ray fluorescence (WD-XRF). *X-Ray Spectrometry*. 2010;39(5):321-7.
213. Beard BL, Johnson CM. Erratum to Brian L. Beard and Clark M. Johnson (2004) "Inter-mineral Fe isotope variations in mantle-derived rocks and implications for the Fe geochemical cycle", *Geochimica et Cosmochimica Acta* 68, 4727–4743. *Geochimica et Cosmochimica Acta*. 2005;69(21):5161.
214. Gupta VK, Dobhal R, Nayak A, Agarwal S, Uniyal DP, Singh P, et al. *Advanced and Hyphenated Techniques for Nano-Level Analysis of Iron in Water*.

215. Barańkiewicz D, Pikoś B, Belter M, Marcinkowska M. Speciation analysis of chromium in drinking water samples by ion-pair reversed-phase HPLC–ICP-MS: validation of the analytical method and evaluation of the uncertainty budget. *Accreditation and Quality Assurance*. 2013;18(5):391-401.
216. Chen Z, Sun Q, Xi Y, Owens G. Speciation of metal–EDTA complexes by flow injection analysis with electrospray ionization mass spectrometry and ion chromatography with inductively coupled plasma mass spectrometry. *Journal of Separation Science*. 2008;31(21):3796-802.
217. Sun H-L, Liu H-M, Tsai S-JJ. Quantitative analysis of manganese, chromium and molybdenum by ion-pair reversed-phase high-performance liquid chromatography with pre-column derivatization and UV-visible detection. *Journal of Chromatography A*. 1999;857(1):351-7.
218. Norkus E, Gaidamauskas E, Stalnionienė I, Crans DC. Interaction of pyridine-2,5-dicarboxylic acid with heavy metal ions in aqueous solutions. *Heteroatom Chemistry*. 2005;16(4):285-91.
219. Michalke B. Review about the manganese speciation project related to neurodegeneration: An analytical chemistry approach to increase the knowledge about manganese related parkinsonian symptoms. *Journal of Trace Elements in Medicine and Biology*. 2016;37:50-61.
220. Gustavo González A, Ángeles Herrador M. A practical guide to analytical method validation, including measurement uncertainty and accuracy profiles. *TrAC Trends in Analytical Chemistry*. 2007;26(3):227-38.
221. Mansilha C, Rocha S, Gameiro P, Pinho C, Ferreira IMPLVO, Silva P, et al. Interlaboratory validation of an environmental monitoring method for

trace analysis of endocrine disrupting compounds. Anal Methods. 2012;4(11):3724-32.

222. Moses CO, Herlihy AT, Herman JS, Mills AL. Ion-chromatographic analysis of mixtures of ferrous and ferric iron. Talanta. 1988;35(1):15-22.

223. Scientific TF. IonPac CS5A Manual - Thermo Fisher Scientific. (07 November 2002).

224. Cardelhoccto N, Cavalli S. Use of ion chromatography for the determination of transition metals in the control of sewage-treatment-plant and related waters. Journal of Chromatography A,. 1997:185-93.

225. Horstkotte B JP, Chocholous P, Sklenarova H, Solich P. Sequential injection chromatography with post-column reaction/derivatization for the determination of transition metal cations in natural water samples. Talanta. 2015;136:75-83.

226. Drinking Water Inspectorate. Water treatment processes London: Drinking Water Inspectorate; 2016 [Available from: <http://dwi.defra.gov.uk/private-water-supply/installations/Treatment-processes.pdf>].